CONVERSION OF GLYCEROL TO PROPANEDIOL USING HETEROGENEOUS CATALYSTS

Ph.D. THESIS

by

SMITA MONDAL

DEPARTMENT OF CHEMICAL ENGINEERING
INDIAN INSTITUTE OF TECHNOLOGY ROORKEE
ROORKEE-247667 (INDIA)
February, 2019

CONVERSION OF GLYCEROL TO PROPANEDIOL USING HETEROGENEOUS CATALYSTS

A THESIS

Submitted in partial fulfilment of the requirements for the award of the degree

of

DOCTOR OF PHILOSOPHY

in

CHEMICAL ENGINEERING

by

SMITA MONDAL

DEPARTMENT OF CHEMICAL ENGINEERING
INDIAN INSTITUTE OF TECHNOLOGY ROORKEE
ROORKEE-247667 (INDIA)
February, 2019

INDIAN INSTITUTE OF TECHNOLOGY ROORKEE ROORKEE

CANDIDATE'S DECLARATION

I hereby certify that the work which is being presented in this thesis entitled **"CONVERSION OF GLYCEROL TO PROPANEDIOL USING HETEROGENEOUS CATALYSTS",** in partial fulfilment of the requirements for the award of the Degree of Doctor of Philosophy and submitted in the Department of Chemical Engineering of the Indian Institute of Technology Roorkee is an authentic record of my own work carried out during a period from January, 2014 to February, 2019 under the supervision of Dr. Prakash Biswas, Associate Professor, Department of Chemical Engineering, Indian Institute of Technology Roorkee, Roorkee-247667, Uttarakhand, India.

The matter presented in the thesis has not been submitted elsewhere by me for the award of any other degree of this or any other Institute.

(SMITA MONDAL)

This is to certify that the above statement made by the candidate is correct to the best of my knowledge.

(Prakash Biswas)
Supervisor

The Ph.D. Viva-Voce Examination of Mrs. SMITA MONDAL, Research Scholar, has been held on 7th June, 2019.

Chairman, SRC

Signature of the External Examiner

This is to certify that student has made all the corrections in the thesis.

Signature of Supervisor
Dated:

Head of the Department

ABSTRACT

In the last two decades, considerable attention has been paid for the value addition of excess glycerol (~10 wt.%), a co-product of transesterification process, for the economic feasibility of biodiesel industry. In the recent literature, several routes have been proposed for the glycerol value addition process such as esterification, oxidation, hydrogenolysis, steam reforming etc. Conversion of glycerol to 1,2-propanediol (1,2-PDO) is one of the promising routes among all proposed glycerol conversion processes. 1,2-PDO is an essential commodity chemical used as a monomer for the production of polyester resin, antifreeze agent, paints, food additives, cosmetics, and pharmaceuticals. Globally, ~2.2 million tons of 1,2-PDO is produced per year and its increasing demand rate is 4% per annum. The formation of 1,2-PDO from renewable glycerol is an eco-friendly process compared to the existing commercial process.

Hydrogenolysis of glycerol is the splitting of C-C and/or C-O bond of a glycerol molecule with the concurrent addition of hydrogen at elevated temperature and pressure. It has been observed that the transformation of glycerol to 1,2-PDO requires a suitable catalyst with the capability to cleave the C-O bond selectively. Presence of acidic and/or basic sites on the catalyst surface favored the dehydration of glycerol and the active metal sites are necessary for hydrogenation of glycerol dehydrated product to produce 1,2-PDO.

In this thesis, Cu, Ni, Zn, Fe, Co monometallic as well as bimetallic (Cu:Ni, Cu:Zn, Co:Zn, Cu:Fe, Co:Fe) catalysts supported on γ-Al_2O_3, MgO, BaO_2, La_2O_3 and MgO-La_2O_3 and also Cu-Zn-Mg-Al-O catalysts derived from a layered double hydroxides (LDHs) precursor were developed and their performances were evaluated for selective transformation of glycerol to 1,2-PDO in an autoclave reactor in liquid phase. Various techniques were employed to characterize the developed catalysts such as specific surface area (BET), X-ray Diffraction (XRD), NH_3-temperature programmed desorption (TPD), H_2-temperature programmed reduction (TPR), CO_2-temperature programmed desorption (TPD), X-ray photoelectron spectroscopy (XPS), transmission electron microscopy (TEM), field emission scanning electron microscopy (FE-SEM), atomic absorption spectroscopy (AAS). Further, to enhance the selectivity/yield of 1,2-PDO, the reaction parameters were optimized experimentally by performing the experiment at the different reaction temperature (170-220 ^oC), pressure (3-6 MPa), glycerol concentration (10-40 wt.%) and catalyst loading (2-10 wt.%), respectively. Stability and reusability of Cu-Zn-Mg-Al-O LDHs, Cu:Zn(4:1)/MgO and Cu:Zn(4:1)/MgO-La_2O_3 catalysts were also performed.

Hydrogenolysis activity of 20 wt.% Cu/γ-Al_2O_3, Ni/γ-Al_2O_3 and Cu-Ni(1:1)/γ-Al_2O_3 catalysts were evaluated. Hydrogenolysis results demonstrated that the bimetallic Cu-Ni(1:1)/γ-Al_2O_3 catalyst was the most active and selective to 1,2-PDO in comparison to other monometallic catalysts synthesized. Maximum glycerol conversion of 70.3% with 85.6% selectivity towards 1,2-PDO was obtained in presence of this bimetallic catalyst. The higher catalytic activity of bimetallic Cu-Ni(1:1)/γ- Al_2O_3 catalyst was due to the presence of a new mixed oxide phase as confirmed by XRD, smaller crystallite size, highest acidity and highest degree of reduction.

Bi-functional Cu-Mg-Al-O and Cu-Zn-Mg-Al-O catalysts derived from LDHs precursor were synthesized by urea hydrolysis method and the performances of these catalysts were evaluated. Ball-flower shaped particles were identified in SEM images of all the catalysts and a well-defined layered structure of solid lamella has also been identified. Very high catalytic activity (> 85%) with > 90% selectivity towards 1,2-PDO was achieved in presence of all the LDHs catalysts synthesized. Cu-Zn-Mg-Al-O catalyst was the most active which showed ~98% conversion with very high (~92%) selectivity towards 1,2-PDO at 210 ^oC, at 4.5 MPa pressure after 12 h of reaction. The synergic interaction between the copper and ZnO on LDHs support, higher reducibility, smaller copper particle size, and well-developed curved platelet structure were solely responsible for the better catalytic activity of Cu-Zn-Mg-Al-O catalyst as compared to Cu-Mg-Al-O catalyst. Further, it was found that the inclusion of small amounts of NaOH as an additive in the reaction mixture significantly improved the selectivity (~94.3%) to 1,2-PDO. However, recycle study showed severe deactivation of the catalyst in the successive reuse.

Further, a series of monometallic (Cu, Co, Zn, and Fe) catalysts supported on MgO with 35% metal loading were synthesized and their performance was examined. Cu and Co metals were found to be more active as compared to Zn and Fe. Although the selectivity towards 1,2-PDO was ~100% over Zn and Fe based catalyst. It was also found that 35% Cu/MgO catalyst exhibited 96.6% conversion with 92.6% selectivity towards 1,2-PDO at 210 °C, 4.5 MPa pressure after 12 h of reaction. Presence of acidic and/or basic sites, bi-functional nature, high metallic surface area (4.4 $m^2.g^{-1}$), lower copper crystallite size (~28 nm) were the main reasons behind the high catalytic activity and 1,2-PDO selectivity. Further, Zn and Fe were incorporated with Cu and Co to increase the overall selectivity and/or the yield of 1,2-PDO. A series of MgO supported bimetallic catalysts were also prepared and their performances were verified. This study aims to optimize the reaction parameters to maximize glycerol conversion and 1,2-PDO selectivity/yield, catalyst stability, and reusability. Among all the catalyst examined, Cu:Zn(4:1)/MgO catalyst exhibited a maximum of 98.4% conversion with 93.4% selectivity

towards 1,2-PDO at 210 ºC and 4.5 MPa pressure. The addition of zinc into the Cu/MgO catalyst increased the degree of reduction of Cu:Zn(4:1)/MgO catalyst and also lowered its reduction temperature significantly. Zinc enhanced basicity and also the reducibility of catalyst by hydrogen spillover effect. NH_3 –TPD and CO_2 –TPD results revealed that copper introduced the acidic sites, whereas, Zn introduced the additional basicity in the catalyst. Very high catalytic activity and selectivity over Cu:Zn(4:1)/MgO catalyst was due to the presence of an appropriate combination of acidic (2.13 mmol NH_3 $gcat^{-1}$) and/or basic (1.81 mmol CO_2 $gcat^{-1}$) sites concentration on the catalyst, high hydrogen consumption (6.7 mmol $gcat^{-1}$), very high degree of reduction (91.7%), and the presence of small average copper particle size (37.1 nm) in the reduced catalyst. Catalyst stability and reusability experiments were performed up to 3rd cycle. Glycerol conversion was found to reduce by ~ 14% after 3rd successive reuse. However, the selectivity towards 1,2-PDO was almost remained same (~94%).

The effects of various basic supports (La_2O_3, CaO, BaO_2, and MgO-La_2O_3) on the performance of Cu-Zn bimetallic catalysts were investigated. The best catalytic activity was obtained in presence of Cu:Zn(4:1)/MgO-La_2O_3 catalyst, which showed 100% conversion with 93% selectivity towards 1,2-PDO at 210 °C and at 4.5 MPa pressure. After the addition of La_2O_3 to Cu:Zn(4:1)/MgO catalyst, average crystallite size of the catalyst was decreased from 33.2 to 27.8 nm and the degree of reduction of the catalyst was increased significantly from ~92% to 97%. Higher activity of Cu:Zn(4:1)/MgO-La_2O_3 catalyst was associated with the presence of smallest average crystallite size (27.8 nm), higher acidic strength (2.12 $mmol.gcat^{-1}$)/basic strength (1.87 $mmol.gcat^{-1}$) and higher degree of reduction (97%).

To understand the intrinsic kinetic behaviour of glycerol hydrogenolysis reaction, kinetic studies were performed in presence of Cu:Ni(1:1)/γ-Al_2O_3, Cu:Zn(4:1)/MgO and Cu:Zn(4:1)/MgO-La_2O_3 catalyst, respectively. Over Cu:Ni(1:1)/γ-Al_2O_3 catalyst, the kinetic experiments were conducted at the different reaction temperature (180-220 ºC) and pressure (3-6 MPa), respectively. A series reaction scheme of glycerol conversion to 1,2-PDO followed by the hydrogenolysis of 1,2-PDO to propanol was considered to develop the kinetic model. To develop the kinetic model, 1,2-PDO and propanol (1-PO + 2-PO) were considered as the main reaction products. A more realistic heterogeneous kinetic model based on combined Langmuir–Hinshelwood-Hougen-Watson (LHHW) and an Eley-Rideal (ER) approach was developed. The calculated activation energy was found to be 70.5 $kJ.mol^{-1}$ for the conversion of glycerol to 1,2-PDO and it was 79.5 $kJ.mol^{-1}$ for the production of PO from 1,2-PDO, respectively. The parity plot of the experimental and model simulated concentration of reactant and products were fitted

very well. Further, in presence of Cu:Zn(4:1)/MgO-La_2O_3 and Cu:Zn(4:1)/MgO catalyst, a simple reaction scheme from glycerol to 1,2-PDO was considered and a kinetic model based on Langmuir–Hinshelwood-Hougen-Watson (LHHW) approach was also developed.

Finally, the overall economic feasibility of the liquid phase hydrogenolysis of glycerol to 1,2-PDO was carried out in presence of Cu:Zn(4:1)/MgO catalyst which showed best activity among all the catalysts. Per day 60 kg production of 1,2-PDO was assumed to be the basis of calculation. Production cost included total fixed cost and operating cost. Annual income tax rate (φ) was considered as 30% of profit. Operating cost included material cost, energy cost, reaction cost, and catalyst separation cost and product purification cost. Production cost per kilograms of 1,2-PDO was estimated to be Rs. 1502.4/-, whereas the market price of 1,2 PDO is Rs. 4437.5/- per kg (Alfa aesar = 99.5% 1,2 PDO, Item no 030948). The selling price of one kilogram 1,2-PDO was considered to be Rs. 2000/-. Based on that, the return on investment after taxes (ROI) was found to be 82.82% and the payback period was calculated as 1.12 years. Therefore, the economic analysis suggested that the production of 1,2-PDO from renewable glycerol is extremely profitable and it is very promising for commercial application.

ACKNOWLEDGEMENTS

It gives me an immense pleasure to express my deep sense of respect to my thesis supervisor, **Dr. Prakash Biswas**, Associate professor, Department of Chemical Engineering, Indian Institute of Technology (IIT) Roorkee for his guidance, motivation and extreme moral support throughout my Ph.D. work. His valuable suggestions, scientific expertise, and insightful discussions gave me the right direction to carry out the research work successfully. It is an honour to have had the great opportunity to work with him. I am very grateful for believing in me and giving me freedom, which helped me to be an independent researcher. Without his guidance and intensive scrutiny, this thesis would not have been possible.

I would like to thank **Dr. Shishir Sinha**, Professor and Head, Department of Chemical Engineering, IIT Roorkee for providing me the opportunity to access all existing facilities in the department to carry out my thesis work. I would like to thank all the member of my Student Research Committee (SRC) as well as Departmental Research Committee for their valuable suggestions, constructive feedback, and critical review during the course of my Ph.D. I am sincerely grateful to all the faculty members in the Department of Chemical Engineering, IIT Roorkee, for their valuable guidance and sharing knowledge during my coursework as well as a teaching assistant.

I am thankful to IIT Roorkee for providing me such an excellent environment to carry out my research work so effectively. I acknowledge the Dean of Resources & Alumni Affairs (DORA) for providing financial assistance to participate and present my works in various national and international conferences.

I am grateful to the Ministry of Human Resources Development (MHRD), Government of India for financial assistance during the tenure of my Ph.D. program. I would like to thank the Department of Science and Technology (DST), Government of India, for providing me the financial support to participate in AIChE (American Institute of Chemical Engineers) annual meeting-2018, at Pittsburgh, USA.

I wish to express my sincere gratitude to my senior laboratory mates, Dr. Satyanarayana Murti Pudi and Dr. Nitin Naresh Pandhare for their immense help and valuable suggestions during early days of my Ph.D. program, whenever it was necessary. They taught me the handling of many sophisticated laboratory equipments including the operation of the batch reactor, gas chromatography, Micromeritics pulse chemisorb 2720 and also various data analysis methods. I

am also thankful to my lab mates Dinesh Kumar Pandey, Richa Tomer for their enthusiastic support, motivation during my work in the laboratory. I want to extend my thanks to Al Ameen Arifa, Arun Pankajasan, Rathikanti Janardhan, Najish, Tushar, Himanshu Malviya, Mohan Lal Meena, Sandeep Joshi, Somsubhra Maity, Jaina Shivnani, Shyam Pratap Singh, Akansha Pandey for providing the cheerful atmosphere in our laboratory.

I greatly appreciate the help of staff members of Instrument Analysis Laboratory, Department of Chemical Engineering, IIT Roorkee, especially Mr. Satyapal and Mr. Arvind to carry out the catalyst characterizations studies.

I would like to thank my best friend Mrs. Vibha Devi who has been a constant source of happiness during my stay at IIT Roorkee. I could not even imagine my Ph.D. days without her. I am indebted to my friends Rachna Arora, Baljinder Kaur Riyar, Sneha Malhotra, Bhupendra Suryawansi, Bhogadi Bhaskar Rao, Mahendra, Anju Goswami, Jyoti Jain, Priti Kumari, Palash Maity for their enthusiastic support, encouragement and providing joyous environment during my stay at IIT Roorkee. I would like to thank my husband Dr. Arkadeb Saha for being by my side during ups and downs and also for giving happiness in my life. His constant emotional support and motivation helped me to stay focused on my research work.

I express my deep gratitude to my father Mr. Netai Chandra Mondal, mother Mrs. Jharna Mondal, for their unconditional love, moral support and providing strength throughout my life. Their blessings, affection, care, and encouragement helped me to acquire this position. I wish to acknowledge my gratitude to my elder sisters Mrs. Chhanda Mondal (Roy), Late Ms. Snigdha Mondal for always being there for me. Their love, continual support and having faith in me boosted my morale. Without their inspiration and advice, I could not even start this journey. I take this opportunity to thank my brother in law, Dr. Pronab Roy, maternal uncle Mr. Prasenjit Kayal and Mr. Abhijit Kayal for being constant source of inspiration and for their valuable advice throughout my career. At this juncture today, I want to dedicate this thesis to my beloved sister, Late Ms. Snigdha Mondal.

Thanks to almighty GOD for showering me all the blessings and giving me patience, strength to complete this journey successfully.

SMITA MONDAL

CONTENTS

LIST OF SCHEMES		**Page No**
Scheme 1.1	Transesterification of triglyceride for the production of biodiesel	1
Scheme 1.2	Reaction mechanism of glycerol hydrogenolysis	3
Scheme 4.1	Reaction mechanism for hydrogenolysis of glycerol over 20 wt.% Cu:Ni(1:1)/γ-Al_2O_3 catalyst	58
Scheme 4.2	Reaction mechanism for hydrogenolysis of glycerol to 1,2-PDO over Cu:Zn(4:1)/MgO catalyst	103
Scheme 5.1	LHHW-ER type reaction mechanism for glycerol hydrogenolysis reaction over Cu:Ni(1:1)/γ-Al_2O_3 catalyst	150
Scheme 5.2	LHHW type reaction mechanism for glycerol hydrogenolysis reaction over Cu:Zn(4:1)/MgO catalyst	162
Scheme 6.1	Cost analysis of the overall process	179

LIST OF FIGURES		**Page No**
Figure 3.1	Schematic diagram of reactor setup	40
Figure 4.1	(A) XRD pattern of γ-Al_2O_3 based monometallic and bimetallic catalyst (B) H_2-TPR profiles of γ-Al_2O_3 supported catalysts (C) NH_3-TPD profiles of γ-Al_2O_3 supported catalysts	45-46
Figure 4.2	Effect of calcination temperature on glycerol conversion and products selectivity over 20 wt.% Cu:Ni(1:1)/γ-Al_2O_3 catalyst.	49
Figure 4.3	Variation in (A) glycerol conversion and (B) product selectivity with time at different temperatures = 180-220 °C, pressure = 4.5 MPa, feed = 20 wt.% glycerol (20 g), catalyst = 2 g. Variation in (C) glycerol conversion and (D) product selectivity with time at	52-54

NOMENCLATURE

Symbol	Nomenclature
PDO	Propanediol
LDH	Layered double hydroxide
C_{AS}	Reactant concentration at the external particle surface (mol. cm^{-3})
C_G	Concentration of glycerol ($mol.L^{-1}$)
C_P	Concentration of 1,2-PDO ($mol.L^{-1}$)
$C^i_{G,exp}$	Experimental concentration of glycerol ($mol.L^{-1}$)
$C^i_{G,sim}$	Simulated concentration of glycerol ($mol.L^{-1}$)
$C^i_{PG,exp}$	Experimental concentration of 1,2-PDO ($mol.L^{-1}$)
$C^i_{PG,sim}$	Simulated concentration of glycerol of 1,2-PDO ($mol.L^{-1}$)
$C^i_{PO,exp}$	Experimental concentration of propanol ($mol.L^{-1}$)
$C^i_{PO,sim}$	Simulated concentration of propanol ($mol.L^{-1}$)
$C_{G.\$}$	Concentration of glycerol at catalyst surface, ($mol.gcat^{-1}$)
$C_{H_2.\$}$	Concentration of hydrogen at catalyst surface, ($mol.gcat^{-1}$)
$C_{P.\$}$	Concentration of 1,2-PDO at catalyst surface, ($mol.gcat^{-1}$)
$C_{W.\$}$	Concentration of water at catalyst surface, ($mol.gcat^{-1}$)
$C_{\$}$	Concentration of the vacant sites, ($mol.gcat^{-1}$)
$C_{T\$}$	Total concentration of catalyst active sites, ($mol.gcat^{-1}$)
D_e	Effective diffusivity, ($cm^2.s^{-1}$)
D_k	Knudsen diffusivity of glycerol ($cm^2.s^{-1}$)
E	Activation energy, ($kJ.mol^{-1}$)
G	Reactant species, glycerol
H_2	Reactant species, hydrogen
P	Product species, 1,2-PDO
PO	Product species, propanol
k_0	Frequency factor, ($mol.gcat^{-1}.\ h^{-1}$)

k_i	Forward reaction rate constant for adsorption of i^{th} reaction on catalyst active site, $((mol/L)^{1-n}/gcat.\ h)$
k_{-i}	Backward reaction rate constant for the desorption of i^{th} reaction from the catalyst active site, $((mol/L)^{1-n}/gcat.\ h)$
K_i	Equilibrium constant of i^{th} reaction on catalyst active site
n	Overall reaction order
N	number of experimental runs
P_{H2}	Hydrogen pressure (MPa)
R	Gas constant, $(kJ.mol^{-1}.K^{-1})$
r_i	Rate of i^{th} reaction, $((mol.\ L^{-1}).\ gcat^{-1}.\ h^{-1})$
r_{obs}	Observed reaction rate at bulk concentration, $(mol\ glycerol.\ gcat^{-1}.\ s^{-1})$
R_p	Radius of the catalyst particle, (cm)
T	Reaction temperature, (K)
W	Product species, water
T_S	Surface temperature (K)
$-\Delta H_{Rx}$	Heat of reaction
Greek Letters	
ρ_p	True density of the catalyst, $(g.cm^{-3})$
φ	Weisz-Prater parameter
α	Pore radius (cm)
$\lambda_{eff} = \lambda_S \left(\frac{\lambda_f}{\lambda_S} \right)^{\xi}$	Effective thermal conductivity of catalyst pellet $(W\ m^{-1}\ K^{-1})$
λ_S	Thermal conductivity of catalyst pellet $(W\ m^{-1}\ K^{-1})$
λ_f	Thermal conductivity of fluid (glycerol + water + solubility of hydrogen) $(W\ m^{-1}\ K^{-1})$
ξ	Porosity of catalyst pellet
β	Prater no

PUBLICATIONS

INTERNATIONAL JOURNAL

[1] **Smita Mondal**, Al Ameen A and Prakash Biswas, Production of 1,2-propanediol from renewable glycerol over highly stable and efficient Cu–Zn(4:1)/MgO catalyst, *Catalysis Letters*, 147 (2017) 2783-2798.

[2] **Smita Mondal**, Rathikanti Janardhan, Mohan Lal Meena and Prakash Biswas, Highly active Cu-Zn-Mg-Al-O catalyst derived from layered double hydroxides (LDHs) precursor for selective hydrogenolysis of glycerol to 1,2-propanediol, *Journal of Environmental Chemical Engineering*, 5 (2017) 5695-5706.

[3] **Smita Mondal**, Himanshu Malviya and Prakash Biswas, Kinetic modelling for the hydrogenolysis of bio-glycerol in presence of a highly selective Cu-Ni-Al_2O_3 catalyst in a slurry reactor. *Reaction Chemistry & Engineering*, 4 (2019) 595-609. DOI: 10.1039/C8RE00138C.

[4] Al Ameen A, **Smita Mondal**, Satyanarayana Murty Pudi, Nitin Naresh Pandhare, and Prakash Biswas, Liquid phase hydrogenolysis of glycerol over highly active 50%Cu–Zn(8:2)/MgO catalyst: Reaction parameter optimization by using Response Surface Methodology, *Energy & Fuels*, *31* (8) (2017) 8521–8533.

[5] Nitin Naresh Pandhare, Satyanarayana Murty Pudi, **Smita Mondal**, Keval Pareta, Manish Kumar, and Prakash Biswas, Development of kinetic model for hydrogenolysis of glycerol over Cu/MgO catalyst in a slurry reactor, *Industrial and Engineering Chemistry Research*, 57 (2018) 101-110. DOI: 10.1021/acs.iecr.7b03684.

[6] **Smita Mondal** and Prakash Biswas, Effect of various oxides on the performance of Cu-Zn catalyst for conversion of glycerol to 1,2-propanediol. (Manuscript under preparation)

PATENT FILED

Prakash Biswas, Al Ameen A, **Smita Mondal,** Satyanarayana Murty Pudi and Nitin Naresh Pandhare, "Copper-Zinc-Magnesium catalyst for highly selective conversion of glycerol to 1,2-propanediol in liquid phase", CINIITR0000100028 (CRN028) (allotted application no. 201711017272 dated 17/05/2017).

INTERNATIONAL CONFERENCE

[1] **Smita Mondal**, Al Ameen A, Prakash Biswas, Conversion of glycerol to propanediol using heterogeneous catalysts. 7th *Asia Pacific Congress on Catalysis.*17-21st January 2017, Mumbai, India.

[2] **Smita Monda**l and Prakash Biswas, Selective conversion of glycerol to 1,2-propanediol over various metal oxide supported copper catalysts, *8th IUPAC International Conference on Green Chemistry*, 9-14th September 2018, Bangkok, Thailand.

[3] **Smita Monda**l and Prakash Biswas, Effect of different metal oxide supported Cu catalysts for 1,2-propanediol production via glycerol hydrogenolysis route, *AIChE annual meeting - 2018*, 28th October-2nd November 2018, Pittsburgh, PA, USA.

[4] Dinesh Kumar Pandey, **Smita Monda**l and Prakash Biswas, Selective hydrogenolysis of glycerol to 1,2-propanediol over an effective copper-zinc bi-metallic catalyst in a continuous and slurry batch reactor, *2nd International Conference on Catalysis and Chemical Engineering (CCE-2018)*, 19-21st February 2018, Paris, France.

NATIONAL CONFERENCE

[1] **Smita Mo**ndal, Al Ameen A, Satyanarayana Murty Pudi, Prakash Biswas**,** Liquid phase hydrogenolysis of glycerol to 1,2-propanediol over MgO supported transition metal (Cu, Co, Ni, Zn, and Fe) catalysts, *Chemcon-2014, IICHE***,** 27-30th December 2014, 864-865, India.

[2] **Smita Mondal,** Rathikanti Janardhan, Prakash Biswas, Hydrogenolysis of glycerol to 1,2-PDO over $Cu_{0.45}Zn_{0.15}Mg_{5.4}Al_2O_9$ catalyst optimized by response surface methodology, *Chemcon-2017, IICHE*, 27-30th December 2017, Haldia, India.

CHAPTER 1

INTRODUCTION

Energy is the backbone of socio-economic development of the modern era. At present, most of the energy comes from fossil fuel which is centralized only in some parts of the world. The developing countries like India, China needs to import crude petroleum from foreign countries to meet their energy requirement. India imports nearly 80% of its crude oil requirement from Middle East and organization of the petroleum exporting countries (OPEC) [Pal and Mitra (2015)]. In 2011, approximately 78% of global energy consumed was petroleum-based [REN-21-Renewable energy policy network]. Dwindling fossil fuel sources, its ever rising cost and its negative impact on the environment have triggered the necessity of alternative fuel from the past two decades [Wang et al., (2010), Maity (2015a)]. Recently, Indian national biofuel policy has fixed a target to reduce its crude oil import by 10% by 2022 [National policy on biofuel 2018, Government of India]. In US, it has been targeted that 30% of existing petroleum-based fuel will be replaced by 2022 [Balan (2014)]. As a result, many attempts have been made for finding an alternative fuel which will be cheaper, environment-friendly and also renewable. In this regard, conversion of biomass to value-added chemicals such as biodiesel, bio-butanol, and bio-ethanol by employing various processes such as thermochemical, chemical and biochemical are growing research interests in recent years [Maity (2015b)]. In this context, biodiesel has emerged as a potential alternative renewable, non-toxic, biodegradable clean fuel. The world production of biodiesel is expected to be around 36.9 million metric tons by the end of 2020 [Dieuzeide et al., (2017)]. Biodiesel, a monoalkyl ester of long chain fatty acid is produced by the transesterification of vegetable oils, animal fats, and waste cooking oil. Scheme 1.1 [Naik et al., (2010)] is showing a typical transesterification process.

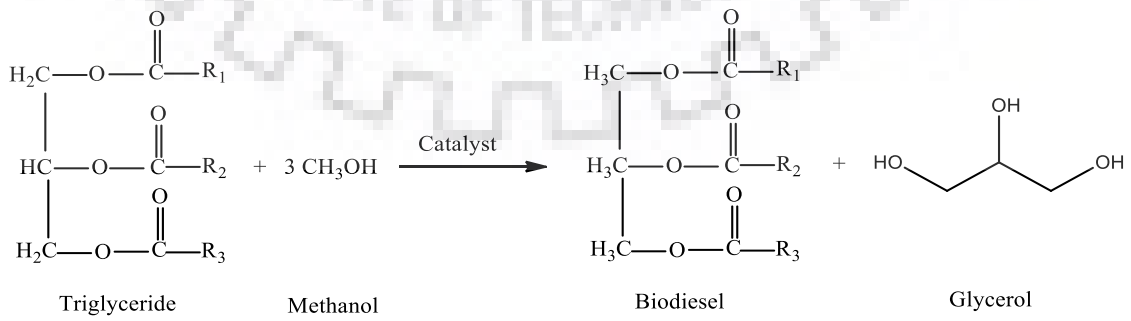

Scheme 1.1. Transesterification of triglyceride for the production of biodiesel

One of the major issues in the biodiesel industry is value addition of the excess amount (~10 wt.%) of crude glycerol obtained as a by-product [Karinen and Krause (2006)]. The commercial biodiesel industry has ended up with large surplus amounts of crude glycerol. This has led to decreasing the price of glycerol and also direct disposal of crude glycerol is a serious environmental concern. In light of this, value addition of these excess amounts of crude glycerol is essential to make the biodiesel industry economically viable [Pathak et al., (2010)]. In addition to this, glycerol also can be obtained as a by-product in saponification process, hydrogenolysis of sorbitol, microbial fermentation etc. According to global glycerol analysis (GIA) report, global glycerol market will reach 6.7 billion pounds by 2020 [Special chem., (2014)].

Glycerol, known as 1,2,3-propanetriol, is a clear, colourless, non-toxic, high functionalized molecule. Glycerol has been identified as one of the top 12 building block compounds. Numerous glycerol value addition processes such as catalytic reforming, oxidation, hydrogenolysis, dehydration, oxidation, etherification, esterification, fermentation and carboxylation have been discussed in the current literature [Nakagawa et al., (2011), Namdeo et al., (2016), Pagliaro et al., (2007)]. Stream reforming of glycerol for the production of H_2 is also well studied [Bepari et al., (2017a)]. Among the various methods proposed, hydrogenolysis of glycerol to 1,2-propanediol (1,2-PDO) is an innovative, attractive and promising route due to the high market demand of 1,2-PDO.

1.1 Hydrogenolysis of glycerol

Hydrogenolysis of glycerol process involves cleavage of C-C bond and/or C=O bond and subsequent addition of hydrogen. The previous study has shown that the cleavage of C=O bond led to the formation of propanediols and cracking of C-C bond produced ethylene glycol, methanol, ethanol, and methane, respectively [Schlaf (2006)]. Therefore, development of an efficient and active catalyst for selective production of propanediols is a great challenge till now. In order to develop a highly active and selective catalyst, many authors have proposed the possible reaction mechanism for hydrogenolysis of glycerol. Two-step and three-step mechanism have been suggested for this reaction process (Scheme-1.2) [Nakagawa et al., (2014)]. In two-step mechanism, initially, glycerol is dehydrated to the intermediate product: either hydroxyacetone or 3-hydroxypropanal. If hydroxyacetone is produced as an intermediate product it is further hydrogenated to 1,2-PDO, whereas, if 3-hydroxypropanal is produced as an intermediate product it is then hydrogenated to 1,3-propanediol. It was observed from the previous literature that hydroxyacetone is thermodynamically more stable as compared to 3

hydroxypropanal which led to the formation of 1,2-PDO much easily in comparison with 1,3-PDO.

Two-steps mechanism (dehydration and hydrogenation):

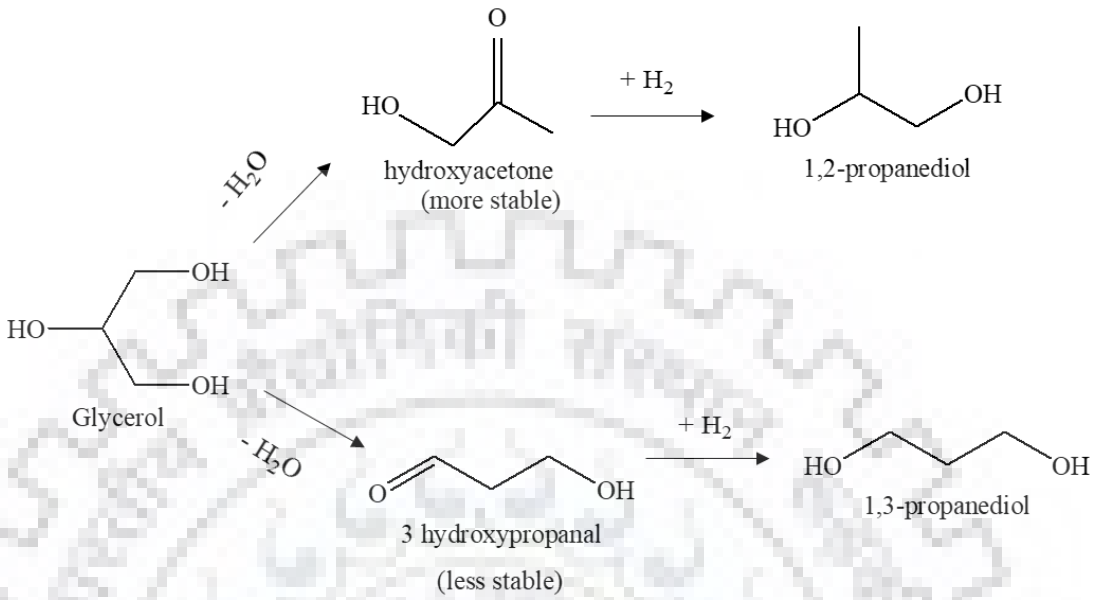

Three steps mechanism (dehydrogenation, dehydration and hydrogenation)

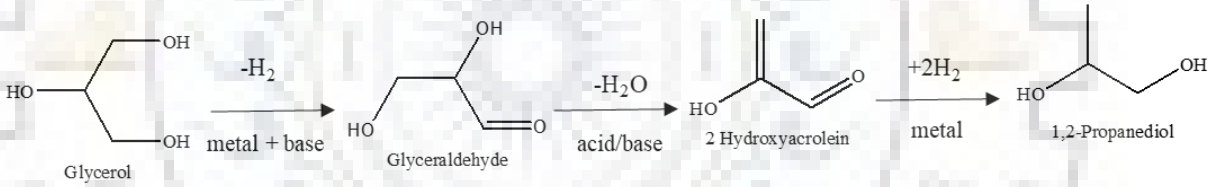

Scheme 1.2. Reaction mechanism of glycerol hydrogenolysis [Nakagawa et al., 2014]

In the three steps process, it was found that glycerol was dehydrogenated to glyceraldehyde followed by dehydration to 2-hydroxyacrolein. Further, 2-hydroxyacrolein was transformed to hydroxyacetone by keto-enol tautomerism followed by the hydrogenation of hydroxyacetone to 1,2-PDO. Now-a-days, 1,2-propanediol (1,2-PDO) is produced from petroleum-derived propylene oxide and the selling cost of 1,2-PDO is $ 1.0–2.2/ kg [Nakagawa and Tomishige (2011)]. 1,2-PDO is used as a monomer for polyester resin, antifreeze agent, solvents, paints, food additives, hydraulic brake fluids, sugar refining, cosmetics, and pharmaceuticals. Globally, ~2.2 million tons of 1,2-PDO is produced per year and its increasing demand rate is 4% per annum. [Rekha et al., (2015), Dasari et al., (2005), Pandhare et al., (2016)]. Archer Daniels Midland Company has opened the 1st commercial plant of 1,2-PDO production from glycerol with a capacity of 0.1 million tons [Mane et al., (2012b)].

1,3 propanediol (1,3-PDO) is another glycerol hydrogenolysis product reported which is used as a monomer of polypropylene terephthalate (PPT) resin, which is a biodegradable polyester. World production of 1,3-PDO is 10^5 tons per year [Silva et al., (2009)]. 1,3-PDO is commercially produced by shell method or degussa-dupoint method. In shell method, 1,3-PDO is produced from hydroformylation of ethylene oxide (petroleum-derived chemical) and successive hydrogenation. Hydration of acrolein is employed in degussa-dupont method, but the main problems associated with these commercially available raw materials are the dependency on non-renewable energy sources and the generation of corrosive chemicals as by-products.

Ethylene glycol (EG), hydroxyacetone, 1-propanol (1-PO), 2-propanol (2-PO), ethanol, were also obtained as by-products of glycerol hydrogenolysis process. EG is used as an antifreeze, lubricant or precursor for the synthesis of polymer, plasticizer and surfactant [Zhu et al., (2010)]. Commercially, EG is produced by the oxidation of petroleum-derived ethylene followed by the hydrolysis of ethylene oxide. 1-propanol is used for the manufacture of waxes, natural and synthetic resin, polyamides, cellulose esters etc. 2-propanol is a common ingredient in antiseptic, detergents, mainly used as a solvent and ethanol is commonly used as a food additive, fuel for motors and also used as a fuel additive in gasoline.

Various previous studies focused on the development of supported monometallic as well as bimetallic noble metals catalyst for selective hydrogenolysis of glycerol to 1,2-PDO [Xia et al., (2012b), Maris et al., (2007), Kusunoki et al., (2005), Ma and He (2009)]. Noble metals including Pt [Maris et al., (2007), Kusunoki et al., (2005)], Ru [Maris et al., (2007), Kusunoki et al.; (2005)], Rh [Maris et al., (2007), Kusunoki et al., (2005)], Pd [Kusunoki et al., (2005)], Re [Ma and He (2009)] and Ag [Zhou et al., (2012)] have been reported previously. However, the major drawbacks of noble metals were the low economic viability and poor selectivity towards 1,2-PDO due to overhydrogenolysis activity. To overcome these limitations, various studies focused on the development of less expensive supported non-noble metals including Cu, Co and Ni catalyst to increase the yield of 1,2-PDO. [Sharma et al., (2014), Yuan et al., (2010), Huang et al., (2008), Dasari et al., (2005), Balaraju et al., (2008), Guo et al., (2009), Guo et al., (2011), Pudi et al., (2015a), Pudi et al., (2015b)]. It was reported that Cu based catalysts are highly selective to 1,2-PDO due to its inherent capability to cleave the C-O bond preserving the C-C bond of glycerol. Co, Ni have more tendency to break C-C bond of glycerol which facilitated the formation of lower alcohols and some gaseous products. [Dhanala et al., (2015)]. The catalyst structure, surface acidity and/or basicity, orientation of bi-

functional active centres including dehydration and hydrogenation sites played important roles on the selectivity to the desired 1,2-PDO [Xia et al., (2012b)]. It is reported that acidic centers favour dehydration of glycerol to hydroxyacetone and the metallic sites facilitate the conversion of hydroxyacetone to 1,2-PDO. In presence of basic sites on the catalyst, hydrogenolysis reaction follows three-step process including dehydrogenation, retro-aldol condensation, and hydrogenation, respectively. For Cu based catalyst, it is investigated that the presence of both Cu^{o} and Cu^{+} plays an important role in their catalytic performance. Cu^{o} provides the catalytic active sites and Cu^{+} provides lewis acid sites which inhibit the aggregation of Cu^{o} particle during the reaction, as a result, the stability of the catalyst increase significantly [Xiao et al., (2014)]. It was observed that the addition of Ni to the Cu based monometallic catalyst exhibited higher catalytic activity as it changes the electronic and geometry of the catalyst [Lin et al., (2010)]. Bimetallic Cu-Ni catalyst has been used for many industrially important reactions such as water gas shift reaction, methanol decomposition etc. [Lin and Guliants (2009)]. Several studies also reported that different catalyst synthesis condition such as pH, time, and calcination temperature of the catalyst and flow rate of the gas-stream affects the metal surface area and crystallite size of the particle. [Shiju et al., (2009), Tsoncheva et al., (2011), Vasiliadou et al., (2013)]. The spillover effect is another important parameter which enhances the reducibility of metal. As a result, the active metallic surface area of the catalyst also increases. Previously, Cu, Ni, Cu-Co metals based ZnO nano-structured catalysts were developed and tested for various reaction [Gupta et al., (2009, 2012, 2016), Lee et al., (2015)]. Few studies focused on the use of hydrogen donor molecules such as methanol, ethanol, 1-propanol, butanol and isopropanol as a solvent instead of molecular hydrogen [Bej P et al., (2017)]. Various supports such as γ-Al_2O_3 [Mane et al., (2010), Mane and Rode (2012) Mane and Rode (2012), Guo et al., (2009)], chromite [Dasari et al., (2005)], MgO [Yuan et al., (2010), Yue et al., (2014), Balaraju et al., (2012)], SiO_2 [Dasari et al., (2005)], ZnO [Balaraju et al., (2008)] and ZrO_2 [Balaraju et al., (2012)] have been explored for glycerol hydrogenolysis reaction. Various previous studies also discussed about the performances of γ-Al_2O_3, TiO_2, MCM-41, silica, molybdenum oxide supported catalysts for many important reactions [Mogalicherla and Kunzru (2010), (2011), Rao and Deo (2007), Rao et al., (2008), Rao et al., (2009), Unnarkat et al., (2016), (2018)].

Recently, hydrotalcite-type layered double hydroxides (LDHs) catalysts have attracted substantial attention in heterogeneous catalysts due to their unique structure [Xia et al., (2012a, 2012b), Yang et al., (2007), Bepari et al., (2017b)]. The usages of LDHs catalyst is very

promising for a reaction where multi-functionality of the catalyst is desirable to improve the selectivity of the desired product. The report based on the activity of LDHs type catalyst for hydrogenolysis of glycerol to 1,2-PDO is only a few [Xia et al., (2012a, 2012b), Xia et al., (2013), Yuan et al., (2011), Meher et al., (2009)]. It is also reported that the acidic and basic properties of the catalysts were significantly affected by the variation of metal compositions (M^{2+}/M^{3+}) in the catalysts [Meher et al., (2009)]. A series of hydrotalcite catalyst having different (Cu+Mg)/Al ratio were prepared and $Cu_{0.4}Mg_{5.6}Al_2O_{8.6}$ catalyst showed good catalytic activity as compared to the remaining series of Cu/Mg/Al catalysts [Xia et al., (2013)]. Maximum 80% conversion with 98.2% selectivity towards 1,2-PDO was reported over $Cu_{0.4}Mg_{5.6}Al_2O_{8.6}$ catalyst at 180 °C and at 3 MPa H_2 pressure after 20 h of reaction [Yuan et al., (2011)]. Xia et al., (2011, 2012a, 2012b) developed various layer double hydroxide based catalysts and evaluated for hydrogenolysis of glycerol. It is reported that different primary alcohols such as methanol, ethanol, 1-propanol, butanol, and isopropanol as a hydrogen donor were very effective towards 1,2-PDO formation from glycerol. Among all the primary alcohol studied, ethanol is suggested as the best hydrogen donor and maximum 95% conversion with 92.2% selectivity towards 1,2-PDO was obtained over $Cu_{0.4}Mg_{6.28}Al_{1.32}O_{8.26}$ catalyst at 210 ^oC and at 3 MPa of nitrogen pressure in presence of ethanol as a hydrogen donor.

Based on the previous literature information, it has been observed that 1,2-PDO was mainly formed by the removal of oxygen from the hydroxyl group of a glycerol molecule with simultaneous addition of hydrogen at elevated hydrogen pressure. It is also disclosed that the bi-functional acidic-basic sites concentration on the catalyst surface, metal particle size and the dispersion of active metal played a significant role to control the selectivity towards 1,2-PDO. Selective conversion of glycerol into 1,2-PDO required a suitable catalyst with bi-functional acid/base and metallic sites. The acid/base sites favoured the dehydration steps whereas the active metal sites favoured the hydrogenation process. Therefore, development of bi-functional catalyst having dehydration as well as hydrogenation sites with an appropriate surface orientation is highly desirable for higher selectivity and yield of 1,2-PDO.

CHAPTER II

LITERATURE REVIEW

This chapter summarizes the development of various catalysts and their activity for the conversion of glycerol and the products selectivity obtained in the glycerol hydrogenolysis process. Liquid phase as well as vapor phase hydrogenolysis of glycerol in presence of various catalysts have been discussed in the previous literature. It has been suggested that selective conversion of glycerol to propanediols requires a suitable catalyst which is active to cleave C=O bond without affecting the C-C bond of glycerol. Previous reports also help to understand the basic role of heterogeneous catalysts and reaction kinetics of the process. The review presented in this chapter is mainly focused on the synthesis of catalysts and their characterization, catalytic activity, hydrogenolysis process conditions used, and the product selectivity obtained. Kinetic study and the development of various kinetic models for this reaction are also discussed in this chapter.

2.1 Glycerol hydrogenolysis to 1,2-PDO over noble metal catalysts

2.1.1 Noble metal based monometallic catalysts

Glycerol hydrogenolysis reaction were studied in presence of various noble metals such as Ru, Pt based monometallic catalysts.

Maris and Davis (2007a) evaluated the catalytic activity of monometallic Ru/C and Pt/C catalysts for liquid phase glycerol hydrogenolysis reaction at 200 °C and at 4 MPa H_2 pressure. At neutral pH, Ru was found to be more active which showed ~40% conversion of glycerol as compared to Pt-based catalyst which showed only ~13%. However, Pt/C catalyst was more selective to 1,2-PDO ($S_{79\%}$) in comparison to Ru/C catalyst ($S_{26\%}$). It was also reported that Ru/C catalyst boosted the formation of lower alcohol and the obtained selectivity to ethylene glycol was very high ($S_{68\%}$). Further, the effect of addition of bases (NaOH, CaO) in the reaction mixture was examined and it was found that the inclusion of base enhanced the catalytic activity of Pt/C significantly than Ru/C catalyst. However, a significant amount of lactate was produced along with 1,2-PDO in presence of base over both the Ru and Pt-based catalyst. It was concluded that, in presence of Ru/C catalyst, C-C bond cleavage of glycerol was metal catalyzed reaction, whereas, in presence of Pt/C catalyst the reaction was a base catalyzed reaction.

Further, the effects of different supports (γ-Al_2O_3, SiO_2, ZrO_2) on the performance of Ru metal was investigated for glycerol hydrogenolysis reaction in liquid phase. [Vasiliadou et al., (2009)]. Ru metal on different oxide supported catalysts with chloride and nitrate precursors were synthesized by wetness impregnation method. The activity of the catalysts in terms of glycerol conversion was directly correlated with the acidic strength of the catalysts. Acidity of the catalysts and the activity in glycerol conversion followed the order as: $RuAl(Cl_3)$ > $RuZr(NO_3)$ > $RuAl(NO_3)$ > $RuSi(Cl_3)$ > $RuSi(NO_3)$. Among all these catalysts, $RuAl(Cl_3)$ exhibited highest glycerol conversion of 69% with lowest 1,2-PDO selectivity of 37.9% at 240.8 ^oC, and at 8 MPa H_2 pressure, after 5 h of reaction. On the other hand, $RuSi(NO_3)$ catalyst showed the lowest glycerol conversion of 21.7% with the highest selectivity of 65% to 1,2-PDO. TEM and XRD-analysis suggested that RuO_2 particle size was comparatively smaller on SiO_2 support rather than γ-Al_2O_3, ZrO_2. Poor selectivity towards 1,2-PDO in presence of chloride precursor suggested that higher acidity facilitated excessive hydrogenolysis resulting 1,2-PDO to 1-propanol production.

Later on, Hamzah et al., (2012) studied effects of different metal oxides (SiO_2, TiO_2, Al_2O_3 and bentonite) on the performance of Ru metal catalysts for liquid phase hydrogenolysis of glycerol. Results suggested that the activity of these catalysts were decreased in the following order Ru/SiO_2 < Ru/TiO_2 ≈ Ru/Al_2O_3 < Ru/bentonite. Among all these, Ru/bentonite catalysts exhibited the maximum glycerol conversion of 62.8% with 80% selectivity towards 1,2-PDO at 150 ^oC and at 2–3 MPa of H_2 pressure. Although Ru/TiO_2 catalyst showed less activity (X = 38.8%), however, the obtained 1,2-PDO selectivity was highest (~83.7%) with respect to all other catalysts. In order to improve the performance of Ru/TiO_2 catalyst, Ru/bentonite-TiO_2 (1:2) catalyst was prepared. After the addition of bentonite to Ru/TiO_2, glycerol conversion was found to be increased from 38.8% to 69.8%, however, the selectivity (80%) to 1,2-PDO was remained unchanged. NH_3-TPD analysis revealed that the combination of bentonite and TiO_2 helped to increase the acidity of the catalyst which helped to increase the catalytic activity.

In order to enhace the acidity of the catalysts solid acids were introduced into the noble metal based catalyst during synthesis. Balaraju et al., (2009) evaluated the performance of Ru/C catalyst along with four solid acid co-catalysts such as niobia, 12-tungstophosphoric acid (TPA) supported on zirconia, cesium salt of TPA and cesium salt of TPA supported on zirconia, respectively, for liquid phase reaction. Catalysts were prepared by impregnation method. Among different solid catalysts, niobia and 12-tungstophosphoric acid (TPA)

supported on zirconia showed almost similar activity (X = 44%) and selectivity towards 1,2-PDO (S = 60.9-64.9%) at 180.8 ºC and at 6 MPa H_2 pressure in presence of 20 wt.% aqueous glycerol solution as feed. Higher activity of Ru/C catalyst in presence of Nb_2O_5 and 12-TPA/ZrO_2 acid catalysts were correlated with the higher acidic strength of the catalyst with respect to other catalysts. Effects of reaction temperature, catalyst weight, H_2 pressure, glycerol concentration and reaction time on the glycerol conversion and 1,2-PDO selectivity were studied to optimize the operating condition. Maximum 62.8% conversion with 66.5% selectivity towards 1,2-PDO was achieved at 180 ^oC, at 6 MPa H_2 pressure, after 8 h of reaction in presence of 20 wt.% glycerol as a feed.

Apart from conventional impregnation methods, other methods were also applied to increase the catalytic activity. Vanama et al., (2015) developed a series of Ru/MCM-41 catalysts having different metal loading (1-6 wt.%) by micro-emulsion method. Catalytic performance was assessed for vapour phase hydrogenolysis of glycerol in a down-flow glass reactor. Reaction parameters were optimized by varying temperature, H_2 flow rate, glycerol concentration and flow rate of H_2. 3 wt.% Ru/MCM-41 catalyst exhibited 62% conversion with 38% selectivity towards 1,2-PDO, 20% selectivity towards 1,3-PDO and 12% towards the other degraded products at 230 ^oC temperature. Experiments were conducted in presence of 20 wt.% aqueous glycerol solution as feed and the total H_2 flow rate of 140 ml min^{-1}. It was proposed that, initially, glycerol was dehydrated to hydroxyacetone and 3-hydroxypropionaldehyde as intermediates followed by the hydrogenation to 1,2-PDO and 1,3-PDO, respectively. High Ru metal dispersion on MCM-41 support, metal particle size obtained from CO-chemisorption, and strong metal-support interaction enhanced the catalytic activity. It was observed that catalytic activity was increased sharply with increasing the Ru metal loading from 0-3% and at higher metal loading (4-6%), it was found to decrease due to agglomeration of Ru metal.

In addition to the Ru based catalysts, several studied showed that Pt based catalysts were also highly active. Yuan et al., (2009) studied the effect of various supports such as Al_2O_3, MgO, hydrotalcite and different types of zeolite (H-beta and HZSM-5) on the performance of Pt metal catalysts for liquid phase hydrogenolysis of glycerol reaction and the results were compared. It was demonstrated that hydrotalcite ($Mg_6Al_2(OH)_{16}CO_3.4H_2O$) precursor supported Pt catalyst was the best active which exhibited 92.1% conversion with 93% selectivity towards 1,2-PDO at 3.0 MPa pressure after 20 h of reaction. The obtained activity of other catalysts was quite low (< 10%). It was reported that strong alkalinity, the small particle size of Pt and high Pt metal dispersion on the support was the primary reasons for very high

hydrogenolysis activity and 1,2-PDO selectivity over Pt/hydrotalcite catalyst. Catalyst recycle study suggested that Pt/hydrotalcite catalyst was quite stable, which showed ~70% conversion with ~94% selectivity towards 1,2-PDO even after 5th cycle.

The activity of TiO_2, SnO_2, ZnO and ZrO_2 supported Pt catalysts was examined in a high-pressure autoclave reactor by Checa et al., (2012) and Pt/ZnO was reported as the most active catalyst. Further, ZnO supported various other noble metals catalysts were also developed and their activity was compared. The obtained catalytic activity followed the order as Pt > Rh >> Pd >> Au. It was also noticed that catalyst reduced at low temperature (473 K) was more active than the catalyst reduced at a higher temperature (673 K) due to the alloy formation. Reduction temperature of 473 K was reported as effective.

Delgado et al., (2013) developed a series of Pt catalysts supported on Al_2O_3, Al_2O_3–SiO_2 and TiO_2, respectively, for liquid phase hydrogenolysis reaction. Among all these supported catalysts, TiO_2 supported Pt catalyst exhibited highest activity and selectivity towards C_3 products and the oxide sites of TiO_2 was reported as the active sites for C-O bond cleavage. Small particle size (~1.3 nm) of Pt in Pt/TiO_2 catalyst played a key role for the higher activity in glycerol hydrogenation reaction. Acidic sites of catalysts were involved in the glycerol dehydration reaction. However, it was also observed that too many acidic sites on the catalysts surface accelerated the C-C bond cracking.

2.1.2 Noble metal based bimetallic catalysts

In order to enhance the activity and selectivity to propanediol, bimetallic noble metal based catalysts were developed and their performances were investigated which is discussed below.

Bimetallic Au-Ru/C and Pt-Ru/C catalyst were synthesized by surface redox reaction and the catalysts were characterized by H_2 chemisorption, X-ray absorption spectroscopy and analytical electron microscopy [Maris et al., (2007b)]. Characterization study revealed that Au and Pt were successfully deposited on the surface of Ru/C catalysts and the average diameter of the catalyst was around 2-3 nm. It was found that, at neutral pH, Pt-Ru/C catalyst was more active than Au-Ru/C catalyst. The activity of both catalysts was increased significantly in presence of the base. Products selectivity obtained over both the bimetallic catalysts were almost similar with the monometallic Ru/C catalyst at neutral and higher pH condition. Pt-Ru catalyst was reported as a stable catalyst, whereas, the catalytic activity of Au-Ru catalyst was decreased as Au migrated off to Ru resulting the agglomeration on the supported carbon.

Further, reaction mechanism study was performed in presence of Pt-Ru/C catalyst and it was proposed that glycerol was converted to 1,2-PDO via three steps process. Initially, glycerol was dehydrogenated to glyceraldehyde followed by dehydrated to pyruvaldehyde which produced lactic acid in presence of the base. Further, subsequent hydrogenation of pyruvaldehyde produced 1,2-PDO in presence of metallic sites of the catalyst.

Later, effects of various supports [ZrO_2, SiO_2, TiO_2, and zeolites (H-beta and HZSM-5)] on the performance of Ru-Re bimetallic catalysts prepared by impregnation method were investigated [Ma and He (2009)]. Catalysts were characterized by N_2 adsorption-desorption, XRD, H_2-TPR, CO-chemisorption, and TEM, respectively. Among all these catalysts, Re promoted Ru–Re/ZrO_2 bimetallic catalyst showed the maximum glycerol conversion of 56.9% with 47.2% selectivity towards 1,2-PDO in liquid phase at 160 ºC temperature, 8 MPa H_2 pressure after 8 h reaction. H_2-TPR study revealed strong interaction of Re and Ru which increased H_2 consumption significantly as compared to the monometallic Ru and Re catalysts. XRD and CO chemisorption results suggested that addition of Re significantly improved the Ru metal dispersion on the support of the catalyst and also the presence of Re inhibited the aggregation of Ru particles. Small average metal particle size (3.2-5 nm), highest Ru metal dispersion (~34%) on the support were reported as the primary reason for the highest catalytic activity of the catalyst.

Addition of Re as a second metal to Pt based catalysts increased the production of 1,3-PDO significantly. For liquid phase reaction, Daniel et al., (2010) reported the maximum 34% selectivity towards 1,3-PDO and 33% selectivity towards 1,2-PDO in presence of bimetallic Pt–Re nanoparticles catalyst supported on activated carbon (Norit SX-1G) at 170 °C and at 4 MPa H_2 pressure. Spillover of H from Pt to Re promoted the reduction of Re during H_2 treatment at 473 K. As a result, the charged Re atoms were dispersed widely on the support which enhanced the catalytic activity.

A series of carbon nanotube supported bimetallic Pt-Re (1:1) catalysts were developed by varying Pt metal loading from 1-30% [Deng et al., (2014)]. It was observed that the particle size increased from 1.5 - 4.9 nm with increasing the metal loading. Turn over frequency (TOF) data showed a volcano-shaped graph with the variation of particle size of the catalysts. Turn over frequency increased from 32-62 h^{-1} as the average particle size enhanced from 1.5 to 1.9 nm. Further, it gradually decreased to 8 h^{-1} when the catalyst particle size was ~4.9 nm. X-ray photoelectron spectroscopy revealed that the ratio of Pt/Re decreased with decreasing of particle size. The higher surface concentration of Re at smaller particle size led to increasing

the surface acidity of the catalyst which might enhance the catalytic activity. Furthermore, in order to reveal the reaction pathway with changing of particle size, hydrogenolysis of glycerol, 1,2-PDO and 1,3-PDO were examined in presence of different particle sized catalysts. It was elucidated that larger particle size favoured the cleavage of secondary C-O bond only and smaller particle size accelerated the cracking of C-C bond and the primary C-O bond, simultaneously.

Apart from Pt, Ru, Re based catalysts some efforts has been made to develop a special type of catalysts where noble as well as non-noble metals were incorporated simultaneously.

Xia et al., (2011) prepared a series of layered double hydroxides (LDHs) $Pd_xCu_{0.4}Mg_{5.6x}Al_2(OH)_{16}CO_3$ catalyst and tested their catalytic activity. It was disclosed that Cu metal dispersion on the catalyst surface was improved after the addition of Pd. Maximum 88% glycerol conversion and 99.6% selectivity towards 1,2-PDO was attained in presence of $Pd_xCu_{0.4}Mg_{5.6x}Al_2(OH)_{16}CO_3$ catalyst at 180 °C and at 2.0 MPa of H_2 pressure. However, the catalytic activity was decreased by ~35% after 5 cycles by keeping the 1,2-PDO selectivity almost unchanged. High catalytic activity was ascribed to the synergistic interaction of Cu and Pd particles and hydrogen spillover effect of Pd on Cu metals. Later this group [Xia et al., (2012a)] developed LDHs derived $Rh_{0.02}Cu_{0.4}/Mg_{5.6}Al_{1.98}O_{8.57}$ catalyst by thermal decomposition method. Rh promoted Cu/solid based catalyst exhibited higher glycerol conversion (91.0%) and higher selectivity (98.7%) to 1,2-PDO than the monometallic solid based catalyst at 180 °C and at 2.0 MPa when bio-ethanol was used as a solvent. Reusability study suggested that the catalyst was deactivated by ~45.8% with a slight decrease in 1,2-PDO selectivity after the 5^{th} cycle.

Deng et al., (2015) investigated the role of Al on the formation of Ir-Re alloy structure by impregnating Ir-Re metals on amorphous silica-alumina (ASA) and dealuminated ASA (D-ASA), respectively. Characterization study revealed that ASA inhibited the formation of Ir-Re alloy structure due to the interaction of Re and Si-Al-OH sites of ASA. As a result, the comparatively larger particle size of Ir and finely dispersed Re species were observed on ASA support. The catalytic result suggested that only 4.1% glycerol conversion with 40.7% 1,3-PDO selectivity and 36.1% 1,2-PDO selectivity was observed over Ir-Re bimetallic catalyst supported on ASA. Further, ASA was dealuminated by treating with HNO_3 followed by Ir-Re was impregnated on it. It was observed that dealuminated ASA acted as an inert material. As a result, the mobility of Re species stimulated the formation of Ir-Re alloy structure which significantly improved the catalytic activity. Maximum 54.5% conversion with 38.9%

selectivity to 1,3-PDO and 13.2% selectivity towards 1,2-PDO was achieved over Ir–Re/D-ASA catalyst at 120 ^{o}C temperature and at 8 MPa of H_2 pressure.

Wang et al., (2016) investigated the effects of the incorporation of noble metals (Ru, Rh and Ir) and different metal oxide (La, Re, Zr, Fe, Sn and Ce oxides) onto the performance of Pt/WOx and Pt/WOx/Al_2O_3 catalysts. Among all these promoters, La showed higher promotional effects on both of the catalysts. Incorporation of 0.1% La to Pt/WOx catalyst increased the conversion of glycerol from 37.4% to 39.9%, the selectivity towards 1,2-PDO remained almost constant (2.3-2.8%) and the selectivity to 1,3-PDO enhanced from 35.1 to 41.3%. Further, incorporation of La onto Pt/WO_x/Al_2O_3 catalyst decreased glycerol conversion from 65.4% to 47.4%, whereas, the selectivity towards 1,2-PDO and 1,3-PDO increased from 7.2-12.5% and 48.2-56.9%, respectively. Characterization studies such as TEM, NH_3-TPD, and high angle annular dark field scanning tunnelling electron microscopy revealed that introduction of La increased the acidic strength of the catalysts, which improved the products selectivity especially the selectivity to 1,3-PDO. The effect of the introduction of other promoters was insignificant on the activity and/or product selectivity.

Fernandez et al., (2017) performed liquid phase hydrogenolysis of glycerol in an autoclave reactor in presence of Pt/WO_X/Al_2O_3 catalyst. In this study, the role of tungsten oxide for the formation of 1,3-PDO from glycerol was investigated by using an in-situ and ex-situ attenuated total reflection infrared spectroscopy. Characterization study suggested that tungsten oxide played three important roles i,e. anchoring of primary hydroxyl groups of glycerol, the supply of H+ and stabilization of secondary carbocation. Maximum 38.5% yield to 1,3-PDO and 6.3% yield to 1,2-PDO were achieved with Pt8WAl catalyst at 200 ^{o}C, 9.0 MPa H_2 pressure after 4 h of reaction. The reaction was also performed in presence of N_2 instead of H_2 and 12.7% yield to 1,2-PDO with 22.2% glycerol conversion was obtained. This result revealed that the presence of brönsted acidic centers and higher exposure of H_2 were necessary for the production of 1,3-PDO.

In this section, it was observed that though catalytic activity were very high in presence of noble metal based catalysts, they are poor selective to 1,2-PDO. 1,2-PDO further converted to lower alcohols such as propanols, ethanol and methanol etc. As a result it is difficult to achieve high yield of 1,2-PDO over noble metal based catalysts. Therfore, various studies focused on the development of non-noble metal based comparatively cheaper catalysts to enhance high yield of 1,2-PDO. The development of non-noble metal based catalysts for glycerol hydrogenolysis process is discussed in the following section.

2.2 Glycerol hydrogenolysis to 1,2-PDO over non-noble metal catalysts

2.2.1 Non-noble metal based monometallic catalysts

Dasari et al., (2005) performed liquid phase glycerol hydrogenolysis reaction in an autoclave reactor in presence of Ni, Pd, Pt, Cu, and Cu-Cr based catalysts. Among all the catalysts studied, maximum 54.8% glycerol conversion with 85% selectivity to 1,2-propanediol (1,2-PDO) was obtained in presence of Cu-Cr catalyst at 200 °C and at 1.37 MPa pressure. Various reaction parameters; temperature, pressure, glycerol concentration, catalyst amount and reduction temperature of the catalyst was optimized over Cu-Cr catalyst. It was found that the higher temperature (>200°C) and pressure (>1.37 MPa) were not beneficial for higher selectivity towards 1,2-PDO due to overhydrogenolysis of diol. Effect of glycerol concentration study suggested that, with increasing glycerol concentration from 20-100%, the yield of 1,2-PDO was increased from 21.7% - 49.7%. Effect of catalyst loading result showed that glycerol conversion increased from 28.3% to 78.5% with increasing the catalyst loading from 1% to 20%, as more number of catalytic active sites were available for the hydrogenolysis reaction with increasing catalyst loading. To understand the reaction pathway, reactions were carried out in two steps. In the first step, the reaction was performed at 200 °C and at 0.06 MPa pressure in absence of H_2 over Cu-Cr catalyst. Further, hydroxyacetone, which was formed in the first step was isolated and further hydrogenation reaction was carried out with hydroxyacetone as a feed at 200 °C and at 1.37 MPa H_2 pressure. From the experimental results obtained, it was proposed that initially glycerol was dehydrated to hydroxyacetone which was further hydrogenated to 1,2-PDO.

Chaminand et al., (2004) tested different metals (Cu, Pd, Rh), supported on ZnO, C, Al_2O_3. The effect of various solvents (H_2O, sulfolane, dioxane) and additives (H_2WO_4) on the products (1,2-PDO and 1,3-PDO) selectivity were also studied. Results disclosed that CuO/ZnO catalyst exhibited 100% selectivity towards 1,2-PDO, however, the conversion was very low (19%). The additive H_2WO_4 showed a very small effect on catalytic activity however it propagated the cracking of C-C bond of glycerol. Solvents had a significant effect on catalytic activity and products selectivity. In presence of sulfolane, 1-propanol was produced as the main product. However, dioxane favoured a higher number of C-C bond cleavage products i,e. ethanol, glycol, and methanol, respectively.

Copper metal supported on γ-Al_2O_3, HY zeolite, HZSM-5 zeolite, 13X zeolite, H zeolite and copper-chromite catalysts were investigated by Guo et al., (2009) and achieved

maximum 96.8% selectivity towards 1,2-PDO with a conversion of 50% in presence of Cu/γ-Al_2O_3 catalyst at 220 ^oC and at 1.5 MPa pressure.

Further, Akiyama et al., (2009) evaluated the activity of Cu based catalysts supported on various oxides (Al_2O_3, Cr_2O_3, ZnO and SiO_2) for glycerol hydrogenolysis reaction in vapour phase. In this study, two steps reaction mechanism was proposed: dehydration of glycerol to hydroxyacetone subsequently hydrogenation of hydroxyacetone to 1,2-PDO. It was observed that dehydration of glycerol to hydroxyacetone was higher at elevated temperature, whereas, hydrogenation of hydroxyacetone was favorable at low temperature and elevated pressure. The yield of 1,2-PDO was limited to 80% due to the trade-off problem between 1st and 2nd step. The thermodynamic analysis suggested that the yield of 1,2-PDO was controlled by the equilibrium of 2nd step reaction i.e. hydrogenation of hydroxyacetone. Therefore, to enhance the catalytic activity, reactions were performed at the gradient temperatures. By employing this method, top and bottom temperature of the catalyst bed were kept at 200 °C and 120 °C, respectively. Among all the catalysts, Cu/Al_2O_3 catalyst exhibited the highest catalytic activity which showed ~100% conversion with 96.9% selectivity towards 1,2-PDO in presence of 30 wt.% glycerol as feed. In this study, the experiment was conducted at a higher flow rate of H_2 (360 $cc.min^{-1}$).

Yuan et al., (2010) developed a series of Cu-MgO catalyst with different copper content by impregnation and co-precipitation method, respectively. CuO-15/MgO catalyst synthesized by co-precipitation method exhibited the highest catalytic activity of 72% with 97.6% selectivity towards 1,2-PDO at 180 °C and at 3.0 MPa of H_2 pressure. 75 wt.% aqueous glycerol solution was used as feed and the reaction data was reported after 20 h of reaction. Higher activity was correlated with the smaller particle size of copper and MgO. Further, after the addition of NaOH to the reaction mixture increased the catalytic activity significantly from 72% to 82% with a slight decrease of 1,2-PDO selectivity from 97.6% to 95.8%. This result demonstrated that with increasing pH of the reaction mixture, the overall reaction rate was increased.

Similar type of catalysts (a series of Cu/MgO catalyst with different composition) were also developed by Balaraju et al., (2012). Various techniques such as BET, XRD, TPR, N_2O-adsorption were used for catalyst characterization. It was reported that 20 wt.% Cu/MgO catalyst showed the highest catalytic activity which showed a maximum of 49.3% conversion with 92.3% selectivity towards 1,2-PDO at 200 °C and at 4 MPa of H_2 after 8 h of reaction. 20 wt.% aqueous glycerol solution was used as feed and the catalyst loading was 6 wt.% with

respect to glycerol. Highly dispersed copper metals and the presence of basic sites on MgO played the key role for high catalytic activity. Influences of temperature, pressure, and catalyst weight were also studied to optimize the reaction parameters. It was observed that maximum 50% glycerol conversion with 92% selectivity towards 1,2-PDO was achieved at 220 ^{o}C, 4.0 MPa of H_2, after 8 h. 20 wt.% glycerol concentration and 0.6 g catalyst in the reaction mixture was the optimum value.

Wu et al., (2013) synthesized four different catalysts such as Cu/γ-Al_2O_3, Ru/C, Cu/boehmite, Cu/SiO_2, respectively, by aqueous chemical reduction method and compared their efficiency for the conversion of glycerol to 1,2-PDO. Among all these catalysts, Cu/boehmite displayed the highest conversion of 77.5% with very high 1,2-PDO selectivity to 92.5%. Higher activity and selectivity was reported due to the higher Cu clusters dispersion (0.91%) on boehmite, which led to the higher surface concentration of active metal and lewis acidic sites of boehmite, which enhanced glycerol to hydroxyacetone formation. Based on the product selectivity obtained in presence of copper catalysts, two possible reaction pathways were proposed for glycerol hydrogenolysis process. First one was that, directly dehydration of glycerol to hydroxyacetone, whereas, another one suggested the dehydrogenation of glycerol to glyceraldehyde followed by the dehydration glyceraldehyde to pyruvic aldehyde and subsequent hydrogenation of pyruvic aldehyde to hydroxyacetone.

A series of Cu metal (2.5-25 wt.%) supported on SBA-15 catalysts were synthesized and their activity was tested in a fixed bed-reactor at 0.1 MPa. [Harishekhar et al., (2015)]. XRD results revealed that higher dispersion of CuO was observed in 5 wt.% Cu/SBA-15 catalyst. NH_3-TPD profile suggested acidity of the catalysts increased up to 5 wt.% Cu loading followed by decreased. Catalytic results suggested that, in presence of 5 wt.% Cu/SBA-15 catalyst, maximum 90% conversion with 84% selectivity towards 1,2-PDO was obtained at 220 ^{o}C when 20 wt.% glycerol was used as feed mixture. This result was correlated with the highly dispersed CuO species and with higher acidity.

A study has been carried out to investigate the deactivation behaviour of Cu-ZnO catalyst for the selective production of 1,2-PDO from glycerol by the hydrogenolysis reaction [Du et al., (2016)]. The activity of Cu-ZnO catalyst synthesized by co-precipitation method was evaluated in a liquid phase autoclave reactor up to cycle-8 at 220 ^{o}C and at 5 MPa of H_2 pressure. Results showed that glycerol conversion was decreased by 56.7%, whereas the selectivity towards 1,2-PDO was almost stable even after the 8th cycle. The used catalyst was characterized by N_2-adsorption-desorption isotherm, XRD, NH_3-TPD, H_2-TPD, FE-SEM, EDS,

HRTEM, N_2O-chemisorption, XPS and ICP, respectively. After successive reuse, the lowering of surface area, porosity, acidity, H_2-uptake capacity, dispersion, aggregation of Cu and ZnO crystals were identified as the primary reasons for catalyst deactivation. XPS analysis showed that copper contents were decreased from ~13% to ~3% after 8th cycle. However, leaching of copper was not observed which was confirmed by XPS analysis.

The deactivation behaviour of Cu-Zn based catalysts were studied by Duran-Martin et al., (2017). This group synthesized Cu-Zn bimetallic catalyst with different Cu:Zn ratio (1, 2.5 and 6) by co-precipitation method and their performance were evaluated in a 100 ml autoclave reactor. The bimetallic catalysts were reused several times and their activities were reported. Maximum 16.2% glycerol conversion with 60.2% selectivity towards 1,2-PDO was observed at 200 ^{o}C, 2.4 MPa pressure, in presence of 0.4 g of 1CuZn catalyst. 80 wt.% glycerol aqueous solution was used as feed. 1CuZn exhibited almost similar glycerol conversion after 1st use (16.2%), however, activity was decreased gradually and showed ~5.2% conversion after 5th cycle. The used catalysts were characterized by XRD, TEM-analysis, XPS etc. The reason behind the deactivation behaviour of the catalyst was sintering of copper metal which was facilitated by leaching of Zn metal into the reaction mixture.

The performance of a series of Cu/oxide (SiO_2, MgO, Al_2O_3, ZnO) catalysts prepared by co-precipitation method was evaluated by Zhou et al., (2017). Glycerol hydrogenolysis reactions were performed in an autoclave reactor in absence of hydrogen or any other external gas. Various techniques such as XRD, CO_2-TPD, TEM, and XPS were used to characterize the catalysts. CO_2-TPD results dictated that basic sites strength of MgO and ZnO supported catalyst were higher as compared to SiO_2 and Al_2O_3 supported catalyst. Among all the catalysts tested, Cu/MgO catalyst showed the highest glycerol conversion of 55% with 68% selectivity towards 1,2-PDO at 473 K after a reaction time of 6 h. Reusability study showed that glycerol conversion was decreased by ~ 50 % after 2nd use. The reused catalyst was characterized by TEM, XPS and XRD analyses to identify the primary cause of deactivation of the catalyst. Characterization study of used catalyst revealed the aggregation of the copper particles on MgO support after reuse. In addition to that, ICP-OES analysis confirmed ~ 31.3% metal leaching after 2nd cycle. Further, the effect of solvent studies (methanol, isopropanol, ethanol, formic acid) was carried out with fresh and reused Cu/MgO catalyst. It was reported that methanol was the most effective solvent for hydrothermal hydrogenolysis reaction. Fresh Cu/MgO catalyst showed 72% conversion with ~38% selectivity towards 1,2-PDO in presence of methanol as a solvent, whereas 79% conversion with ~68% 1,2-PDO selectivity was achieved in presence of

used catalyst. It was elucidated that methanol reforming was beneficial due to more number of hydrogen production as compared to other solvents used.

Mitta et al., (2018) synthesized a series of Y-zeolite supported Cu metal (3-15%) catalysts and their catalytic activity was tested in a fixed bed reactor at 0.2 MPa pressure. Among all the catalysts developed, 3 wt.% CuO/Y-zeolite exhibited the highest catalytic activity and selectivity towards 1,2-PDO. Experimental results were in good agreement with the characterization results reported. Higher catalytic activity of 3 wt.% CuO/Y-zeolite catalyst was correlated with the higher BET surface area (580 $m^2.g^{-1}$), higher pore diameter (0.129 $cc.g^{-1}$), higher lewis acidic sites (480 $\mu mol.g^{-1}$) along with total acidic sites (512 $\mu mol.g^{-1}$), higher total basic sites (773 $\mu mol.g^{-1}$), high dispersion (58%), smaller Cu particle size (2.1 nm), small crystallite size (2.8 nm) and higher metal surface area (480 $m^2.g^{-1}$). Further, the effects of reaction parameters i.e. temperature, glycerol to hydrogen feed ratio and H_2 flow rate were investigated in presence of 3 wt.% CuO/Y-zeolite catalyst. It was observed that 92% conversion with 82% selectivity towards 1,2-PDO was achieved at 210 °C, at 0.2 MPa of H_2 pressure. Time on stream study was performed up to 20 h to verify the stability of the catalyst. It was observed that catalyst was highly stable up to 11 h. After 20 h of reaction, 20% conversion of glycerol along with 50% selectivity towards 1,2-PDO was obtained. Characterization study revealed that deactivation of catalyst was due to the sintering and agglomeration of Cu particle, which decreased the acidic sites significantly.

Recently, Li et al., (2019) synthesized copper metal catalyst supported on hierarchically structured M-SAPO-11 zeolite and its performance was compared with conventional zeolites such as SAPO-11, M-Hbeta, and M-HZSM-5. It was found that Cu/M-SAPO-11 catalyst exhibited higher glycerol conversion (~80%) with very high selectivity (~78%) towards 1,2-PDO as compared to the other catalysts at 240 °C and at 4 MPa pressure in presence of 8 wt.% glycerol as feed. It was observed that mesopores nature of M-SAPO-11 zeolite helped to reduce the diffusional barrier of reagents which reduced mass transfer resistance significantly. It was also found that the presence of medium strength acidic sites in M-SAPO-11 zeolite increased the selectivity to 1,2-PDO. Cu on M-Hbeta and M-HZSM-5 catalysts showed lower selectivity towards 1,2-PDO due to overhydrogenolysis of 1,2-PDO to propanol. Presence of higher number of strong strength acidic sites in conventional zeolites were solely responsible for overhydrogenolysis of 1,2-PDO to other degradation products. Further, incorporation of an appropriate amount of nickel metal to Cu/M-SAPO-11 catalyst (Cu_2Ni/M-SAPO-11) increased its performance remarkably and showed ~93% conversion of glycerol with 97.7% selectivity

towards 1,2-PDO due to the formation of Cu-Ni alloy. TEM images of the catalysts revealed that after the addition of nickel to Cu/M-SAPO-11 catalyst, average particle size was decreased. This result suggested that Ni enhanced the dispersion of Cu metals which promoted the cleavage of more number of C-O bond and suppressed the cracking of C-C bond. Reusability study of Cu_2Ni/M-SAPO-11 catalyst suggested that 90.2% glycerol conversion with 96.5% selectivity towards 1,2-PDO was achieved after 4^{th} successive use.

Few studies focused on the evaluation of the performance of Co-based catalyst. Co/MgO catalyst gave highest glycerol conversion (44% conversion) alongwith 42% selectivity towards 1,2-PDO at 200 °C and at 2 MPa H_2 pressure [Guo et al., (2009)]. Calcination temperature of the catalysts, basic sites of MgO, crystallite size played an important role in the catalytic activity. It was also observed that hydration of MgO to $Mg(OH)_2$ during the reaction caused the aggregation of cobalt particle which led to the deactivation of the catalyst.

2.2.2 Non-noble metal based bimetallic catalysts

Apart from monometallic catalysts, bimetallic non-noble metal based cataysts were also developed to increase the activity of the catalyst.

In order to produce both 1,2-PDO as well as 1,3-PDO, Niu et al., (2013) prepared a series of acid-base bi-functional catalysts Cu(x)-MgO(y) supported on ultra-stable Y type zeolite (USY) for hydrogenolysis reaction. Copper metal was used due to its inherent ability to cleave the C-O bond without affecting C-C bond. USY was introduced to provide acidic sites into the catalyst for the production of 1,3- PDO. Use of an appropriate amount of Cu and MgO improved conversion and also selectivity towards 1,2-PDO. Maximum 83.7% conversion was obtained with 40% selectivity towards 1,2-PDO and 19.4% selectivity to 1,3-PDO at 200 ºC, 3.5 MPa H_2 in presence of 6 wt.% 0.2Cu-MgO/USY catalyst loading. High copper metal dispersion (from TEM image), the strong interaction between MgO and USY was reported as the main reasons for better catalytic activity and 1,3-PDO selectivity.

Sharma et al., (2014) synthesized Cu:Cr (3:1) catalyst which was further modified by the addition of Zn and Zr and their catalytic activity was evaluated in liquid phase in an autoclave reactor. It was revealed that after the inclusion of Zn and Zr to the Cu:Cr matrix, glycerol conversion and selectivity towards 1,2-PDO was increased from 40 to 100% and 60 to 97%, respectively. NH_3-TPD study revealed that after the addition of Zn and Zr to Cu:Cr matrix, the acidity of the catalyst was increased significantly. It was also observed that the addition of Zn and Zr also helped to increase copper metal dispersion on the catalyst. Zn

increased the catalytic activity due to its H_2-spillover effect. Reaction parameters were optimized by varying temperature, pressure, catalyst loading, and glycerol concentration. Cu:Zn:Cr:Zr (3:2:1:3) catalyst showed best performance (100% conversion and 97% selectivity towards 1,2-PDO) at 240 °C and at 4 MPa hydrogen pressure in presence of 80 wt.% aqueous glycerol solution as feed. Catalyst stability study revealed that the catalyst was moderately active and showed 86% conversion with 96% selectivity towards 1,2-PDO even after cycle five. Further, LHHW type model was proposed to understand the reaction mechanism for glycerol hydrogenolysis process over Cu:Zn:Cr:Zr (3:2:1:3) catalyst. The apparent activation energy for the formation of 1,2-PDO from glycerol was found to be 31.7 kcal/mol.

Further, Rekha et al., (2016) prepared a series of Cu-ZrO_2-MgO catalyst by varying composition of Cu and ZrO_2 and their performance was evaluated in liquid phase glycerol hydrogenolysis reaction. XRD, BET, CO_2-TPD, TPR, N_2O-chemisorption and XPS techniques were used to characterize the catalysts. Catalytic activity was correlated with the number of copper active sites and moderate basic strength of the catalysts. Among all the catalysts synthesized, 20%Cu-10%ZrO_2-MgO catalyst exhibited the highest catalytic activity. To optimize the reaction parameters, the effect of reaction temperature, glycerol concentration, hydrogen pressure and reaction time were studied in presence of 20%Cu-10%ZrO_2-MgO catalyst. Maximum 62% conversion with 97% selectivity towards 1,2-PDO was obtained at 180 ^oC temperature, 4.0 MPa H_2 after 8 h of reaction. 20 wt.% glycerol and 0.6 g of catalyst were reported as optimum. Further, power-law type kinetic model was proposed. Results suggested that apparent reaction order of 0.6955 with respect to glycerol and the order was 0.6069 with respect to hydrogen, respectively. The activation energy for this reaction over 20%Cu-10%ZrO_2-MgO catalyst was reported as 22.78 kJ/mol.

Huang et al., (2008) screened several catalysts on the basis of their performance in liquid phase reaction. Among various catalysts examined in the liquid phase, Ni/Al_2O_3 and Cu/ZnO/Al_2O_3 catalysts were selected for gas phase reaction in a fixed bed reactor. Ni/Al_2O_3 catalyst exhibited complete conversion with 31.0% selectivity towards 1,2-PDO and 30.1% selectivity to [CO + CH_4] at 210 ^oC temperature, at 0.1 MPa of pressure and in presence of the weight hourly space velocity (WHSV) of 0.18 h^{-1}. This result suggested that Ni/Al_2O_3 catalyst had more tendency to cleave C-C bond which increased the selectivity to gaseous products. However, Cu/ZnO/Al_2O_3 catalyst exhibited high catalytic activity, which showed ~100% conversion with 77.4% selectivity towards 1,2-PDO at 210 °C, atmospheric pressure and at the WHSV of 0.08h^{-1}. It was also proposed that hydroxyacetone was produced as an intermediate

product during glycerol hydrogenolysis to 1,2-PDO reaction. The thermodynamic analysis suggested that dehydration of glycerol to hydroxyacetone was thermodynamically favorable and hydrogenation of hydroxyacetone to 1,2-PDO formation was limited by thermodynamic equilibrium.

H-beta supported Zr based monometallic and bimetallic (Ni-Zr, Cu-Zr, and Zn-Zr) catalysts were synthesized by wetness impregnation method [Kant et al., (2017)]. Bi-functional properties due to the presence of brönsted and lewis acid sites on the catalysts were reported to be the key factors for higher catalytic activity and diol selectivity. Catalytic activity results suggested that, with increasing of Zr metal loading in Zr/H-beta catalyst, moderate acidic strength of the catalyst was increased, which essentially increased the selectivity to lower alcohol at the expense of 1,3-PDO selectivity. This result depicted that, for the catalyst having higher acidic strength favoured over hydrogenolysis of 1,3-PDO to lower alcohols. Incorporation of 2nd metal in Zr/H-beta catalyst improved the catalytic activity and the selectivity towards 1,2-PDO and 1,3-PDO significantly. Higher activity of the bimetallic catalyst was because of the interaction of metals which led to increasing the total acidic strength of the catalysts. Among all of the catalysts, Ni-Zr/H-beta catalyst showed the highest activity. Further, reaction parameter optimization study was carried out to understand the influence of reaction temperature, H_2 pressure and reaction time on the catalytic activity and diol selectivity. Maximum 77% conversion with 14% selectivity to 1,3-PDO and 26% selectivity towards 1,2-PDO was observed at 200 ^oC, at 600 psi H_2 pressure. 50 wt.% glycerol solution and 0.5 g of catalyst were reported as the optimum values for higher 1,2-PDO selectivity.

Recently, a series of cerium promoted Cu/MgO catalyst was synthesized by co-precipitation method. Physico-chemical properties i.e. surface area, oxidation states, acidity and basicity of these catalysts were analysed by BET, TPR, NH_3-TPD, CO_2-TPD, XPS, XRD, and Raman spectroscopy [Mallesham et al., (2017)]. With increasing the Ce loading into the Cu/MgO catalyst, BET surface area was found to be increased up to Cu/Ce3/Mg. H_2-TPR results revealed that the addition of Ce to Cu/MgO catalyst lowered the reduction temperature of CuO. Among all the catalysts, Cu/Ce3/Mg exhibited a low-temperature peak around 127 ^oC, which ascribed the strong interaction of CuO species with CeO_2 and MgO. NH_3-TPD study revealed that Cu/Ce3/Mg catalyst showed the highest acidic strength (521 $\mu mol.g^{-1}$) among all other catalysts and Cu/Ce3/Mg catalyst showed smaller CuO crystallite size which suggested the well-dispersion of CuO species on the catalyst surface. XPS spectra demonstrated the

presence of more number of Ce^{+3} ions in the Cu/Ce3/Mg catalyst. Raman spectra proclaimed that Cu/Ce3/Mg catalyst showed a maximum number of oxygen defects, which might be the vital reason for the reduction of more number of Ce^{+4} ions to Ce^{+3} ions. Glycerol hydrogenolysis activity of the catalysts was evaluated in liquid phase and Cu/Ce3/Mg catalyst exhibited the maximum glycerol conversion of 56.4% with 97.4% selectivity towards 1,2-PDO at 200 ºC, 6 MPa pressure after 10 h of reaction time. Reusability test of the catalyst depicted that glycerol conversion was decreased by 31.4% with almost constant 1,2-PDO selectivity (97.4%) after 4^{th} cycle.

It can be concluded that among non-noble metals Cu based catalysts are highly active and selective to 1,2-PDO compared to Co and Ni based catalysts. Ni based catalysts have more tendency to break C-C bond cleavage which increases selectivity to lower alcohols. It was also observed that bimetallic catalysts were more active compared to monometallic catalysts due to synergic metal support interaction. Cu supported on acidic (γ-Al_2O_3) or basic carrier (MgO, ZnO) are highly promising for glycerol hydrogenolysis reaction. Incorporation of ZnO to Cu based catalysts enhances the catalytic activity of Cu due to its hydrogen spillover effect. Moreover, appropriate amount of acidic and/or basic sites, highly dispersed Cu^0, small particle size, small crystallite size are highly desirable for higher catalytic activity, selectivity to 1,2-PDO and stability of the catalysts.

2.3 Glycerol hydrogenolysis to 1,2-PDO over hydrotalcite-type catalysts

Recently, hydrotalcite-type layered double hydroxides (LDHs) catalysts have received considerable attention in heterogeneous catalysts due to their unique structure [Xia et al., (2012a), Yang et al., (2004)]. Hydrotalcite compounds are layered double hydroxide (LDH), consists of negatively charged anions intercalated between the positively charged hydroxide layers combined with H_2O molecule. The empirical formula of LDH catalyst is $[M^{II}_{1-x}\ M^{III}_{x}(OH)_2]^{x+}[A^{n-}_{x/n}]^{x-}.m\ H_2O$ where x is the ratio of $M^{III}/[M^{III} + M^{II}]$ (range is 0.20 to 0.40). M^{II} is divalent metals (Cu, Zr, Zn, Ti, and Ni) and M^{III} is trivalent metals (Al, Cr and Ga). A^{n-} is anion charged compounds (CO_3^{2-}, Cl^-, SO_4^{2-} and NO_3^-) and m is the molar amount of water between hydroxide layer [Xia et al., (2012a)]. The usages of LDHs catalyst is very promising for a reaction where multi-functionality of the catalyst is desirable to improve the selectivity of the desired product. The report based on the performance of LDHs type catalyst for hydrogenolysis of glycerol to 1,2-PDO is only a few [Xia et al., (2012a), Xia et al., (2012b), Yang et al., (2004), Xia et al., (2013), Yuan et al., (2011), Meher et al., (2009)].

The performance of Cu/Zn/Al mixed metal oxides based hydrotalcite catalyst was evaluated and maximum 52% conversion with 94% selectivity towards 1,2-PDO was achieved in presence of Cu/Zn/Al (1:1:4) mixed metal oxides based hydrotalcite catalyst at 200 ^{o}C and at 1.4 MPa of H_2 pressure [Meher et al., (2009)]. It is also reported that the acidic and basic properties of the catalysts were significantly affected with the variation of metal compositions (M^{II}/M^{III}) in the catalysts [Meher et al., (2009)].

Xia et al., (2012a) developed various layered double hydroxide based catalysts and their performance was evaluated for glycerol hydrogenolysis in liquid phase. It is reported that different primary alcohols such as methanol, ethanol, 1-propanol, butanol, and isopropanol as a hydrogen donor were very effective for selective conversion of glycerol to 1,2-PDO. Among all these primary alcohols, ethanol is suggested as the best hydrogen donor, and maximum 95% conversion with 92.2% selectivity towards 1,2-PDO was achieved over $Cu_{0.4}Mg_{6.28}Al_{1.32}O_{8.26}$ catalysts at 210 ^{o}C and at 3 MPa nitrogen pressure in presence of ethanol as a hydrogen donor. Later this group [Xia et al., (2012b)] prepared a series of $Cu_{0.4}/Zn_{5.6-x}Mg_xAl_2O_{8.6}$ catalysts derived from layered double hydroxide precursors. It was found that after the addition of Zn to $Cu_{0.4}Mg_{5.6}Al_2O_9$ catalyst, surface area and pore size of the catalysts were decreased gradually. N_2O adsorption data revealed that copper metal dispersion was increased with the addition of Zn up to $Cu_{0.4}Zn_{0.6}Mg_{5.0}Al_2O_9$ composition of catalyst and further it was decreased. The smallest copper particle size of 2.02 nm was detected for $Cu_{0.4}Zn_{0.6}Mg_{5.0}Al_2O_9$ catalyst. NH_3-TPD and CO_2-TPD study demonstrated that $Cu_{0.4}/Zn_{5.6}Al_2O_{8.6}$ catalyst exhibited highest acidic strength, whereas, $Cu_{0.4}/Mg_{5.6}Al_2O_{8.6}$ catalyst showed highest basic strength. H_2-TPR result showed that with increasing the Zn amount in the catalysts, new reducible CuO sites were evolved due to hydrogen spillover effect between Cu and ZnO. To ensure the spillover effect, H_2-TPD analysis of reduced catalyst was carried out. With increasing Zn content in the catalysts, two types of H_2-desorption peaks were observed. Peaks detected in the temperature range of 80–170°C was because of desorption from ZnO sites and peaks in the temperature range of 240–360°C was due to the desorption from copper particle sites. Catalytic activity result suggested maximum 78.2% glycerol conversion and 99.3% selectivity towards 1,2-PDO over $Cu_{0.4}Zn_{0.6}Mg_{5.0}Al_2O_9$ catalyst at 180 °C, and at 2.0 MPa H_2 pressure after 10 h of reaction. The highest catalytic activity of $Cu_{0.4}Zn_{0.6}Mg_{5.0}Al_2O_9$ catalyst was reported due to the optimum basic strength of the catalyst and H_2 spillover effect of ZnO, small Cu particle size (~2.02 nm) and higher copper metal dispersion (49.4 ± 6%). This group also prepared a series of hydrotalcite catalyst having different (Cu+Mg)/Al ratio and $Cu_{0.4}Mg_{5.6}Al_2O_{8.6}$ catalyst showed

good catalytic activity as compared to the remaining series of Cu/Mg/Al catalysts [Xia et al., (2013)].

A series of double layered base $Cu_x/Mg_{6-x}Al_2O_{9-x}$ catalysts were developed via co-precipitation, impregnation and ion exchange method, respectively [Yuan et al., 2011]. N_2-adsorption study revealed that with increasing copper content, surface area and pore volume of the catalysts were decreased. This was because of uniformity of crystallites were decreased with increasing of Cu content in the catalyst. XRD-pattern of calcined catalysts showed that only $Cu_{0.4}/Mg_{5.6}$ $Al_2O_{8.6}$ catalyst had lamellar-like structure after calcination and this lamellar-like structure was collapsed at higher Cu^{+2}/Mg^{+2} ratio because of agglomeration of CuO particle. H_2 TPR profile of $Cu_{0.4}/Mg_{5.6}Al_2O_{8.6}$ catalyst showed only one reduction peak at 150-260 °C region which ascribed the presence of Cu^{+2} species in the lamellar-like structure. However, with increasing Cu^{+2}/Mg^{+2} ratio, two H_2 consumption peaks were detected. This result indicated the presence of reducible Cu^{+2} species in the lamellar-like structure as well as the bulk Cu^{+2} species outside the lamellar surface. N_2O chemisorption study suggested that very high dispersion (~80 %) and copper surface area (1083 $m^2.g^{-1}$) of $Cu_{0.4}/Mg_{5.6}Al_2O_{8.6}$ catalyst. CO_2-TPD study showed that the basic strength of the catalysts was increased with decreasing Cu^{+2}/Mg^{+2} ratio. $Cu_{0.4}/Mg_{5.6}$ $Al_2O_{8.6}$ catalyst showed the highest glycerol conversion of 80% with 98.2% selectivity towards 1,2-PDO at 180 °C and at 3.0 MPa H_2 pressure after 20 h of reaction. 75 wt.% aqueous glycerol solution was used as feed. Further, it was found that the addition of small amounts of NaOH in the reaction mixture was beneficial for glycerol conversion without significant loss of selectivity towards 1,2-PDO. However, catalyst stability and reusability were not reported in this study.

Kolena et al., (2018) developed various Cu-Zn-Al based hydrotalcite catalysts by co-precipitation method and catalysts were calcined at different temperatures (350-700 °C) followed by the reduction at their respective reduction temperature. TEM images of the catalysts revealed that at lower calcination temperature (350 °C), particle sizes were in the range of 10-50 nm, whereas, the particle sizes were increased significantly (100-400 nm) at higher calcination temperatures (> 450 °C). Glycerol hydrogenolysis results suggested that catalyst calcined at 350 °C showed the best catalytic performance which showed 82.6% selectivity towards 1,2-PDO at 83% conversion of glycerol. Lower activity of catalysts calcined at higher temperature attributed to the agglomeration of particles, lower surface area, pore volume and disintegration of structure. Further, the same catalyst (Cu-Zn-Al catalyst) was developed by one step activation process. In this process, the dried hydrotalcite catalyst was

directly reduced in an autoclave reactor at 350 °C and at 7 MPa pressure and the catalytic activity was investigated at similar reaction condition. Results showed that both the catalysts exhibited similar activity (~80% conversion). However, selectivity to 1,2-PDO increased significantly (~93.1%) when catalyst was developed by one step activation process.

Co-Zn-Al layered double hydroxide, a efficient and stable catalyst as compared to Co-based monometallic catalyst was developed [GuO et al., (2011)]. Co-Zn-Al LDHs catalysts reduced at 673 K and 873 K, were synthesized and designated as Co-Zn-Al-673 and Co-Zn-Al-873, respectively. Maximum 70% conversion with 57.8% selectivity towards 1,2-PDO was achieved over Co-Zn-Al-873 catalyst at 200 °C and at 2 MPa H_2 pressure. Co-Zn-Al-873 catalyst containing smaller Co particle size (~16 nm) showed higher catalytic activity as compared to Co-Zn-Al-673 catalyst having large Co particle size (~50 nm).

Overall, Cu based layered double hydroxide catalysts are highly promising for selective production of 1,2-PDO from glycerol at mild reaction condition. Higher metal dispersion, higher surface area are the key factors for higher selectivity to 1,2-PDO in presence of Cu based LDHs catalysts.

2.4 Kinetic study

Very limited literature information is available on the kinetic studies of glycerol hydrogenolysis.

Lahr and Shanks (2003) developed Langmuir-Hinshelwood type kinetic model for glycerol hydrogenolysis reaction in presence of Ru/C catalysts. The reaction was performed in a batch reactor at two pH levels to obtain kinetic data. In the model development, competitive adsorption of three compounds i.e. glycerol, ethylene glycol, and propylene glycol were taken into account. H_2 was considered as in excess in the reaction mixture. The final rate equation was developed as follows:

$$-r_G = \frac{k_G' C_G^{1.5}}{1 + k_G C_G + k_{PG} C_{PG} + k_{EG} C_{EG}} \qquad (2.1)$$

where, k_G' is the reaction rate constant and k_G, k_{PG}, k_{EG} are the adsorption constants of glycerol, propylene glycol, and ethylene glycol, respectively. The degradation rate of glycols at different pH were determined from the model which helped to comprehend the instantaneous selectivity toward both glycols at different pH of the solution. The values of glycerol rate constant (k_G) and glycerol adsorption constant (k_G') were 50 L.mol^{-1} and 0.57 L$^{3/2}$/min.(kg of catalyst).mol$^{1/2}$,

respectively, with an R^2 value of 0.88. Results suggested that propylene glycol selectivity was not affected with pH of the solution, whereas, the selectivity to ethylene glycol was decreased with increasing the pH of the reaction mixture. Competitive adsorption suggested that affinity of propylene glycol towards the catalyst active sites was lower as compared to glycerol and ethylene glycol. The affinity of glycerol to the catalyst surface was twice than the ethylene glycol. These phenomena gave an overall reaction pathway for glycerol hydrogenolysis reaction. In this study, the effect of temperature on reaction rate was not considered in the model.

Torres et al., (2010) studied aqueous phase hydrogenolysis of glycerol to 1,2-PDO in a slurry reactor in the temperature and pressure range of 220 -240 ºC and 2.4-9.6 MPa H_2 pressure, respectively, in presence of bimetallic Ru-Re/C catalyst. The bimetallic catalyst showed the highest conversion of 57.7% with 36.6% selectivity towards 1,2-PDO. Monometallic Ru based catalyst showed a 52.1% conversion with 18.9% selectivity towards 1,2-PDO whereas monometallic Re catalyst was not at all active. To develop the kinetic model, experiments were performed at the different reaction temperature, pressure and catalyst loading. In this study, both liquid and gaseous products were considered for the development of kinetic model. A simple power-law type kinetic model was proposed for the hydrogenation of glycerol to 1,2-PDO due to the complexity of the reaction scheme. The rate equations were defined as follows:

$$-r_G = wC_G \frac{(C_{H_2})_g}{H_{H_2}} \left[k_1 + k_2 + \frac{H_{H_2}}{(C_{H_2})_g} k_5 \right] \tag{2.2}$$

The obtained rate equations were solved by using Rosenbrock algorithm in MATLAB coupled with Levenberg-Marquardt method. According to the kinetic model, predicted data showed in good agreement with the experimental data in terms of goodness of fit and activation energy parameters. The calculated activation energy for the formation of 1,2-PDO and EG were 54.2 and 63.8 kJ/mol, respectively.

Xi et al., (2010) presented a three-step model of glycerol dehydrogenation-dehydration-hydrogenation for the production of 1,2-PDO in a trickle-bed reactor. The rate equation (2.3) was solved by Euler's method in MATLAB.

$$-r_G = \frac{k_G K_G C_{OH^-} C_{H_2}^2}{1 + C_G C_{OH^-} + C_{H_2}^3} \tag{2.3}$$

The result showed that the developed kinetic model was fitted well with the experimental data. Pre-exponential factor, activation energy and adsorption constant were reported as 8.2×10^{10}, 86 kJ/mol, 4.6×10^{4} m^3/kmol, respectively.

Zhou et al., (2010) prepared a series of Cu-ZnO-Al_2O_3 catalyst by co-precipitation method and the maximum 93.5% selectivity towards 1,2-PDO at 81.5% glycerol conversion was obtained over Cu-ZnO-Al_2O_3 catalyst with 1:1:0.5 molar ratio. Kinetic studies were conducted in a fixed-bed reactor over Cu-ZnO-Al_2O_3 catalyst at reaction temperature varying from 493-513 K and at H_2 pressure varying from 3.0-5.0 MPa. A two-site Langmuir-Hinshelwood type model was proposed based on two steps (dehydration-hydrogenation) mechanism. The rate equation was as follows:

$$-r_G = \frac{k_G K_G C_G}{1 + K_G C_G + K_A C_A + K_P C_P} \tag{2.4}$$

where C_G, C_P, C_A are the concentrations of glycerol, 1,2-PDO and hydroxyacetone, respectively. Competitive adsorption of glycerol, hydroxyacetone, and propylene glycol were assumed. Results showed that the predicted concentration data were in a good match with the experimental data with the relative error of 6.3% for glycerol and 7.6% propylene glycol, respectively. The kinetic and adsorption factors were calculated by using 4th order Runge-Kutta method coupled with Rosenbrock algorithm. The activation energies obtained for dehydration to hydroxyacetone and hydrogenation to 1,2-PDO were 86.56 and 57.80 kJ·mol^{-1}, respectively. This result suggested that the first step dehydration to hydroxyacetone was slower than the second step hydrogenation of hydroxyacetone to 1,2-propanediol.

Vasiliadou and Lemonidou (2013) carried out a kinetic study over Cu/SiO_2 catalyst in an autoclave reactor in the temperature range of 180-240 °C and the pressure range of 2-8 MPa. A simple reaction scheme of two parallel routes leading to the formation of 1,2-PDO and 1,3-PDO was considered to develop the kinetic model. The kinetic parameters were calculated by assuming a Power-law type kinetic model. In this study, the overall reaction rate exhibited an almost zero order with respect to initial glycerol concentration and ~1st order with respect to H_2 in liquid phase. The production rate of 1,2-PDO was not affected by the initial glycerol concentration, however, it was strongly depended (almost first order) on H_2 concentration. Furthermore, the formation rate of 1,3-PDO was strongly dependent on glycerol concentration and to nearly first order on H_2 concentration. The activation energies obtained for the overall reaction (96.8 kJ/mol), 1,2-PDO (94.3 kJ/mol) and 1,3-PDO (135.3 kJ/mol) formation

demonstrated the selective formation of the 1,2-PDO at lower temperatures. Recently, this group [Yfanti et al., (2018)] has developed a Langmuir-Hinshelwood type kinetic model for glycerol hydrogenolysis reaction by using methanol as a hydrogen donor in presence of a Cu:Zn:Al catalyst. For the development of a kinetic model, four reaction steps including aqueous phase reforming (APR) of methanol for the production of hydrogen, dehydration of glycerol to hydroxyacetone, hydrogenation of hydroxyacetone to 1,2-PDO and glycerol hydrogenolysis for the formation of ethylene glycol, respectively, were considered. Kinetic experiments were carried out at different reaction temperatures (200-270 ^{o}C) and at different reaction times (0-75 min). The obtained activation energies for dehydration of glycerol to hydroxyacetone and hydrogenation of hydroxyacetone to 1,2-PDO were estimated to be 87 kJ/mol and 68.4 kJ/mol, respectively. Further, the kinetic models were validated with the experimental runs collected at different initial glycerol concentration (1-5 wt.%) and different methanol concentration (7-30 wt.%).

Gandarias et al., (2013) performed glycerol hydrogenolysis reaction over 17Ni–13Cu/Al_2O_3 catalyst using formic acid as a hydrogen donor. In this study, Langmuir-Hinshelwood type kinetic model was developed where a series reaction scheme of glycerol to 1,2-PDO and hydrogenolysis of 1,2-PDO to 1-propanol (1-PO) were considered. Competitive adsorption between glycerol and 1,2-PDO was proposed in the reaction model. It is concluded that initial conversion of glycerol to 1,2-PDO was higher than the decomposition of formic acid which indicated that initially, H^+ was generated from aqueous phase reforming of glycerol or any other source. At higher glycerol conversion, the H^+ ions generated from formic acid were captured by 1,2-PDO and was not transferred to glycerol. These H^+ ions finally were converted to molecular H_2 which eventually escaped in the gas phase. Briefly, to achieve higher hydrogen donor efficiency and to avoid further degradation of 1,2-PDO to 1-PO, optimum glycerol conversion was required. The major drawback of this study was that the effect of reaction temperature was not taken into account.

Sharma et al., (2014) proposed Langmuir-Hinshelwood-Hougen-Watson type kinetic model over Cu:Zn:Cr:Zr (3:2:1:3) mixed metal catalyst. The obtained overall rate equation was

$$-r_G = \frac{k_3 C_{t,s}^2 K_1 K_2 C_G P_H}{(1 + K_1 C_G + K_2 P_H + (C_P / K_4) + (C_W / K_5))^2} \qquad (2.5)$$

In the kinetic model, only 1,2-PDO was considered as a product and the inhibition terms were neglected. As a consequence, the kinetic model was reduced to a simple power-law kinetic model as follows:

$$-r_G = k_{SR} C_G P_H \tag{2.6}$$

It was concluded that the reaction was followed pseudo 1st order kinetics relating to glycerol and the apparent activation energy was estimated as 132 kJ.mol^{-1}.

Rajkhowa et al., (2017) carried out the kinetic experiments for hydrogenolysis of glycerol reaction in a trickle-bed reactor at the temperature and pressure range of 190-240 ºC and 6.5-8 MPa, respectively. The spacetimes were varied from 25 to 340 kg s mol^{-1}. It was proposed that glycerol was dehydrated to hydroxyacetone predominantly and subsequently hydrogenated to 1,2-PDO. In addition, 1,3-propanediol and ethylene glycol were also formed as side products. The degradation of 1,2-PDO to lower alcohols such as ethanol, methanol, and propanol were also reported. In the proposed kinetic model, all the reaction products were considered. The activation energy for the dehydration of glycerol to hydroxyacetone and hydroxyacetone to 1,2-PDO were found to be 84 kJ.mol^{-1} and 59.3 kJ.mol^{-1}, respectively. It was elucidated that high selectivity towards 1,2-PDO was obtained because of the lower reaction rate of the parallel and side reactions and lower adsorption affinity of hydroxyacetone as compared to glycerol.

2.5 Knowledge gaps and hypothesis

Hydrogenolysis of glycerol to 1,2-PDO is a promising route for the value addition of excess amounts of glycerol obtained in the biodiesel industry. For successful commercialization of glycerol hydrogenolysis process, development of selective and stable catalysts is highly desirable. In the last two decades, various catalysts were developed and examined for liquid phase hydrogenolysis of glycerol. Noble metals have been reported as very active for this reaction. However, the primary drawback associated with the noble metals is that these metals facilitate the overhydrogenolysis process which produces more degradation products and noble metals are also very expensive. As a result, the development of highly active, selective, relatively cheaper and higher resistance to poisoning, non-noble metal-based catalysts are highly desirable. The heterogeneous catalysed glycerol hydrogenolysis process is not yet fully commercialized due to lower 1,2-PDO yield, adverse reaction condition, poor catalyst reusability, and catalyst leaching.

Regarding the catalyst development, previous literature information dictated that acidic and/or basic sites on the catalyst surface favour the dehydration of glycerol and the active metal sites are necessary for hydrogenation of glycerol dehydrated product to produce 1,2-PDO. High active metallic surface area, good dispersion of active metals onto the support, higher reducibility, small particle size are the important factors for higher catalytic activity and the selectivity towards 1,2-PDO. Morphology and structure of the catalysts also have significant roles on the catalytic activity and product selectivity. Among the various transition metal catalysts, Cu, Co based catalyst showed very decent performance for selective hydrogenolysis of glycerol to 1,2-PDO and Ni metal is known as for its hydrogenation ability. It was also observed from the literature that addition of Zn enhanced the activity as well as 1,2-PDO selectivity mainly for copper-based catalysts. Several previous reports dictated that ZnO can act as a reservoir for atomic hydrogen which enhances the hydrogen spillover, thereby increase the hydrogenation capability of the catalyst.

Several previous studies were focused on the development of catalysts and the optimization of reaction parameters to maximize the 1,2-PDO selectivity. However, a very less attention was paid to develop the kinetic model and the estimation of kinetic parameters for this industrially important reaction. The fundamental understanding of reaction kinetics, development of kinetic models and the estimation of kinetic parameters are very important to design a suitable reactor and process before commercialization. Therefore, more study is required regarding the development of new and efficient catalysts, kinetic models and the estimation of kinetic parameters for successful commercialization of glycerol hydrogenolysis process. The aim of this study was to develop a highly active, selective, stable and environment-friendly catalyst for selective conversion of bio-glycerol to 1,2-PDO at mild reaction condition. In this regard, bi-functional Cu-Mg-Al-O and Cu-Zn-Mg-Al-O catalysts derived from layered double hydroxide (LDHs) precursors, and a series of monometallic (Cu, Ni, Co, Zn and Fe), bimetallic catalysts supported on MgO, Al_2O_3, CaO, La_2O_3, MgO-La_2O_3 were developed for selective production of 1,2-PDO by the hydrogenolysis of glycerol in liquid phase in a slurry batch reactor. Different supports such as γ-Al_2O_3, MgO, CaO, La_2O_3 etc. were selected to incorporate the acidic and/or basic sites and metals (Cu, Zn, Co) were selected to incorporate the hydrogenation sites on the catalysts surface, respectively. Various kinetic models including power-law, modified power-law, Eley-Rideal (ER), Langmuir–Hinshelwood-Hougen-Watson (LHHW), and a new kinetic model based on in a combination of ER and LHHR approach were developed. The kinetic models were validated with the help of the

experimental data generated in presence of Cu:Ni(1:1)/γ-Al_2O_3, Cu:Zn(4:1)/MgO and Cu:Zn(4:1)/MgO-La_2O_3 catalyst, respectively. Finally, an economic analysis was performed for the overall glycerol hydrogenolysis process in presence of the best catalyst developed in this thesis. Economic analysis suggested that the production of 1,2-PDO from renewable glycerol is extremely profitable and it is very promising for commercial application.

2.6 Objectives

In this thesis work, the following objectives were set:

(i) Synthesis of following supported monometallic and bimetallic catalysts for liquid phase hydrogenolysis of glycerol.
20 wt.% Cu/γ-Al_2O_3, Ni/γ-Al_2O_3, Cu:Ni(1:1)/γ-Al_2O_3, 35 wt.% Cu/MgO, Zn/MgO, Co/MgO, Fe/MgO, Ni/MgO, 50 wt.% Cu:Fe(1:1)/MgO, Co:Fe(1:1)/MgO, Co:Zn(1:1)/MgO, Cu:Zn(1:1)/MgO, Cu:Zn(4:1)/MgO, Cu/MgO, Zn/MgO , 50 wt.% Cu:Zn(4:1)/BaO_2, Cu:Zn(4:1)/La_2O_3, Cu:Zn(4:1)/CaO, Cu/La_2O_3, Cu:Zn(4:1)/MgO-La_2O_3.

(ii) Characterization of the catalysts by several techniques such as
BET surface area, X-ray diffraction (XRD), temperature programmed reduction (TPR), NH_3-temperature programmed desorption (NH_3-TPD), CO_2-temperature programmed desorption (CO_2-TPD), transmission electron microscopy (TEM), field emission scanning electron microscopy (FE-SEM), X-ray photoelectron spectroscopy (XPS), atomic absorption spectroscopy (AAS) etc.

(iii) Performance evaluation of the synthesized catalysts in an autoclave reactor.
Study the effect of various reaction parameters such as reaction temperature, hydrogen pressure, glycerol to water ratio, reaction time and amount of catalyst on the glycerol conversion and 1,2-PDO selectivity/yield.

(iv) To investigate the stability and reusability of the catalysts.

(v) To develop a suitable kinetic model and the estimation of kinetic parameters for glycerol hydrogenolysis reaction in presence of Cu:Ni(1:1)/γ-Al_2O_3, Cu:Zn(4:1)/MgO and Cu:Zn(4:1)/MgO-La_2O_3 catalyst, respectively.

CHAPTER III

EXPERIMENTAL DETAILS

Previous literature suggested that for selective production of 1,2-PDO from glycerol hydrogenolysis reaction requires heterogeneous catalyst having bi-functional acidic-basic properties, small average particle size, higher reducibility, higher dispersion of active metals on the support. In this chapter, the synthesis of various catalysts and their characterization techniques are discussed. Details of the experimental set-up, experimental procedure, and the product analysis techniques are also described.

3.1 Catalyst Preparation

3.1.1 Materials

$Cu(NO_3)_2.3H_2O$ (>99%, Thomas baker, India), $Ni(NO_3)_2.6H_2O$ (>99.9%, Thomas Baker, India), $Co(NO_3)_2.6H_2O$ (>98%, Alfa Aesar India), $Zn(NO_3)_2.6H_2O$ (>99%, Thomas baker, India), $Fe(NO_3)_3.9H_2O$ (>99.9%, Merck specialities, India), $Mg(NO_3)_2.6H_2O$ (99.0%, Thomas Baker Chemicals, India), $Al(NO_3)_3.9H_2O$ (95%, Thomas Baker Chemicals, India) were used as metal precursors. Aluminium oxide (>99.9%, Thomas Baker, India), MgO light (Thomas Baker, India, 98%), CaO (>95%, Thomas Baker, India), BaO_2 (>90%, Thomas Baker, India) and La_2O_3 (>99.9%, Thomas Baker) were used as catalyst supports. $NaHCO_3$ (>99.8%, Thomas Baker, India) and urea (99.0%, Sisco Research Lab, India) were used as precipitating agents. Glycerol (>99.9%, Thomas baker, India), 1,2-PDO (>99%, Merck specialities, India), Hydroxyacetone (95%, Alfa Aesar, India), Ethylene glycol (>95%, Sigma Aldrich-Fluka, India) were used as feed and product calibration, respectively. The hydrogen (99.99%) and nitrogen (99.99%) were purchased from Sigma gases, India and used directly without any further purification.

3.1.2 Preparation of γ-Al_2O_3 supported catalysts

Copper (II) nitrate trihydrate, nickel (II) nitrate hexahydrate were used as metal precursors and aluminium oxide was used as catalyst support. 20 wt.% Cu/γ-Al_2O_3, 20 wt.% Ni/γ-Al_2O_3 and 20 wt.% Cu:Ni(1:1)/γ-Al_2O_3 catalysts were synthesized by wetness impregnation method. γ-Al_2O_3 was added to the aqueous solution of the calculated amount of metal precursors [$Cu(NO_3)_2.3H_2O$ and/or $Ni(NO_3)_2.6H_2O$]. The resulting slurry was stirred for 15 min and kept for aging for 12 h at 25-30 °C. Further, the resulting slurry was dried overnight in an oven at 110 ^oC followed by calcination at 400 ^oC for 4 h in presence of air. Prior to each

reaction, catalysts were reduced in ex-situ under the flow of H_2 for 3 h at their respective reduction temperatures obtained from TPR peak. 20 wt.% Cu:Ni(1:1)/γ-Al_2O_3 signified that unit mass of catalyst contained 80 wt.% of γ-Al_2O_3 and 20 wt.% of total Cu and Ni metals, where weight ratio of Cu/Ni =1.

3.1.3 Preparation of layered double hydroxides (LDHs) catalysts

$Cu(NO_3)_2.3H_2O$, $Zn(NO_3)_2.6H_2O$, $Mg(NO_3)_2.6H_2O$, $Al(NO_3)_3.9H_2O$ were used as metal precursors and urea was used as precipitating agent. Glycerol, 1,2-PDO, hydroxyacetone, ethylene glycol were used as feed and product calibration, respectively. The hydrogen and nitrogen were purchased from Sigma gases, India.

Table 3.1. Catalyst designation and their composition

Urea concentration (M)	Catalyst	Catalyst	Theoretical			
			Cu (wt.%)	ZnO (wt.%)	MgO (wt.%)	Al_2O_3 (wt.%)
1.5	$Cu_{0.40}Mg_{5.6}Al_2O_9$	Cu-Mg-Al-O-1	35	-	48.8	16.3
2	$Cu_{0.40}Mg_{5.6}Al_2O_9$	Cu-Mg-Al-O-2	35	-	48.8	16.3
2.5	$Cu_{0.40}Mg_{5.6}Al_2O_9$	Cu-Mg-Al-O-3	35	-	48.8	16.3
2	$Cu_{0.64}Mg_{5.37}Al_2O_9$	Cu-Mg-Al-O-4	45	-	38.8	16.3
2	$Cu_{0.45}Zn_{0.15}Mg_{5.4}Al_2O_9$	Cu-Zn-Mg-Al-O	35	15	33.8	16.3
2	$Zn_{0.15}Mg_{5.85}Al_2O_9$	Zn-Mg-Al-O	-	15	68.8	16.3

Layered double hydroxides **(**LDHs) Cu-Mg-Al-O and Cu-Zn-Mg-Al-O catalysts were synthesized by homogenous co-precipitation via urea hydrolysis method [Jingfa et al., (1996), Turco et al., (2004), Ogawa et al., (2002)]. An aqueous solution of the required amounts of metal precursors was mixed with the aqueous solution of urea and heated at 100 ^oC for 2 h in a three-necked round bottom flask equipped with a reflux and a magnetic stirrer. After two hours, the solution turned into a slurry and the resulting slurry was continuously refluxed at 100 ^oC for 12 h under stirring. Further, the obtained slurry was cooled to room temperature, filtered, and washed thoroughly with deionized water. The solid obtained was dried in an oven

at 110 ºC for 10 h followed by calcination at 400 ºC for 4 h in presence of air. Prior to each reaction, catalysts were reduced in ex-situ under the flow of H_2 for 3 h at their respective reduction temperature obtained from TPR peak. The catalysts were prepared in presence of three different urea concentration i,e. 1.5M, 2M, and 2.5M, respectively. The reaction mechanism of the formation of LDHs catalysts by following urea hydrolysis method is discussed elsewhere [Costantino et al., (2013), Basahel et al., (2014)]. Theoretical composition of the catalyst synthesized and their designations are shown in Table 3.1.

3.1.4 Preparation of MgO supported catalysts

$Cu(NO_3)_2.3H_2O$, $Co(NO_3)_2.6H_2O$, $Zn(NO_3)_2.6H_2O$, $Fe(NO_3)_3.9H_2O$ were used as metal precursors and MgO light was used as catalyst support. $NaHCO_3$ was used as a precipitating agent. Glycerol, 1,2-PDO, Hydroxyacetone, Ethylene glycol were used as feed and product calibration, respectively. The hydrogen (99.99%) and nitrogen (99.99%) were purchased from Sigma gases, India and used directly without any further purification.

MgO supported monometallic and bimetallic catalysts were prepared by precipitation-deposition method [Pudi et al., (2015a)]. Total metal loading in the final catalyst was kept constant at 50 wt.%. In a typical catalyst synthesis, an aqueous solution of $NaHCO_3$ (1 $mol.L^{-1}$) was added dropwise to the aqueous solution of the nitrate salts of metal precursors with an appropriate ratio with constant stirring until the pH of the solution was 8-9. After precipitation, the required amount of MgO light was added to the solution under vigorous stirring for 6 h followed by aging for 12 h at room temperature. The slurry obtained was filtered, washed thoroughly with deionized water and dried at 110 ºC for 12 h. The dried solid was calcined in air at 400 ºC for 4 h. Prior to each reaction, catalysts were reduced in ex-situ under the flow of H_2 for 3 h at their respective reduction temperature obtained from TPR peak. Catalysts prepared and their composition is shown in Table 3.2. The catalysts prepared by this method were designated as Cu/MgO, Zn/MgO, Cu:Zn(4:1)/MgO, Cu:Zn(1:1)/MgO, Cu:Fe(1:1)/MgO, Co:Fe(1:1)/MgO, Co:Zn(1:1)/MgO, respectively.

3.1.5 Preparation of different metal oxide supported Cu-Zn bimetallic catalysts

$Cu(NO_3)_2 \cdot 3H_2O$ and $Zn(NO_3)_2 \cdot 6H_2O$ were used as metal precursors. CaO, BaO_2 and La_2O_3 were used as supports without any further treatment. All the various metal oxide supported Cu-Zn bimetallic catalysts were prepared by precipitation- deposition method [Pudi et al., (2015a)]. Total metal loading in the final catalysts were kept constant at 50 wt.%. For catalyst synthesis, 0.1 M $NaHCO_3$ solution was added drop by drop to the aqueous solution of

nitrate precursors with continuous stirring until pH of the solution reached 8-9. Further, respective supports [CaO, BaO_2, La_2O_3, MgO:La_2O_3 (1:1)] were added to the aqueous solution under continuous stirring for 6 h. After that, the solution was kept for aging for 12 h at room temperature. The obtained precipitate was filtered under vacuum and washed thoroughly with distilled water to remove the Na^+ ion. The solid residue was dried in an oven at 110 ^oC for 24 h followed by calcination at 400 ^oC for 4 h in presence of air for the removal of nitrate (NO_3^-), bicarbonate (HCO_3^-) and hydroxyl (OH^-) ions present if any. Prior to each reaction, catalysts were reduced in ex-situ under the flow of H_2 for 3 h at their respective reduction temperature obtained from TPR peak. The final catalysts were designated as Cu-Zn(4:1)/CaO, Cu-Zn(4:1)/La_2O_3, Cu-Zn(4:1)/BaO_2, Cu-Zn(4:1)/MgO-La_2O_3, respectively. 50 wt.% Cu-Zn(4:1)/CaO, Cu-Zn(4:1)/La_2O_3, Cu-Zn(4:1)/BaO_2, Cu-Zn(4:1)/MgO-La_2O_3 signified that per unit mass of different supported catalysts contained 50 wt.% of supports [i.e. CaO, La_2O_3, BaO_2, MgO-La_2O_3 (1:1)] and 50 wt.% of total Cu and Zn metals, where weight ratio of Cu/Zn =1.

3.2 Catalyst characterization

The physico-chemical properties of the fresh and used catalysts were characterized by various techniques such as specific surface area (BET), X-ray powder diffraction (XRD), temperature programmed reduction (TPR), temperature programmed desorption (TPD), scanning electron microscope with energy-dispersive X-ray analysis (FESEM-EDX), transmission electron microscopy (TEM) and atomic absorption spectroscopy (AAS) etc.

Nitrogen adsorption-desorption isotherm was used to determine the specific surface area of the catalysts by using a Micromeritics Accelerated Surface Area and Porosimetry (ASAP 2020, USA) instrument at liquid nitrogen temperature (-196 ^oC). Prior to the adsorption process, the catalyst was degassed under vacuum for 4 h to remove the moisture from the catalyst sample. Specific surface area was determined by the multipoint Brunauer-Emmett-Teller (BET) method and Barret-Joyner-Halendra (BJH) method was used to measure the pore size distribution by considering the desorption branch.

X-ray diffraction patterns were collected on a Bruker AXS D8 advanced diffractometer coupled with Ni-filtered Cu-Kα radiation (40 KV, λ = 1.5418 ^oA). Data were recorded at the scanning range of 10-90^o with a ramp rate of 1^o min^{-1}. Expert-Pro software and Joint committee on powder diffraction standards (JCPDS) were used to identify the XRD peaks. The average crystallite sizes of the metal and/or oxides were determined by using the Scherrer's formula

from the line width of the XRD peaks corresponding to their respective crystal planes. Scherrer's equation: $D = 0.90\lambda/\beta \cos\theta$, where β is the full width at half-maximum (FWHM) and θ is the diffraction angle

The reduction behavior of the catalysts was determined on a Micromeritics Pulse Chemisorb 2720 equipment coupled with a thermal conductivity detector (TCD) to determine the amounts of hydrogen consumed. Prior to each experiment, 50 mg of calcined catalysts was degassed at 200 ^{o}C for 2 h under the flow of argon (20 cc.min^{-1}) followed by cooling at room temperature. Temperature programmed reduction (TPR) profile was monitored by heating the sample linearly at a rate of 10^{o} min^{-1} from room temperature to 800 ^{o}C under the flow of 10% H_2/Ar gas mixture (20 cc.min^{-1}).

NH_3-temperature programmed desorption (NH_3-TPD) was performed to measure the acidic property of the catalyst. NH_3-TPD analyses were performed on a Micrometrics Pulse Chemisorb 2720 equipped with a TCD. Before the analysis, catalyst was degassed at 200 ^{o}C for 2 h under the flow of helium (20 cc.min^{-1}) followed by cooling at 25-30 ^{o}C. After degassing, the sample was saturated with NH_3 under the flow of 27% NH_3/He (20 cc.min^{-1}) for 1 h and the sample was purged with helium for 1 h to remove the physically adsorbed ammonia. NH_3 desorption was monitored by heating the sample from 40 to 900 ^{o}C at a heating rate of 10 ^{o}C min^{-1}.

Surface morphology of the catalyst was determined by field emission scanning electron microscopy (FE-SEM) on a quanta scanning electron microscope (QUANTA, Model 200 FEG) coupled with energy dispersive X-ray (EDX). A small amount of sample was dispersed on the specimen stub and coated with gold using a sputter coater (Edward S150) under argon flow to avoid the charging of particles and analysis was performed at an accelerating voltage of 20 kV under vacuum.

Average particle size and distribution of the particles on the support were determined by transmission electron microscope (TEM) on a Tecnai G^2 20 S-Twin microscope attached with EDAX. A small amount of samples was dispersed in ethanol solution by ultrasonic and a few drops of the solution was placed in a carbon-coated copper grid.

Thermal stability of catalysts was investigated by differential thermal analysis (DTA) and thermo-gravimetric analysis (TGA) by using an EXSTAR TGA/DTA 6300 machine.

Table 3.2. Catalysts composition and their designation

Catalyst composition (theoretical)	Catalyst designation	Theoretical metal composition Metal 1: Metal 2 (wt.%)	Actual metal composition [a] (wt.%)
Pure MgO	MgO	-	-
50 wt.% Cu/MgO	Cu/MgO	50:0	49.7 : 0
50 wt.% Zn/MgO	Zn/MgO	0:50	0 : 48.7
50 wt.% [40 wt.% Cu:10 wt.% Zn]/MgO	Cu:Zn(4:1)/MgO	40:10	38.8 : 7.8
50 wt.% [25 wt.% Cu:25 wt.% Zn]/MgO	Cu:Zn(1:1)/MgO	25:25	25.6 : 20.7
50 wt.% [25 wt.% Cu: 25 wt.% Fe]/MgO	Cu:Fe(1:1)/MgO	25:25	25.9 : 26.5
50 wt.% [25 wt.% Co: 25 wt.% Fe]/MgO	Co:Fe(1:1)/MgO	25:25	21.3 : 20.2
50 wt.% [25 wt.% Co: 25 wt.% Zn]/MgO	Co:Zn(1:1)/MgO	25:25	24.0 : 24.5

[a] composition obtained from FESEM-EDX

in mass of the sample with temperature was recorded. Whereas, the temperature difference between sample and reference material were recorded in DTA.

The metal concentration in the fresh reduced and reused catalysts were determined by atomic absorption spectroscopy (AAS) in an AVANTA M, GBC scientific equipment. For the analysis, 20-30 mg of samples and 2 ml of aqua regia solution (HNO_3:HCl = 1:3) were taken in a 15 ml borosilicate glass vessel equipped with a Teflon lined cap and digested at 130 ^oC for 45 min. Prior to analysis, the solution was diluted up to the required concentration.

The metal concentrations in the fresh and spent catalysts were also determined by X-Ray Fluorescence (XRF) analysis on a Bruker S4 Poinner instrument. The working principle of XRF analysis is based on wavelength dispersive spectroscopy technique. In this analysis technique, the sample was excited initially with the primary X-ray source and the emitted X-ray was measured.

X-ray photoelectron spectra (XPS) were recorded on a PHI 5000 Versa Probe III to determine the oxidation states of the metal element. Monochromatic Al-Kα X-ray radiation source (hv = 1,486.6 eV) with 100 µm of spot size was operated in the constant pass energy mode at 23.50 eV. The analysis was carried out at room temperature under an ultra-high vacuum of 10^{-13} MPa for charge neutralization. All the spectra were collected with reference to C1s peak at 284.6 eV and with a step size of 0.025 eV.

3.3 Catalytic activity test

3.3.1 Experimental set-up and procedure

Hydrogenolysis of glycerol was performed in an autoclave reactor equipped with a 250 ml Teflon lined reaction vessel (Amar equipment, India, Model No. 2000), turbine impeller, temperature controller (PID), pressure indicator and a sampling port. The schematic diagram of the reactor set-up is shown in Figure 3.1. Prior to each experiment, fresh calcined catalyst was reduced ex-situ in a separate tubular flow reactor at their respective reduction temperature obtained from TPR analysis for 3 h under the flow (25-30 cc min^{-1}) of pure hydrogen. The catalysts were loaded into the reactor as synthesized without any pelletization. The average catalyst particle size were < 50 nm obtained from TEM analysis. After reduction, the catalyst was allowed to cool to room temperature under the flow of hydrogen. After cooling, reduced catalysts were immediately charged into the autoclave reactor. The time lag of shifting the reduced catalyst into the autoclave was <1 min. Therefore, it was assumed that the re-oxidation

of the catalyst within this short period of time at room temperature was almost negligible. Further, the required amount of reduced catalyst and 100 g of aqueous glycerol solution (20 wt.%) was taken into the autoclave reactor and then the reactor was purged several times with hydrogen to remove air inside the reactor and pressurized the reactor with hydrogen up to 3-6 MPa. Experiments were carried out at 170-220 ^{o}C under constant stirring speed at 800 rpm. After the reaction, the reactor was allowed to cool to 25-30 °C and the products were separated from the catalyst particle by centrifugation (Heraeus Biofuges Stratos, Thermo Scientific) if any. All the experiments were conducted atleast two times, in some cases multiple experiments were also carried out to verify the consistency of the results. Data reported in this thesis are the average values of the multiple experiments performed.

3.3.2 Product analysis

The products were analysed by gas chromatography (GC 6800, Newchrom Technologies, India). A chromosorb 101 packed column (1.52 m × 3.1 mm OD × 2 mm OD) attached with a flame ionization detector (FID) was used for the separation and the products were quantified by an internal standard process (Appendix I). In this study, n-butanol was used as an internal standard.

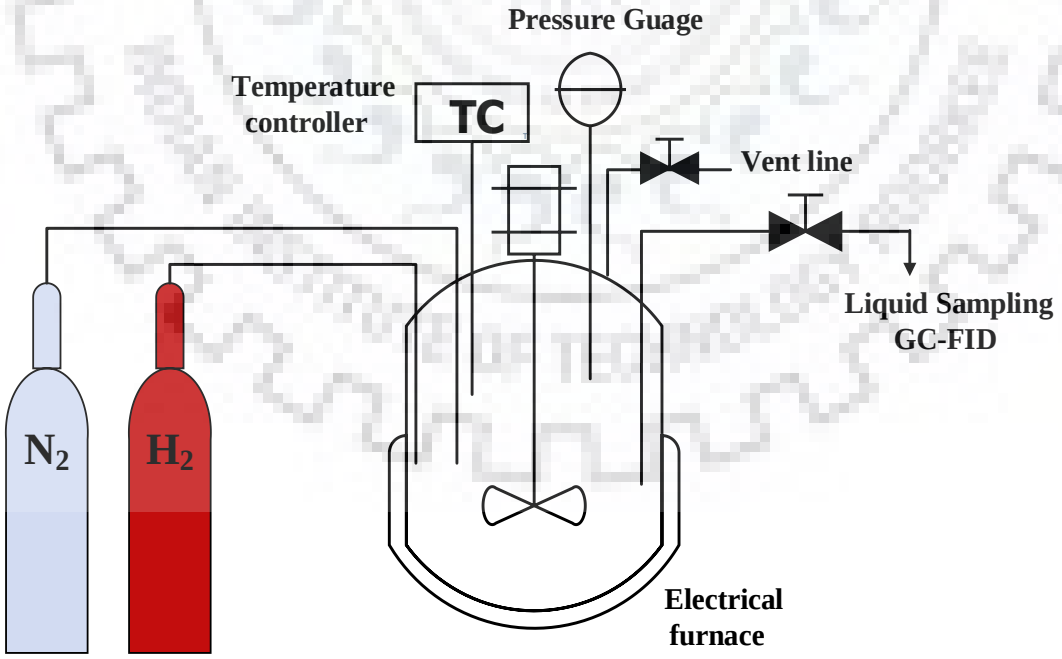

Figure 3.1. Schematic diagram of reactor set-up

Glycerol conversion, products selectivity, and yield were calculated as follows:

$$\text{Conversion}\,(\%) = \frac{\text{Moles of glycerol converted}}{\text{Total moles of glycerol in feed}} \times 100$$

$$\text{Selectivity}\,(\%) = \frac{\text{Moles of carbon in specific product}}{\text{Total carbon moles in all liquid products}} \times 100$$

$$\text{Yield}\,(\%) = \frac{\text{Conversion}\,(\%) \times \text{Selectivity}\,(\%)}{100}$$

CHAPTER IV

RESULTS AND DISCUSSION

This chapter describes the activity of γ-Al_2O_3 supported Cu, Ni mono-metallic and bi-metallic catalyst, Cu based hydrotalcite catalysts, MgO supported Cu, Co, Zn, Fe monometallic and bimetallic catalysts for selective glycerol hydrogenolysis to 1,2-PDO. The role of various supports i.e. CaO, BaO_2, La_2O_3 and MgO-La_2O_3 on the performance of Cu:Zn bi-metallic catalysts are also discussed. The physico-chemical properties such as oxidation state of Cu, presence of bi-metallic phase, bi-functional acidic/basic sites, H_2 spillover effect were explored and the correlation between the catalyst characterization results with the catalytic activity and product selectivity were also investigated. Various reaction parameters such as temperature, pressure, glycerol concentration, catalyst loading, reaction time were optimized to maximize the glycerol conversion and 1,2-PDO selectivity. The possible reaction pathway for the conversion of glycerol to 1,2-PDO was also investigated in presence of various catalysts. In addition, the catalyst stability and their reusability were verified and the obtained results were explained with the help of the used catalyst characterization results.

4.1 Selective hydrogenolysis of glycerol to 1,2-PDO over Cu/γ-Al_2O_3, Ni/γ-Al_2O_3 and Cu:Ni(1:1)/γ-Al_2O_3 catalysts

γ-Al_2O_3 supported Cu, Ni monometallic and Cu-Ni bi-metallic catalysts were synthesized by incipient wetness impregnation method. The catalysts were characterized by BET surface area measurement, X-ray diffraction study, NH_3-temperature programmed desorption, H_2-temperature programmed reduction etc. The hydrogenolysis activity of these catalysts was examined in a batch reactor. Activity data were correlated with the catalyst characterization results. In presence of γ-Al_2O_3 supported Cu and/or Ni, a possible reaction pathway was proposed.

4.1.1 Catalyst characterization

4.1.1.1 Textural properties

The BET surface area and pore volume of the catalysts determined from their N_2-adsorption-desorption isotherm are listed in Table 4.1. The BET surface area and pore volume were in the range of 71-78 m^2g^{-1}, and 0.12-0.15 $cm^3.g^{-1}$, respectively (Table 4.1). The obtained BET surface area of all the catalysts was followed the order as Cu:Ni(1:1)/γ-Al_2O_3 > Cu/γ-Al_2O_3 > Ni/γ-Al_2O_3.

Table 4.1. Physico-chemical property of catalysts

Catalyst	S_{BET} [a] ($m^2 g^{-1}$)[#]	V_p [a] ($cm^3 g^{-1}$)	Total acidity [b] (mmol NH_3 $gcat^{-1}$) [#]	Average reduced particle size [c] (nm)	
				Cu	Ni
Cu/γ-Al_2O_3	77	0.15	0.562	89	-
Cu:Ni(1:1)/γ-Al_2O_3	78	0.15	0.609	33	22
Ni/γ-Al_2O_3	71	0.12	0.407	-	39

[#]Analytical instruments error for BET surface area, active volume for TPD: x ± 2%
[a] Calculated based on the desorption branch of isotherm
[b] Calculated from NH_3-TPD data
[c] Average crystallite size calculated from XRD pattern by using Scherrer's formula

4.1.1.2 X-Ray diffraction pattern (XRD)

The XRD pattern of reduced catalysts is shown in Figure 4.1 (A). The diffraction peaks obtained at the 2θ of 43.3º, 50.4º, 74.2º represented the presence of cubic metallic copper corresponding to (111), (200) and (220) crystal planes, respectively [JCPDS: 85-1326]. Peaks detected at 2θ = 45.5º, 51.8º and 76.4º represented the cubic nickel metal corresponding to (111), (200) and (220) crystal planes, respectively [JCPDS: 04-0850]. The peaks at the 2θ range of 43.3º- 45.5º and 50.4º-52º, corresponded to the copper-nickel mixed oxide phase [JCPDS: 78-1602] [Pudi et al., (2015b), Lee et al., (2004), Rogatis et al., (2008)]. The formation of mixed oxide phase indicated the strong interaction of metals (Cu, Ni) with alumina support. The average crystallite size of copper, nickel particle from the line width of their corresponding crystal planes were calculated by using the Scherrer's formula and the calculated values are summarized in Table 4.1. Results suggested that after incorporation of Cu and Ni metal on γ-Al_2O_3, the average crystallite size was decreased significantly. The small average crystallite size of Cu:Ni(1:1)/Al_2O_3 bimetallic catalyst indicated the synergetic interaction of Cu and Ni metal with γ-Al_2O_3 support.

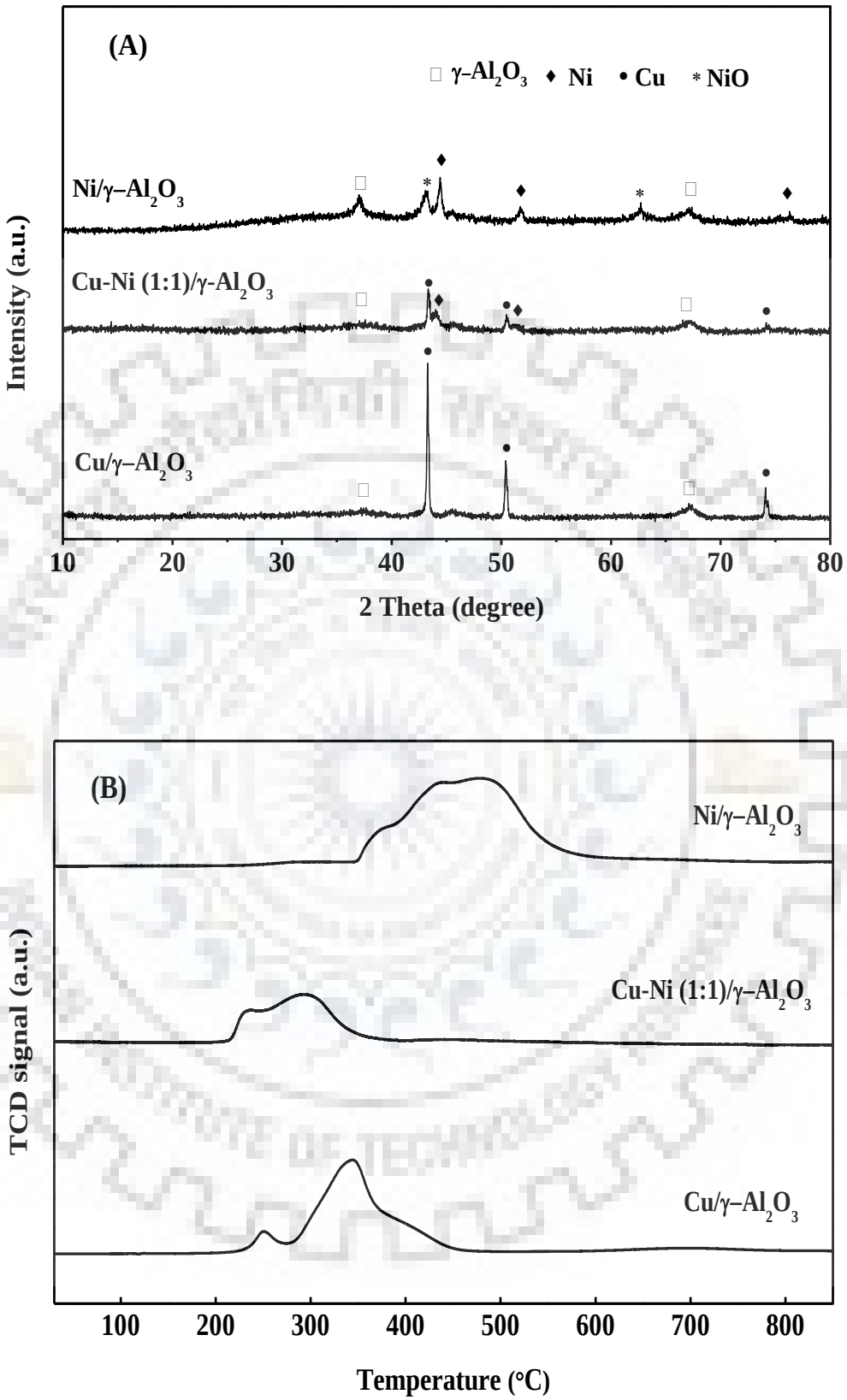

Figure 4.1. (A) XRD pattern of γ-Al_2O_3 based monometallic and bimetallic catalyst (B) H_2-TPR profiles of γ-Al_2O_3 supported catalysts

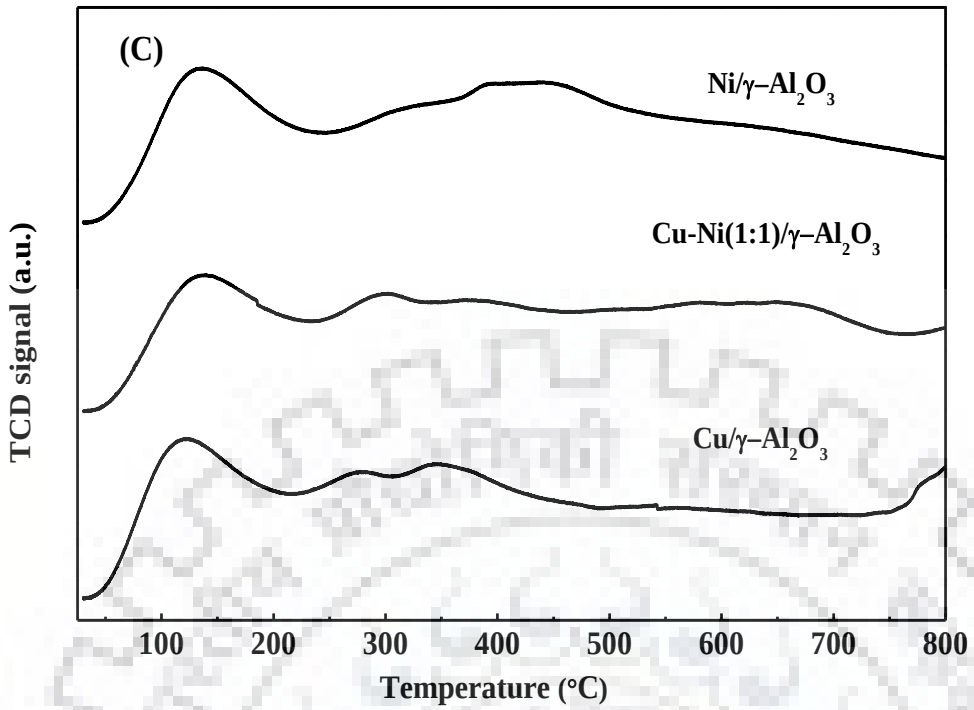

Figure 4.1. (C) NH_3-TPD profiles of γ-Al_2O_3 supported catalysts

4.1.1.3 H_2-temperature programmed reduction (TPR)

H_2-TPR profile of γ-Al_2O_3 supported catalysts is shown in Figure 4.1 (B). 20 wt.% Cu/γ-Al_2O_3 catalyst showed two reduction peaks of Cu metal at 250 °C and 350 °C, respectively. The peak at 250 °C represented the highly dispersed CuO to Cu metal, whereas, the reduction peak at 350 °C indicated the reduction of bulk CuO to Cu cubic metal [Jiang et al., (2005)]. 20 wt.% Ni/γ-Al_2O_3 catalyst exhibited a broad reduction peak at the temperature range of 350-610 °C, with a shoulder peak at 366 °C. This low-temperature reduction peak at 366 °C was because of weakly bonded NiO to Ni. Two major reduction peaks detected at 431 °C and 477 °C indicated the bulk reduction of NiO to Ni metal [Yu et al., (2010)]. The reduction peak at higher temperature was because of strongly bonded NiO with γ-Al_2O_3 support. For Cu-Ni bimetallic catalyst, a broad reduction peak was observed at the temperature range of 230-350 °C, which indicated the combined reduction of CuO and NiO. It was observed that the reduction temperature of CuO and NiO in the bimetallic catalyst was shifted towards the lower side, which suggested the variation of metal support interaction after the addition of Cu and Ni metals on γ-Al_2O_3 support.

4.1.1.4 NH_3-temperature programmed desorption (TPD)

NH_3-TPD pattern (Figure 4.1 (C)) of γ-Al_2O_3 supported catalysts showed the acidic sites on all the catalysts were distributed in three different temperature regions i,e. 80-250 °C, 250-500 °C and above 500 °C, respectively. Desorption of ammonia from the temperature region of 80-250 °C corresponded to weak strength acidic sites, desorption at 250-500 °C indicated the presence of moderate strength acidic sites and the desorption at > 500 ºC characterized the presence of strong strength acidic sites, respectively [Khandan et al., (2008)]. The TPD pattern (Figure 4.1 (C)) of γ-Al_2O_3 supported copper, nickel catalysts suggested the presence of primarily weak strength acidic sites on the surface. The calculated total acidic strength of all the catalysts are summarized in Table 4.1. Results showed that the highest acidic strength of 0.609 mmol $NH_3.gcat^{-1}$ was obtained for the bimetallic Cu:Ni(1:1)/γ-Al_2O_3 catalyst as compared to monometallic catalysts.

4.1.2 Catalytic performance

In presence of all the γ-Al_2O_3 supported catalysts, catalytic activity was evaluated in liquid phase autoclave reactor at 210 °C temperature, 4.5 MPa of H_2 pressure in presence of 2 g of catalyst. The obtained glycerol conversion and products selectivity are summarized in Table 4.2. Carbon balances of all the experiments reported in Table 4.2 were closely 100 ± 5%. Monometallic Cu, Ni catalysts showed lower catalytic activity as compared to the bimetallic catalyst. Monometallic Cu/γ-Al_2O_3 and Ni/γ-Al_2O_3 catalysts showed glycerol conversion of 21% and 14.5%, respectively. Lower glycerol conversion was because of lower acidic strength (0.407-0.562 $mmol.gcat^{-1}$) of the catalyst, presence of larger metal particle size and lower metal dispersion in the catalysts. However, Cu:Ni(1:1)/γ-Al_2O_3 catalyst exhibited significantly higher glycerol conversion (71.6%). The higher catalytic activity of bimetallic Cu:Ni(1:1)/γ-Al_2O_3 catalyst was because of higher surface area (78 $m^2.g^{-1}$), higher acidity (0.609 $mmol.gcat^{-1}$), smaller average particle size (27 nm). The highest 1,2-PDO selectivity of 91.1% was obtained in presence of Cu/γ-Al_2O_3 catalyst with small amounts of hydroxyacetone (3.3%), propanol (4.8%) and 0.8% of others products were also obtained. Ni/γ-Al_2O_3 catalyst exhibited 87.9% selectivity towards 1,2-PDO and trace amounts of hydroxyacetone (3%), propanol (2.8%) and 6.1% of other products including ethylene glycol, 2-propanol, ethanol, and methanol, respectively. More degradation products obtained over nickel catalyst suggested cleavage of C-C bond of glycerol. In presence of Cu:Ni(1:1)/γ-Al_2O_3 catalyst, the obtained 1,2-PDO selectivity was 85.6%, and the selectivity to propanol, hydroxyacetone, and other products were 8.9% 1.4% and 4.1%,

respectively. Lower degradation products in presence of bimetallic Cu:Ni(1:1)/γ-Al_2O_3 catalyst suggested that this catalyst stimulated the cleavage of C-O bond by suppressing the C-C bond of glycerol. The maximum overall yield of 61.2% was obtained in presence of Cu:Ni(1:1)/γ-Al_2O_3 catalyst due to the bi-functional behavior of the catalyst. The bi-functional behavior of this catalyst was may be due to the presence of a new copper-nickel bimetallic phase on the catalyst as shown in the XRD pattern (4.1 (A)).

Table 4.2. Catalytic results in presence of γ-Al_2O_3 supported Cu, Ni catalysts

Catalyst	Conversion (%)	Selectivity (%)				1,2-PDO yield (%)
		1,2-PDO	Hydroxy-acetone	Propanol	Others[a]	
Cu/γ-Al_2O_3	21.0	91.1	3.3	4.8	0.8	19.1
Cu:Ni(1:1)/γ-Al_2O_3	71.6	85.6	1.4	8.9	4.1	61.2
Ni/γ-Al_2O_3	14.5	87.9	3.0	2.8	6.1	12.7

[a] Others: ethylene glycol, 2-propanol, ethanol, methanol
Reaction condition: 210 °C, 4.5 MPa, 20 wt.% glycerol, 12 h reaction time, 2 g of catalyst, 700 rpm
Experimental errors for all the values (conversion, selectivity and yield) : x ± 1 %

4.1.3 Effect of calcination temperature

Bimetallic Cu:Ni(1:1)/γ-Al_2O_3 catalyst was found to be more active and the highest 1,2-PDO yield was obtained in presence of this catalyst due to the presence of new copper-nickel bimetallic phase in this catalyst. The effect of catalyst calcination temperature on the formation of this new bimetallic phase and the variation of catalytic activity and 1,2-PDO selectivity/yield of the catalyst calcined at different temperature were examined. Catalyst calcination temperature significantly affected the physico-chemical properties of Cu:Ni(1:1)/γ-Al_2O_3 catalyst (Appendix-1). The reaction was performed at standard reaction condition (210 °C, 4.5 MPa), the results obtained are shown in Figure 4.2. As shown in Figure 4.2, with increasing the catalyst calcination temperature from 350 °C to 400 °C, glycerol conversion was increased from 70.3% to 71.6% and further, the glycerol conversion was decreased gradually and reached to 58.5% for the catalyst calcined at 550 °C. The decrease in conversion was might be due to the agglomeration of particles in the

catalyst calcined at the higher temperature. The selectivity towards 1,2-PDO was found to be increased from 85.6% at 300 °C to 90.4% at 550 °C with a simultaneous decrease in selectivity to propanols (PO). The maximum 1,2-PDO yield of ~61% was achieved in presence of 20 wt.% Cu:Ni(1:1)/γ-Al_2O_3 catalyst calcined at 400 °C. This result suggested that the calcination temperature of ~400 °C was the optimum for higher conversion and yield to 1,2-PDO.

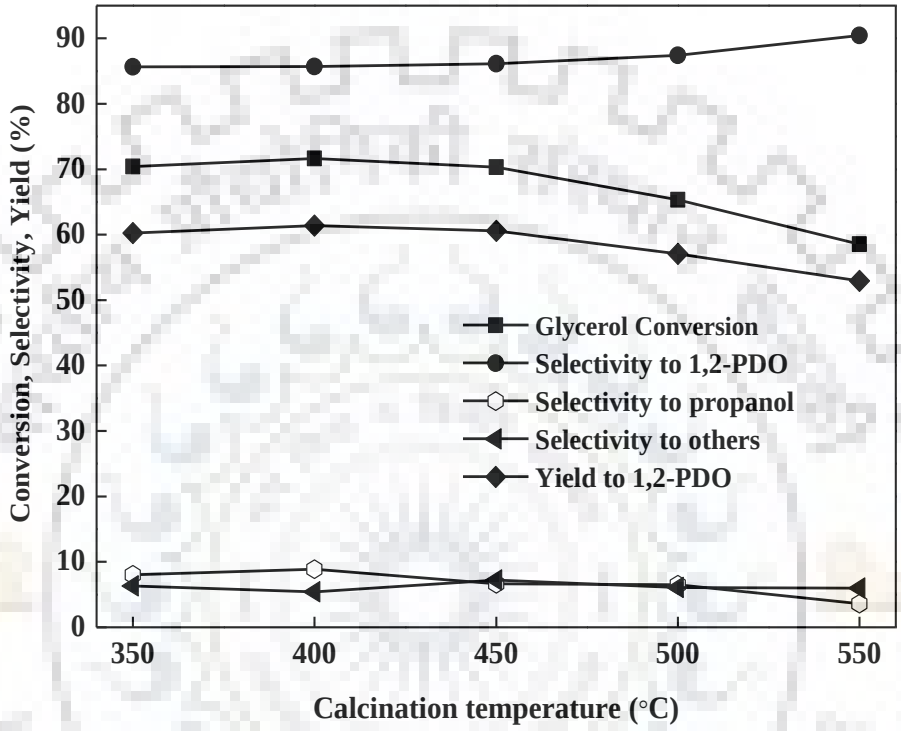

Figure 4.2. Effect of calcination temperature on glycerol conversion and products selectivity over 20 wt.% Cu:Ni(1:1)/γ-Al_2O_3 catalyst

4.1.4 Parameter studies

The influences of reaction temperature, pressure, glycerol concentration and catalyst loading on the activity and product selectivity over 20 wt.% Cu:Ni(1:1)/γ-Al_2O_3 catalyst calcined at 400 °C is discussed in the following section. Experimental errors for all the values in Figure 4.3 are x ± 1 %.

4.1.4.1 Effect of temperature

A variation in reaction temperature had a significant effect on glycerol conversion (Figure 4.3 (A)). The glycerol conversion increased with an increase in reaction time and temperature at a constant pressure (4.5 MPa). At 180 °C, the glycerol conversion increased from 10% after 2 h to 37% after 12 h of reaction. However, at 220 ºC, glycerol conversion varied from 48% to 85% with a variation in reaction time from 2 h to 12 h. In presence of Cu:Ni(1:1)/γ-Al_2O_3 catalyst, 1,2-PDO and propanol (1-PO + 2-PO) were identified as the major reaction products. Although, slight amounts of hydroxyacetone, ethylene glycol, ethanol, and methanol were also detected. After 12 h, the selectivity towards hydroxyacetone, ethylene glycol, ethanol and methanol varied as 0.6-3.6%, 1.7-2.3%, 1.18-2.3%, and 0.9-1.0%, respectively, with an increase in the reaction temperature from 180-220 °C. The 1,2-PDO selectivity decreased slightly by simultaneously increasing the selectivity towards propanol with reaction time at all reaction temperatures (Figure 4.3 (B)). The effect was more pronounced at higher reaction temperature (220 ºC). After 12 h of reaction, the selectivity towards 1,2-PDO decreased from ~95% at 180 °C to 68% at 220 °C, and the selectivity to propanol increased from ~1% to ~21%. At higher temperature, more propanol was produced due to further hydrogenolysis of 1,2-PDO [Sepulveda et al., (2017)]. The investigation on the effect of temperature study disclosed that the selective conversion of glycerol to 1,2-PDO was not favourable at the higher reaction temperature (>210 °C).

4.1.4.2 Effect of pressure

The glycerol conversion and products selectivity at different pressures (3-6 MPa) and at a constant temperature (210 °C) is shown in Figure 4.3 (C) and 4.3 (D), respectively. The conversion was found to increase with reaction time as well as pressure. After 12 h, with increasing pressure from 3 to 6 MPa, glycerol conversion increased from 58% to 85%. As shown in Figure 4.3 (D), apart from 1,2-PDO and propanol, hydroxyacetone, ethylene glycol, ethanol, and methanol were also detected in the reaction mixture. After 12 h of reaction, selectivity towards hydroxyacetone, ethylene glycol, ethanol and methanol varied in the range of 7.5 - 1.3%, 1.5 - 2.3%, 1.0 - 2.0%, 0.4 - 1.2%, respectively, with raising the pressure from 3 MPa to 6 MPa. The selectivity towards 1,2-PDO showed a decreasing trend and selectivity to PO showed an increasing trend with reaction time at all pressures (Figure 4.3 (D)). The decrease in selectivity towards 1,2-PDO with increasing time was mainly due to the sequential conversion of 1,2-PDO to propanol and the C-C bond scission of glycerol which led to the formation of other

lower alcohols [Hamzah et al., (2012)]. The selectivity towards 1,2-PDO increased with a simultaneous decrease in selectivity towards PO with an increase in reaction pressure. The variation in selectivity towards both products was insignificant at > 4.5 MPa [Amada et al., (2011)]. At higher pressures, hydroxyacetone was produced as an intermediate by the dehydration of glycerol, which was instantaneously hydrogenated to 1,2-PDO, hence the selectivity towards 1,2-PDO increased [Pandhare et al., (2016)]. However, in this study, at a lower pressure, a significant amount of propanol was obtained, which suggested that propanol was formed due to the sequential hydrogenation of glycerol, hydroxyacetone, and 1,2-PDO. However, the decrease in the selectivity towards propanol with hydrogen pressure suggested that its formation was not favoured by the increase in hydrogen partial pressure. These results indicated that a high reaction pressure (> 4.5 MPa) favoured the selective hydrogenolysis of glycerol to 1,2-PDO and minimized the formation of other lower alcohols.

4.1.4.3 Effect of glycerol concentration

Influence of glycerol concentration on glycerol conversion and products selectivity is shown in Figure 4.3 (E). It can be observed that glycerol conversion decreased from 73.5% to 42.4% with increasing the glycerol concentration from 10-40 wt.%. Decreasing of glycerol conversion with glycerol concentration was because of less number of catalyst active sites [Balaraju et al., (2012)]. Selectivity towards 1,2-PDO decreased from 95.2% to 72.8% with simultaneous increasing the selectivity to 1-propanol from 1-20%. This result suggested that at higher glycerol concentration (> 20%), overhydrogenolysis of 1,2-PDO took place which produced 1-propanol.

4.1.4.4 Effect of catalyst loading

Effect of catalyst loading is shown in Figure 4.3 (F). Glycerol conversion was found to be increased from 43% to 84% with increasing the catalyst loading from 1-2 g. The sharp increase in catalytic activity with increasing the catalyst loading was because of increasing of catalyst active sites. It was also observed that selectivity towards 1,2-PDO increased from 86.5% to 93% at the range of catalyst loading from 1-2 g. However, selectivity to 1-propanol decreased from 10.5% to 2.5% with increasing the catalyst amount. These results suggested that with increasing the catalyst amount, total active sites were increased, which promoted selective glycerol conversion of 1,2-PDO by suppressing the degradation products.

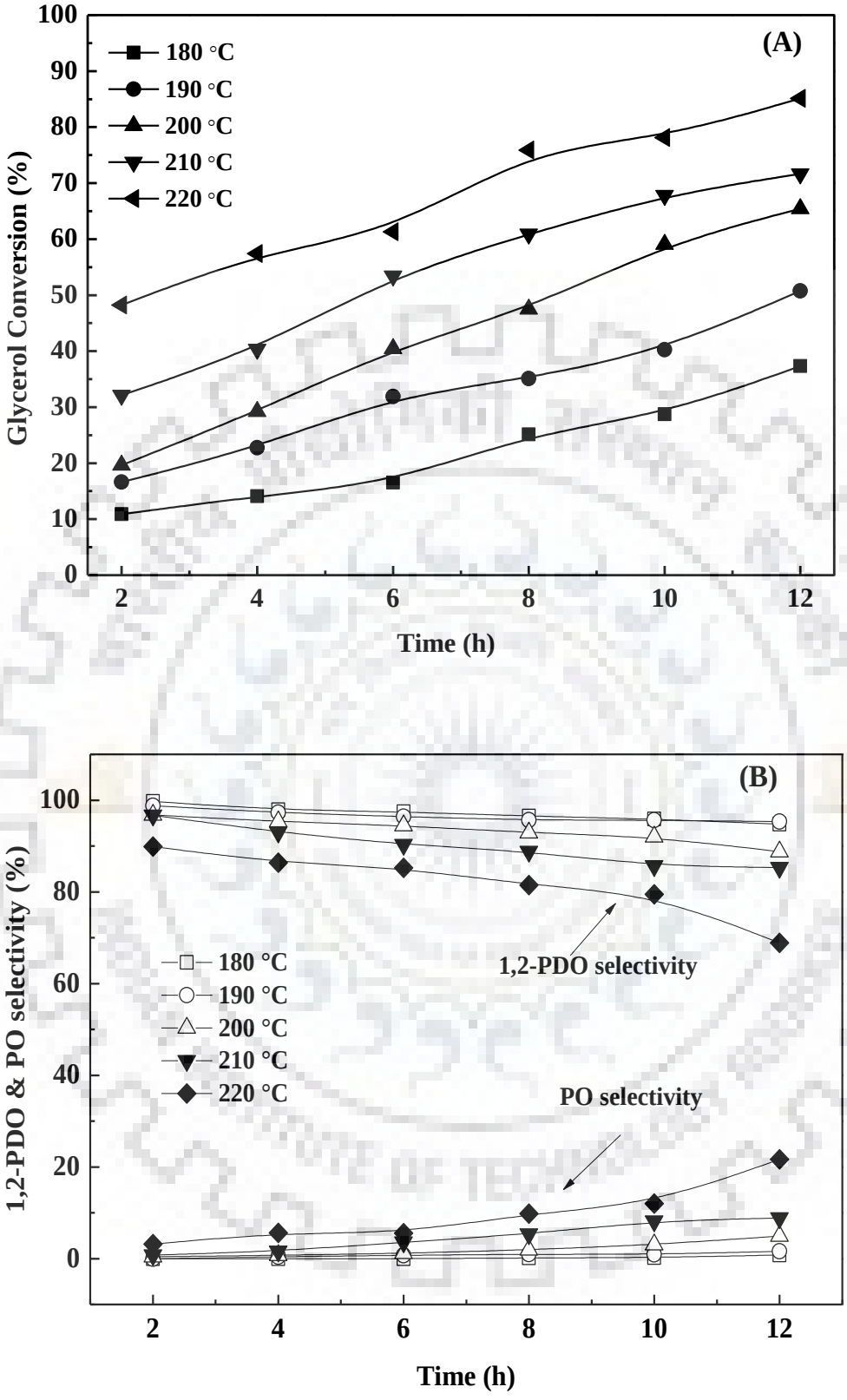

Figure 4.3. Variation in (A) glycerol conversion and (B) product selectivity with time at different temperatures = 180-220 °C, pressure = 4.5 MPa, feed = 20 wt.% glycerol (20 g), catalyst = 2 g

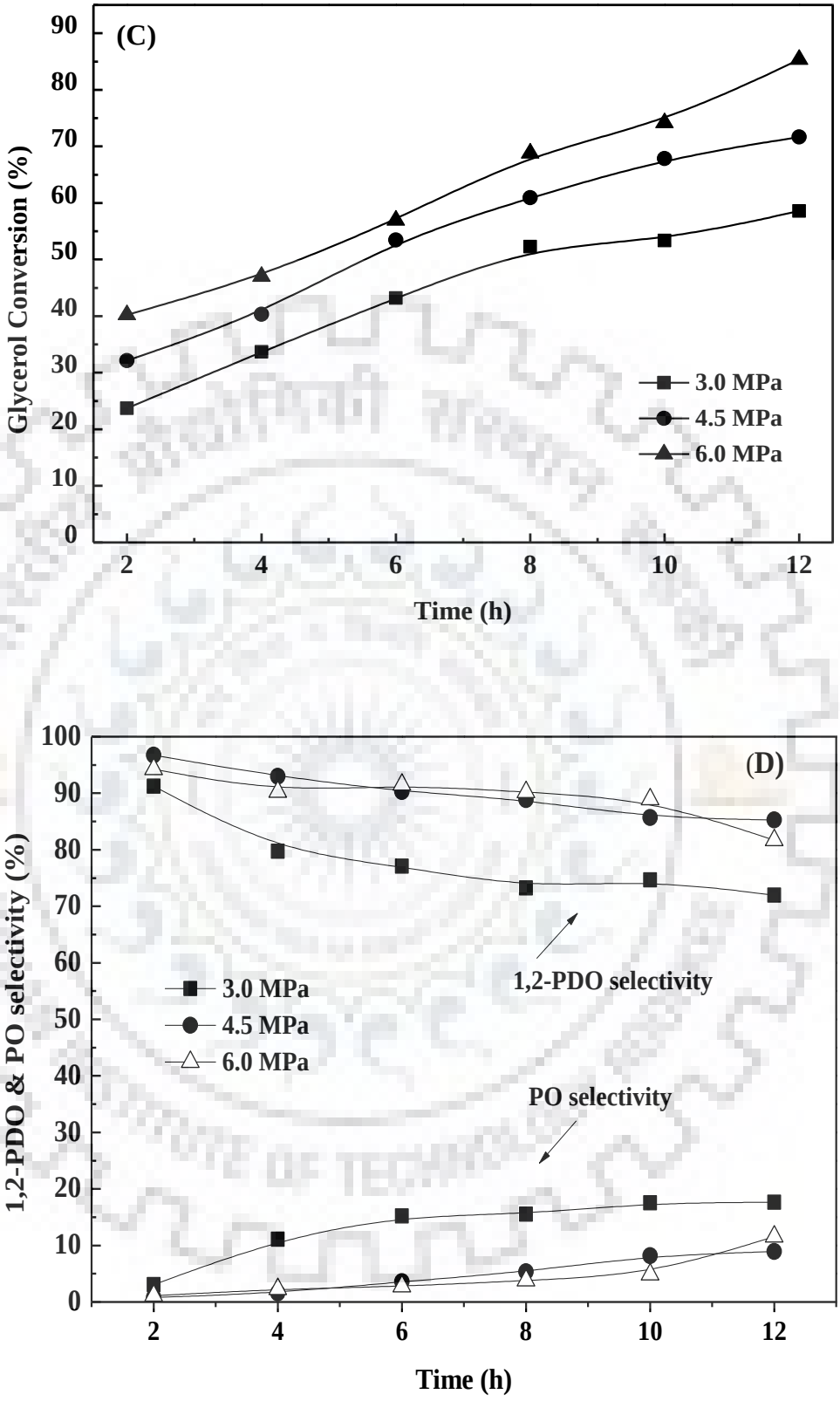

Figure 4.3. Variation in (C) glycerol conversion and (D) product selectivity with time at different pressures = 3 MPa – 6 MPa, temperature = 210 °C, feed = 20 wt.% glycerol (20 g), catalyst = 2 g

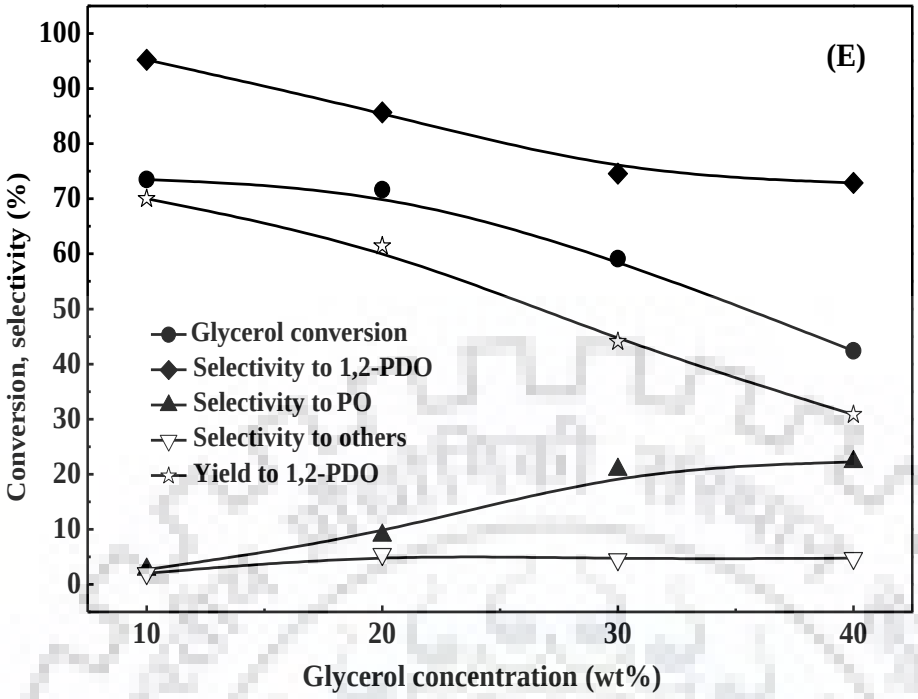

Figure 4.3. (E) Effect of glycerol concentration on conversion and selectivity. Reaction Conditions: reaction temperature = 210 ^{o}C, H_2 pressure = 4.5 MPa, reaction time = 12 h, catalyst = 2 g

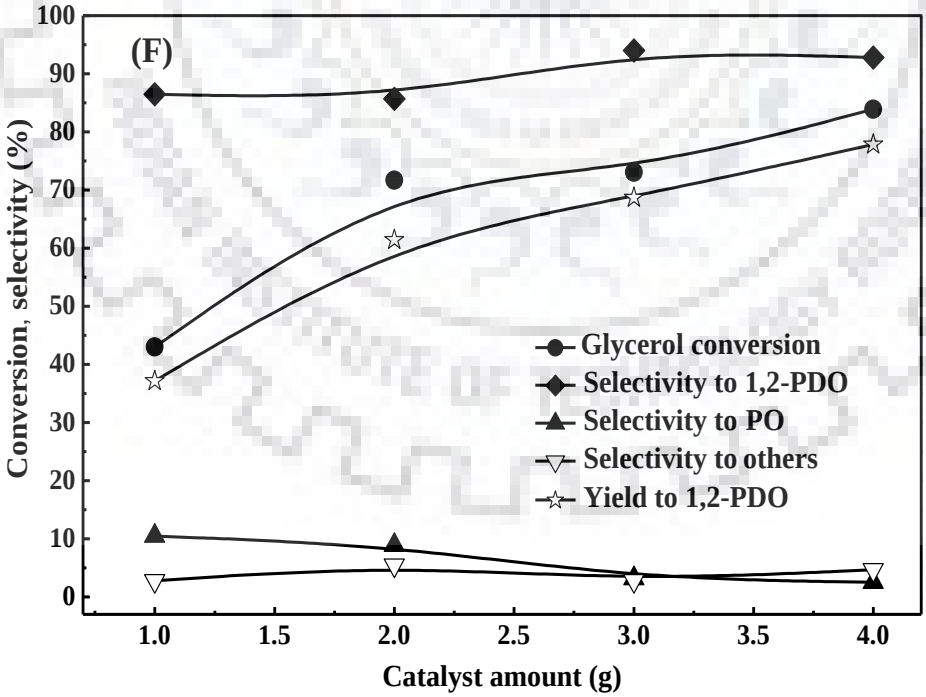

Figure 4.3. (F) Effect of catalyst amount on conversion and selectivity. Reaction Conditions: feed = 20 wt.% glycerol (20 g), reaction temperature = 210 ^{o}C, H_2 pressure = 4.5 MPa, reaction time = 12 h

4.1.5 Reaction mechanism study

It is very important to understand the actual reaction pathway followed for the production of 1,2-PDO and other reaction products in liquid phase hydrogenolysis of glycerol. The reaction mechanisms for liquid phase hydrogenolysis of glycerol have been studied previously and discussed the possible reaction path over various catalysts [Wang et al., (2010), Dasari et al., (2005), Xia et al., (2012b), Maris et al., (2007), Wang et al., (2015b), Menchavez et al., (2017)]. Existing literature information suggested two different reaction mechanisms for hydrogenolysis of glycerol to 1,2-PDO. A two-step mechanism described the formation of metastable hydroxyacetone as an intermediate by dehydration of glycerol over the acidic-basic sites of the catalytic surface followed by the formation of 1,2-PDO by the hydrogenation of hydroxyacetone over the active metallic sites of the catalyst [Wang et al., (2010), Dasari et al., (2005), Maris et al., (2007), Vasiliadou and Lemonidou (2011)]. The dehydration step followed the homogenous E1 mechanism, where the primary -OH group of glycerol was removed and formed carbocation intermediate i.e: hydroxyacetone. Another possible path discussed three steps hydrogenolysis process [Xia et al., (2012b), Wang et al., (2015b)]. Initially, glycerol dehydrogenated to glyceraldehyde followed by dehydration to 2-hydroxyacrolein. Further, 2-hydroxyacrolein was converted to pyruvaldehyde by keto-enol tautomerism followed by hydrogenation to hydroxyacetone and finally hydroxyacetone hydrogenated to 1,2-PDO [Maris et al., (2007), Maris and Davis (2007), Xiao et al., (2012), Xia et al., (2012b), Wang et al., (2015b)]. Glyceraldehyde was formed primarily in the presence of basic sites of the catalyst surface. It was also reported that hydroxyacetone was more stable and its formation was thermodynamically more favourable as compared to glyceraldehyde.

Reaction mechanism study was performed in presence of Cu:Ni(1:1)/γ-Al_2O_3 catalyst at the optimum reaction condition, i.e. at 210 °C, 4.5 MPa pressure, in presence of 10 wt.% catalyst and 20 wt.% aqueous glycerol solution as feed [Pudi et al., (2015b)]. Experimental results suggested that the primary reaction products were 1,2-PDO and propanol (1-PO + 2-PO). Although small amounts (~ 5.4%) of other products, such as hydroxyacetone, ethylene glycol (EG), ethanol and methanol, were also detected. The maximum of 85.7% selectivity towards 1,2-PDO and 8.9% selectivity to propanol was achieved with 71.6% conversion of glycerol. The obtained selectivity to hydroxyacetone (~1.9%), EG (2.1%), ethanol (0.9%) and methanol (0.5%) were very low.

Table 4.3. Hydrogenolysis of glycerol, hydroxyacetone, 1,2-PDO and EG over Cu:Ni(1:1)/γ-Al_2O_3 catalyst

Reactant	Conversion (%)	Selectivity (%)					
		1,2-PDO	Hydroxy-acetone	EG	1-PO + 2-PO	Ethanol	Methanol
Glycerol	71.6	85.7	1.8	2.1	8.9	0.9	0.5
Hydroxy-acetone	97.4	94.3	-	-	4.1	1.6	0
1,2-PDO	9.6	-	-	-	13.2	83.2	3.6
EG	14.7	-	-	-	-	10.5	89.5

Experimental errors for all the values (conversion, selectivity and yield) : x ± 1 %
Reaction condition: Feed = 20 wt.% aqueous glycerol solution (100 g), pressure = 4.5 MPa, temperature = 210 °C, catalyst loading = 2 g, time = 12 h

To find out the probable reaction pathway followed in presence of bi-functional Cu:Ni(1:1)/γ-Al_2O_3 catalyst the primary reaction products i,e. hydroxyacetone, 1,2-PDO and ethylene glycol (EG) were used as reactants and hydrogenolysis reactions were conducted at the similar optimized reaction condition. For each experiment, the reactant i.e. hydroxyacetone, 1,2-propanediol, and ethylene glycol concentration was 20 wt.% of the feed mixture. The products distribution obtained for each reactant as a feed is shown in Table 4.3. In the presence of hydroxyacetone as a reactant, 97.4% conversion of hydroxyacetone with 94.3% selectivity towards 1,2-PDO and ~4% selectivity to propanol was achieved. This result indicated that hydroxyacetone was obtained as an intermediate and primarily transformed into 1,2-PDO and a trace amount of propanol. This reaction mechanism suggests that glycerol was initially converted to hydroxyacetone by dehydration and 1,2-propanediol was obtained by the hydrogenation of hydroxyacetone. Further, with 1,2-PDO as the reactant, 9.6% conversion of 1,2-PDO was achieved and 1,2-PDO was mainly converted to ethanol ($S_{83\%}$), propanol ($S_{13.2\%}$) and a small amount of methanol ($S_{3.6\%}$). This result suggested that 1,2-PDO was the main contributor of ethanol (0.9%) and propanol (1-PO + 2-PO) (8.9%), when glycerol was used as the feed. EG as a reactant showed only 14.7% conversion with 89.5% selectivity to methanol and 10.5 %

selectivity to ethanol. This result suggested that ethanol and methanol were mainly obtained by the degradation of EG or 1,2-PDO, whereas propanol may have been formed via the overhydrogenolysis of 1,2-PDO. Based on these experimental observations (Table 4.3), the probable reaction pathway was proposed (Scheme 4.1) in the presence of the Cu:Ni(1:1)/γ-Al_2O_3 catalyst.

4.1.6 Summary

This study focused on the development of γ-Al_2O_3 supported Cu, Ni monometallic and Cu-Ni bimetallic catalysts for hydrogenolysis of glycerol in a liquid phase batch reactor. Experimental results demonstrated that bimetallic copper-nickel catalysts were more active and selective to 1,2-PDO as compared to monometallic catalysts due to bi-functional behaviour. Further, the influences of temperature and pressure on glycerol conversion and products selectivity were investigated to maximize the yield to 1,2-PDO. Results suggested that 20 wt.% Cu:Ni(1:1)/γ-Al_2O_3 catalyst calcined at 400 °C exhibited very high catalytic activity (70.3%) and 1,2-PDO selectivity (85%) at mild reaction condition. The reaction mechanism study suggested two steps hydrogenolysis process i.e. dehydration of glycerol to hydroxyacetone on the acidic centres of the catalyst followed by hydrogenation of hydroxyacetone to 1,2-PDO on the metallic sides of the catalyst.

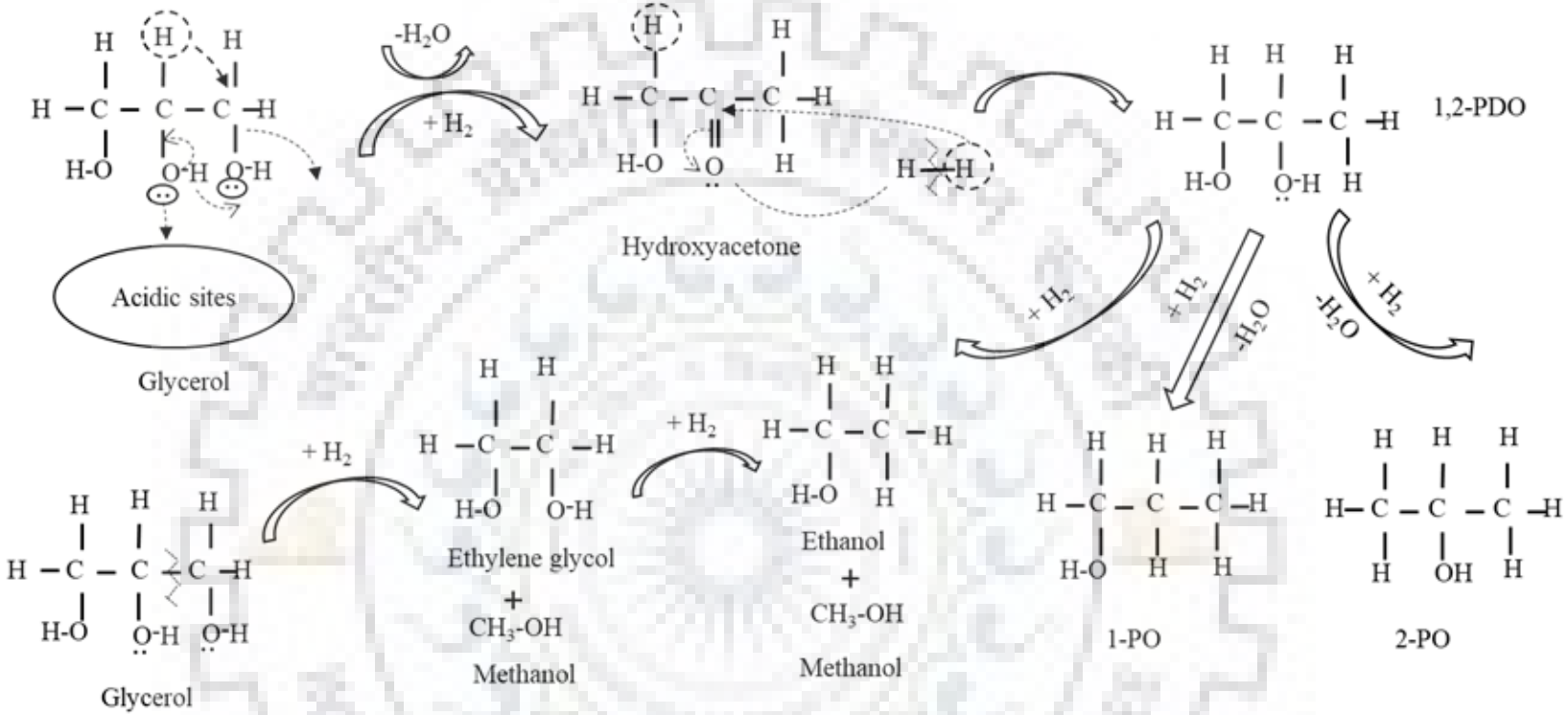

Scheme 4.1. Reaction mechanism for hydrogenolysis of glycerol over 20 wt.% Cu:Ni(1:1)/γ-Al_2O_3 catalyst

4.2 Selective hydrogenolysis of glycerol to 1,2-propanediol over Cu-Mg-Al-O catalyst derived from layered double hydroxides (LDHs) precursor

It was observed in the previous section that 20 wt.% Cu:Ni(1:1)/γ-Al_2O_3 catalyst was moderately active and selective to 1,2-PDO. It was also observed that, although the addition of Ni increased the catalytic activity of Cu/γ-Al_2O_3, however, the catalyst was not selective to 1,2-PDO at the higher temperature because of overhydrogenolysis of 1,2-PDO to propanol. Therefore, to increase the catalytic activity as well as 1,2-PDO selectivity, instead of nickel, magnesium metal was introduced into the Cu-Al catalyst. The following section discusses the selective hydrogenolysis of glycerol to 1,2-PDO in presence of bi-functional layered double hydroxide (LDHs) type Cu-Mg-Al-O and Cu-Zn-Mg-Al-O catalysts prepared by urea hydrolysis method. The physico-chemical properties of these catalysts were characterized by various techniques such as specific surface area (BET), X-ray Diffraction (XRD), H_2-temperature programmed reduction (H_2-TPR) and scanning electron microscopy (FE-SEM) etc. Ball-flower shaped particles were identified in FE-SEM images of all the catalysts and a well-defined layered structure of solid lamella has also been identified. Further, the effect of concentration of urea in catalysis synthesis, the effect of metal loading and influences of the addition of bases in the reaction mixture on catalytic activity were also studied. Reaction parameters were optimized experimentally by studying the effect of temperature, pressure, glycerol concentration and catalyst loading. Catalyst stability and reusability of Cu-Zn-Mg-Al-O catalyst were also verified.

4.2.1. Catalyst characterization

4.2.1.1 Textural properties

BET surface area (S_{BET}), cumulative pore volume (V_P) and average pore diameter (D_P) of the catalysts are shown in Table 4.4. The surface area, pore volume (V_P) and average pore diameter of the catalysts were in the range of 22.9-70.3 $m^2.g^{-1}$, 0.029-0.097 $cm^3.g^{-1}$ and 5.1-6.2 nm, respectively. The surface area, pore volume and pore diameter of the Cu-Mg-Al-O catalyst were increased from 22.9 to 70.3 $m^2.g^{-1}$, 0.029 to 0.097 $cm^3.g^{-1}$ and 5.1 to 5.5 nm, respectively, with increasing the urea concentration from 1.5 to 2.5 M. With increasing Cu metal in Cu-Mg-Al-O-2 catalyst, surface area, and pore volume were decreased to 16.1 $m^2.g^{-1}$ and 0.022 $cm^3.g^{-1}$, respectively. The surface area, pore volume and pore diameter of the Cu-Zn-Mg-Al-O catalyst were 23.5 $m^2.g^{-1}$, 0.036 $cm^3.g^{-1}$ and 6.2 nm, respectively.

Table 4.4. Physico-chemical properties of catalysts

Catalyst	Urea concentration (M)	BET surface area (S_{BET}, $m^2.g^{-1}$)[a #]	Pore volume (V_p, $cm^3.g^{-1}$)[a]	Average pore size (D_p, nm)[a]	Average crystallite size of Cu[b] (nm)
Cu-Mg-Al-O-1	1.5	22.9	0.029	5.1	25.4
Cu-Mg-Al-O-2	2.0	54.1	0.063	5.3	22.5
Cu-Mg-Al-O-3	2.5	70.3	0.097	5.5	16.2
Cu-Mg-Al-O-4	2.0	16.1	0.022	5.5	28.8
Cu-Zn-Mg-Al-O	2.0	23.5	0.036	6.2	21.6

[a] Data obtained from BET surface analyzer
[b] Crystallite size calculated by using Scherrer's formula
[#]Analytical instruments error for BET surface area: x ± 2%

4.2.1.2 XRD

The XRD pattern (Figure 4.4 (A)) of all the fresh dried catalysts showed the diffraction peaks at the 2θ value of 11.7º, 23.6º, 35.0º, 39.7º, 47.1º, 60.9º and 62.4º corresponding to the (003), (006), (009), (105), (108), (110) and (113) crystal planes of LDHs structure (JCPDS 35-0965) [Xia et al., (2012a), Meher et al., (2009)].

The XRD patterns of reduced Cu-Mg-Al-O catalyst are shown in Figure 4.4 [(B) and (C)]. The sharp and symmetrical reflection peaks obtained at the 2θ value of 43.3º and 50.3º were corresponding to the (111) and (200) diffraction planes of cubic metallic copper (JCPDS: 85-1326). Whereas, the diffraction peak obtained at 2θ = 35.5º was corresponding to the (002) plane of crystalline monoclinic CuO phase (JCPDS: 80-1987). Diffraction due to the (111) and (220) crystal planes of typical cubic MgO phase were detected at 2θ = 36.9º and 62.2º, respectively (JCPDS:78-0430). The peak obtained at 2θ = 74º was corresponding to the Al_2O_3 (JCPDS: 78-0430). XRD patterns of Cu-Mg-Al-O catalyst suggested that the crystal morphology of the catalysts was varied with the variation of urea concentration during the

synthesis of these catalysts. With increasing the urea concentration, the intensity of the diffracted Cu^o peaks decreased (Figure 4.4 (B)). On the contrary, the intensity of the diffracted peaks related to Cu^o increased with increasing copper metal loading in the catalyst (Figure 4.4 (C)) [Nagaraja et al., (2007), Balaraju et al., (2012)]. For Cu-Zn-Mg-Al-O catalyst (Figure 4.4 (C)(c)), an additional peak was obtained at $2\theta = 36.2^o$ corresponding to the (002) plane of ZnO (JCPDS: 04-0831). The average crystallite sizes of copper calculated by using Scherrer's equation are summarized in Table 4.4. The average crystallite size of copper was decreased from 25.4 nm to 16.2 nm with increasing the urea concentration from 1.5M to 2.5M [Fernandez et al., (2009), Ansari et al., (2009)]. The average copper crystallite size was 28.8 nm and 21.6 nm for the catalyst Cu-Mg-Al-O-4 and Cu-Zn-Mg-Al-O, respectively.

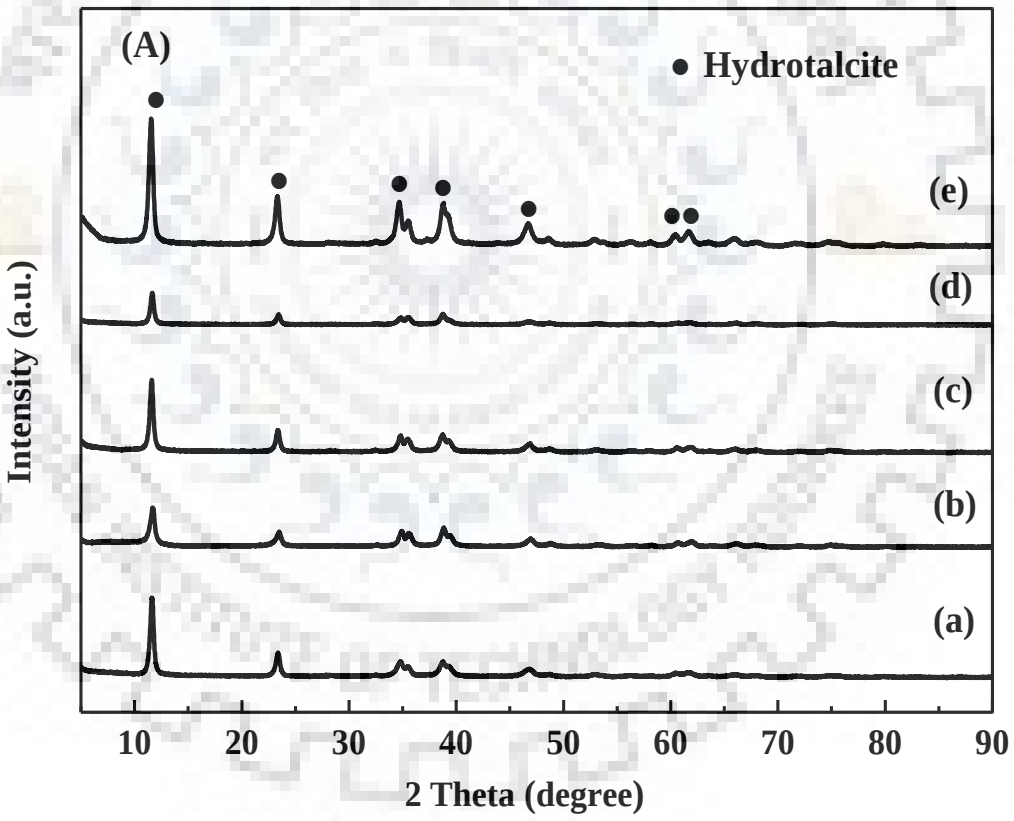

Figure 4.4. (A) XRD pattern of fresh dried LDHs (a) Cu-Mg-Al-O-1 (1.5M), (b) Cu-Mg-Al-O-2 (2M), (c) Cu-Mg-Al-O-3 (2.5M), (d) Cu-Mg-Al-O-4 (2M), (e) Cu-Zn-Mg-Al-O (2M)

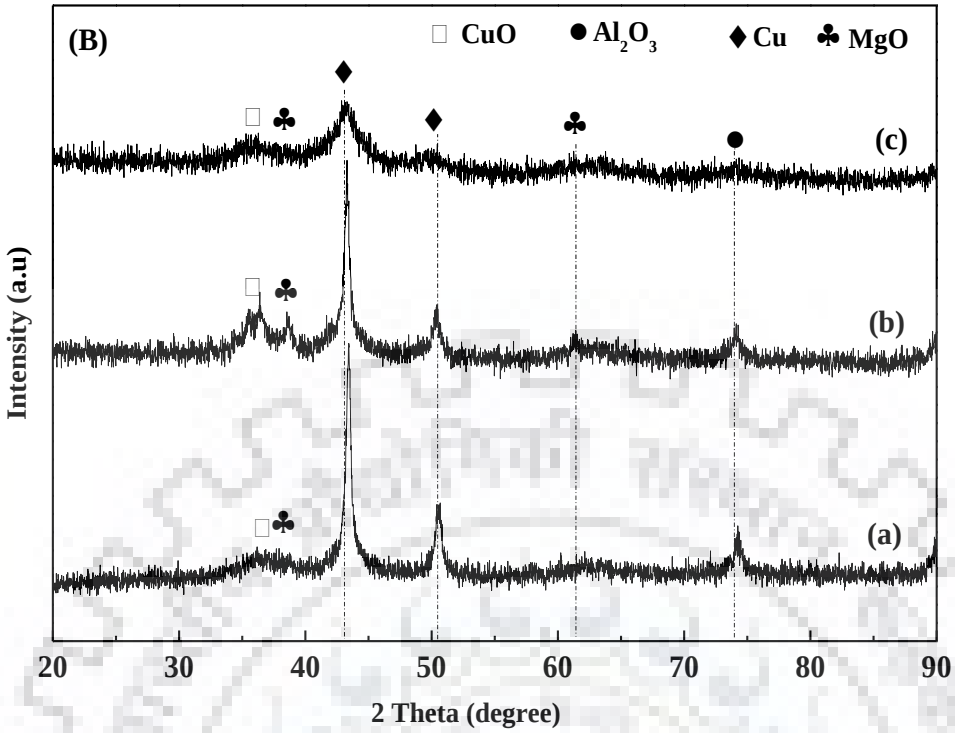

Figure 4.4. (B) XRD patterns of fresh reduced catalysts (a) Cu-Mg-Al-O-1 (1.5M), (b) Cu-Mg-Al-O-2 (2M), (c) Cu-Mg-Al-O-3 (2.5M)

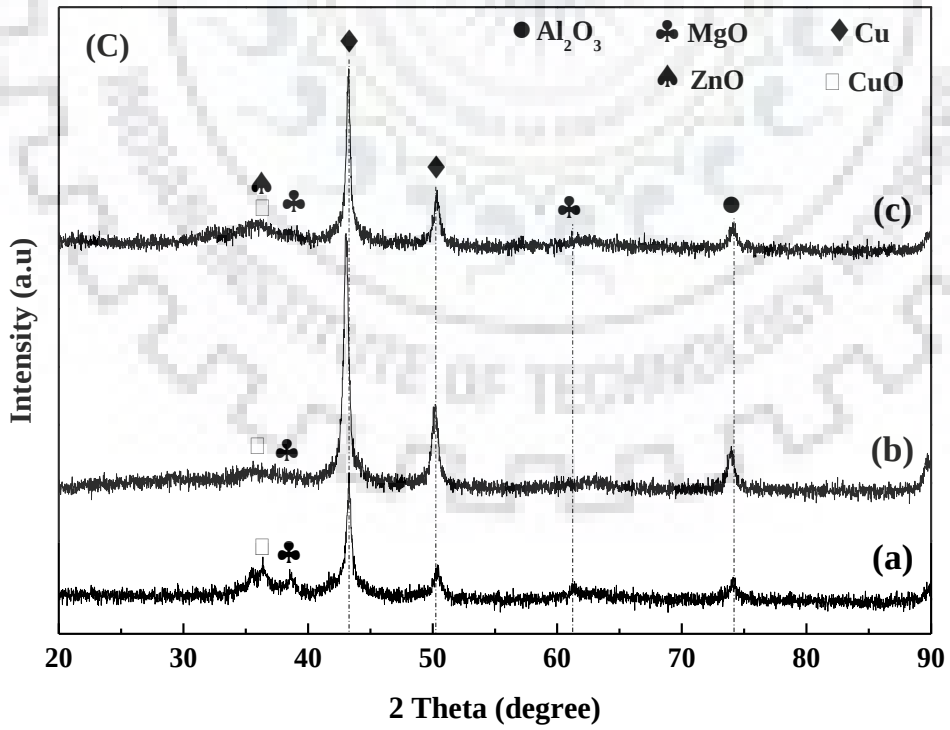

Figure 4.4. (C) XRD patterns of the reduced catalysts synthesized in presence of 2M urea solution: (a) Cu-Mg-Al-O-2, (b) Cu-Mg-Al-O-4, (c) Cu-Zn-Mg-Al-O

4.2.1.3 H_2-TPR

The reduction profile of calcined LDHs catalysts is shown in Figure 4.5. For Cu-Mg-Al-O-1 catalyst, one major reduction peak at 294 ^oC could be ascribed to the reduction of CuO to Cu^o [Kim et al., (2003), Dedecek et al., (1995)]. The reduction peaks corresponding to MgO, Al_2O_3, and ZnO was not observed in the temperature range studied [Balaraju et al., (2008), Pudi et al., (2014), Pudi et al., (2015a)]. For Cu-Mg-Al-O-2 catalyst, combined reduction peaks were obtained at 215 ^oC and 318 ^oC, respectively. The low temperature (215 ^oC) reduction peak was attributed the reduction of CuO to Cu^+ [Kim et al., (2003), Dedecek et al., (1995)] and the reduction peak at higher temperature (318 ^oC) was due to the reduction of Cu^+ to Cu° [Pudi et al., (2015)]. The reduction profile of Cu-Mg-Al-O-3 catalyst was almost similar to the reduction peak obtained for Cu-Mg-Al-O-1 catalyst. However, the reduction peak was shifted slightly towards lower temperature (285 ^oC) side. This result indicated that the concentration of urea played a significant role in the LDHs structure as well as the reduction behaviour of these catalysts. The reduction temperature of the catalyst (Cu-Mg-Al-O-4) having higher copper content was shifted towards higher temperature (327 ^oC). For Cu-Zn-Mg-Al-O catalyst, a broad combined reduction peak was detected and the reduction peak was shifted towards lower temperature (196-285 ^oC) due to the strong synergetic interaction in the LDHs structure [Xia et al., (2012a)]. The hydrogen consumption and the total degree of copper metal reduction was calculated based on the TPR results obtained for all the catalysts and summarized in Table 4.5. The hydrogen consumption for Cu-Mg-Al-O catalyst prepared in presence of 1.5-2.5 (M) urea solution was almost similar (7.1-7.6 mmol $gcat^{-1}$). For the catalyst having higher copper metal loading (Cu-Mg-Al-O-4), the hydrogen consumption was maximum (11.4 mmol H_2 $gcat^{-1}$) due to the presence of more reducible copper. The hydrogen consumption was lower (5.5 mmol H_2 $gcat^{-1}$) for Cu-Zn-Mg-Al-O catalyst. The degree of reduction of all the catalysts was estimated from the difference in theoretical and experimental H_2 consumption following the relation given in Table 4.5. The total degree of reduction of all the catalyst was very high (93.1-98.6 %).

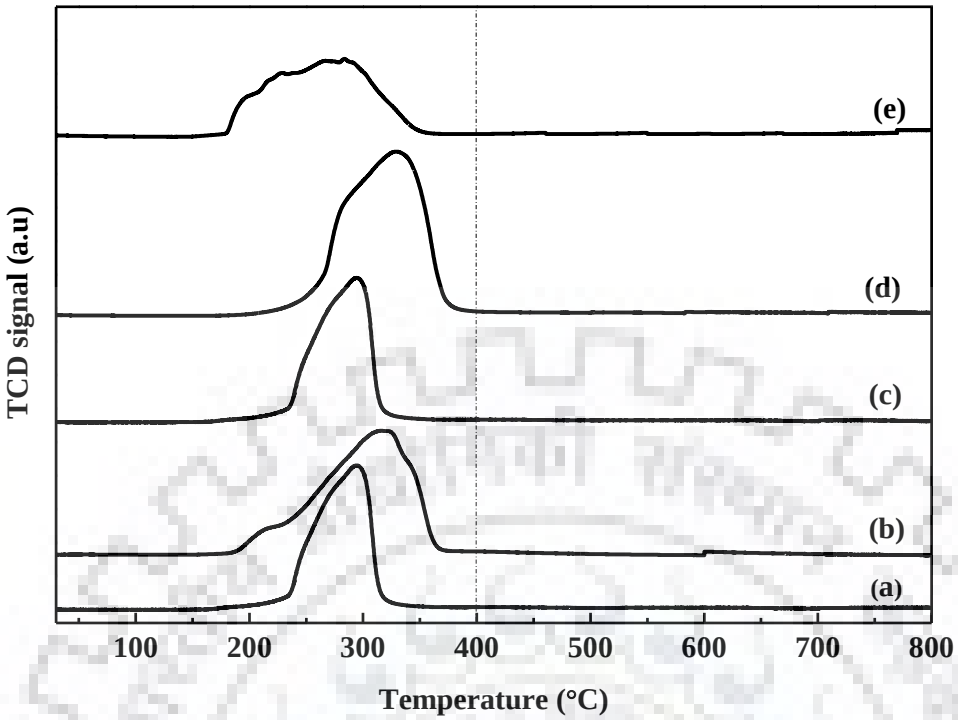

Figure 4.5. TPR patterns of fresh calcined catalysts (a) Cu-Mg-Al-O-1, (b) Cu-Mg-Al-O-2, (c) Cu-Mg-Al-O-3, (d) Cu-Mg-Al-O-4, (e) Cu-Zn-Mg-Al-O

Table 4.5. Summary of TPR and TPD results for LDHs catalyst

Catalyst	TPR results			TPD results
	Reduction peak (^oC)	H_2 consumption (mmol H_2 $gcat^{-1}$)[a #]	Degree of reduction of copper (%)[b]	Acidity (mmol NH_3 $gcat^{-1}$)[c #]
Cu-Mg-Al-O-1	294	7.1	97.3	1.8
Cu-Mg-Al-O-2	215, 318	7.6	96.9	2.6
Cu-Mg-Al-O-3	285	7.3	98.6	3.1
Cu-Mg-Al-O-4	327	11.4	95.1	2.0
Cu-Zn-Mg-Al-O	196, 231, 285	5.5	93.1	2.6

[a]Consumption of H_2 calculated from TPR peaks.

[b]Degree of reduction of copper (%) = [(experimental consumption of H_2)]/(theoretical consumption of H_2) × 100

[c]Acidity calculated from NH_3-TPD data

[#]Analytical instruments error for the active volume obtained in TPR, TPD: x ± 2%

4.2.1.4 NH_3-TPD

Surface acidity of the reduced catalysts was determined via NH_3-TPD and the obtained TPD patterns are shown in Figure 4.6. The quantitative estimation of the acidity of the catalysts is listed in Table 4.5. As shown in Figure 4.6, the acidic sites were classified into three different temperature regions, i,e. 80-300 ^oC, 300-550 ^oC and above 550 ^oC, respectively. These temperature regions were characterized by desorption of ammonia from the weak, medium and strong strength acidic sites, respectively [Pudi et al., (2015a), Pudi et al., (2015b)]. Total acidic strength was calculated based on the total amount of ammonia desorbed (mmol NH_3.$gcat^{-1}$) at different temperature regions (Table 4.5). The total acidity of the catalysts was increased from 1.8 to 3.1 mmol NH_3 $gcat^{-1}$ with increasing the urea concentration from 1.5M to 2.5M. The acidic strength of Cu-Mg-Al-O-4 and Cu-Zn-Mg-Al-O catalyst was 2.0 mmol NH_3 $gcat^{-1}$ and 2.6 mmol NH_3 $gcat^{-1}$, respectively.

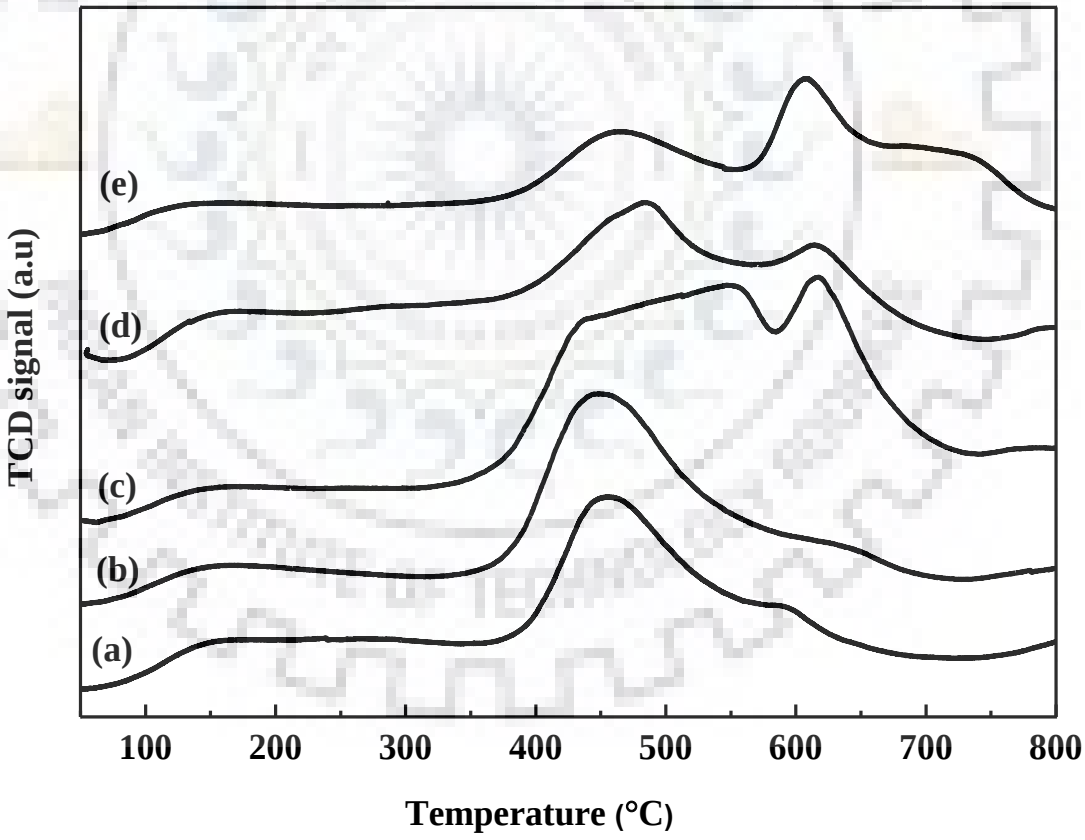

Figure 4.6. NH_3-TPD patterns of the fresh reduced catalysts: (a) Cu-Mg-Al-O-1, (b) Cu-Mg-Al-O-2, (c) Cu-Mg-Al-O-3, (d) Cu-Mg-Al-O-4, (e) Cu-Zn-Mg-Al-O

4.2.1.5 FE-SEM

Figure 4.7 [(A) to (E)] represent the FE-SEM images of the LDHs catalysts. Ball-flower shaped particles were identified in FE-SEM images of all the catalysts and a well-defined layered structure of solid lamella has also been identified in each particle under high resolution [Xia et al., (2012b)]. The FE-SEM images confirmed the formation and stability of LDHs type structure of the catalysts even after calcination and reduction.

4.2.2 Catalytic activity

The catalytic activity of all the catalysts was evaluated at a standard reaction condition which was experimentally optimized in the previous section. The conversion of glycerol and products distribution obtained over all the catalysts are shown in Table 4.6. Carbon balances of all the experiments reported in Table 4.6 were closely 100 ± 5%. Cu-Mg-Al-O-1, Cu-Mg-Al-O-2, and Cu-Mg-Al-O-3 catalysts exhibited very high glycerol conversion (85-89%) and 1,2-PDO was identified as the primary reaction product ($S_{1,2\text{-PDO}} \geq 90.2\%$). Small amounts of ethylene glycol (EG) (~5%) and other products (< 5%) such as hydroxyacetone, propanols, ethanol, and methanol were also detected. The higher glycerol conversion and 1,2-PDO selectivity was due to the presence of bi-functionality [Yuan et al., (2011)], higher acidic strength (1.8-3.1 mmol NH_3 $gcat^{-1}$) [Balaraju et al., (2008)], high hydrogen consumption (7.1-7.6 mmol H_2 $gcat^{-1}$) [Pudi et al., (2015a)], high reducibility (96.9%) and small average copper crystallite size (~16.2-24.7 nm) [Liu et al., (2014)]. As shown in Table 4.6, with increasing urea concentration from 1.5M to 2.0M during the catalyst synthesis, the conversion of glycerol increased from 85% to 89% and the selectivity of 1,2-PDO increased from 90.2% to 93.4% with a simultaneous decrease in selectivity to other products from 4.7% to 1.8%. However, further increase in urea concentration up to 2.5M, the glycerol conversion and 1,2-PDO selectivity were almost unchanged. These results suggested that higher urea concentration (>2M) for catalyst synthesis was not favourable for higher selectivity towards 1,2-PDO. Therefore, 2M urea solution was selected for the preparation of other catalysts.

To determine the effect of copper metal loading on the catalytic performance, copper wt.% in the catalyst was increased at the expense of magnesium wt.% and the resulting catalyst was designated as Cu-Mg-Al-O-4. The performance of this catalyst was also evaluated at the same reaction condition and the results obtained were compared with the other Cu-Mg-Al-O catalysts.

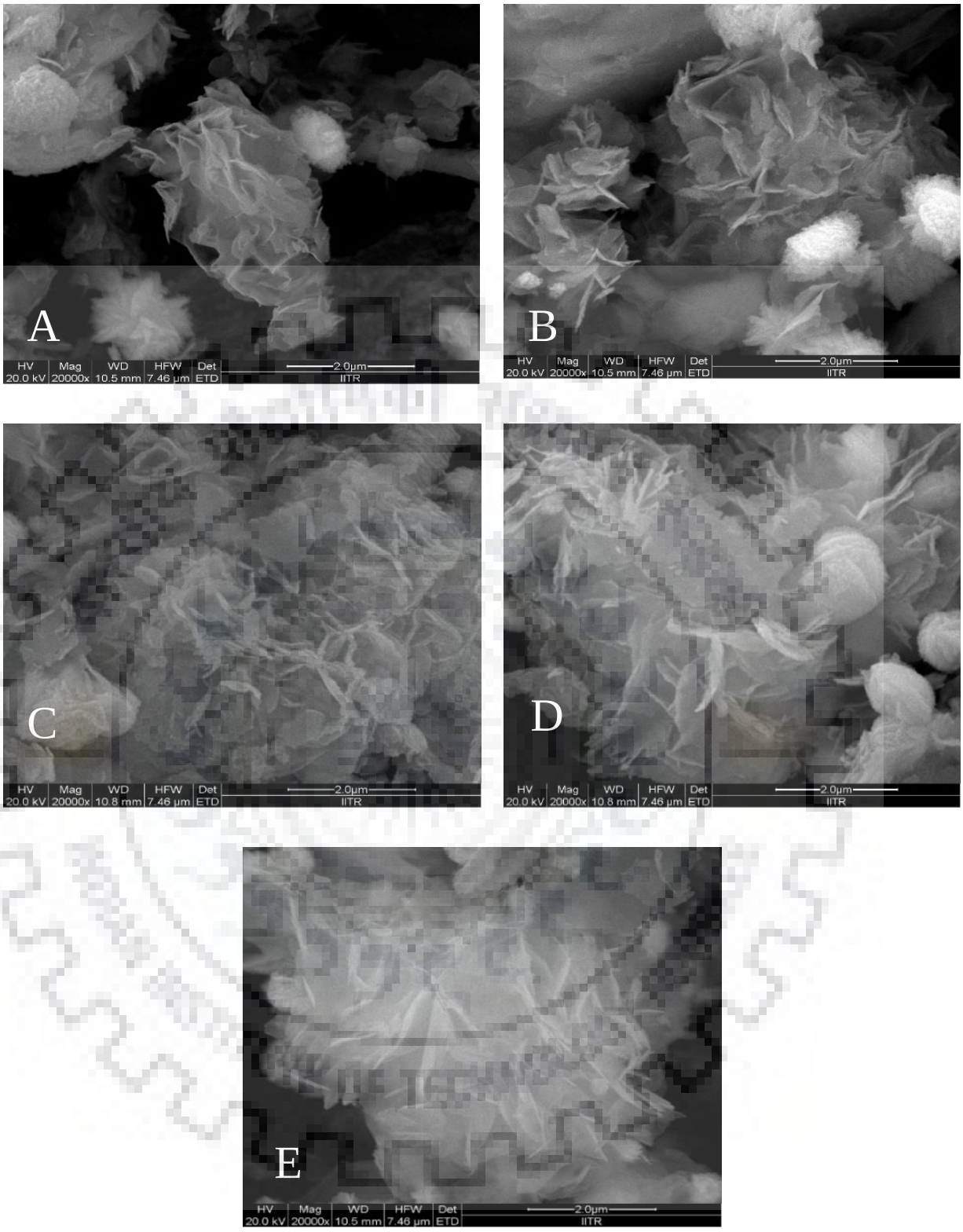

Figure 4.7. FE-SEM images of fresh reduced catalysts: (A) Cu-Mg-Al-O-1, (B) Cu-Mg-Al-O-2, (C) Cu-Mg-Al-O-3, (D) Cu-Mg-Al-O-4, (E) Cu-Zn-Mg-Al-O

The results depicted that, with increasing copper metal loading at the expense of magnesium, the glycerol conversion (88.5%) and product selectivity ($S_{1,2\text{-PDO}}$ = 94%, S_{EG} = 4.6%, S_{others} =1.4%) was not affected. To determine the effect of addition of zinc on Cu-Mg-Al-O moiety in the LDHs structure as well as catalytic performance, a small amount of zinc was added in the Cu-Mg-Al-O catalyst and the corresponding catalyst was designated as Cu-Zn-Mg-Al-O. It is interesting to note that, after the addition of small amount of zinc on the Cu-Mg-Al-O LDHs catalyst, glycerol conversion increased significantly (98.3%). The increase in glycerol conversion after the addition of Zn in the catalyst was due to the presence of strong strength acidic sites on the catalyst surface and the hydrogen spillover effect of ZnO [Xia et al., (2012), Feng et al., 2013]. As shown in Figure 4.6 (e), the presence of high-intensity peak at >550 ^{o}C for Cu-Zn-Mg-Al-O catalyst indicated the presence of strong strength acidic sites at the catalyst surface. Rode et al., (2010) reported that lewis acidic characteristics of Zn species played a key role in catalytic activity. It is also observed from Figure 4.5 that, the addition of Zn significantly lowered the reduction temperature of the catalyst. After the addition of Zn, new reducible CuO species were formed at lower reduction temperature. This enhancement of reducibility of CuO was solely responsible for increasing catalytic activity [Xia et al., (2012b)]. It was also observed that after incorporation of Zn to the catalyst, the selectivity towards 1,2-PDO was decreased by 2.5%, the selectivity to EG was increased by 2% and the selectivity to other products was almost constant (1.4%). However, the overall yield of 1,2-PDO was increased significantly i.e. from 83% to 90%. The increase in catalytic activity after the addition of zinc in the LDHs catalyst $Cu_{0.4}/Zn_{5.6x}Mg_xAl_2O_{8.6}$ is also reported in the previous literature [Xia et al., (2012b)]. Addition of zinc might increase the activity of H_2 on the surface of the catalyst by hydrogen spillover effect of ZnO which enhanced the catalytic activity.

It can be seen from Figure 4.6, with increasing urea concentration from 1.5M to 2M, the intensity of the peak corresponding to the moderate acidic sites strength of the catalysts was increased. As a result, the surface acidity of the catalyst was increased from 1.8 to 2.6 mmol NH_3 $gcat^{-1}$ (Table 4.5). This increase in acidity on the catalyst surface enhanced the glycerol conversion from 85.1% to 88.9%. Further increasing the urea concentration up to 2.5M during catalyst synthesis, in addition to the peak corresponding to the moderate acidic sites strength of the catalysts, the peaks corresponding to the strong acidic sites strength were also detected (Figure 4.6 (c)). Therefore, the total surface acidity of this catalyst (Cu-Mg-Al-O-3) was further increased to 3.1 mmol NH_3 $gcat^{-1}$ (Table 4.5). Although the acidity was increased for Cu-Mg-Al-O-3 catalyst, the glycerol conversion was almost unaffected (~ 88.5%). These results

indicated that optimum concentration of acidity on the catalyst surface is essential for higher glycerol conversion. Further, Cu-Mg-Al-O-4 catalyst was synthesized in presence of 2M urea solution and copper wt.% in the catalyst was increased at the expense of magnesium wt. % with respect to the Cu-Mg-Al-O-2 catalyst. The acidity (2.0 mmol. $gcat^{-1}$) of Cu-Mg-Al-O-4 catalyst was slightly lower than the acidity (2.6 mmol. $gcat^{-1}$) of the Cu-Mg-Al-O-2 catalyst. For these two catalysts, the glycerol conversion was almost similar (~88.5 %) and selectivity towards 1,2-PDO was slightly (~1%) increased for Cu-Mg-Al-O-4 catalyst due to the presence of higher copper metal [Feng et al., (2013)]. The acidity value was not affected the glycerol conversion obtained over Cu-Mg-Al-O-4 catalyst may be because of the value was within the optimum concentration of the acidic sites on the catalyst surface. For zinc loaded catalyst (Cu-Zn-Mg-Al-O), the acidity was further increased to ~2.6 mmol. $gcat^{-1}$ which was similar to the value obtained for Cu-Mg-Al-O-2 catalyst. Although the acidity value was almost similar, the glycerol conversion was increased by ~10% for Cu-Zn-Mg-Al-O catalyst due to the presence of strong strength acidic sites on the catalyst surface and the hydrogen spillover effect of ZnO [Feng et al., (2013)]. After the addition of Zn, new reducible CuO species were formed at lower reduction temperature. This enhancement of reducibility of CuO was solely responsible for increasing catalytic activity [Xia et al., (2012b)]. To verify the role of copper, the catalytic activity of copper-free catalyst (Zn-Mg-Al-O) was also evaluated. Results demonstrated that in absence of copper the catalytic activity was very low (Table 4.6).

The products distribution obtained over various copper, magnesium and aluminum-based catalyst suggested that hydrogenolysis process primarily followed two steps process. Initially, hydroxyacetone was formed as an intermediate via dehydration of glycerol over the acidic and/or basic sites of the catalyst. In the second step, hydroxyacetone further hydrogenates over active metal sites and produced 1,2-PDO. EG and other products formed due to the over hydrogenolysis of glycerol, hydroxyacetone and 1,2-PDO, respectively [Pudi et al., (2015a), Dasari et al., (2005), Vasiliadou et al., (2011), Nakagawa et al., (2011)]. It is also known that the products selectivity is a strong function of nature of the catalyst as well as the reaction condition. Over Cu-Mg-Al-O-2 catalyst, the selectivity towards 1,2-PDO was highest (93.4%), EG selectivity was ~5% and other products selectivity was 1.5%. These results suggested that Cu-Mg-Al-O-2 catalyst favoured the selective breakage of C-O bond by suppressing the breakage of C-C bond of glycerol which produced very high selectivity towards 1,2-PDO, and formed very small amount of degradation products (1.5%). EG was formed via dehydration of glycerol [Xia et al., (2013), Yuan et al., (2011)]. In presence of Cu-

Zn-Mg-Al-O catalyst, the conversion of glycerol increased whereas the selectivity towards 1,2-PDO decreased with simultaneous increase in selectivity to EG by keeping the selectivity to other products almost constant. These results demonstrated that the addition of zinc favoured direct conversion of glycerol to EG through dehydration step [Rode et al., (2010)].

Table 4.6. Conversion and product selectivity obtained over LDHs catalysts

Catalyst	Urea Concentration (M)	Base additives	Conversion (%)	Selectivity (%)			1,2-PDO yield (%)
				1,2-PDO	EG	Others*	
Cu-Mg-Al-O-1	1.5	-	85.1	90.2	5.1	4.7	76.7
Cu-Mg-Al-O-2	2.0	-	88.9	93.4	4.8	1.8	83.1
Cu-Mg-Al-O-3	2.5	-	88.5	93.5	4.7	1.8	82.7
Cu-Mg-Al-O-4	2.0	-	88.5	94.0	4.6	1.4	83.2
Cu-Zn-Mg-Al-O	2.0	-	98.3	91.5	7.1	1.4	90.0
Zn-Mg-Al-O	2.0		2.9	59.2	29.2	11.6	17.1
		NaOH (1g)	98.4	94.3	3.7	2.0	92.8
		KOH (1g)	95.1	93.2	3.9	2.9	88.6
		$Ca(OH)_2$ (1g)	94.7	93.1	3.7	3.2	88.1

Reaction conditions: 20 wt.% glycerol (20 g), 7.5 wt.% catalyst with respect to glycerol, 800 rpm, 210 ^{o}C, 4.5 MPa pressure, 12 h reaction time.
*Others: hydroxyacetone, 1-propanol, 2-propanol, ethanol and methanol.
Experimental errors for all the values (conversion, selectivity and yield) : x ± 1 %

The reduction of 1,2-PDO selectivity after the addition of zinc was also observed previously [Xia et al., (2011), Rode et al., (2010)]. The effect of the addition of different bases such as NaOH, KOH and $Ca(OH)_2$ on the conversion of glycerol and product selectivity was investigated over Cu-Zn-Mg-Al-O catalyst. Results obtained showed that the addition of 1 g of

NaOH in the 100 g of reaction mixture (1 (wt./wt.) %), the conversion of glycerol was unaffected. However, the selectivity towards 1,2-PDO was increased to 94.3% at the expense of EG. This result suggested that selective conversion of glycerol to 1,2-PDO by following dehydration followed by hydrogenation step was favoured in presence of suitable basic environment in the reaction mixture. Addition of base also reduced the formation of degradation products due to the C-C bond cleavage of glycerol. The addition of other bases was not very effective [Yadav et al., (2012)].

4.2.3 Parameter studies

4.2.3.1 Effect of temperature

As expected, the glycerol conversion increased from 93.4% to 99.1% as the temperature increased from 190 ºC to 220 ºC (Figure 4.8 (A)). The selectivity towards 1,2-PDO increased initially from 92.4% at 190 °C to 94.3% at 210 °C and further it slightly decreased to 92% at 220 °C. However, the selectivity to EG was ~4% up to 210 ºC, thereafter it increased to 5.2% at 220 °C. At higher temperature (> 210 ºC), selectivity towards 1,2-PDO decreased slightly while selectivity to EG and other degradation products increased. This results suggested that, at higher temperature, 1,2-PDO was further hydrogenolysed to degradation products and also at higher temperature, the breakage of C-C bond of glycerol molecule predominated which resulted in the higher selectivity to EG, propanols and lower alcohols [Dasari et al., (2005), Balaraju et al., (2012)].

4.2.3.2 Effect of pressure

Influence of pressure (3.5-5 MPa) on glycerol conversion and product selectivity in presence is shown in Figure 4.8 (B). Glycerol conversion increased from 95% to 99.3% with increasing the pressure from 3.5 MPa to 5 MPa. The selectivity towards 1,2-PDO passed through a maxima. It increased from 92.5% at 3.5 MPa to 94.3% at 4.5 MPa and further it decreased to 92.6% at 5 MPa. Initially, with increasing pressure, the solubility of hydrogen in the reaction mixture increased which enhanced selective hydrogenation of glycerol to 1,2-PDO. At pressure higher than 4.5 MPa, selectivity towards 1,2-PDO decreased due to the formation of degradation products [Pudi et al., (2015), Sharma et al., (2014), Guo et al., (2009)].

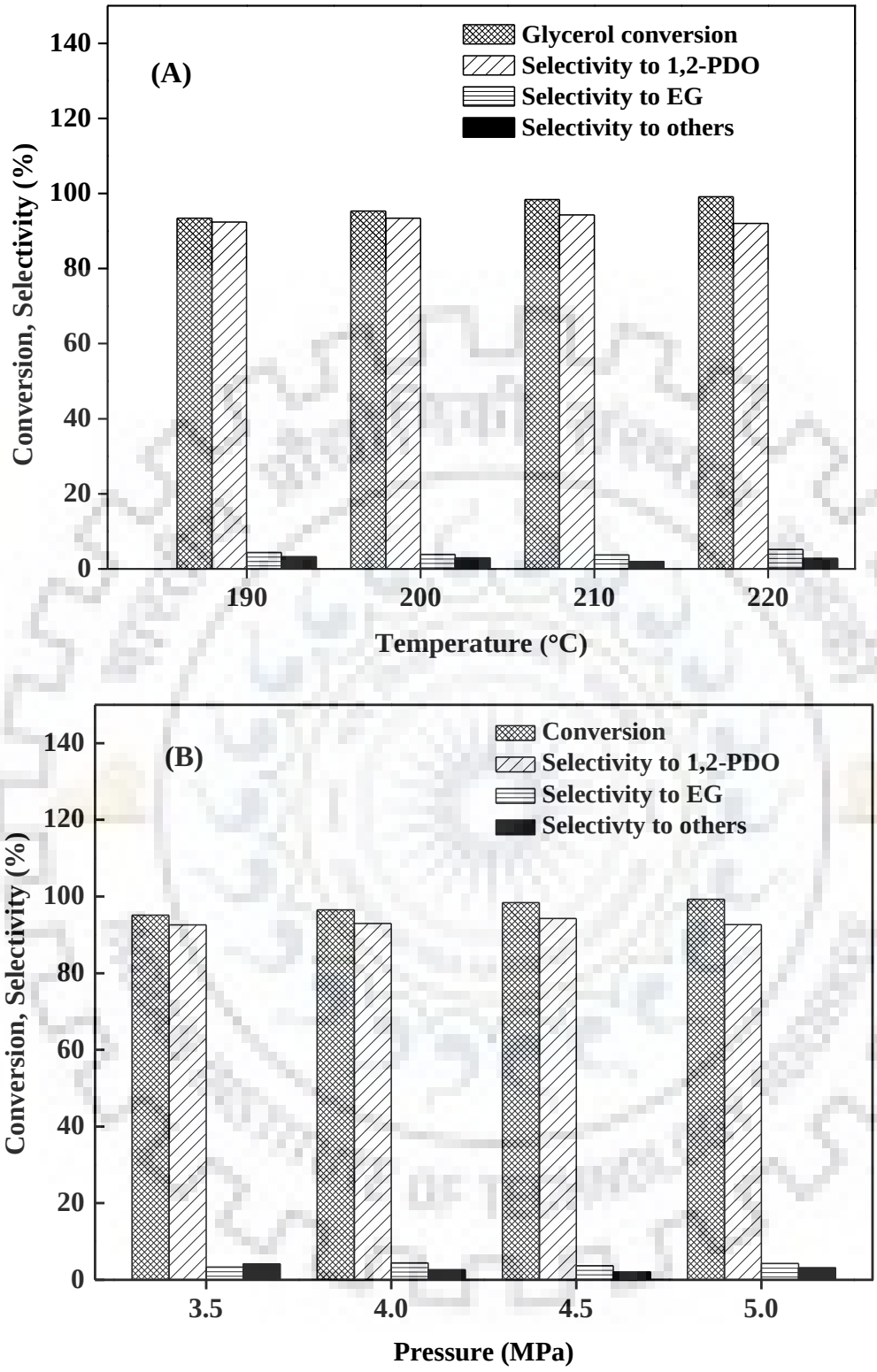

Figure 4.8. Effect of reaction parameters on glycerol conversion, and product selectivity (A) Effect of temperature, Reaction condition: 4.5 MPa pressure, 12 h, 7.5% of catalyst weight with respect to glycerol, 20 wt.% glycerol (20 g), 800 rpm (B) Effect of pressure: Reaction condition: 210 ^{o}C, 12 h, 7.5% of catalyst weight with respect to glycerol, 20 wt.% glycerol (20 g), 800 rpm.

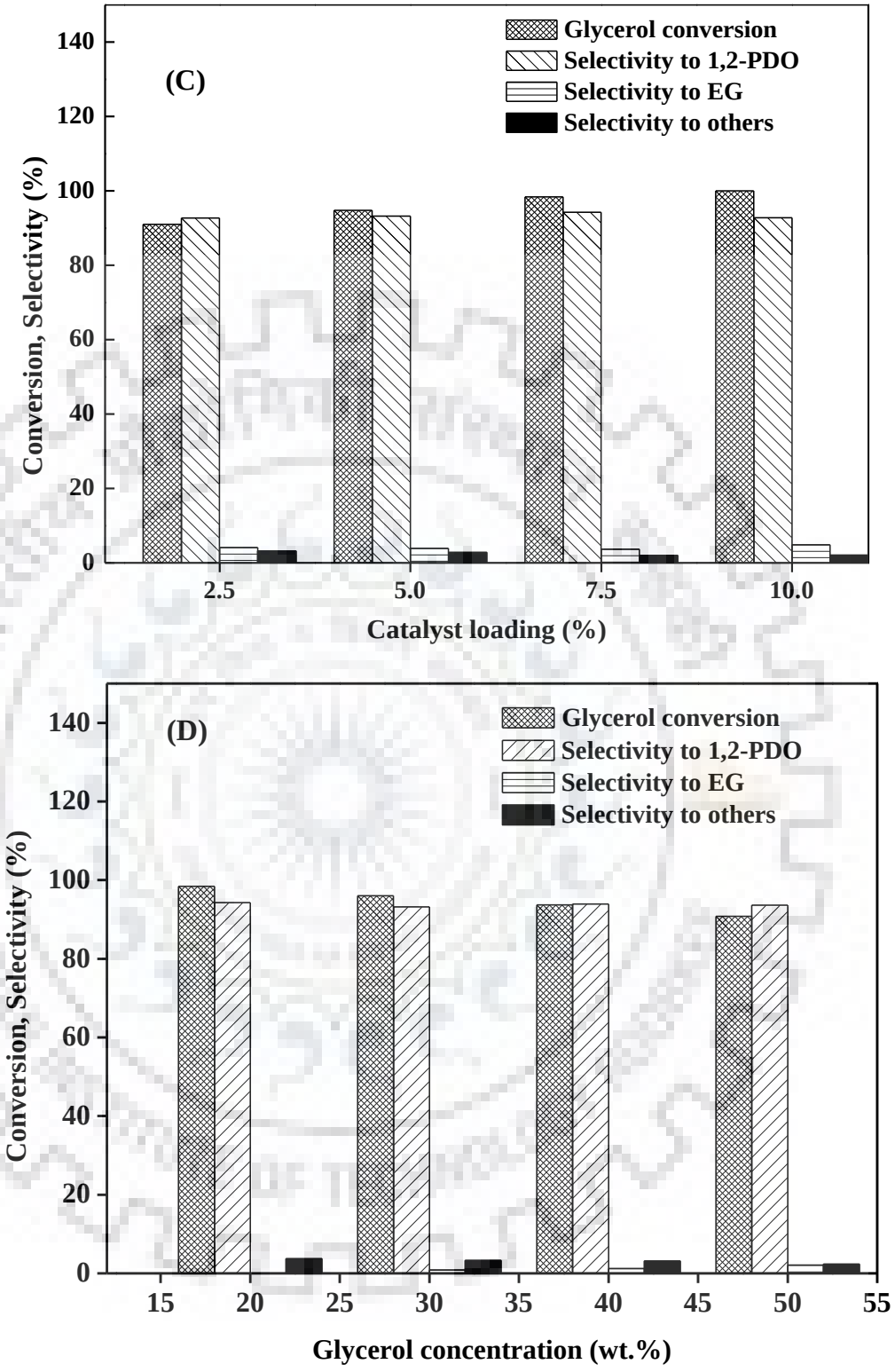

Figure 4.8. Effect of reaction parameters on glycerol conversion, and product selectivity (C) Effect of catalyst loading: Reaction condition: 210 ^{o}C, 4.5 MPa, 12 h, 20 wt.% glycerol (20 g), 800 rpm. (D) Effect of glycerol concentration: Reaction condition: 210 ^{o}C, 4.5 MPa pressure, 12 h, 7.5% of catalyst weight with respect to glycerol, 800 rpm.

4.2.3.3 Effect of catalyst loading

As expected, conversion of glycerol increased from 91% to 100% when catalyst loading was increased from 2.5 wt.% to 10 wt.% (Figure 4.8 (C)). The conversion was increased due to increasing the concentration of the active sites in the reaction mixture with increasing the catalyst amount. However, the selectivity towards 1,2-PDO decreased marginally (~ 1.5 %) at highest catalyst loading (10 wt.%), which was may be due to the over hydrogenolysis of glycerol and 1,2-PDO to other linear alcohols such as methanol, ethanol, 1-propanol and 2-propanol [Meher et al., (2009), Miyazawa et al., (2006)]. Moreover, the overall yield of 1,2-PDO increased with increasing the catalyst loading and achieved ~93% in presence of 7.5 wt.% catalyst loading and higher. These results demonstrated that 7.5 wt.% catalyst loading was optimum for maximum yield (~93%) of 1,2-PDO at 210 ^{o}C, and 4.5 MPa pressure in presence of 20 wt.% glycerol as feed.

4.2.3.4 Effect of glycerol concentration

As shown in Figure 4.8 (D), with increasing glycerol concentration from 20 to 50 wt.%, glycerol conversion was decreased by ~8% because of the availability of a limited number of metallic sites in the reaction mixture [Miyazawa et al., (2007), Feng et al., (2008)] and the solution viscosity which might enhance the mass transfer resistance. The selectivity towards 1,2-PDO decreased marginally (94-94%). Whereas, the selectivity to hydroxyacetone and ethylene glycol increased to ~2.1% and ~2.3%, respectively. These results suggested that, for higher selectivity towards 1,2-PDO, lower glycerol (~20 wt.%) concentration was beneficial.

4.2.4 Comparison of performance of Cu-Zn-Al-Mg-O catalyst with previous reported LDHs catalysts

The performance of LDHs catalyst for hydrogenolysis of glycerol is very limited [Xia et al., (2012b), Xia et al., (2013), Yuan et al., (2011), Meher et al., (2009)]. Xia et al., (2012a) reported maximum glycerol conversion of 91% with 98.7% selectivity towards 1,2-PDO at 180 ^{o}C and 2 MPa pressure when 75 wt.% glycerol was used as feed. In this study, the catalyst concentration used was very high (12.5 wt.%). Meher at al., (2009) reported the performance of Cu/Zn/Al mixed metal oxide derived from a hydrotalcite precursors and showed maximum glycerol conversion of 52% with 93-94% selectivity towards 1,2-PDO in presence of 80 wt.% aqueous glycerol concentration at 200 ^{o}C and at 1.36 MPa pressure. In their study, 5 wt.% catalyst loading was used and the reaction data was collected after a longer period of reaction

time (24 h). In comparison with the previous results reported, in this study, the glycerol conversion and 1,2-PDO selectivity obtained was significantly high. Maximum 98.4% glycerol conversion with 94.3% selectivity towards 1,2-PDO was observed after 12 h of reaction at 210 °C temperature, 4.5 MPa pressure when 20 wt.% glycerol concentration and 7.5% catalyst loading was used. The effect of glycerol concentration on conversion and 1,2-PDO selectivity results suggested that Cu-Zn-Mg-Al-O catalyst developed in this study was very active even in presence of very higher concentration (50 wt.%) of glycerol. Higher than 90% conversion with very high selectivity towards 1,2-PDO (> 93%) was obtained when 50 wt.% of glycerol was used as a feed (Figure 4.8). The experimental results reported in this study demonstrated that Cu-Zn-Mg-Al-O LDHs catalyst was very active and selective to 1,2-PDO in presence of wide range of glycerol concentration (20-50 wt.%) as a feed. Therefore, the Cu-Zn-Mg-Al-O LDHs catalyst developed in this study is efficient and showed better performance in comparison to the LDHs catalysts reported in the literature.

4.2.5 Catalyst reusability

Reusability of the catalyst is very important for an industrial application. Previous literature reported non-noble metal (Cu, Co and Ni) based LDHs catalyst undergoes a serious deactivation problem in hydrogenolysis of glycerol due to the damaging of LDHs structure of catalyst during recycling and reactivation process [Meher et al., (2009), Montassier et al., (1995), Vasiliadou et al., (2011)]. To verify the stability and reusability of Cu-Zn-Mg-Al-O LDH catalyst, a series of recycle experiments were performed at the optimum reaction condition. After each experiment, the used catalyst was recovered by filtration followed by drying at 120 ^{o}C for 12 h. In each recycle experiment there was a loss in the weight of the catalyst particles. Therefore, to verify the reusability of the catalyst, the constant catalyst to glycerol ratio was maintained in each recycle batch [Sharma et al., (2014), Vasiliadou et al., (2011)]. Prior to each experiment, used Cu-Zn-Mg-Al-O catalyst was reactivated in a tubular reactor under hydrogen flow at 400 ^{o}C for 2 h. As shown in Table 4.7, after 1st recycle, glycerol conversion was decreased from 98.4% to 70% i,e. nearly (1/3rd) catalytic activity was lost. The glycerol conversion was decreased severely to 30% after cycle-3. It is very interesting to note that, although the catalyst activity was decreased significantly, the selectivity of 1,2-PDO was almost unchanged (~95%).

Table 4.7. Glycerol conversion and product selectivity obtained over Cu-Zn-Mg-Al-O catalyst and average copper crystallite size in the catalyst in successive cycles

No. of cycle	Glycerol conversion (%)	Product selectivity (%)			1,2-PDO yield (%)	Average copper crystallite size[a] (nm)	Cu wt.(%)[b]
		1,2-PDO	EG	Others*			
Fresh catalyst	98.4	94.3	3.7	2.0	92.7	21.6	35.7
1st reuse	70.0	94.9	2.4	2.7	66.4	34.6	33.7
2nd reuse	54.5	95.8	1.2	3.0	52.2	35.3	32.6
3rd reuse	30.0	96.4	1.1	2.5	28.9	46.9	30.3

Reaction conditions: 20 wt.% glycerol (20 g), 7.5% catalyst weight with respect to glycerol, 800 rpm, 210 ^{o}C, 4.5 MPa pressure, 12 h.
*Others: Hydroxyacetone, 1-propanol, 2-propanol, ethanol and methanol.
[a]Calculated by using Scherrer's formula.
[b]Obtained from XRF data
Experimental errors for the values (conversion, selectivity and yield) : x ± 1%

To understand the reason for deactivation of the catalyst, the used catalyst was characterized by FE-SEM, TEM, and XRD, respectively.FE-SEM images of the used catalyst (Figure 4.9) showed that the well-developed lamella-like structure of the fresh Cu-Zn-Mg-Al-O catalyst was destroyed in successive recycles due to repetitive reactivation of catalyst via reduction at 400 ^{o}C for 2 h before each cycle. XRD pattern of fresh and used catalysts was compared (Figure 4.10). The XRD profile of the used catalyst showed highly crystalline diffraction patterns of copper metal. In addition to the peaks corresponding to copper metal detected for fresh reduced catalyst (Figure 4.10 (a)), additional peaks at $2\theta = 31.7^{o}$ corresponding to the diffraction of (100) crystal plane of ZnO (JCPDS: 80-0075) and at $2\theta = 36.9^{o}$ corresponding to the diffraction pattern of (111) crystal plane of MgO phase (JCPDS:78-0430) became very prominent. XRD pattern of the used catalyst also indicated the variation in metal interaction in the catalyst due to the agglomeration of particles which is in agreement with the FE-SEM micrograph.

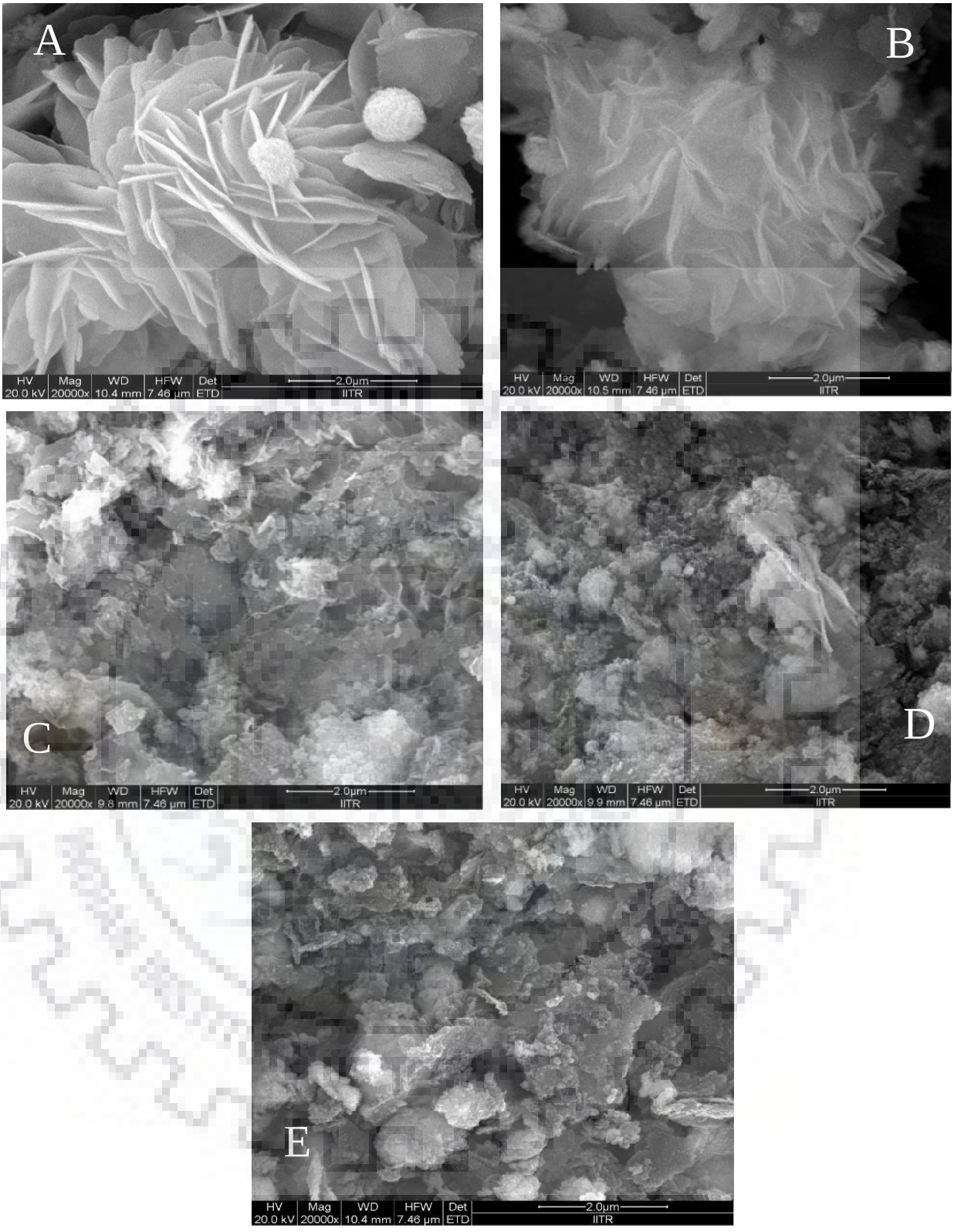

Figure 4.9. FE-SEM micrographs of fresh and used catalysts (A) fresh dried, (B) fresh reduced, (C) after cycle-1, (D) after cycle-2 and (E) after cycle-3

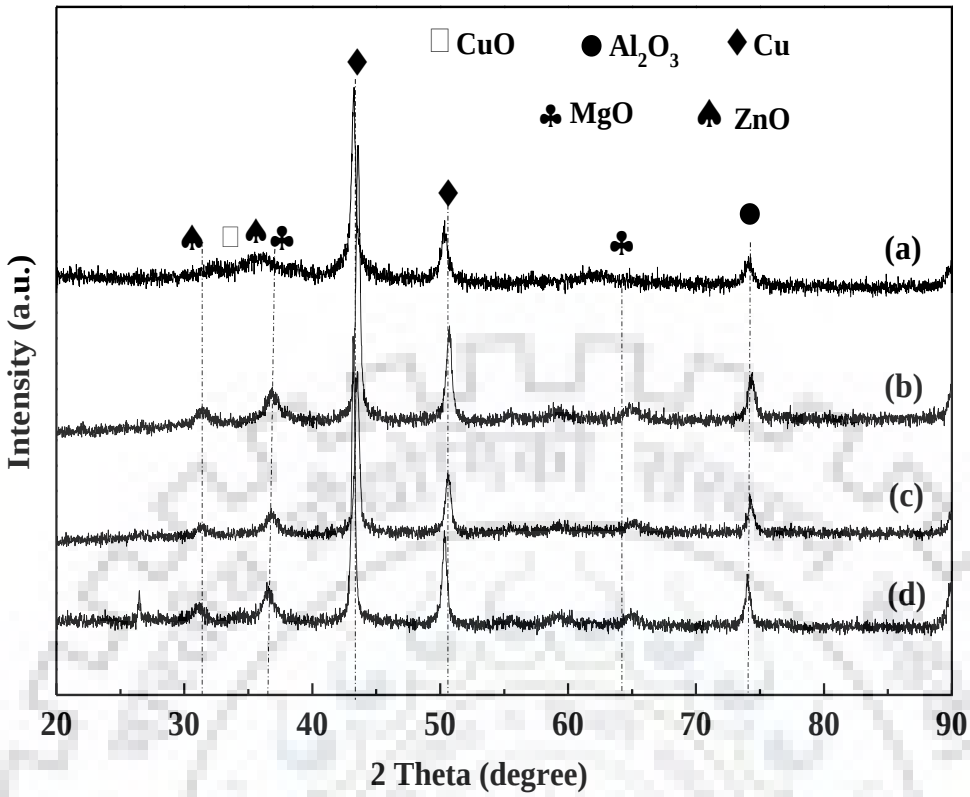

Figure 4.10. XRD pattern of fresh and used Cu-Zn-Mg-Al-O catalysts (a) fresh reduced, (b) after cycle-1, (c) after cycle-2 and (d) after cycle-3

The copper crystallite size of the used catalyst after each cycle was calculated by using Scherrer's equation. The result showed that the copper crystallite size was increased from 21.6 nm to 46.9 nm after cycle-3 due to agglomeration. Similar kind of results were also observed in the previous reports [Yun et al., (2014), Huang et al., (2012)]. X-ray fluorescence (XRF) data disclosed the elemental composition of fresh and used catalysts (Table 4.7). It was observed that Cu content was slightly decreased (~5%) after cycle-3. TEM images and corresponding metal particle size histogram of fresh reduced and used catalyst (Figure 4.11) suggested agglomeration of the particle after 3rd cycle. Average mean catalyst particles size was increased from 31.4 nm to 46.1 nm which is in agreement with the XRD results.

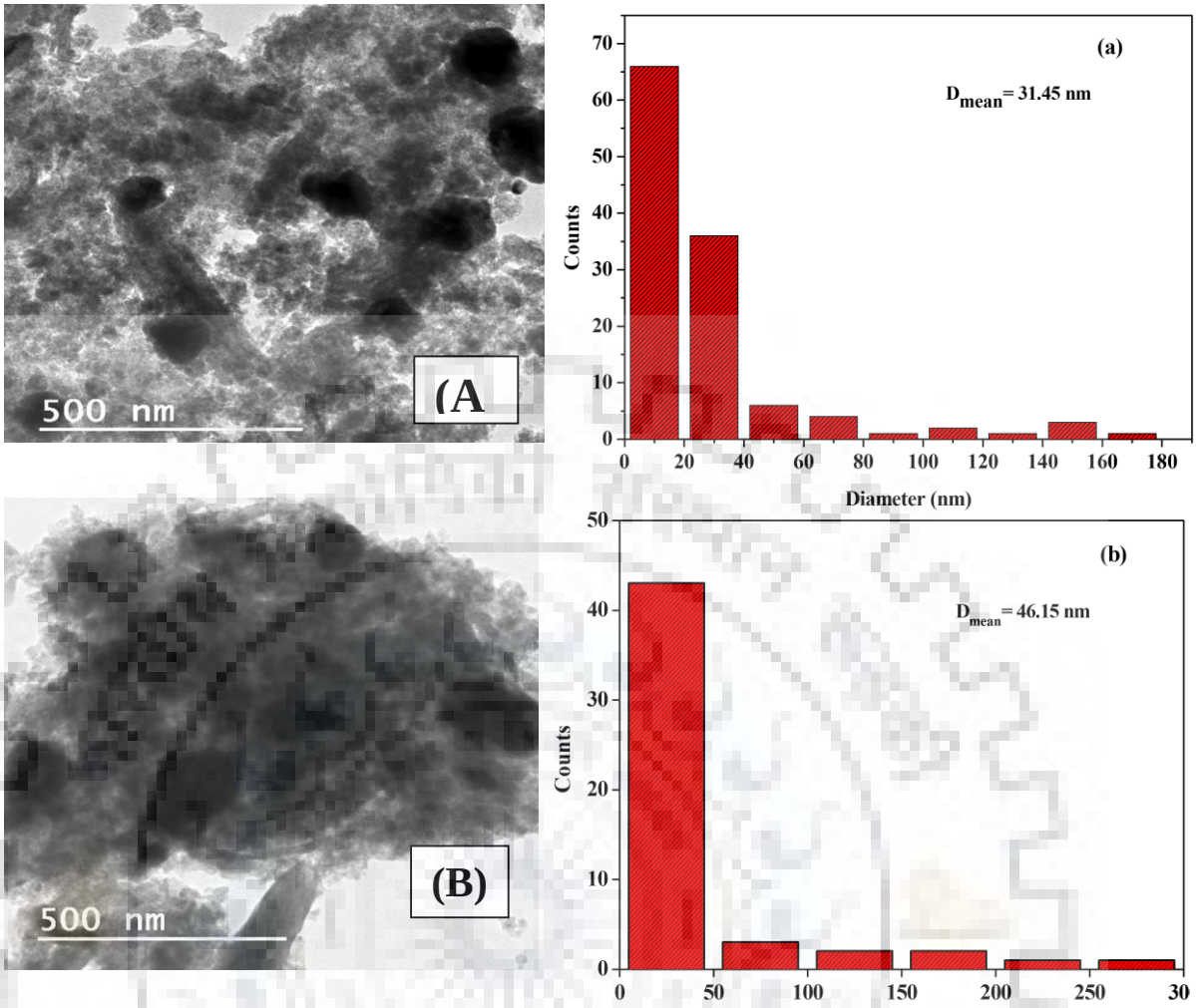

Figure 4.11. TEM micrograph and corresponding metal particle size histogram: [(A) and (a)] fresh reduced Cu-Zn-Mg-Al-O catalyst; [(B) and (b)] Cu-Zn-Mg-Al-O catalyst after cycle-3

4.2.6 Summary

In this study, highly active Cu-Mg-Al-O based LDHs catalysts were synthesized by homogenous urea hydrolysis method. Ball-flower shaped particles were identified for all the catalysts and a well-defined layered structure of solid lamella has also been identified. The characterization results confirmed the formation and stability of LDHs type structure of the catalysts even after calcination and reduction. Effects of urea concentration on the physico-chemical properties as well as catalytic performance were evaluated for liquid phase hydrogenolysis of glycerol to 1,2-PDO. Results demonstrated that the catalysts synthesized in presence of 2M urea showed best catalytic activity due to the presence of optimum acidity, small copper crystallite size, and well developed curved lamellae structure. Higher urea

concentration (> 2M) for catalyst synthesis was not beneficial for higher selectivity towards 1,2-PDO. In order to improve the catalytic activity and 1,2-PDO selectivity, zinc was incorporated in Cu-Mg-Al-O catalyst. Catalyst characterization results suggested that ZnO helped to reduce the reduction temperature of the catalyst by hydrogen spillover effect of ZnO to copper metal. In presence of Cu-Zn-Mg-Al-O catalyst, the conversion of glycerol was increased whereas the selectivity towards 1,2-PDO was decreased with simultaneous increase in selectivity to EG by keeping the selectivity to other products almost constant. These results demonstrated that the addition of zinc favoured direct conversion of glycerol to EG through dehydration step. Addition of zinc might increase the activity of H_2 on the surface of the catalyst by hydrogen spillover effect of ZnO which enhanced the catalytic activity. The highest 94.3% selectivity towards 1,2-PDO at 98.4% glycerol conversion was achieved over Cu-Zn-Mg-Al-O-3 catalyst at 210 ^{o}C and at 4.5 MPa pressure when 20 wt.% glycerol was used as feed. The reaction was carried out up to 12 h in the presence of 1g of NaOH. Effect of addition of different bases such as NaOH, KOH and $Ca(OH)_2$ on glycerol conversion and product selectivity over Cu-Zn-Mg-Al-O catalyst were also studied. Results showed that addition of 1 g of NaOH in the reaction mixture increased the selectivity towards 1,2-PDO to 94.3% at the expense of EG. The addition of other bases was not very effective. Effect of glycerol concentration in the feed revealed that increasing glycerol concentration from 20% to 30%, the variation in glycerol conversion and selectivity towards 1,2-PDO was insignificant. However, at higher glycerol concentration (>30%), the conversion was dropped by ~7%. The product distribution obtained over Cu-Zn-Mg-Al-O catalyst suggested that glycerol was converted to 1,2-PDO selectively by dehydration followed by hydrogenation step in presence of suitable basic environment in the reaction mixture. Addition of base also reduced the formation of degradation products due to the cleavage of C-C bond of glycerol. Catalyst reusability results revealed that conversion of glycerol decreased significantly due to structural changes of the catalyst after successive reuse and sintering of copper and ZnO species during the reaction. However, the selectivity to 1,2-PDO was increased from 94.3% to 96.3% at the expense of EG after 3rd cycle.

4.3 Selective hydrogenolysis of glycerol to 1,2-PDO over MgO supported catalysts

It was observed from the previous section (4.2) that LDHs type catalysts were highly active and selective for glycerol hydrogenolysis to 1,2-PDO. However, the catalyst was severely deactivated after successive reuses. In further study, MgO supported monometallic and bimetallic catalysts were developed by co-precipitation method and their activity is discussed. In preliminary catalyst screening study, a series of monometallic (Cu, Co, Zn and Fe) catalysts supported on MgO with 35% metal loading were synthesized and their performance for liquid phase hydrogenolysis of glycerol was evaluated (Table 4.8).

Table 4.8. Screening of catalysts

Catalyst	Conversion (%)	Selectivity (%)		
		1,2-PDO	EG	Others*
35% Cu/MgO	96.4	92.0	6	2
35% Co/MgO	79.7	72.8	13.9	13.4
35% Zn/MgO	11.6	100	0	0
35% Fe/MgO	2.5	100	0	0

Reaction condition: 20 wt.% glycerol (20 g), catalyst: 1.6 g, temperature: 210 ^{o}C, H_2 pressure: 4.5 MPa, speed of agitation: 700 rpm, time: 12 h

*Others: hydroxyacetone, 1-PO, 2-PO, ethanol, and methanol

Experimental errors for all the values (conversion, selectivity and yield) : x ± 1 %

The obtained results demonstrated that the catalytic activity followed the order: Cu > Co > Zn > Fe. Cu and Co exhibited best catalytic activity and Zn and Fe were less active although the selectivity towards 1,2-PDO was ~100% over Zn and Fe based catalyst. It was also found that 35% Cu/MgO catalyst exhibited 96.6% conversion with 92.6% selectivity towards 1,2-PDO at 210 °C, 4.5 MPa pressure after 12 h of reaction. It was observed from our earlier study that presence of acidity and basicity, bi-functional nature, high metallic surface area (4.4 $m^2.g^{-1}$), lower copper crystallite size (~28 nm) were the main reasons behind the high catalytic activity and 1,2-PDO selectivity [Pudi et al., (2015)]. Therefore, in further study, Zn

and Fe were incorporated with Cu and Co to increase the overall selectivity and/or yield of 1,2-PDO. A series of MgO supported bimetallic catalysts were developed by co-precipitation method and their performance was assessed. The primary emphasis was given to optimizing the reaction parameters to maximize glycerol conversion and 1,2-PDO yield, catalyst stability, and reusability. Among all the catalysts tested, bimetallic 50wt.% Cu:Zn(4:1)/MgO catalyst showed almost complete conversion with very high selectivity (~94%) to 1,2-PDO under mild reaction condition. A number of experiments were also performed in the presence of various reaction intermediates to establish the reaction mechanism for the hydrogenolysis of glycerol and a possible reaction path of the formation of 1,2-PDO is proposed over the Cu:Zn(4:1)/MgO catalyst. Catalytic stability and reusability test was also performed.

4.3.1 Catalyst characterization

4.3.1.1 Textural properties

The specific surface area (S_{BET}), and cumulative pore volume (V_p) of MgO support and reduced catalysts are listed in Table 4.9. The specific surface area of MgO support was 92 $m^2.g^{-1}$ and after the inclusion of Cu and Zn metal precursors, the specific surface area of the catalysts decreased significantly (17-37 $m^2.g^{-1}$) due to the coverage of metals over MgO support as well as the formation of metal clusters [Yuan et al., (2010), Pudi et al., (2015)]. The pore volume of the catalysts was in the range of 0.01-0.18 $cm^3.g^{-1}$.

4.3.1.2 XRD

The XRD pattern of the calcined catalysts is shown in Figure 4.12 (A). Diffraction peaks [4.12 (A) (h)] corresponding to MgO were obtained at the 2θ values of 36.9°, 42.8°, 62.2°, 74.6°, respectively, corresponding to the (111), (200), (220), (311) crystal planes of the cubic MgO phase, respectively (JCPDS: 78-0430). However, after the inclusion of CuO [4.12 (A) (a)], additional peaks corresponding to CuO were detected at the 2θ values of 35.5°, 38.8°, 48.6°, 58.3°, 66.1°, and 68.0° corresponding to (002), (111), (202), (202), (311), and (220) crystal planes of monoclinic CuO phase, respectively (JCPDS: 80-1987) [Pudi et al., (2015a)]. For Zn/MgO catalyst [4.12 (A) (b)], the diffraction peaks at 31.7°, 34.5°, 47.7° and 56.5° were ascribed the presence of hexagonal ZnO phase corresponding to (100), (002), (110) and (101) crystal planes, respectively (JCPDS: 80-0075). Crystalline Co_3O_4 phase corresponding to (311) crystal plane was detected at the 2θ values of 36.8° (JCPDS: 781970) for Co:Fe(1:1)/MgO catalyst [4.12 (A) (g)]. The diffraction peaks corresponding to iron oxides were not detected for

iron doped catalysts. The XRD patterns of reduced catalysts were quite similar to calcined catalysts [Figure 4.12 (B)]. For copper-based catalyst, additional diffraction peaks corresponding to metallic copper were detected at the 2θ angle of 43.3°, 50.4° and 74.1° corresponding to (111), (200) and (220) crystal planes, respectively (JCPDS: 85-1326). In the reduced cobalt catalyst, the diffraction peaks corresponding to metallic cobalt was absent indicated dispersion of cobalt phase [Guo et al., (2009)]. For iron-based reduced catalyst, very low-intensity diffraction peaks corresponding to iron crystallite was detected at the 2θ angle of 44.6° (JCPDS: 85-1410).

The average crystallite size of metals and their oxides of both calcined and reduced catalysts are reported in Table 4.9. For calcined catalyst, the average crystallite size of CuO was calculated from the peaks corresponding to (002), (111), (202), (311) and (220) crystal planes, respectively. The calculated size of CuO crystallite was in the range of 20.1-36.6 nm. The average crystallite size of ZnO calculated from the line width of (100), (002), (110) and (101) crystal planes was in the range of 30-40.8 nm. For Co_3O_4, the average crystallite size was in the range of 22.4-28.9 nm calculated from the line width of (311) crystal plane of the XRD pattern of the respective catalysts. For reduced catalysts, the average copper crystallite size was in the range of 37.1-43.9 nm. The average crystallite size of Fe^o was higher (55.3-59.6 nm).

4.3.1.3 H_2-TPR

The reduction behaviour of the catalysts is shown in Figure 4.13. As shown in Figure 4.13 (h), MgO was not reduced in the temperature range of 40-800 °C [Mirzaei et al., (2015)]. However, Cu/MgO catalyst showed a single major reduction peak at 294 °C which attributed to the direct reduction of CuO to Cu^o [Pudi et al., (2015a), Kim et al., (2003)]. For Zn/MgO catalyst [Figure 4.13(b)], a broad peak with small intensity was detected at ~550 °C which indicated that ZnO was slightly reducible in the range of temperature (40-800 °C) studied [Yu et al., (2007)]. TPR profile of Cu:Zn(4:1)/MgO catalyst showed a single broad reduction peak at a mean temperature of 260 °C. This result indicated that after the addition of ZnO in the Cu/MgO catalyst, the reduction temperature of catalyst shifted towards the lower temperature due to the strong interaction between ZnO and CuO. ZnO primarily increased the reducibility of CuO due to the hydrogen spillover effect as reported earlier [Xia et al., (2012b)].

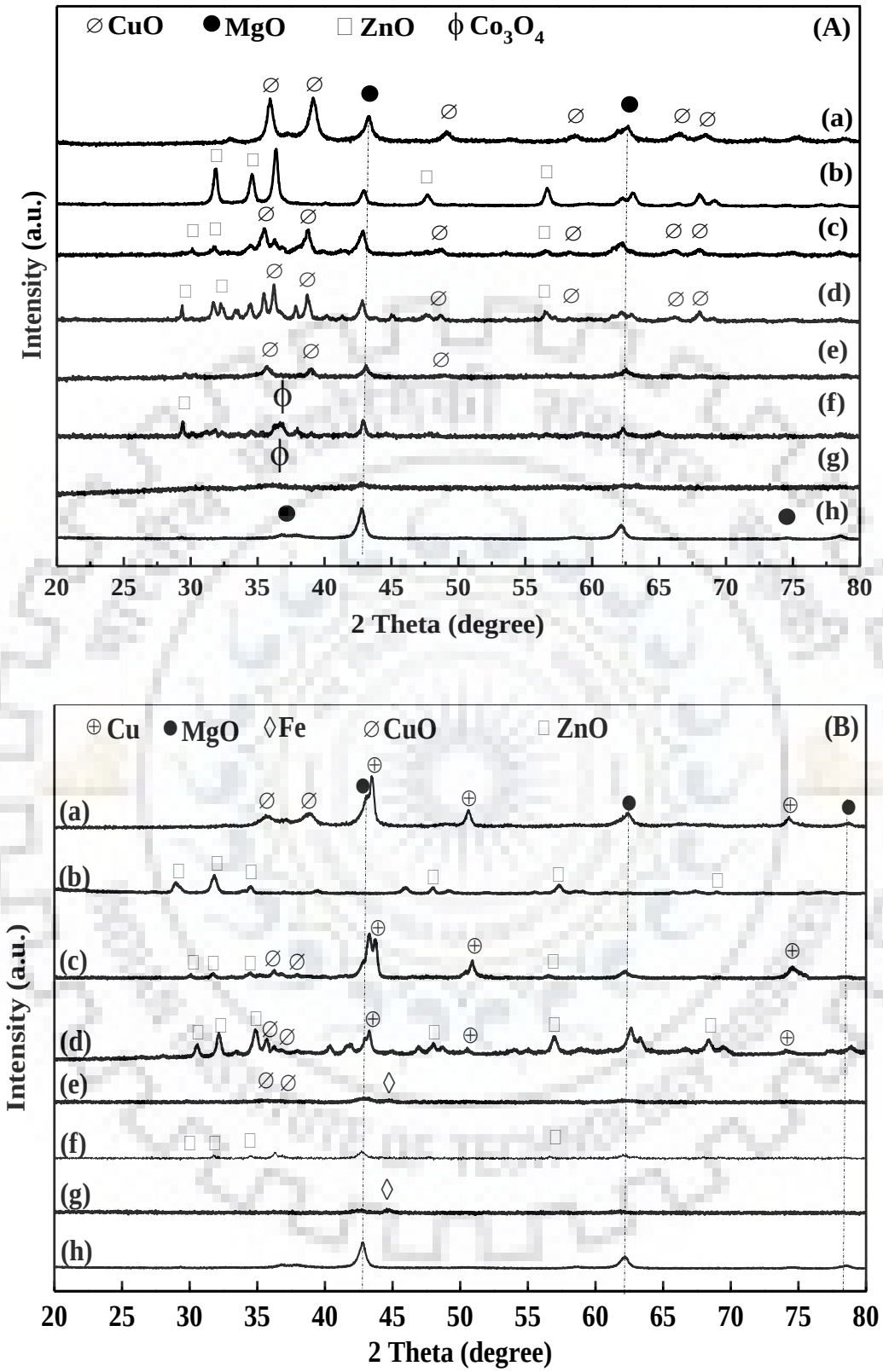

Figure 4.12. XRD pattern of catalysts (A) Fresh calcined (B) Fresh and reduced [(a) Cu/MgO, (b) Zn/MgO, (c) Cu:Zn(4:1)/MgO, (d) Cu:Zn(1:1)/MgO, (e) Cu:Fe(1:1)/MgO, (f) Co:Zn(1:1)/MgO, (g) Co:Fe(1:1)/MgO, (h) MgO]

Table 4.9. BET surface area, pore volume and average crystallite sizes of calcined and reduced catalysts

Catalyst	Theoretical metal composition Metal 1: Metal 2 (wt.%)	Actual metal composition [a] (wt.%)	S_{BET} [b] ($m^2.g^{-1}$)†	V_P [b] ($cm^3.g^{-1}$)	Average crystallite size (nm) [c]						
					Fresh-calcined			Fresh-reduced			
					CuO	ZnO	Co_3O_4	Cu	CuO	Fe	ZnO
MgO			92.0	0.180	-	-	-	-	-	-	-
Cu/MgO	50:0	49.7 : 0	17.0	0.030	20.1	-	-	41	28.6	-	-
Zn/MgO	0:50	0 : 48.7	21.4	0.010	-	30	-	-	-	-	28.9
Cu:Zn(4:1)/MgO	40:10	38.8 : 7.8	23.6	0.012	28.1	30.0	-	37.1	29.4	-	33.2
Cu:Zn(1:1)/MgO	25:25	25.6 : 20.7	29.0	0.014	36.6	31.2	-	43.7	33.7	-	30.2
Cu:Fe(1:1)/MgO	25:25	25.9 : 26.5	37.0	0.018	25.4	-	-	43.9	36.5	55.3	-
Co:Fe(1:1)/MgO	25:25	21.3 : 20.2	21.4	0.010	-	-	28.9	-	-	59.6	-
Co:Zn(1:1)/MgO	25:25	24.0 : 24.5	19.4	0.010	-	40.8	22.4	-	-	-	27.6

[a] Composition obtained from SEM-EDX

[b] Calculated based on the desorption branch of isotherm.

[c] Average crystallite size calculated from XRD pattern by using Scherrer's formula.

†Analytical instruments error for BET surface area: x ± 2%

Similar reduction temperature (~300 ^{o}C) for $Cu_{0.4}Zn_{0.3}Mg_{5.3}Al_2O_9$ catalyst was reported earlier [Xia et al., (2012b)]. The broad reduction temperature peak (152-350 ^{o}C) obtained for Cu:Zn(4:1)/MgO catalyst demonstrated the direct reduction of highly dispersed CuO to Cu^{o} [Pudi et al., (2015a), Kim et al., (2003)]. For Cu:Zn(1:1)/MgO catalyst (4.13 (d)), one major reduction peak was detected at 227 ^{o}C due to the direct reduction of CuO species to Cu^{o} [Xia et al., (2015), Kim et al., (2003)]. Synergistic interaction between CuO with ZnO and hydrogen spillover effect of ZnO were solely responsible for shifting the reduction temperature towards lower side for the ZnO loaded Cu/MgO catalysts. For Cu:Fe(1:1)/MgO catalysts, two major reduction peaks were detected [Figure 4.13 (e)]. The low temperature (~237 °C) peak was for the reduction of CuO to Cu^{o} and the high-temperature reduction peak at 460 °C was for the reduction of Fe_2O_3 to Fe_3O_4 [Mokhonoana et al. (2009)]. Another broad reduction peak with very low intensity was observed at ~600 °C which might be due to the reduction of Fe_3O_4 to Fe [Mokhonoana et al. (2009)]. It was reported earlier that cobalt oxide was reduced in two steps. Initially, Co_3O_4 was reduced to CoO at ~385 °C and CoO was further reduced to Co metal at 550°C and higher [Rekha et al., (2015), Vantblik and Prins (1986)]. The reduction profile [Figure 4.13 (f)] of Co:Zn(1:1)/MgO catalyst showed one reduction peak at 386 °C corresponding to the reduction of Co_3O_4 to CoO and a broad peak with very low intensity was observed at higher temperature (~598 °C) can be related to the reduction of CoO to Co. For Co:Fe(1:1)/MgO catalyst [Figure 4.13 (g)], reduction peak obtained at ~400 °C was due to the combined reduction of Co_3O_4 to CoO and Fe_2O_3 to Fe_3O_4, respectively. The high temperature (686 °C) broad peak was may be due to the combined reduction of CoO to Co and Fe_3O_4 to Fe, respectively [Rekha et al., (2015), Mokhonoana et al., (2009), Vantblik and Prins (1986)].

The hydrogen consumption and degree of reduction of all the catalysts were calculated based on the TPR result and the values obtained are shown in Table 4.10. The hydrogen consumption was in the range of 0.53-6.9 mmol. $gcat^{-1}$. The degree of reduction of the catalyst was calculated based on the following equation: degree of reduction (%) = (H_2 consumption from TPR peak/ H_2 consumption theoretical) × 100. The peak area obtained in the TPR profile for different catalysts was corresponding to the hydrogen consumption ($ml.g^{-1}$ catalyst) from TPR peak of the respective catalysts. For complete reduction of metal oxides, theoretical hydrogen consumption was calculated based on the following stoichiometric equations [Kim et al., (2003), Yu et al., (2007), Mokhonoana et al., (2009), Vantblik and Prins (1986)]:

$$CuO + H_2 = Cu + H_2O \quad (4.1)$$

$$ZnO + H_2 = Zn + H_2O \quad (4.2)$$

$$Fe_2O_3 + 3H_2 = 2Fe + 3H_2O \quad (4.3)$$

$$Co_3O_4 + 4H_2 = 3Co + 4\ H_2O \quad (4.4)$$

Since MgO was not reduced in the temperature range of 40-800 ^oC (Figure 4.13 (h)), therefore, it was assumed that the total hydrogen consumption was used to reduce the total other metal oxides (CuO, ZnO, Co_3O_4, Fe_2O_3) presents in the catalyst apart from MgO. The actual composition of the catalyst obtained from FESEM-EDX (Table 4.9) was used to determine the theoretical hydrogen consumption.

The obtained degree of reduction was in the range of 7.1%-91.7% (Table 4.10). The degree of reduction followed the order Cu:Zn(4:1)/MgO > Cu:Zn(1:1)/MgO > Cu/MgO > Cu:Fe(1:1)/MgO > Co:Zn(1:1)/MgO > Co:Fe(1:1)/MgO > Zn/MgO. Cu/MgO showed the reduction of 83.5% whereas the degree of reduction of Zn/MgO catalyst was only ~7%. After the addition of Zn on Cu/MgO catalyst, the degree of reduction increased significantly (87.5-91.7%). The obtained TPR profile of catalysts suggested a partial reduction of ZnO. ZnO mainly enhanced the reducibility of CuO species due to the hydrogen spillover effect, as a result, the reduction peak of Cu:Zn/MgO catalysts was shifted towards lower temperature. This results also depicted strong interaction between ZnO and CuO in the catalyst. The degree of reduction of Cu:Fe(1:1)/MgO catalyst was lower (61.6%) as compared to Cu:Zn/MgO catalyst (87.5-91.7%) which indicated that iron oxide was not as effective as ZnO to enhance the reducibility of the catalyst. Co-containing catalyst showed a lower degree of reduction (26.7-30%) than Cu containing catalysts (61.6-91.7%) because of the formation of Mg-Co-O mixed oxide solid solution which was consistent with the previous literature [Guo et al., (2009), Mirzaei et al., (2015)].

Table 4.10. NH_3-TPD, CO_2-TPD and H_2-TPR data of catalysts

Calcination temperature	TPD results		TPR results		
	Acidity [a] (mmol NH_3. $gcat^{-1}$)[#]	Basicity [b] (mmol CO_2. $gcat^{-1}$)[#]	Reduction peak (maximum) (°C)	H_2 consumption [c] (mmol. $gcat^{-1}$)[#]	Degree of reduction [d] (%)
MgO	-	1.92	-	-	-
Cu/MgO	1.67	1.34	294	6.54	83.5
Zn/MgO	0.80	2.54	550	0.53	7.1
Cu:Zn(4:1)/MgO	2.13	1.81	260	6.70	91.7
Cu:Zn(1:1)/MgO	1.15	2.10	227	6.30	87.5
Cu:Fe(1:1)/MgO	0.70	0.79	237, 460,600	6.90	61.6
Co:Fe(1:1)/MgO	0.27	0.39	400, 686	2.80	26.7
Co:Zn(1:1)/MgO	0.44	0.75	386, 598	2.75	29.9

[a] Calculated from NH_3-TPD data

[b] Calculated from CO_2-TPD data

[c] H_2 consumption calculated from TPR peaks

[d] Degree of reduction (%) = (H_2 consumption from TPR peak/ H_2 consumption Theoretical) × 10

[#]Analytical instruments error for the active volume obtained in TPR, TPD: x ± 2%

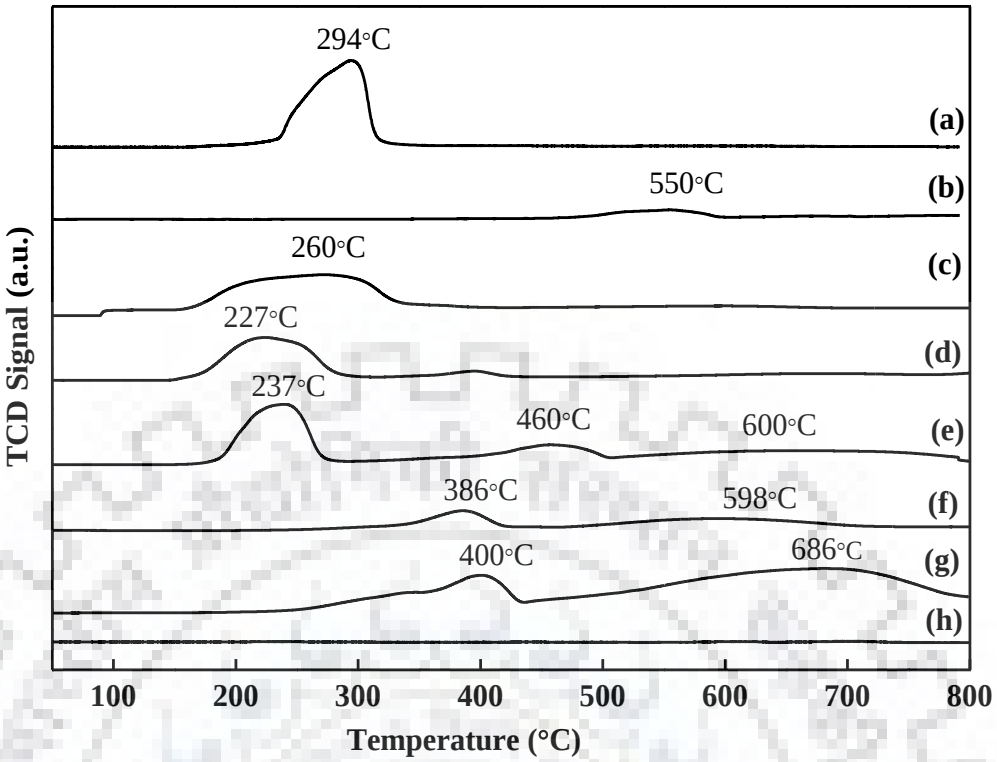

Figure 4.13. H_2–TPR of calcined catalysts (a) Cu/MgO, (b) Zn/MgO, (c) Cu:Zn(4:1)/MgO, (d) Cu:Zn(1:1)/MgO, (e) Cu:Fe(1:1)/MgO, (f) Co:Zn(1:1)/MgO, (g) Co:Fe(1:1)/MgO, (h) MgO

4.3.1.4 NH_3-TPD

NH_3-TPD analysis was performed to determine the strength of the acidic site of catalysts and the obtained TPD pattern is shown in Figure 4.14 (A). Total acidic strength of the catalyst followed the order Cu:Zn(4:1)/MgO > Cu/MgO > Cu:Zn(1:1)/MgO > Cu:Fe(1:1)/MgO > Zn/MgO > Co:Zn(1:1)/MgO > Co:Fe(1:1)/MgO. Among all these catalysts, Cu:Zn(4:1)/MgO catalyst exhibited the highest acidity (2.13 mmol NH_3. $gcat^{-1}$). For Cu:Zn(4:1)/MgO catalyst, the obtained acidity was slightly higher (2.13 mmol NH_3. $gcat^{-1}$) as compared to the acidity value (1.67 mmol NH_3. $gcat^{-1}$) obtained for Cu/MgO catalyst. The slight increase in acidity value was may be due to the presence of higher amount of reducible copper oxide in Cu:Zn(4:1)/MgO catalyst [Jimenez-Morales et al., (2012)] (Table 4.10). The presence of less amounts of reducible copper oxide in Cu/MgO catalyst was due to the agglomeration of copper metal. The higher amount of reducible CuO species in Cu:Zn(4:1)/MgO catalyst was maybe because of hydrogen spillover effect of ZnO which is absent in Cu/MgO catalyst. After addition of 25 wt.% zinc to the Cu/MgO catalyst, the acidity was reduced to 1.15 mmol NH_3. $gcat^{-1}$ and 0.7 mmol NH_3. $gcat^{-1}$ for Cu:Zn(1:1)/MgO and Cu:Fe(1:1)/MgO, respectively. The

acidity of Co:Zn(1:1)/MgO and Co:Fe(1:1)/MgO catalyst was very low i,e. 0.44 mmol NH_3. $gcat^{-1}$ and 0.27 mmol NH_3. $gcat^{-1}$, respectively.

4.3.1.5 CO_2- TPD

The basic sites of the catalyst were analysed by CO_2-TPD and the TPD pattern obtained is shown in Figure 4.14 (B). The estimated total basic sites are summarized in Table 4.10. TPD results demonstrated that the basic sites were classified into weak (80-300 ^oC), moderate (300-500 ^oC) and strong (> 500 ^oC) strength CO_2 desorption sites, respectively. Total basicity of the catalysts followed the order: Zn/MgO > Cu:Zn(1:1)/MgO > MgO > Cu:Zn(4:1)/MgO > Cu/MgO > Cu:Fe(1:1)/MgO > Co:Zn(1:1)/MgO > Co:Fe(1:1)/MgO. As shown in Table 4.10, the maximum basicity of 2.54 mmol CO_2. $gcat^{-1}$ was observed for Zn/MgO catalyst and after the addition of zinc to the copper catalyst, the basicity was increased significantly (1.81-2.10 mmol CO_2. $gcat^{-1}$). Cobalt-containing catalyst exhibited less basicity (0.39-0.75 mmol CO_2. $gcat^{-1}$) as compared to copper containing catalyst (0.79-2.10 mmol CO_2. $gcat^{-1}$).

4.3.1.6 FE-SEM

FE-SEM images of the catalysts demonstrated different types of surface morphologies for different catalysts (Figure 4.15). The morphology evolved due to dehydration, dehydroxylation, denitration, and decarbonation of the metal precursor throughout the thermal treatment. Different morphology suggested different kinds of metal interactions in the catalysts. The FE-SEM image of fresh Cu:Zn(4:1)/MgO and Cu:Zn(1:1)/MgO catalyst showed long rod-like crystal along with aggregated small particles. However, the size of the rod-like crystal increased with increasing the amount of zinc (Cu:Zn(1:1)/MgO) (Figure 4.15 (b)) [Phoohinkong et al., (2017)]. The width of the rod-shaped crystal was increased from ~400 nm to ~600 nm in presence of higher amount of zinc. The FE-SEM image of Cu:Fe(1:1)/MgO and Co:Zn(1:1)/MgO catalyst showed spherical shaped morphology. The flake-like morphology was observed for Co:Fe(1:1)/MgO catalyst [Figure 4.15 (e)]. The actual metal weight percent in the catalyst was investigated by FESEM-EDX analysis and the results showed a good agreement with the theoretical metal loading used for catalyst synthesis (Table 4.9).

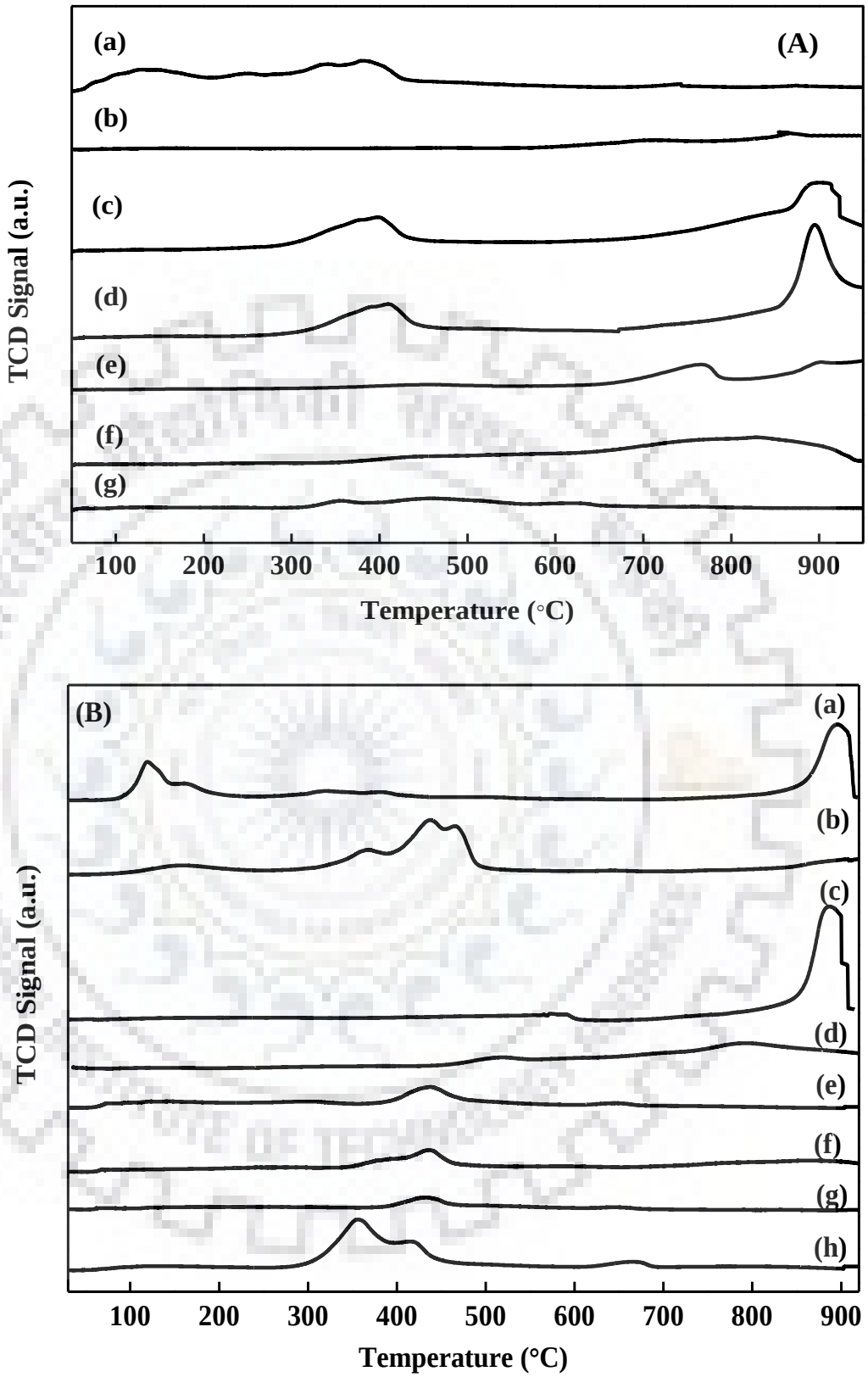

Figure 4.14. (A) NH_3-TPD and (B) CO_2-TPD pattern of the reduced catalyst (a) Cu/MgO, (b) Zn/MgO, (c) Cu:Zn(4:1)/MgO, (d) Cu:Zn(1:1)/MgO, (e) Cu:Fe(1:1)/MgO, (f) Co:Zn(1:1)/MgO, (g) Co:Fe(1:1)/MgO, (h) MgO

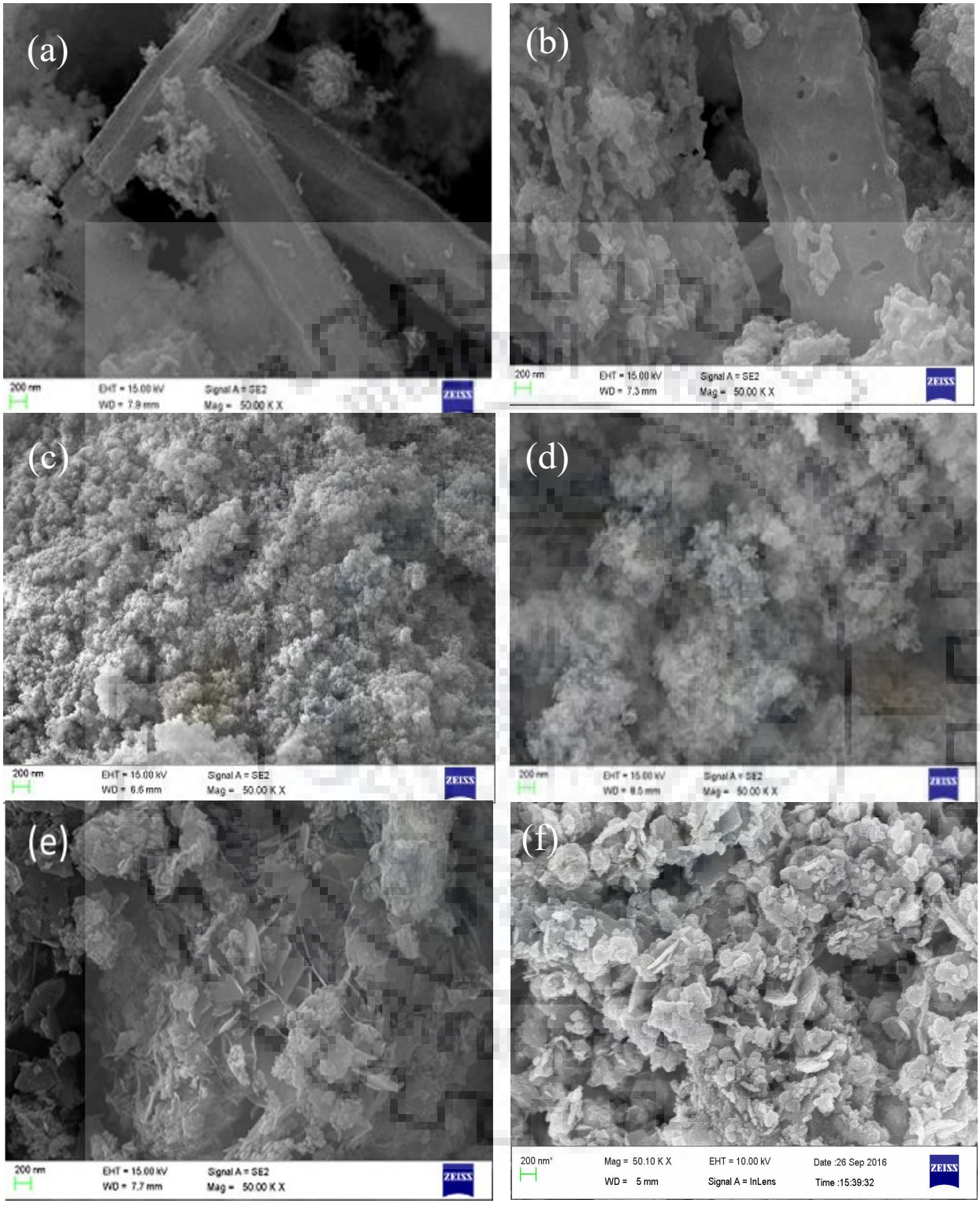

Figure 4.15. FE-SEM images of the catalyst: (a) Cu:Zn(4:1)/MgO, (b) Cu:Zn(1:1)/MgO, (c) Cu:Fe(1:1)/MgO, (d) Co:Zn(1:1)/MgO, (e) Co:Fe(1:1)/MgO, (f) Cu:Zn(4:1)/MgO catalyst after cycle-3

4.3.2 Catalytic activity

Catalytic activity of all the catalysts are shown in Table 4.11. Carbon balances of all the experiments reported in Table 4.11 were closely 100 ± 8%. Initial screening for bimetallic catalysts showed maximum glycerol conversion of ~89% over Cu:Fe(1:1)/MgO and Cu:Zn(1:1)/MgO catalyst, respectively (Table 4.11). The higher activity of copper-based catalyst can be correlated with the presence of higher acidity (0.7-1.15 mmol NH_3. $gcat^{-1}$), basicity (0.8-2.10 mmol CO_2. $gcat^{-1}$), higher hydrogen consumption (6.3-6.9 mmol. $gcat^{-1}$) and the higher degree of reduction (61.6-87.5%) of catalysts. Acidity and/or basicity of the catalyst helped for dehydration of glycerol and the presence of reduced metal facilitated the hydrogenation of dehydrated intermediates. The activity of cobalt-based catalyst was low (≤ 67.1%) and Co:Fe(1:1)/MgO was the least active catalyst. Previously, Co/MgO, Co/ZnO, Co-Zn-Al hydrotalcite catalysts are shown as moderately selective towards the formation of 1,2-PDO and less active as compared to Cu based catalysts [Rekha et al., (2015), Guo et al., (2009), Guo et al., (2011)].

For bimetallic catalysts, 1,2-propanediol (1,2-PDO) and ethylene glycol (EG) was obtained as primary reaction products. However, small amounts of other products including hydroxyacetone, 1-propanol (1-PO), 2-propanol (2-PO), ethanol and methanol were also detected. 1,2-PDO was regarded as the primary hydrogenolysis product, EG and other small linear alcohols such as 1-PO, 2-PO, ethanol, and methanol were regarded as over hydrogenolysis products [Lahr and Shanks (2003), Zhou et al., (2010)]. Over copper-based catalysts, the selectivity towards 1,2-PDO was very high (> 92%) and the selectivity to EG and other degradation products were < 5% and < 3%, respectively. This result suggested that copper-based catalyst was highly selective to 1,2-PDO and overhydrogenolysis of glycerol was not significant [Dasari et al., (2005)]. Although the glycerol conversion over Co:Fe(1:1)/MgO catalyst was very low (38.3%), the selectivity towards 1,2-PDO was significantly high (91.3%) and the total selectivity to EG and other products were only < 10%. The poor glycerol conversion was may be due to the availability of low acidic and/or basic sites on the catalyst surface as well as poor reducibility of catalysts (26.7%). Presence of lower concentration of acidic and/or basic sites as well as the reduced metal sites significantly reduced the available dehydration and hydrogenation centers on the catalyst surface [Du et al., (2016), Wang et al., (2015a)]. For Co:Zn(1:1)/MgO catalyst, glycerol conversion was quite high (67.1%) as compared to Co:Fe(1:1)/MgO catalyst (38.3%). However, the selectivity towards 1,2-PDO was lower (74.7%) and the selectivity to EG (16.7%) and other products (8.6%) were quite higher.

This result demonstrated that overhydrogenolysis of 1,2-PDO and EG to other products were favoured over cobalt-zinc catalyst [Wang et al., (2015a)].

Table 4.11. Glycerol hydrogenolysis reaction over monometallic and bimetallic catalyst

Catalyst	Conversion (%)	Selectivity (%)			1,2-PDO yield (%)
		1,2-PDO	EG	Others*	
Cu:Zn(1:1)/MgO	88.5	94.2	2.9	2.9	83.4
Cu:Fe(1:1)/MgO	89.0	92.3	4.5	3.2	82.2
Co:Zn(1:1)/MgO	67.1	74.7	16.7	8.6	50.2
Co:Fe(1:1)/MgO	38.3	91.3	4.4	4.4	35.0
Effect of copper to zinc weight ratio					
Cu/MgO	95.4	92.6	4.8	2.6	88.3
Cu:Zn(4:1)/MgO	98.7	93.4	3.2	3.4	92.2
Cu:Zn(1:1)/MgO	88.5	94.2	2.9	2.9	83.4
Zn/MgO	4.8	100	0.0	0.0	4.8

Experimental errors for all the values (conversion, selectivity and yield) : x ± 1 %
Reaction condition: 20 wt.% glycerol (20 g), catalyst: 1.6 g, temperature: 210 ^{o}C, H_2 pressure: 4.5 MPa, speed of agitation: 700 rpm, time: 12 h.
*Others: hydroxyacetone, 1-PO, 2-PO, ethanol and methanol.

For the initial catalyst screen, the maximum 1,2-PDO yield of 83.4% was obtained in presence of Cu:Zn(1:1)/MgO catalyst. This result suggested that the addition of zinc into the copper-magnesia catalyst was beneficial to enhance the selectivity and yield of the desired 1,2-PDO. For hydrogenolysis of glycerol, the presence of acid and/or base functionality on the catalyst surface facilitates the removal of -OH group from glycerol molecule and active metal sites were required for hydrogenation of the dehydrated intermediate to 1,2-PDO [Wang et al., (2015a)]. Copper metal has a higher potential for selective cleavage of C-O bond and also its

hydrogenation ability is superior. It is also reported that particle size of copper metal and the presence of acid/basic sites on the catalyst surface played a crucial role on hydrogenolysis activity as well as 1,2-PDO selectivity [Balaraju et al., (2012), Wang et al., (2015), Du et al., (2016)]. Several authors reported that the addition of zinc increases the reducibility of active metals by its H_2 spillover ability and Zn also can alter the electronic configuration of active metal sites [Sharma et al., (2014), Xia et al., (2012b), Li et al., (2014)]. Cu:Zn(1:1)/MgO catalyst was found to be the most active and selective catalyst among all other catalysts examined. Further, the effect of the copper to zinc weight ratio in the catalyst on the catalytic performance was examined and the results obtained are summarized in Table 4.11.

Over Cu/MgO catalyst, 95.4% conversion of glycerol was obtained with 94.2% selectivity towards 1,2-PDO. The selectivity to EG and other products were 4.8% and 2.6%, respectively. Moreover, this is very interesting to observe that Zn/MgO catalyst was poor active ($X_{glycerol} \approx 4.8\%$) and 100% selective to 1,2-PDO. The poor activity of Zn/MgO catalyst was may be due to the poor reducibility (7.1%) of ZnO. Since 1,2-PDO selectivity was 100% and no other intermediate products were detected over Zn/MgO catalyst, hence, it may be resolved that 1,2-PDO was may be formed directly by selective hydrogenolysis of glycerol. After the addition of small amount of zinc in the copper-magnesium system (Cu:Zn(4:1)/MgO), conversion of glycerol ($X_{glycerol}$ ~98.7%) and the selectivity towards 1,2-PDO ($S_{1,2\text{-PDO}}$ ~ 93.4%) was enhanced significantly. The overall yield of 1,2-PDO was very high (92.2%) in presence of Cu:Zn(4:1)/MgO catalyst. Moreover, in presence of higher amounts of zinc (Cu:Zn(1:1)/MgO), the glycerol conversion dropped ~10% by keeping the 1,2-PDO selectivity almost constant (~94%). The overall yield of 1,2-PDO was decreased to 83.4% in presence of Cu:Zn(1:1)/MgO catalyst. Very high catalytic activity and 1,2-PDO yield was obtained over Cu:Zn(4:1)/MgO catalyst because of the presence of an appropriate combination of acidic (2.13 mmol NH_3. $gcat^{-1}$) and/or basic (1.81 mmol CO_2. $gcat^{-1}$) sites concentration on the catalyst, high hydrogen consumption (6.7 mmol. $gcat^{-1}$) [Zelazny et al., (2017)], very high degree of reduction (91.7%) [Zelazny et al., (2017)] and presence of small average copper particle size (37.1 nm) in the reduced catalyst [Yuan et al. (2010)]. The addition of zinc into the Cu/MgO catalyst increased the degree of reduction of Cu:Zn(4:1)/MgO catalyst (91.7%) and also lowered the reduction temperature (Figure 4.13). Zinc helped to increase the basicity and also the reducibility of the catalyst by hydrogen spillover effect [Xia et al., (2012b), Sun et al., (2011), Zou and Shen (2000)]. NH_3 –TPD and CO_2 –TPD results revealed that copper introduced the acidic sites whereas Zn introduced the additional basicity in the catalyst. As compared to other catalysts,

the concentrations of acidic as well as basic sites were higher for Cu:Zn(4:1)/MgO catalyst which was responsible for bi-functional characteristics of the catalyst. Hydrogenolysis of glycerol require both acidic as well as basic sites on the catalyst surface, acid and/or basic site enhance dehydration of glycerol to intermediate such as hydroxyacetone and further hydroxyacetone hydrogenate to 1,2-PDO in presence of the metal sites [Wang et al., (2010), Pudi et al., (2015a), Wang et al. (2015b)]. Iglesia et al., (1997) reported that acid-base sites are required for hydrogenation and dehydration reaction because these sites can stabilize and also discard adsorbed intermediate species. The appropriate combination of acidic and/or basic sites are essential for higher selectivity and yield of 1,2-PDO. It is also reported that the particle size of copper played an important role to control the selectivity towards 1,2-PDO. The presence of more reduced small size (< 50 nm) copper particle is preferable for higher selectivity towards 1,2-PDO [Yuan et al., (2010), Wang et al. (2015b). Cu:Zn(4:1)/MgO catalyst exhibited the highest selectivity (93.4%) to 1,2-PDO due to the synergistic effect of copper and zinc on MgO support, the hydrogen spillover effect of ZnO, the smaller crystallite size of copper particle and the bi-functional characteristics of the catalyst.

4.3.3 Parameter studies

The influences of various reaction parameters such as temperature, pressure, catalyst amount and glycerol concentration were studied in the presence of Cu:Zn(4:1)/MgO catalyst. Influences of different reaction parameters on glycerol conversion, 1,2-PDO selectivity and yield are discussed in the following section. Experimental errors for all the values in Figure 4.16 are x ± 1%.

4.3.3.1 Effect of temperature

Effect of reaction temperature (190-220 °C) on glycerol conversion and product selectivity obtained over Cu:Zn(4:1)/MgO catalyst is shown in Figure 4.16 (A). Results showed that the glycerol conversion increased sharply and achieved ~100% at 210 °C and higher. However, the selectivity towards 1,2-PDO decreased from 95% to 91% with the simultaneous increase in selectivity to other degradation products from 5% to ~9% with temperature. This is in accordance with the previous report over copper-based catalyst that at a higher temperature, the cleavage of C-C bond prevailed along with the C-O bond cleavage causing the formation of overhydrogenolysis products i,e. 1-PO, 2-PO and EG etc [Guo et al., (2009), Pudi et al., (2015a)]. The overall yield of 1,2-PDO was increased from 75% at 190 ^{o}C to 93.4% at 210 ^{o}C

and beyond 210 ^{o}C, 1,2-PDO yield was decreased to ~91% due to the formation of other products.

4.3.3.2 Effect of pressure

Influence of initial hydrogen pressure (4.0-6.0 MPa) demonstrated a significant effect on the catalytic activity, 1,2-PDO selectivity, and yield (Figure 4.16 (B)). Almost complete conversion of glycerol was achieved at 4.5 MPa and higher. However, the selectivity towards 1,2-PDO decreased from 94% at 4 MPa to 92% at higher pressure (6 MPa) due to the formation of other degradation products. Initially, with increasing pressure, glycerol conversion was increased due to the availability of more H_2 species at the catalyst surface which increased hydrogenation [Sharma et al., (2014)]. The selectivity towards 1,2-PDO was decreased slightly at the elevated H_2 pressure due to the formation of degradation products, i.e.: EG, ethanol, and methanol [Balaraju et al., (2009)]. The maximum 1,2-PDO yield of 92.1% was achieved at 4.5 MPa and at 210 ^{o}C.

4.3.3.3 Effect of catalyst loading

The conversion of glycerol increased with catalyst loading and achieved ~100% in presence of 8 wt.% catalyst and higher [Figure 4.16 (C)]. The selectivity towards 1,2-PDO was almost constant ~93% throughout the catalyst loading varied. The increase in glycerol conversion with an increase in metal loading was attributed to the increasing active metal sites on the catalyst surface [Yuan et al., (2010), Niu et al., (2013)]. The maximum 1,2-PDO yield of 92.2% was obtained in presence of 8 wt.% catalyst of glycerol solution.

4.3.3.4 Effect of glycerol concentration

The effect of glycerol concentration (10-40 wt.%) on glycerol conversion and product selectivity is shown in Figure 4.16 (D). Glycerol conversion passed through maxima and almost complete glycerol conversion was obtained in presence of 20 wt.% glycerol as feed. Low glycerol conversion at lower glycerol concentration (10 wt.%) was due to the presence of excess water in the feed. Excess water content decreased the catalytic activity which was in good agreement with previous literature [Sharma et al., (2014), Montassier et al., (1995)]. However, further increase in glycerol concentration beyond 20 wt.%, glycerol conversion showed a decreasing trend.

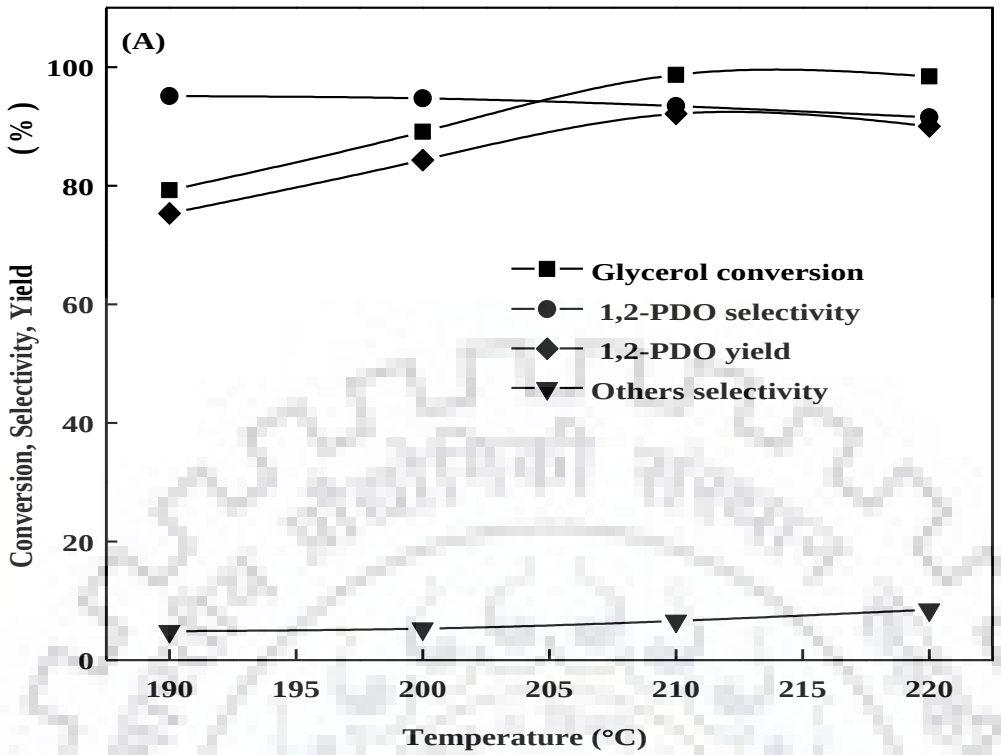

Figure 4.16. (A) Effect of reaction temperature, reaction condition: 4.5 MPa H_2 pressure, 20 wt.% glycerol (20 g), 1.6 g catalyst, reaction time 12 h

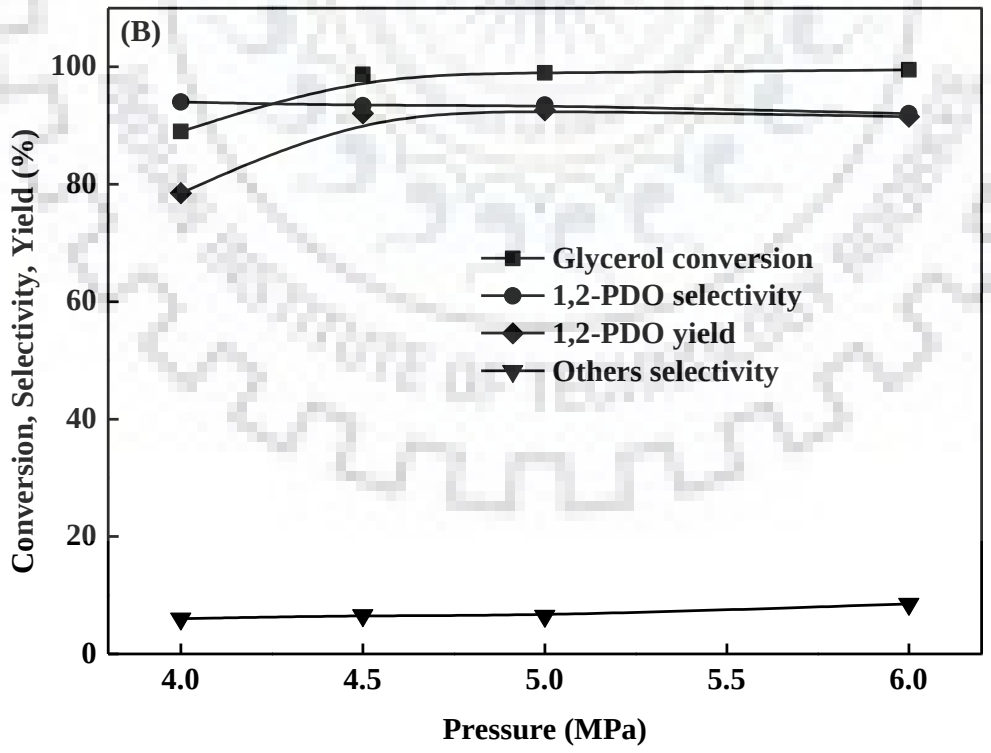

Figure 4.16. (B) Effect of initial hydrogen pressure, reaction condition: 210 °C temperature, 20 wt.% glycerol (20 g), 1.6 g catalyst, reaction time 12 h

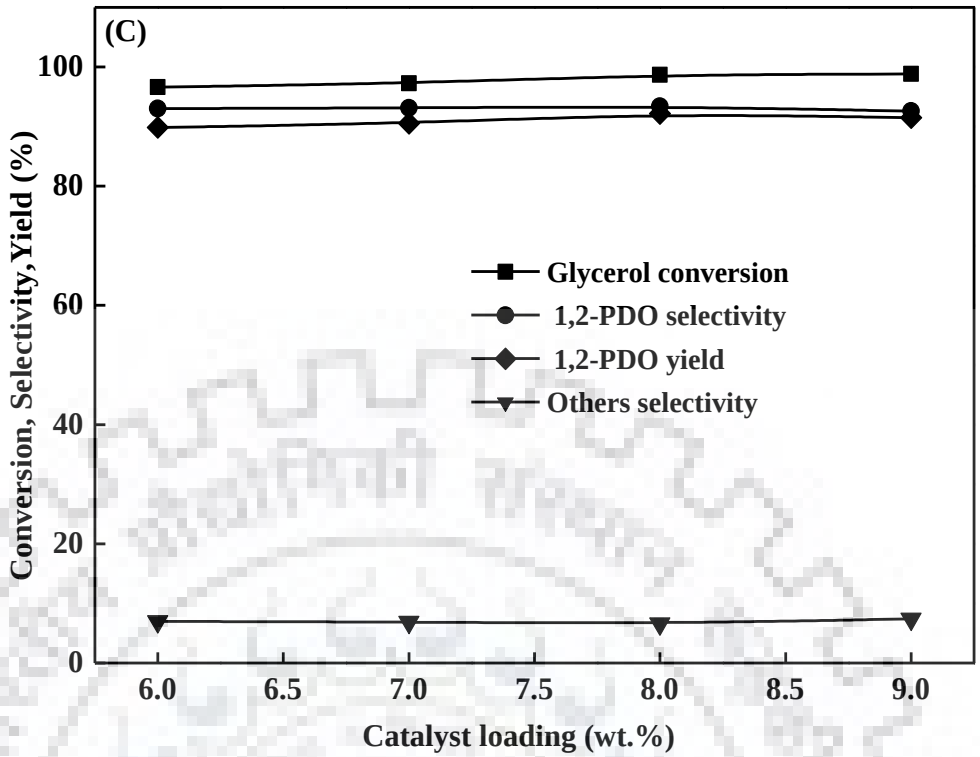

Figure 4.16. (C) Effect of catalyst loading, reaction condition: 210 °C temperature, 4.5 MPa H_2 pressure, 20 wt.% glycerol (20 g), reaction time 12 h

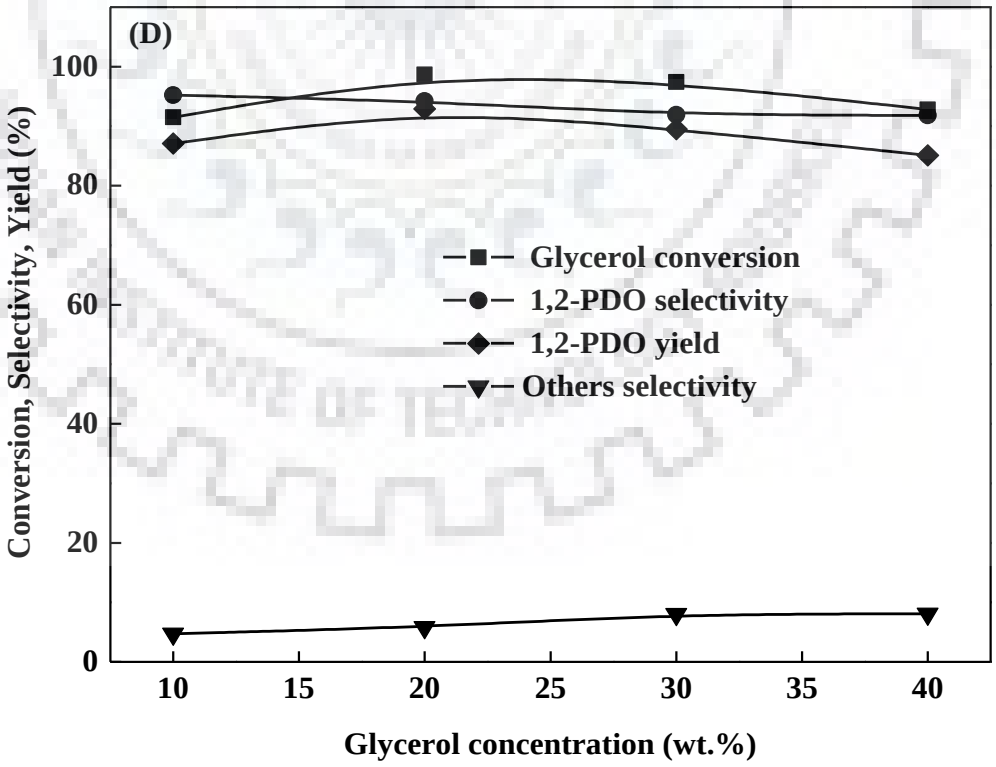

Figure 4.16. (D) Effect of glycerol concentration, reaction condition: 210 °C temperature, 4.5 MPa H_2 pressure, (0.8-3.2) g catalyst, reaction time 12 h

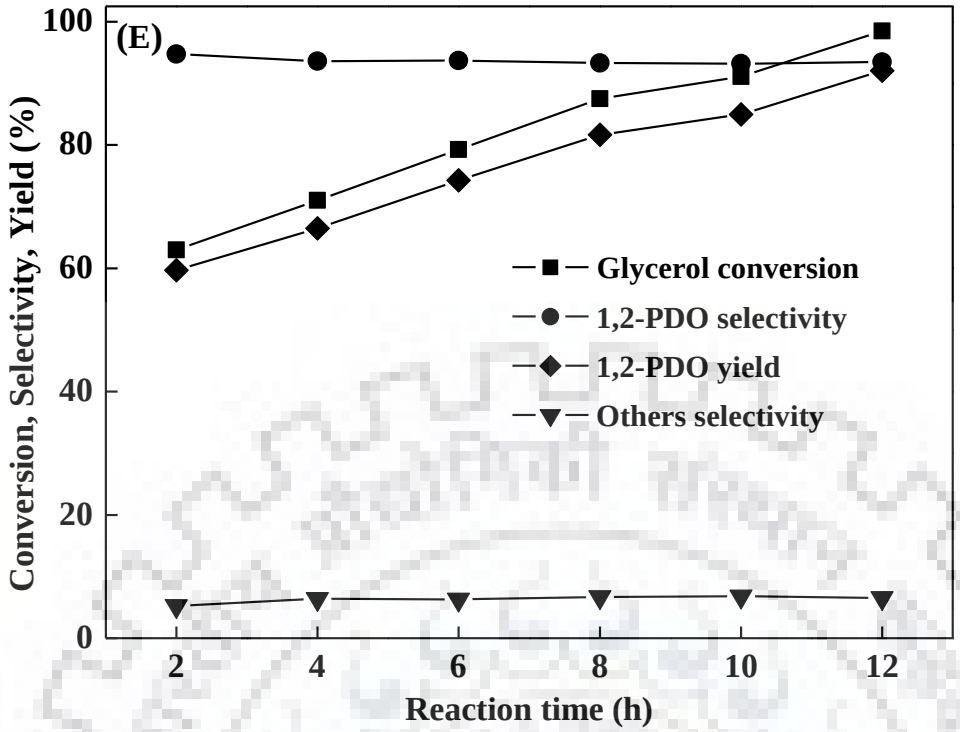

Figure 4.16. (E) Effect of reaction time, reaction condition: 210 °C temperature, 4.5 MPa H_2 pressure, 20 wt.% glycerol (20 g), 1.6 g catalyst

This is because at higher feed concentration, the viscosity of the solution increased and availability of H_2 molecule on the catalyst surface was decreased due to higher diffusion resistance [Sharma et al., (2014)]. The selectivity towards 1,2-PDO slightly decreased with increasing the glycerol concentration with a simultaneous increase in the selectivity to other degradation products [Balaraju et al., (2012)]. The maximum overall 1,2-PDO yield of 92.1% was achieved in presence of 20 wt.% glycerol.

4.3.3.5 Effect of reaction time

As shown in Figure 4.16 (E), glycerol conversion increased with reaction time and achieved ~100% after 12 h [Sharma et al., (2014), Yuan et al., (2010)]. The selectivity towards 1,2-PDO (~94%) and other products (~6%) were almost constant in the entire period of reaction time. The overall yield of 1,2-PDO increased from 59.7% to 92.1% after 12 h of reaction. This result suggested that Cu:Zn(4:1)/MgO catalyst was highly selective to 1,2-PDO and significantly suppressed the cleavage of C-C bond even after a longer period of reaction time [Yuan et al., (2010), Pandhare et al., (2016)].

4.3.4 Reaction mechanism

Reaction mechanism study was performed in presence of Cu:Zn(4:1)/MgO catalyst at the optimum reaction condition. In this study, 1,2-PDO, EG was obtained as the main reaction products over Cu:Zn(4:1)/MgO catalyst and a trace amount of hydroxyacetone, ethanol, methanol, 1-PO, 2-PO were also obtained. To understand the actual reaction path, important products such as 1,2-PDO, hydroxyacetone and EG were taken as a separate reactant and the hydrogenolysis reaction was performed under the same reaction condition. The conversion and product selectivity obtained in each experiment are summarized in Table 4.12.

Table 4.12. Hydrogenolysis of glycerol, hydroxyacetone, 1,2-PDO and EG over Cu:Zn(4:1)/MgO catalyst

Reactant	Conversion (%)	Selectivity (%)				
		1,2-PDO	Hydroxy-acetone	EG	1-PO + 2-PO	Ethanol+ Methanol
Glycerol	98.7	93.4	0.23	3.6	1.7	1.0
Hydroxyacetone	99.4	87.9	-	-	4.1	7.9
1,2-PDO	6.9	-	-	-	90.3	10.0
EG	14.9	-	-	-	-	99.9

Experimental errors for all the values (conversion, selectivity and yield) : x ± 1 %
Reaction condition: 210 °C temperature, 4.5 MPa H_2, 20 wt.% glycerol (20 g), catalyst loading = 1.6 g, 12 h

Previous literature information suggested that if protonation of glycerol occurs at the terminal hydroxyl group, metastable hydroxyacetone was formed as an intermediate and water was eliminated from the reaction [Gandarias et al., (2010)]. Nimlos et al., (2006) investigated dehydration and protonation of glycerol using quantum mechanics calculation. Sato et al., (2008) suggested that hydroxyacetone was produced by protonation of glycerol followed by deprotonation and tautomerism of unstable enol. Yue et al., (2014) found that dehydration of glycerol depended on H_2 spillover of Cu metal and acid/basic sites of support material. In this study, hydrogenolysis of hydroxyacetone showed almost complete conversion with ~88% selectivity towards 1,2-PDO, 4.1% combined selectivity to 1-PO and 2-PO and 7.9% combined

selectivity to ethanol and methanol. This result suggested that hydroxyacetone was formed as an intermediate and immediately converted primarily to 1,2-PDO and others. Approximately 12% of hydroxyacetone was converted to degradation products (1-PO, 2-PO, ethanol, and methanol). Any other intermediate such as glyceraldehydes and 2-hydroxyacrolein was not detected over Cu:Zn(4:1)/MgO catalyst.

Hydrogenolysis of 1,2-PDO as a starting compound showed very low conversion (~7%) and 1,2-PDO was mainly converted to propanols (1-PO+2-PO) with ~90% selectivity and (ethanol + methanol) with ~10% selectivity. This result suggested that 1,2-PDO further hydrogenated to primarily propanols (1-PO + 2-PO) and small alcohols (ethanol + methanol) under the reaction condition used.

Ethylene glycol was detected only from hydrogenolysis of glycerol but not from the hydrogenolysis of hydroxyacetone or 1,2-PDO. This result suggested that EG was formed directly from glycerol by the cleavage of C-C bond although the selectivity was very low (< 4%). The conversion of EG was ~15% and it was converted to only linear alcohol (ethanol + methanol) with ~100% selectivity. Propanols (1-PO + 2-PO) were obtained due to the over hydrogenolysis of 1,2-PDO. Linear alcohols (ethanol + methanol) were obtained due to the degradation of glycerol, 1,2-PDO, hydroxyacetone and EG, respectively. Gandarias et al., (2010) reported a similar kind of reaction mechanism for hydrogenolysis of glycerol over Pt/silico-alumina catalyst. The product distribution obtained over Cu:Zn(4:1)/MgO catalyst suggested two-step hydrogenolysis reaction process for the production of 1,2-PDO from glycerol i,e. dehydration of glycerol to hydroxyacetone followed by the hydrogenation of hydroxyacetone to 1,2-PDO. The reaction pathway proposed is shown in Scheme 4.2.

4.3.5 Reusability of the catalyst

The stability of the Cu:Zn(4:1)/MgO catalyst was investigated up to 3rd cycle under the similar reaction condition. After each cycle, the used catalyst was filtered, washed thoroughly with ethanol followed by deionized water to remove organic species and then dried at 110 °C overnight. Before each cycle, the dried catalyst was treated with H_2 (50 ml.min^{-1}) at 350 °C for 3 h. During the catalyst recovery and reactivation process, some amounts of catalyst were lost in every cycle. However, in every batch, glycerol to catalyst weight ratio was kept constant [Sharma et al., (2014)]. The glycerol conversion and product selectivity obtained in successive recycle are summarized in Table 4.13.

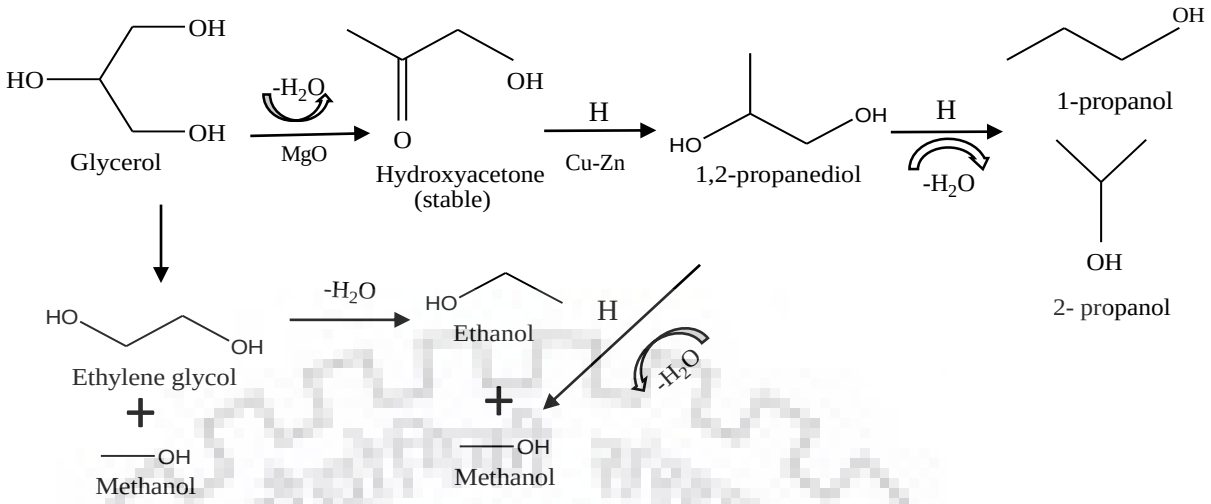

Scheme 4.2. Reaction mechanism scheme for glycerol hydrogenolysis reaction over Cu:Zn(4:1)/MgO catalyst

Glycerol conversion was found to reduce by ~ 14% after cycle-3. However, the selectivity towards 1,2-PDO was almost unaffected (~94%) and the selectivity to EG and other degradation products were varied in the range of 2-3.6% and 1.7-3.6%, respectively. The overall yield of 1,2-PDO was decreased from 92.1% to 79.2% after cycle-3 due to the moderate loss of catalytic activity.

To determine the reason of deactivation of the catalyst, the used catalyst (after cycle-3) was characterized by various techniques such as BET, XRD, TEM, atomic absorption spectroscopy (AAS) etc. The physico-chemical properties of the used (after cycle-3) catalyst were compared with fresh reduced catalysts. As shown in Table 4.13, the BET surface area of the used catalyst was reduced significantly (10 $m^2.g^{-1}$) because of agglomeration of the catalyst particles [Sharma et al., (2014), Du et al., (2016)]. XRD pattern of the used catalyst showed highly intense diffraction peaks corresponding to Cu^0 (Figure 4.17). In the used catalyst, the calculated copper crystallite size by using the Scherrer's equation was increased (~58 nm) significantly as compared to the fresh catalyst (37 nm) (Table 4.13). This result confirmed the agglomeration of the copper particle after cycle-3. Detailed surface morphology of the used (after cycle-3) catalyst was also characterized by FE-SEM and TEM. It can be seen from Figure 4.15 (f), that the rod-shaped morphology of the fresh reduced catalyst was destroyed after

cycle-3 and particles were mostly agglomerated. TEM images of fresh reduced catalyst were compared with the used (after cycle-3) catalyst. The TEM micrographs and corresponding average particle size histograms are shown in Figure 4.18. It was observed that the average particle size in the catalyst was increased from 32 nm to 51 nm after reuse due to the agglomeration of the metal particles which was in good agreement with the XRD result obtained. Finally, the probability of metal leaching in the reaction mixture during the reaction was verified by performing the AAS analysis of fresh and used catalyst. AAS result reported in Table 4.13 suggested that the metal leaching in the solution was insignificant.

Based on catalyst screening and reaction parameter study, it has been observed that Cu:Zn(4:1)/MgO catalyst was the most active, stable and selective to 1,2-PDO. The maximum glycerol conversion of 98.7% with 93.4% selectivity towards 1,2-PDO was obtained at 210 °C, 4.5 MPa pressure in presence of 8 wt.% catalyst loading when 20 wt.% glycerol was used as feed. This catalyst is superior as compared to the results reported in the previous literature [Yuan et al., (2010), Xia et al. (2012a), Xia et al., (2012b), Guo et al., (2009), Guo et al., (2011), Balaraju et al., (2012), Niu et al., (2013)] for MgO based catalyst in terms of activity and 1,2-PDO yield. Xia et al. (2012a) reported maximum 91% conversion with 89.8% yield of 1,2-PDO over $Rh_{0.02}Cu_{0.4}/Mg_{5.6}$ $Al_{1.98}O_{8.57}$ catalyst. However, the stability of $Rh_{0.02}Cu_{0.4}/Mg_{5.6}$ $Al_{1.98}O_{8.57}$ catalysts was very poor and activity was decreased ~38% after 3rd cycle. Yuan et al., (2011) reported 80% conversion with 98.2% selectivity towards 1,2-PDO over $Cu_{0.4}$ $Mg_{5.6}$ $Al_2(OH)_{16}CO_3$ catalyst at 180 °C, at 3.0 MPa H_2 pressure after 20 h of reaction, 75 wt.% glycerol was used as feed. However, catalyst stability and reusability study were not reported.

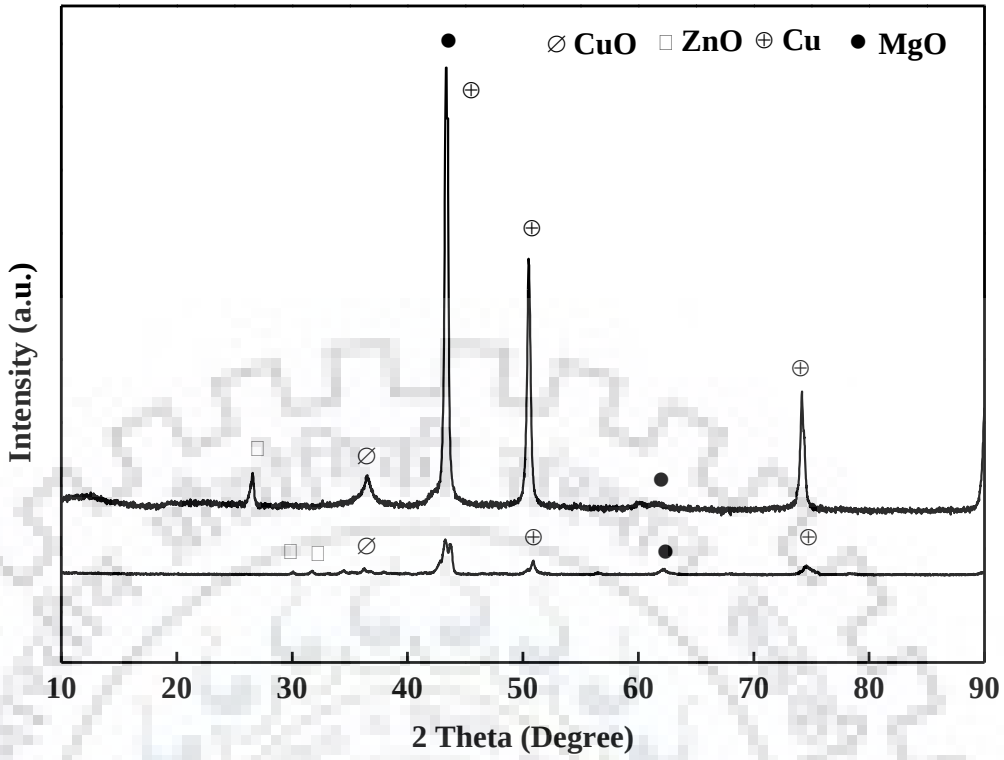

Figure 4.17. XRD- Pattern of fresh and 3rd used Cu:Zn(4:1)/MgO catalyst

4.3.6 Summary

Hydrogenolysis of glycerol is a promising route for value addition of excess glycerol obtained from biodiesel industry. For successful commercialization of selective hydrogenolysis to 1,2-PDO, development of a selective and stable catalyst is highly desirable. In this study, a series of MgO supported Cu, Zn, Fe, Co-based monometallic and bimetallic catalysts were synthesized by precipitation-deposition method. The catalytic performance was evaluated in a high-pressure autoclave reactor in liquid phase. Various catalyst characterization results confirmed the variation of metal support interaction in different catalysts. XRD results demonstrated that the copper crystallite size in the reduced copper catalyst was very low (< 45 nm). The reduction behaviour of the catalysts was significantly different for different catalyst having different composition. TPR result indicated that after the addition of ZnO in the Cu/MgO catalyst, the reduction temperature of the catalysts shifted towards lower temperature side due to the strong interaction between ZnO with CuO. Cu/MgO showed a very high degree of reduction (~83%) whereas the degree of reduction of Zn/MgO catalyst was only ~7%.

Table 4.13. Reusability results of glycerol hydrogenolysis reaction over Cu:Zn(4:1)/MgO catalyst

	Conversion[a] (%)	Selectivity (%)			1,2-PDO yield (%)	Catalyst characterization data after reuse					
						Cu[b] (wt.%)	Zn[b] (wt.%)	S_{BET}[c] ($m^2.g^{-1}$)[#]	D_{Cu} XRD (nm)[d]		
		1,2-PDO	EG	Others					Cu	CuO	ZnO
Fresh catalyst	98.7	93.4	3.2	3.4	92.1	38.7	8.5	23	37.1	29.4	33.2
2nd cycle	89.1	94.4	3.6	2.0	84.1	-	-	-	-		-
3rd cycle	84.2	94.1	2.0	3.6	79.2	40.1	10.1	10	57.6	22.4	43.7

[a] Reaction condition: 210 °C temperature, 4.5 MPa H_2, 20 wt.% glycerol (20 g), catalyst loading = 1.6 g, 12 h

[b] Metal loading calculated from AAS analysis.

[c] Obtained from N_2 adsorption-desorption isotherm data.

[d] Calculated by using Scherrer's formula

[#] Analytical instruments error for BET surface area obtained in TPR, TPD: x ± 2%

Experimental errors for all the values (conversion, selectivity and yield) : x ± 1 %

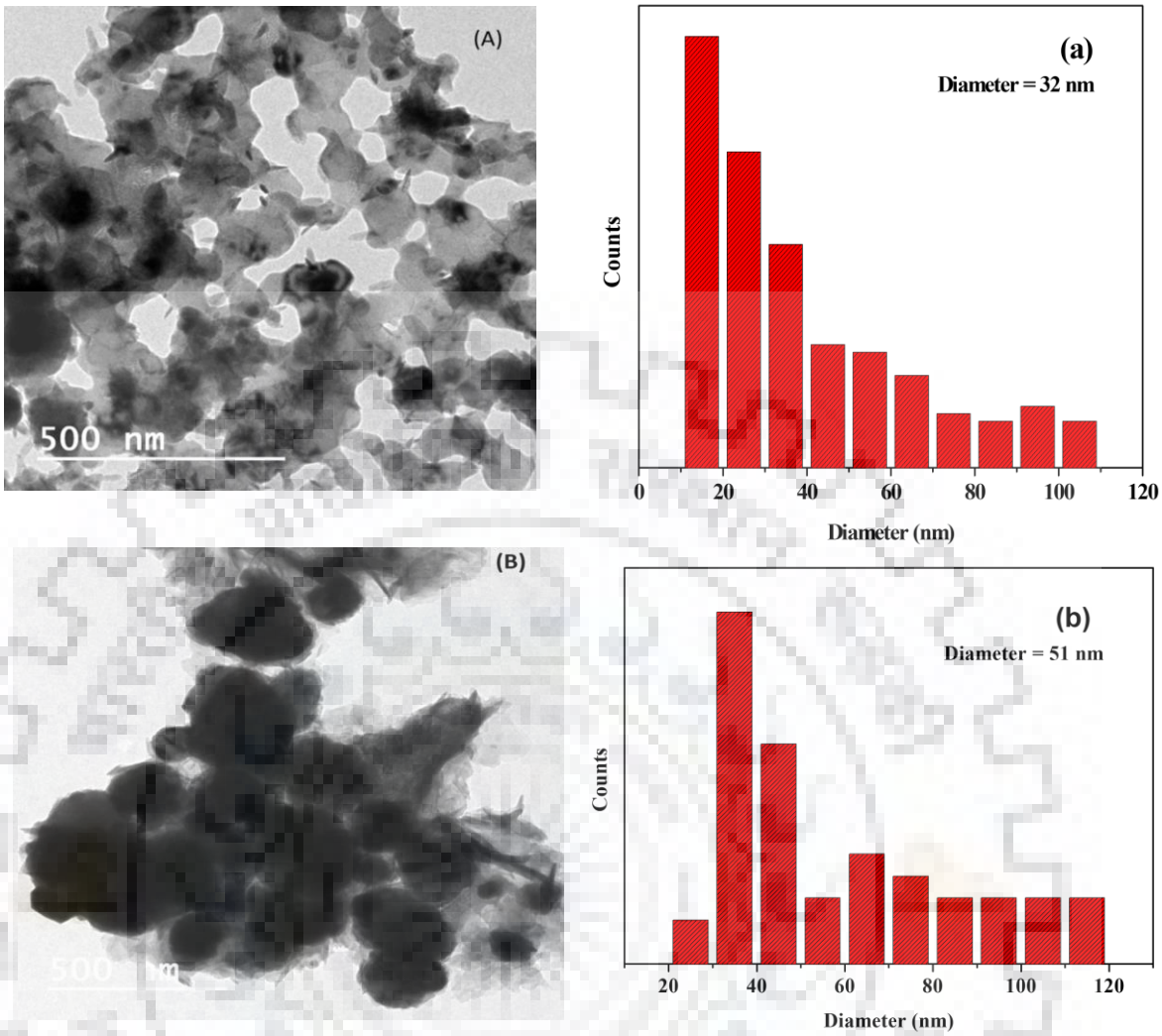

Figure 4.18. TEM micrograph and corresponding average particle size histogram: [(A) and (a)] fresh and reduced Cu:Zn(4:1)/MgO catalyst; [(B) and (b)] Cu:Zn(4:1)/MgO catalyst after cycle-3

After the addition of Zn on Cu/MgO catalyst, the degree of reduction increased significantly (81-86%). The complete reduction of ZnO was quite difficult and ZnO mainly enhanced the reducibility of CuO species due to the hydrogen spillover effect. NH_3 –TPD and CO_2 –TPD results revealed that copper introduced the acidic sites whereas Zn introduced the additional basicity in the catalyst.

Cu/MgO catalyst showed a 95.4% conversion with the 1,2-PDO selectivity to 94.2% at 210 ^oC and 4.5 MPa pressure. The selectivity to EG and other products were 4.8% and 2.6%, respectively. Zn/MgO catalyst was poor active which showed only 4.8% conversion of glycerol

and 100% selective to 1,2-PDO. Glycerol was directly converted to 1,2-PDO through selective hydrogenolysis without forming any intermediates. After the addition of small amount of zinc in the copper-magnesium system (Cu:Zn(4:1)/MgO), conversion (98.7%) of glycerol and the selectivity (93.4%) to 1,2-PDO enhanced significantly. Moreover, in presence of higher amounts of zinc (Cu:Zn(1:1)/MgO), the glycerol conversion dropped ~10% by keeping the 1,2-PDO selectivity almost constant (~94%). Very high catalytic activity and 1,2-PDO selectivity over Cu:Zn(4:1)/MgO catalyst was due to the presence of an appropriate combination of acidic (2.13 mmol NH_3. $gcat^{-1}$) and/or basic (1.81 mmol CO_2. $gcat^{-1}$) sites concentration on the catalyst, high hydrogen consumption (6.7 mmol. $gcat^{-1}$), very high degree of reduction (91.7%), and presence of small average copper particle size (37.1 nm) in the reduced catalyst. As compared to other catalysts, the concentration of acidic as well as basic site was higher for Cu:Zn(4:1)/MgO catalyst which was responsible for bi-functional characteristics of the catalyst. Influences of different reaction parameter suggested that the hydrogenolysis of glycerol was beneficial for higher selectivity and yield of 1,2-PDO at ≤ 210 ºC, at ≤ 4.5 MPa pressure, in presence of 8 wt.% catalyst loading and use of 20 wt.% glycerol as feed was beneficial.

The product distribution obtained over Cu:Zn(4:1)/MgO catalyst suggested two-step hydrogenolysis reaction process for the production of 1,2-PDO from glycerol i,e. dehydration of glycerol to hydroxyacetone followed by the hydrogenation of hydroxyacetone to 1,2-PDO. EG was obtained directly by the hydrogenolysis of glycerol due to the cleavage of C-C bond. EG was converted to only linear alcohol (ethanol + methanol) with ~100% selectivity. Propanols (1-PO + 2-PO) were obtained due to the overhydrogenolysis of 1,2-PDO and linear alcohols (ethanol + methanol) were obtained due to the degradation of glycerol, 1,2-PDO, hydroxyacetone and EG, respectively.

Catalyst reusability study showed that glycerol conversion was decreased by ~ 14% after cycle-3. However, the selectivity towards 1,2-PDO was almost unaffected (~94%) and the selectivity to EG and other degradation products were varied in the range of 2-3.6% and 1.7-3.6%, respectively. The overall yield of 1,2-PDO was decreased from 92.1% to 79.2% after cycle-3 due to the loss of catalytic activity. The physico-chemical properties of the used (after cycle-3) catalyst were compared with the fresh reduced catalysts. The BET surface area of the used catalyst was reduced significantly because of agglomeration of the catalyst particles. The catalyst particles were agglomerated due to the repetitive heat treatment of the catalyst before each cycle and agglomeration of particles was the probable reason of catalyst deactivation.

4.4 Selective hydrogenolysis of glycerol to 1,2-PDO over various basic oxide supported copper-zinc bimetallic catalysts

Cu:Zn(4:1)/MgO catalyst exhibited very high catalytic activity and selectivity for liquid phase glycerol hydrogenolysis to 1,2-PDO reaction. Reusability study suggested that the catalyst was moderately active and selective even after 3rd cycle. To increase the stability of the catalyst further, the effect of various supports ((La_2O_3, BaO_2, CaO, MgO-La_2O_3) on the performance of Cu:Zn bimetallic was investigated. In this section, the catalytic activity of various supported (La_2O_3, BaO_2, CaO, MgO-La_2O_3) Cu:Zn bimetallic catalysts synthesized by co-precipitation method are discussed. Among all of the catalysts, Cu:Zn(4:1)/MgO-La_2O_3 exhibited complete conversion of glycerol at mild reaction condition. The stability and reusability of Cu:Zn(4:1)/MgO-La_2O_3 catalyst was also evaluated.

4.4.1 Catalyst characterization

4.4.1.1 Textural properties

Specific surface area (BET) and pore volume of all the fresh reduced catalyst estimated by N_2-adsorption-desorption technique are summarized in Table 4.14. The maximum surface area of 23.6 $m^2.g^{-1}$ was obtained for 50% Cu:Zn(4:1)/MgO catalyst. Whereas, for 50% Cu:Zn (4:1)/BaO_2 catalyst, it was lowest 1.6 $m^2.g^{-1}$. Pore volume of the catalyst was in the range of 0.006-0.008 $cm^3.g^{-1}$.

4.4.1.2 XRD

To identify the various crystal phase present in the catalyst, X-ray diffraction patterns were collected for all the calcined and reduced catalysts. The obtained diffraction patterns are shown in Figure [4.19 (A) and (B)], respectively. For calcined catalyst, reflection exhibited at 2θ = 35.7°, 38.9°, 56.5°, 68.2°, 72.5° were corresponding to the (002), (111), (021), (220), (311) crystal planes of monoclinic CuO phase, respectively [JCPDS: 80-1917]. The characteristic peaks detected at the 2θ values of 31.6° and 47.3° corresponded to the (100) and (110) crystal planes of hexagonal ZnO phase [JCPDS: 80-0075]. For La_2O_3 supported catalyst, the reflection due to the (004), (020), (115), (114), (204) crystal planes of La_2CuO_4 were detected at the 2θ value of 26.9°, 32.9°, 41.8°, and 43.7°, respectively [JCPDS: 38-0709]. The peak obtained at 49.5° and 44.3° were due to reflection from (200) and (114) crystal planes of La_2CuO_4 phase, respectively [JCPDS: 812450, 81-2448].

Table 4.14. Textural properties of the catalysts

Catalyst	BET Surface area ($m^2.g^{-1}$)[#]	Pore volume ($cm^3.g^{-1}$)
50% Cu:Zn(4:1)/La_2O_3	16.6	0.008
50% Cu:Zn(4:1)/MgO	23.6	0.012
50% Cu:Zn(4:1)/MgO-La_2O_3	15.6	0.008
50% Cu:Zn(4:1)/BaO_2	1.6	0.008
50% Cu:Zn(4:1)/CaO	12.2	0.006

[#] Analytical instruments error for BET surface area: x ± 2%

$La_2O_2CO_3$ phase was detected at the diffraction angle of 22.2°, 25.2°, 25.8°, 30.2° and 54.6° due to the deflection from (004), (100), (101), (103), (203) crystal planes [JCPDS: 841963] [Shi et al., (2010)]. For Cu:Zn/CaO catalyst, diffraction peak detected at 2θ = 48.6° was corresponding to CaO phase [JCPDS: 280775]. $CaCO_3$ phase was detected at the 2θ value of 29.3°, 43.1°, respectively, which referred to (104) and (145) crystal planes of $CaCO_3$ [JCPDS: 86-0174]. For Cu:Zn/BaO_2 catalyst, $Ba_2CuO_{3.39}$ phase was observed at 2θ = 23.9° referred to its (101) crystal plane [JCPDS: 852486].

In the XRD pattern of reduced catalyst (Figure. 4.19 (B)), the reflection due to the metallic copper was detected at the 2θ value of 43.2°, 50.1° and 74.0°, respectively, corresponding to the (111), (200) and (220) crystal planes of monoclinic copper (JCPDS: 85-1326). Together with these, almost all the reduced catalyst, the peaks corresponding to CuO and ZnO were also detected as marked in Figure. 4.19 (B). This result indicated that in the reduced catalyst copper was present in oxide form as well as in reduced form [Pandhare et al., (2016)]. A sharp diffraction peak corresponding to $CaCO_3$ was detected at 2θ = 29.3º in the reduced Cu:Zn/CaO catalyst [JCPDS: 86-0174].

The average crystallite sizes of all the phases present in the fresh calcined and reduced catalysts were calculated from the line width of the respective planes by using Scherer's formula. The calculated values are summarized in Table 4.15. The average crystallite size for calcined catalyst was 29-45 nm whereas it was in the range of 28-57 nm after reduction. The results suggested that the average crystallite size was reduced for 50 wt.% Cu:Zn(4:1)/MgO catalyst after the addition of La_2O_3. For reduced catalyst, the crystallite size of metallic copper was in the range of 30.5-39.5 nm.

4.4.1.3 NH_3-TPD

Acidic sites of the reduced catalysts were identified by NH_3-TPD analysis and the NH_3-TPD profiles are shown in Figure. 4.20 (A). It is known from the previous studies that NH_3 desorption peak evolved at the temperature region from 150-300 °C, 300-550 °C and above 550 °C correspond to weak, medium and strong strength acidic sites, respectively [Pudi et al., (2015a), Pudi et al., (2015b)]. However, in this study, NH_3 desorption peaks of all the catalysts were observed at medium and strong strength acidic region. The total number of acidic sites were estimated by the total amount of NH_3 desorbed per gram of sample at different temperatures which were summarized in Table 4.16. [Rodrigues et al., (2012)]. NH_3-pattern of Cu:Zn(4:1)/MgO and Cu:Zn(4:1)/MgO-La_2O_3 catalysts exhibited medium strength acidic region. All the catalysts exhibited NH_3-desorption peak at higher temperature region which suggested the presence of strong acidic sites. Total acidic sites were estimated and were varied from 1.82-2.36 mmol.gcat^{-1}. Total number of acidic sites were in the order of Cu:Zn(4:1)/MgO > Cu:Zn(4:1)/MgO-La_2O_3 > Cu:Zn(4:1)/La_2O_3 > Cu:Zn(4:1)/BaO_2.

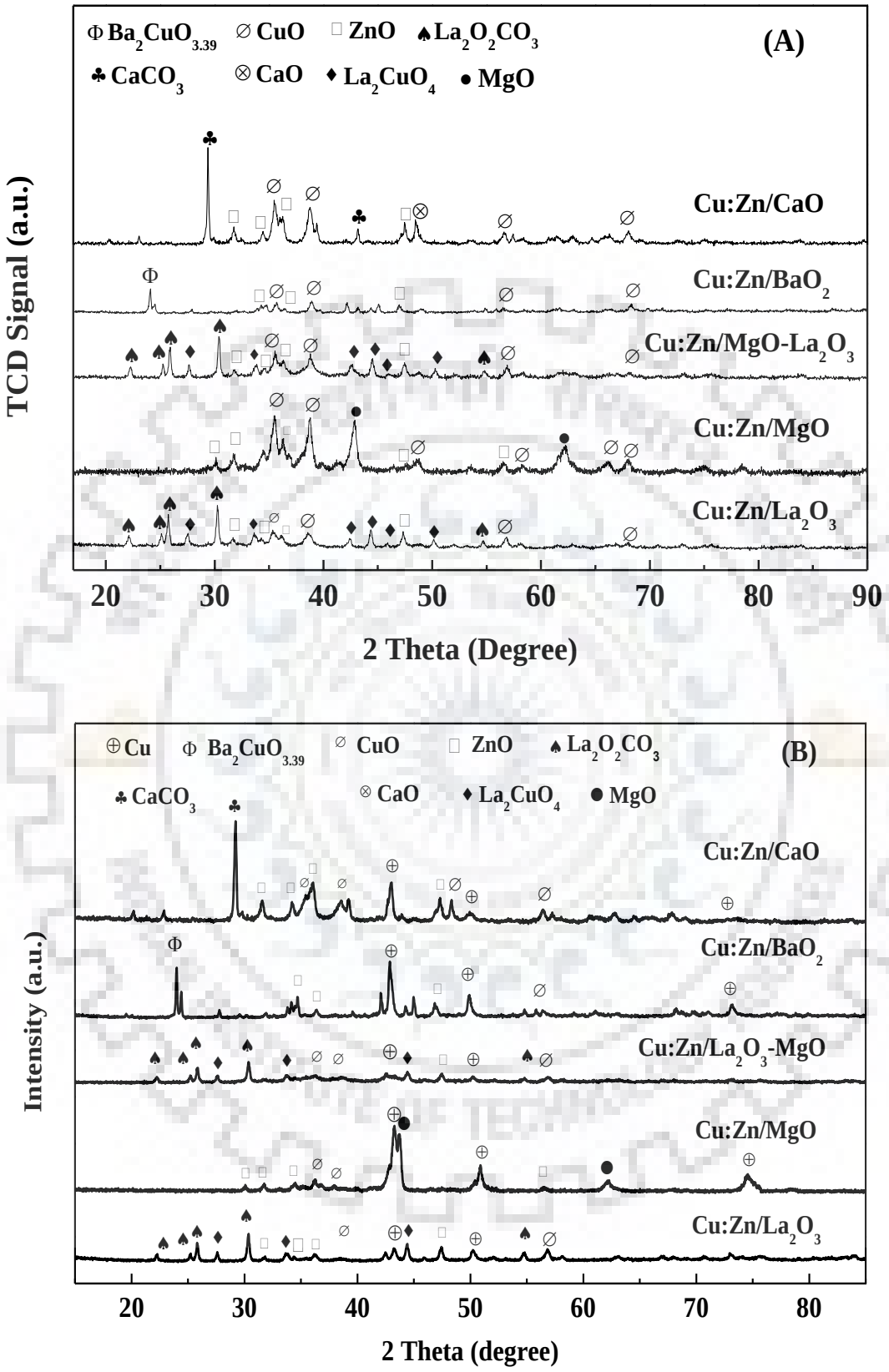

Figure 4.19. XRD pattern of (A) calcined catalysts (B) reduced catalyst

Table 4.15. Crystallite size calculated by using Scherer's formula

Catalyst	Crystallite size (nm) in calcined sample							
	CuO	ZnO	$La_2O_2CO_3$	CaO	$CaCO_3$	La_2CuO_4	$BaCuO_{2.5}$	Average
50% Cu:Zn(4:1)/La_2O_3	20.8	22.2	40.3	-	-	36.6	-	30.0
50% Cu:Zn(4:1)/MgO	28.1	30.0	-	-	-	-	-	29.1
50% Cu:Zn(4:1)/MgO-La_2O_3	22.5	28.2	35.1	-	-	31.3	-	29.3
50% Cu:Zn(4:1)/BaO_2	32.7	33.4	-	-	-	-	71.2	45.8
50% Cu:Zn(4:1)/CaO	34.1	32.7	-	18.5	45.2	-	-	32.6
	Crystallite size (nm) in reduced sample							
	CuO	ZnO	$La_2O_2CO_3$	Cu	La_2CuO_4	$BaCuO_{3.39}$	$CaCO_3$	Average
50% Cu:Zn(4:1)/La_2O_3	17.4	23.2	34.15	30.5	35.0	-	-	28.1
50% Cu:Zn(4:1)/MgO	29.4	33.2	-	37.1	-	-	-	33.2
50% Cu:Zn(4:1)/MgO-La_2O_3	18.3	25.3	37.12	32.2	26.3		-	27.8
50% Cu:Zn(4:1)/BaO_2	-	61.8	-	39.5	-	71.2	-	57.4
50% Cu:Zn(4:1)/CaO	34.3	38.6	-	32.3	-	-	38.2	34.1

4.4.1.4 CO_2-TPD

CO_2-TPD analysis technique was used in order to quantify the basic sites of the reduced catalysts. CO_2-TPD profile of the reduced catalysts is shown in Figure. 4.20 (B). Total basic sites are classified into three regions: weak (150-300 °C), medium (300-550 °C) and strong strength basic sites (above 550 °C), respectively [Pudi et al., (2015a, 2015b)]. In this study, weak basic sites were not detected in the catalysts. Total basic sites were summarized in Table 4.16. Total no of basic sites was calculated by the total amount of CO_2 desorbed per gram of sample and were in the range of 1.21-1.86 mmol. $gcat^{-1}$. Total basic sites of all the reduced catalyst were as follows: Cu:Zn(4:1)/MgO-La_2O_3 > Cu:Zn(4:1)/MgO > Cu:Zn(4:1)/La_2O_3 > Cu:Zn(4:1)/BaO_2. It can be observed from Figure 4.20 (B) that Cu:Zn(4:1)/La_2O_3 and Cu:Zn(4:1)/MgO-La_2O_3 catalyst exhibited a significant amount of medium strength basic sites. All the catalysts showed CO_2 desorption peak at higher temperature region which suggested the presence of strong strength basic sites.

NH_3-TPD and CO_2-TPD pattern of Cu:Zn(4:1)/CaO catalyst is shown in Figure 4.20 (C). For both the cases, similar desorption peaks were detected at 850 °C. These peaks were detected due to the decomposion of $NaHCO_3$ which was used as a precipitation agent during the synthesis of catalysts.

4.4.1.5 TGA

As $NaHCO_3$ was used as a precipitation agent during the synthesis of catalysts, peak evolved at the higher temperature (> 600 °C) were might be from the decomposition of bicarbonate species. To ensure this, TGA study of all the catalysts were carried out at inert atmosphere. TGA pattern of all the supported catalysts is shown in Figure 4.21. It was observed that except CaO supported catalyst, all the catalysts were stable at higher temperature up to 900 °C. Cu:Zn(4:1)/CaO catalyst showed a similar type of NH_3/CO_2-desorption peak at around 850 °C temperature. So, it can be concluded that this peak is not related to the desorption of NH_3 or CO_2 [James et al., (2013)].

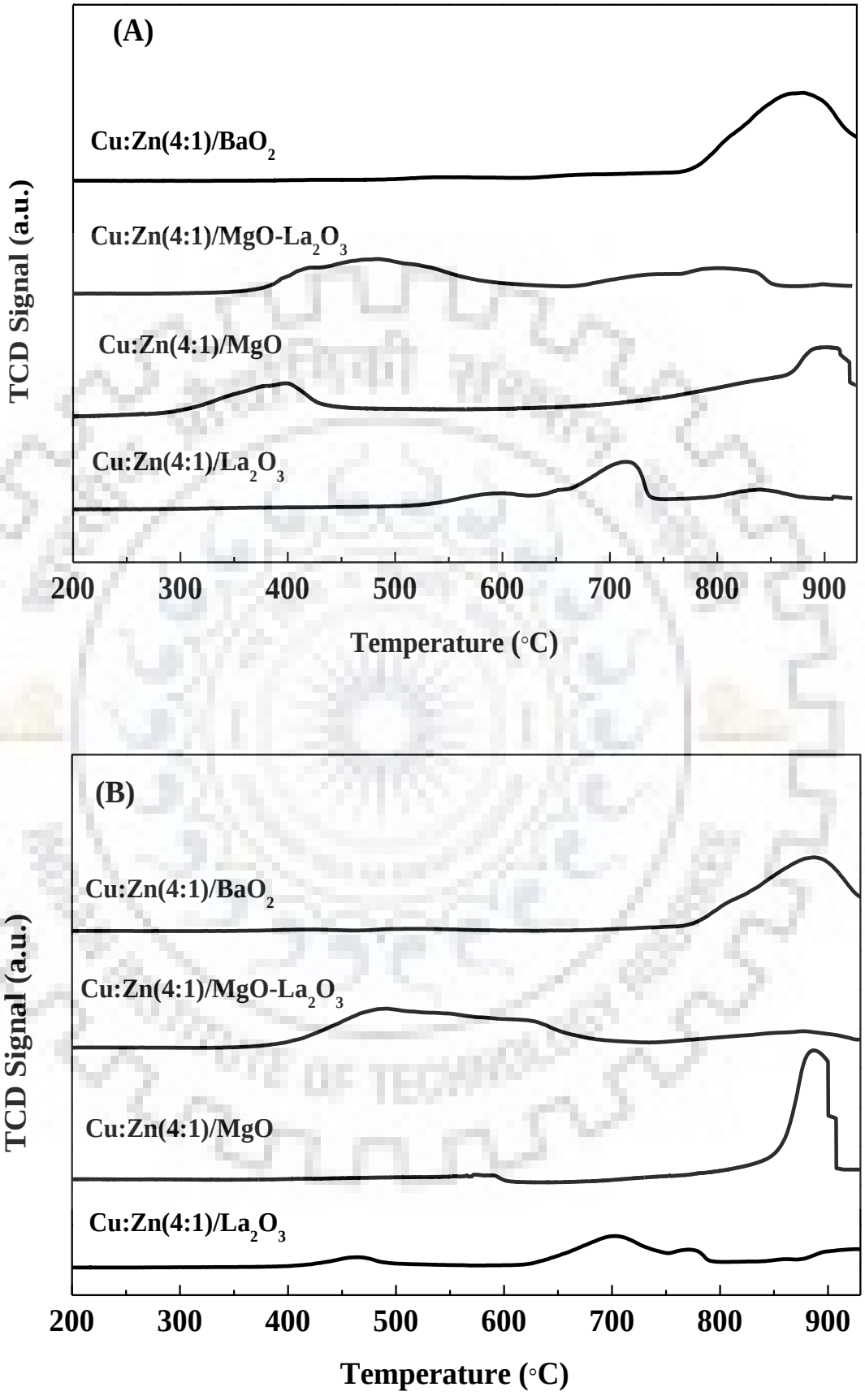

Figure. 4.20. (A) NH_3-TPD of all the catalysts (B) CO_2-TPD pattern of all the catalysts

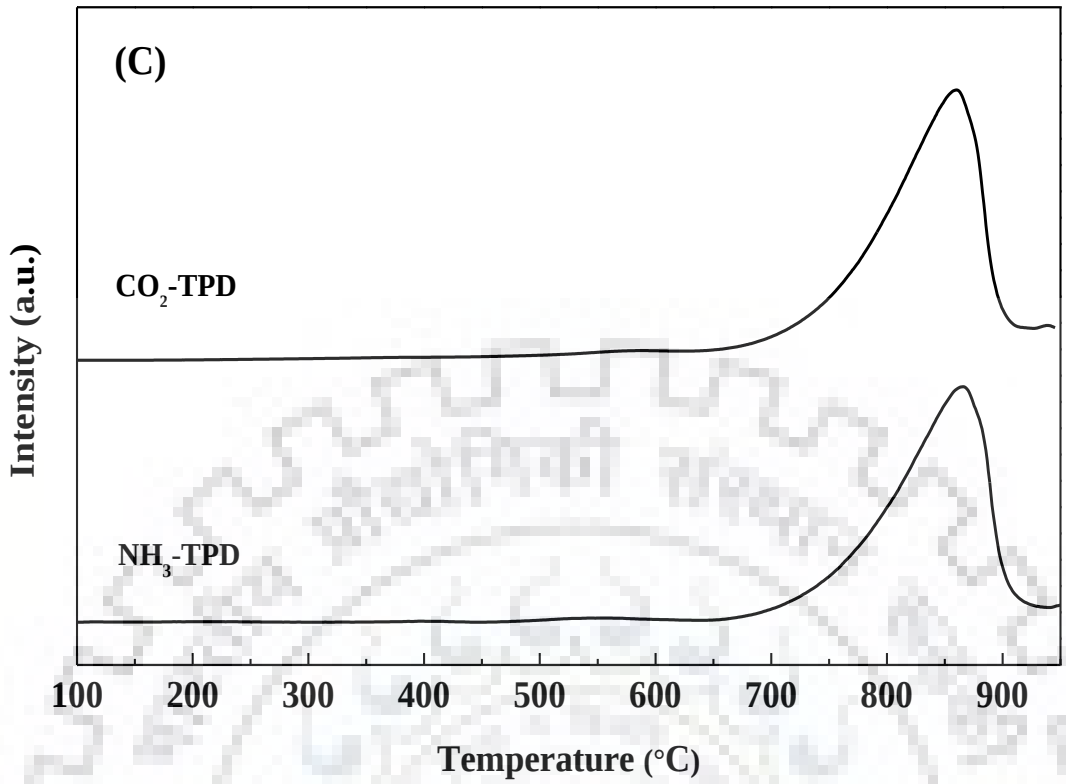

Figure. 4.20. (C) NH_3-TPD and CO_2-TPD pattern of Cu:Zn(4:1)/CaO catalyst

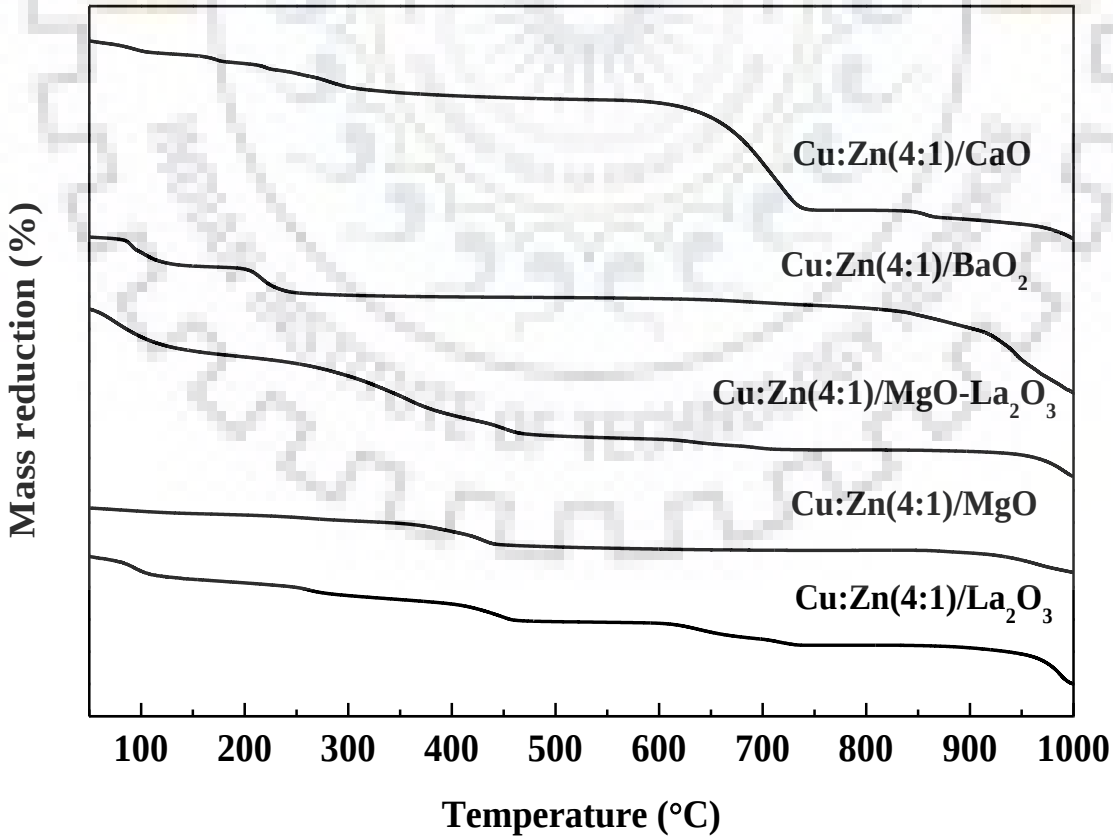

Figure. 4.21. TGA pattern of all the supported catalyst

Table 4.16. NH_3-TPD and CO_2-TPD data of the catalysts

NH_3-TPD data of the catalysts				
Catalyst	(Acidity) (mmol.gcat^{-1}) †			
	Weak	Medium	Strong	Total
Cu:Zn(4:1)/La_2O_3	-	-	1.82	1.82
Cu:Zn(4:1)/MgO	1.238	0.438	0.454	2.13
Cu:Zn(4:1)/MgO-La_2O_3	0.034	1.419	0.67	2.12
Cu:Zn(4:1)/BaO_2	-	-	1.34	1.34
Cu:Zn(4:1)/CaO	-	-	7.09	7.09
CO_2-TPD data of the catalysts				
Catalyst	(Basicity) (mmol.gcat^{-1}) †			
	Weak	Medium	Strong	Total
Cu:Zn(4:1)/La_2O_3	-	0.267	1.179	1.446
Cu:Zn(4:1)/MgO	0.0008	0.165	1.644	1.81
Cu:Zn(4:1)/MgO-La_2O_3	0.004	1.721	0.143	1.87
Cu:Zn(4:1)/BaO_2	-	-	1.33	1.33
Cu:Zn(4:1)/CaO	-	-	3.21	3.21

† Analytical instruments error for the active volume obtained in TPD: x ± 2%

4.4.1.6 H_2-TPR

Temperature programmed reduction (TPR) profiles of all the calcined catalysts are shown in Figure 4.22. MgO, CaO, BaO_2 and La_2O_3 did not show any reduction peak at the temperature range of 50-850 °C [Surendar et al., (2017), Yang et al., (2016)]. In our previous study, it was observed that ZnO was slightly reduced at ~550 °C. In this study, all the catalysts showed a reduction peak between 240-300°C which might be associated to the direct reduction of CuO to Cu^o [Pudi et al., (2015a), Kim et al., (2003)]. Cu:Zn(4:1)/La_2O_3 exhibited a reduction peak of CuO at around 241 °C. For Cu:Zn(4:1)/MgO catalyst, the reduction peak of CuO was shifted towards higher temperature at 266 °C. This result suggested that La_2O_3 facilitated lowering the reduction temperature of CuO significantly as compared to MgO. After addition of La_2O_3 to Cu:Zn(4:1)/MgO catalyst, reduction peak was shifted from 266 °C to 261 °C [Moura et al., (2014)]. Cu:Zn(4:1)/BaO_2 catalyst exhibited reduction peak comparatively higher

temperature at 302 °C. TPR profile of Cu:Zn(4:1)/CaO showed a sharp reduction peak at 264.8 °C. It is suggested from the Figure 4.22, La_2O_3 based catalyst exhibited reduction peak of CuO at lowest temperature compared to all of the supported catalysts. Variation in reduction temperature of CuO with different supported catalysts indicated the variation of metal support interaction. H_2-consumption and calculated degree of reduction of all the catalysts were summarized in Table 4.17. Details calculation procedure for estimating the degree of reduction was discussed in our earlier section (4.3.1.3). The degree of reduction of all the catalysts were in the range of 61.8% to 97.1%. Degree of reduction were varied in the following order Cu:Zn(4:1)/MgO-La_2O_3 > Cu:Zn(4:1)/La_2O_3 > Cu:Zn(4:1)/CaO > Cu:Zn(4:1)/BaO_2. Though Cu:Zn(4:1)/La_2O_3 catalyst showed reduction peak at a lower temperature compared to Cu:Zn(4:1)/MgO catalyst, H_2 consumption amount of Cu:Zn(4:1)/La_2O_3 was much lower compared to the later. Cu:Zn(4:1)/MgO showed ~91.7% degree of reduction. After addition of La_2O_3 to Cu:Zn(4:1)/MgO catalyst, the degree of reduction increases significantly (97.1%). This result indicated that after the addition of lanthanum oxide to Cu:Zn(4:1)/MgO catalyst, more reducible CuO species were formed on the surface of the catalyst.

Table 4.17. H_2-TPR and XPS results of the catalysts

Samples	H_2-TPR		XPS
	H_2-consumption ($mmol.gcat^{-1}$) †	degree of reduction (%)	$(Cu^+ + Cu^o)/Cu$
Cu:Zn(4:1)/La_2O_3	6.15	78.8	0.690
Cu:Zn(4:1)/MgO	6.70	91.7	0.969
Cu:Zn(4:1)/MgO-La_2O_3	7.32	97.1	0.727
Cu:Zn(4:1)/BaO_2	4.82	61.8	0.248
Cu:Zn(4:1)/CaO	6.01	76.7	0.420

†Analytical instruments error for the active volume obtained in TPR: x ± 2%

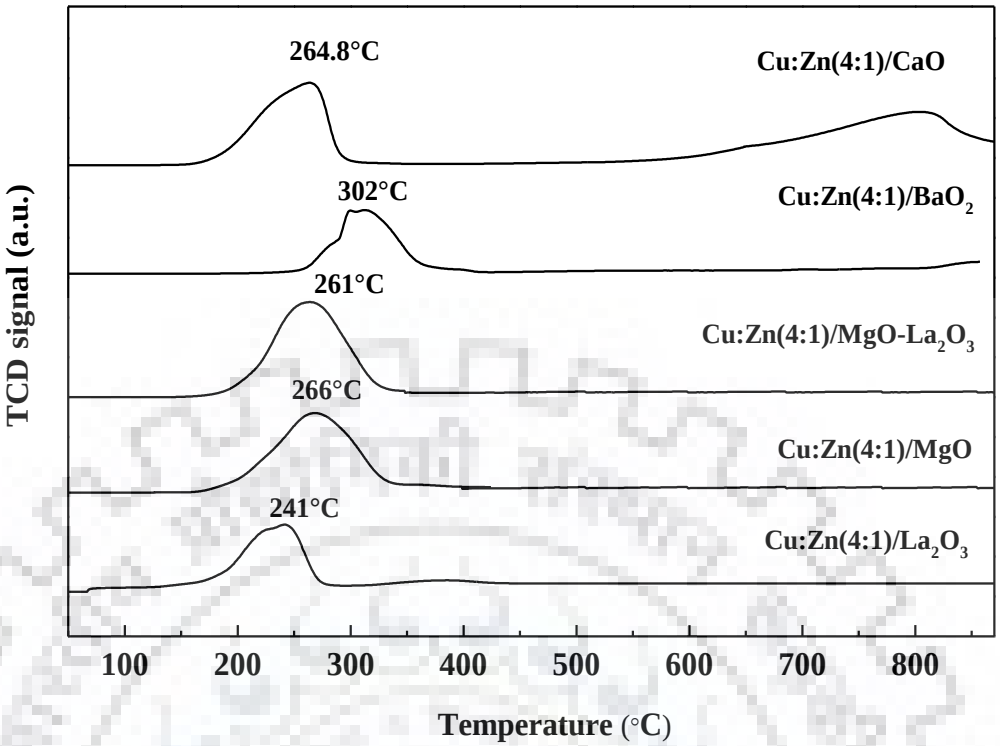

Figure. 4.22. H_2-TPR pattern of all the catalyst

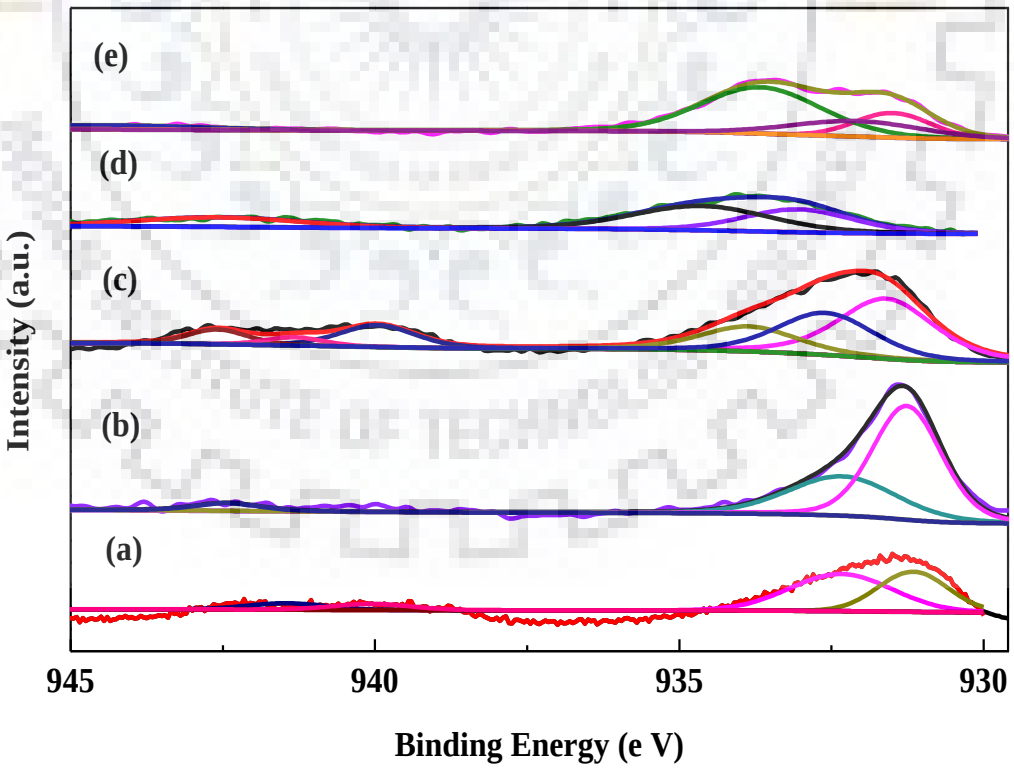

Figure 4.23. XPS pattern of catalysts (a) Cu:Zn(4:1)/La_2O_3, (b) Cu:Zn(4:1)/MgO, (c) Cu:Zn(4:1)/MgO-La_2O_3, (d) Cu:Zn(4:1)/BaO_2, (e) Cu:Zn(4:1)/CaO

4.4.1.7 X-ray photoelectron spectra (XPS)

X-ray photoelectron spectra of $Cu2p_{3/2}$ region was investigated to identify the oxidation state of copper species present on the catalysts surface. The obtained $Cu2p_{3/2}$ spectra of all the catalysts are shown in Figure 4.23. The spectrum obtained between the binding energy of 930-935 eV was de-convoluted into three different peaks. Binding energy corresponded to 931.2 ± 0.2, 932.3 ± 0.3 and higher than 933 eV represented the presence of Cu^{+}, $Cu^{o,}$ and Cu^{+2} species, respectively [Zhong et al., (2008), Kwak et al., (2012), Feng et al., (2015)]. Satellite peaks obtained at higher binding energy i.e. 942.9 and 944 eV confirmed the presence of Cu^{+2} species [Duran Martin et al., (2013)]. Various previous studies [Vila et al., (2012)] reported that surface concentration of both Cu^{+} and Cu^{o} species were solely responsible for higher catalytic activity for selective production of 1,2-PDO from glycerol. The atomic ratio of $(Cu^{+} + Cu^{o})/Cu$ species of all the catalysts was calculated and the obtained values are summarized in Table 4.17. This ratio was attributed to the total active sites present on the catalyst surfaces. The calculated atomic ratio of $(Cu^{+}+Cu^{o})/Cu$ species for all the catalyst followed the order as Cu:Zn(4:1)/MgO > Cu:Zn(4:1)/MgO-La_2O_3 > Cu:Zn(4:1)/La_2O_3 > Cu:Zn(4:1)/CaO > Cu:Zn(4:1)/BaO_2. Earlier Kwak et al., (2012) determined the ratio of Cu^{o}/Cu^{2+} of all the synthesized catalysts which indirectly related to the catalytic performance of glycerol hydrogenolysis reaction. Liu et al., (2016) observed that after addition of WO_x in Cu/Al_2O_3 catalyst, the ratio of $Cu^{+}/(Cu^{+} + Cu^{o})$ increased from 54.6% to 65.1% which suggested the strong interaction between Cu and WO_x species. Vila et al., (2012) reported that selectivity towards 1,2-PDO mostly related to the ratio of Cu^{o}/Cu^{+} and also to the total concentration of Cu species. Xiao et al., (2014) observed that with increasing of Cu^{o}/Cu^{+} ratio from 3.1 to 6.6, glycerol conversion increased and reached the maxima, however beyond 6.6 to 15.7, glycerol conversion followed a decreasing trend. These results suggested that optimum ratio of Cu^{o}/Cu^{+} are required for higher glycerol hydrogenolysis activity.

4.4.1.8 FE-SEM

FE-SEM images (Figure 4.24) obtained for different catalysts indicated different types of surface morphology of the catalyst with the variation of support. As shown in Figure 4.24, the surface morphology of MgO supported Cu:Zn bi-metallic catalyst showed rod-like structure, whereas, La_2O_3 supported catalysts exhibited spherical shaped structure. After the addition of La_2O_3 to Cu:Zn(4:1)/MgO catalyst, the spherical structure was found to be enlarged.

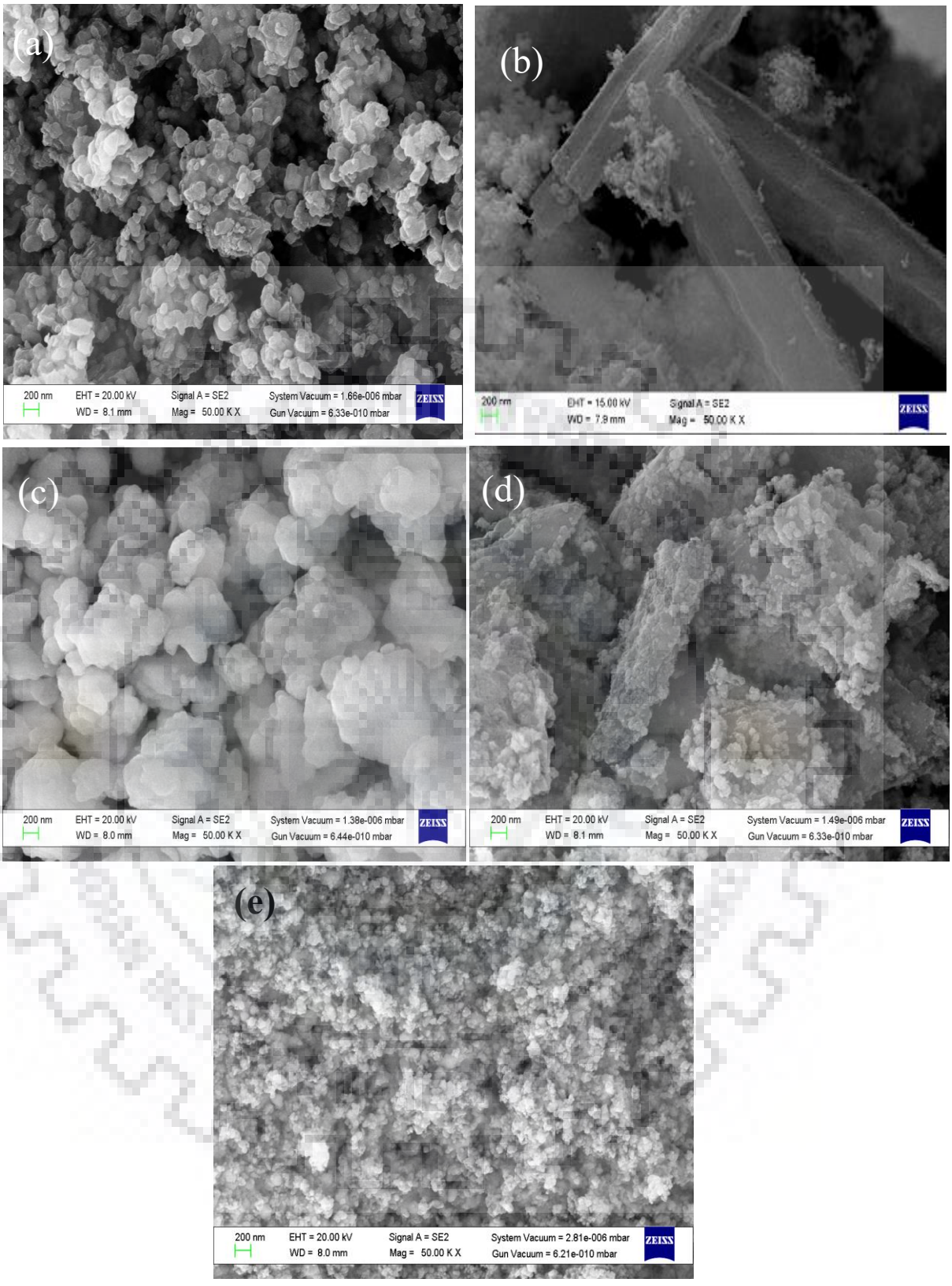

Figure 4.24. FE-SEM images of catalysts (a) Cu:Zn(4:1)/La_2O_3, (b) Cu:Zn(4:1)/MgO, (c) Cu:Zn(4:1)/MgO-La_2O_3, (d) Cu:Zn(4:1)/CaO, (e) Cu:Zn(4:1)/BaO_2

For CaO supported catalyst, cluster-like structure was observed and BaO_2 supported catalyst showed small spherical shaped morphology. This different morphology indicated different types of metal support interactions which provided different types of active centers and hence different catalytic activity were observed for different catalysts.

4.4.2 Catalytic activity

The catalytic activity of Cu:Zn bimetallic catalyst supported on various metal-oxide was investigated for liquid phase glycerol hydrogenolysis reaction at 210 °C temperature and 4.5 MPa pressure. The catalytic activity of all the supported catalysts is shown in Table 4.18. Carbon balances of all the experiments reported in Table 4.18 were closely 100 ± 8%. Except Cu:Zn(4:1)/BaO_2, all other catalysts exhibited very high glycerol conversion (> 96%). It was observed that Cu:Zn(4:1)/BaO_2 catalyst was least active and showed 40% glycerol conversion, whereas, Cu:Zn(4:1)/MgO-La_2O_3 catalyst was most active and revealed complete conversion of glycerol at the reaction condition used. Higher activity of Cu:Zn(4:1)/MgO-La_2O_3 catalyst was associated with the smallest average crystallite size (27.8 nm), higher acidity (2.12 mmol.gcat^{-1}), basicity (1.87 mmol.gcat^{-1}) and higher reducibility (97%). Poor activity of Cu:Zn(4:1)/BaO_2 catalyst was because of smaller surface area (1.6 $m^2.g^{-1}$), higher particle size (57.4 nm), lower basicity (1.34 mmol.gcat^{-1}), lower degree of reduction (61.8%) and the presence of lower active Cu species (Table 4.17). Hydrogen consumption over various catalyst followed the order as Cu:Zn(4:1)/MgO-La_2O_3 > Cu:Zn(4:1)/MgO > Cu:Zn(4:1)/La_2O_3 > Cu:Zn(4:1)/CaO > Cu:Zn(4:1)/BaO_2. These results very well correlated with the catalytic activity obtained over all the catalysts. More hydrogen consumption indicated more degree of reduction, which enhanced the presence of reducible copper on the catalyst and hence activity.

In presence of all the catalysts, 1,2-PDO was obtained as a primary reaction product and the selectivity was very high (82.6-93.4%) (Table 4.18). Small amounts (2.7-4.6 %) of ethylene glycol (EG) and other products including propanol, ethanol, methanol were also obtained over different supported Cu:Zn bimetallic catalysts. The selectivity to other products was varied in the range of 4 - 12.9%. The obtained 1,2-PDO selectivity for La_2O_3, MgO, and La_2O_3-MgO supported catalysts catalyst was almost identical (~93%). Cu:Zn(4:1)/CaO showed slightly lower (~89.9%) selectivity towards 1,2-PDO and it was lowest (82.6%) for BaO_2 supported catalyst. As shown in Table 4.18, in presence of CaO and BaO_2 supported catalyst the selectivity to EG and other products (propanol + ethanol + methanol) were higher as compared to other catalyst and the selectivity to other products was almost 13% in presence of BaO_2

supported catalyst. These results indicated that these two catalysts were less selective to 1,2-PDO and more degradation product were formed due to overhydrogenolysis reaction.

Table 4.18. Catalytic activity

Catalyst	Conversion (%)	Selectivity (%)			Yield (%)
		1,2-PDO	EG	Others*	
50wt.% Cu:Zn(4:1)/La_2O_3	96.3	93.3	2.7	4.0	89.8
50wt.% Cu:Zn(4:1)/MgO	98.7	93.4	3.2	3.4	92.2
50wt.% Cu:Zn(4:1)/MgO-La_2O_3	100	93.4	3.9	2.7	93.1
50wt.% Cu:Zn(4:1)/BaO_2	40.1	82.6	4.5	12.9	33.1
50wt.% Cu:Zn(4:1)/CaO	96.2	89.9	4.6	5.5	86.5

Experimental errors for all the values (conversion, selectivity and yield) : x ± 1 %
Reaction condition: Temperature = 210 °C, H_2 pressure = 4.5 MPa, 20 wt.% glycerol (20 g), catalyst amount = 1.6 g, time = 12 h.
*Others: hydroxyacetone, 1-propanol, 2-propanol, ethanol and methanol.

The overall yield of 1,2-PDO was highest (93.1%) for La_2O_3-MgO supported catalyst and Cu:Zn(4:1)/BaO_2 catalyst showed only 33.1% yield to 1,2-PDO. It was observed that Cu:Zn(4:1)/La_2O_3 and Cu:Zn(4:1)/MgO catalyst provided 89.8% and 92.2% yield to 1,2-PDO, respectively. For hydrogenolysis process, the role of acidic and/or basic strength of the catalyst played an important role to control the product selectivity which is very well discussed in previous literature [Wang et al., (2010), Wang et al., (2015b), Pudi et al., (2015a)]. It is reported that catalytic activity, as well as 1,2-PDO selectivity, was enhanced in presence of appropriate amount of acidic and/or basic sites on the catalyst surface. Cu:Zn(4:1)/MgO catalyst showed very high catalytic activity (~99%) and 1,2-PDO yield (92.2%) with respect to others i,e. La_2O_3, CaO and BaO_2 supported catalysts due to the higher acidic (2.12 mmol NH_3 $gcat^{-1}$) as well as basic strength (1.81 mmol CO_2 $gcat^{-1}$) of the catalyst, higher reducibility (91.7%) and the presence of higher amount of active sites [i.e. (Cu^+ + Cu^o)/Cu atomic ratio]. It was very interesting to note that, after the incorporation of La_2O_3 into Cu:Zn(4:1)/MgO

catalyst, 1,2-PDO yield was increased from 92.2% to 93.1%. XRD-results revealed that after addition of La_2O_3 to Cu:Zn(4:1)/MgO catalyst, average crystallite size was decreased from 33.2 nm to 27.8 nm. CO_2-TPD result also suggested that La_2O_3 enhanced the basic strength of the catalyst from 1.81 mmol.gcat^{-1} to 1.86 mmol.gcat$^{-1.}$ The inclusion of La_2O_3 to Cu:Zn(4:1)/MgO catalyst increased reducibility of CuO to Cu^o remarkably from 91.7% to 97%. These were the possible reason for higher 1,2-PDO yield in presence of La_2O_3 doped Cu:Zn(4:1)/MgO catalyst. Since Cu:Zn(4:1)/MgO-La_2O_3 catalyst was found to be the most active and selective to 1,2-PDO, therefore, this catalyst was selected for further parameter study. The effect of different reaction parameter on the catalytic activity and product selectivity is discussed in the following section.

4.4.3 Parameter studies

Influences of various reaction parameters such as temperature, pressure, catalyst loading and feed concentration were investigated over 50 wt.% Cu:Zn(4:1)/MgO-La_2O_3 catalyst at standard reaction condition i.e. at 210 °C and at 4.5 MPa H_2-pressure in presence of 20 wt.% aqueous glycerol solution as feed with 8 wt.% of catalyst loading. Reaction data were collected after a reaction time of 12 h. Experimental errors for all the values (conversion, selectivity and yield) in Figure 4.25 are x ± 1 %.

4.4.3.1 Effect of temperature

Effect of temperature on glycerol conversion and products selectivity was investigated in the temperature range of 170-210 °C and the results are shown in Figure 4.25 (A). It was observed that conversion of glycerol increased sharply at elevated temperature as expected. Glycerol conversion increased from 81% to 100% as the temperature was increased from 170 °C to 190 °C. Selectivity towards 1,2-PDO was very high and it was almost constant (94%) throughout. The slight decrease in selectivity towards 1,2-PDO at the higher temperature (>200 ^{o}C) was due to the over hydrogenolysis of 1,2-PDO which led to the formation of degradation products such as EG, PO, methanol etc. [Sato et al., (2009), Akiyama et al., (2009)]. The overall yield of 1,2-PDO increased from 78.8% to 93.5% with increasing the temperature from 170 °C to 210 °C [(Figure 4.25 (A)]. Results suggested that approximately 210 ^{o}C was the optimum temperature for higher selectivity towards 1,2-PDO.

4.4.3.2 Effect of pressure

Influence of reaction pressure on glycerol conversion and products selectivity is shown in Figure. [4.25 (B)]. It was observed that 100% conversion of glycerol was achieved at 4.5 MPa and higher. Selectivity towards 1,2-PDO decreased slightly from 97% to 94% when pressure was increased from 3.0 MPa to 6 MPa. This was due to the formation of other products such as ethylene glycol, methanol at higher pressure. It was observed that the selectivity to ethylene glycol increased from ~2.1% at 3.0 MPa to 4.2% at 6 MPa. The overall yield of 1,2-PDO increased from 64% to 93.4% as pressure increased from 3.0 MPa to 4.5 MPa. Further increasing the pressure had no significant effect on the yield of 1,2-PDO. This result suggested that hydrogen pressure within the range of 3-4.5 MPa had a significant effect on the conversion glycerol to 1,2-PDO as more number of hydrogen species was adsorbed on the surface of the catalyst [Huang et al., (2008)]. Pressure beyond 4.5 MPa was not beneficial for 1,2-PDO production as higher pressure propagated overhydrogenolysis to lower alcohols.

4.4.3.3 Effect of catalyst loading

Effect of catalyst loading was studied by varying the catalyst loading from 2-8 wt.% at 210 ^{o}C temperature, 4.5 MPa pressure in presence of 20 wt.% aqueous glycerol solution as feed. Figure 4.25 (C) showed that as the catalyst loading increased from 2-8 wt.%, glycerol conversion was enhanced from 39.5% to 100% and the selectivity towards 1,2-PDO was decreased from ~98% to ~93%. It was also observed that the selectivity to other products increased from ~1.95% to ~6.7%. The overall yield of 1,2-PDO increased from 42.1% to 93.3% with increasing of catalyst loading from 2-8 wt.%. Increasing of glycerol conversion with catalyst loading is due to the availability of a higher number of catalytic active sites at higher catalyst loading. Results demonstrated the optimum catalyst loading of 8 wt.% for higher selectivity towards 1,2-PDO.

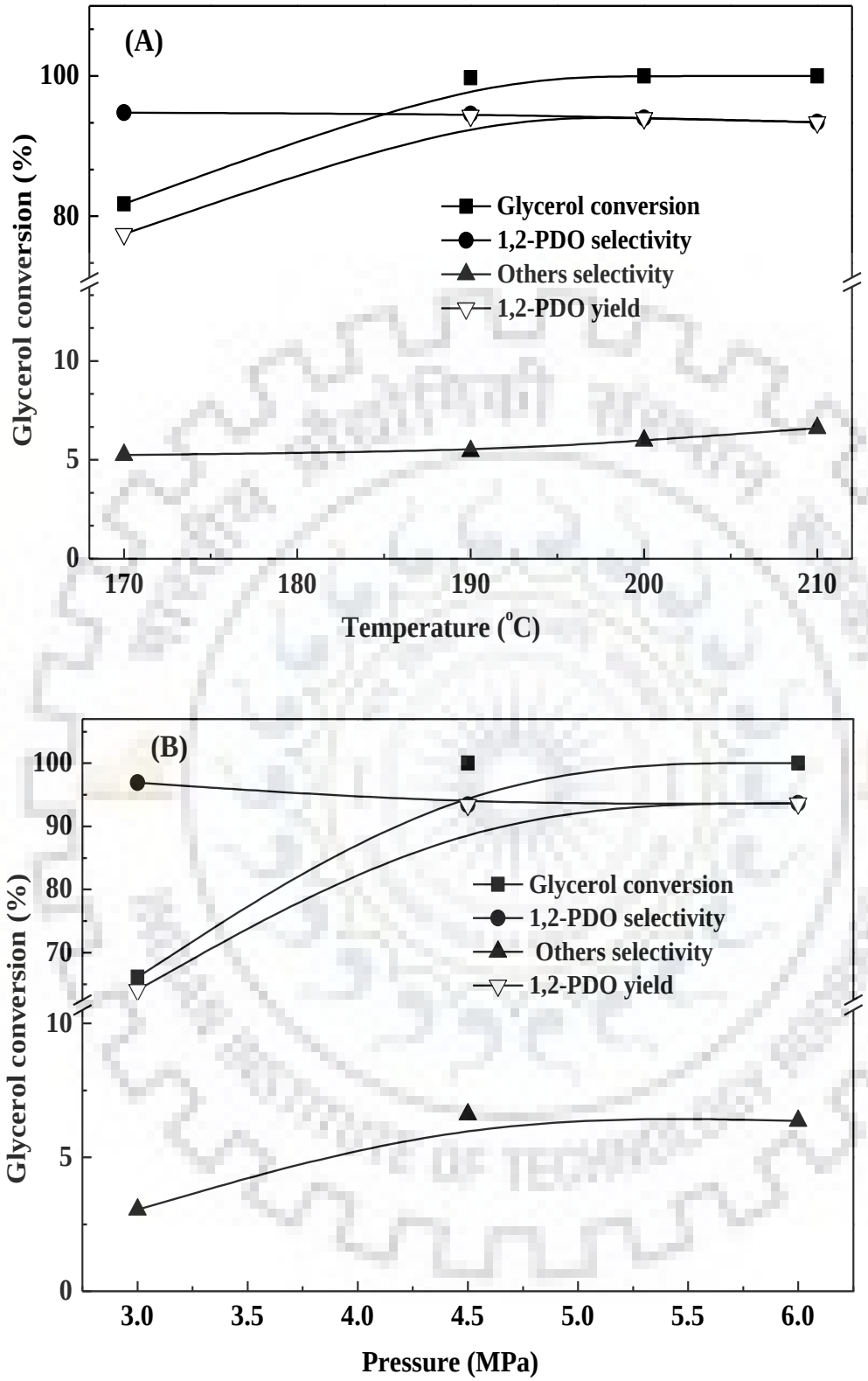

Figure 4.25. (A) Effect of reaction temperature, reaction condition: 4.5 MPa H_2 pressure, 20 wt.% glycerol (20 g), 1.6 g catalyst, reaction time 12 h (B) Effect of initial hydrogen pressure, reaction condition: 210 °C temperature, 20 wt.% glycerol (20 g), 1.6 g catalyst, reaction time 12 h

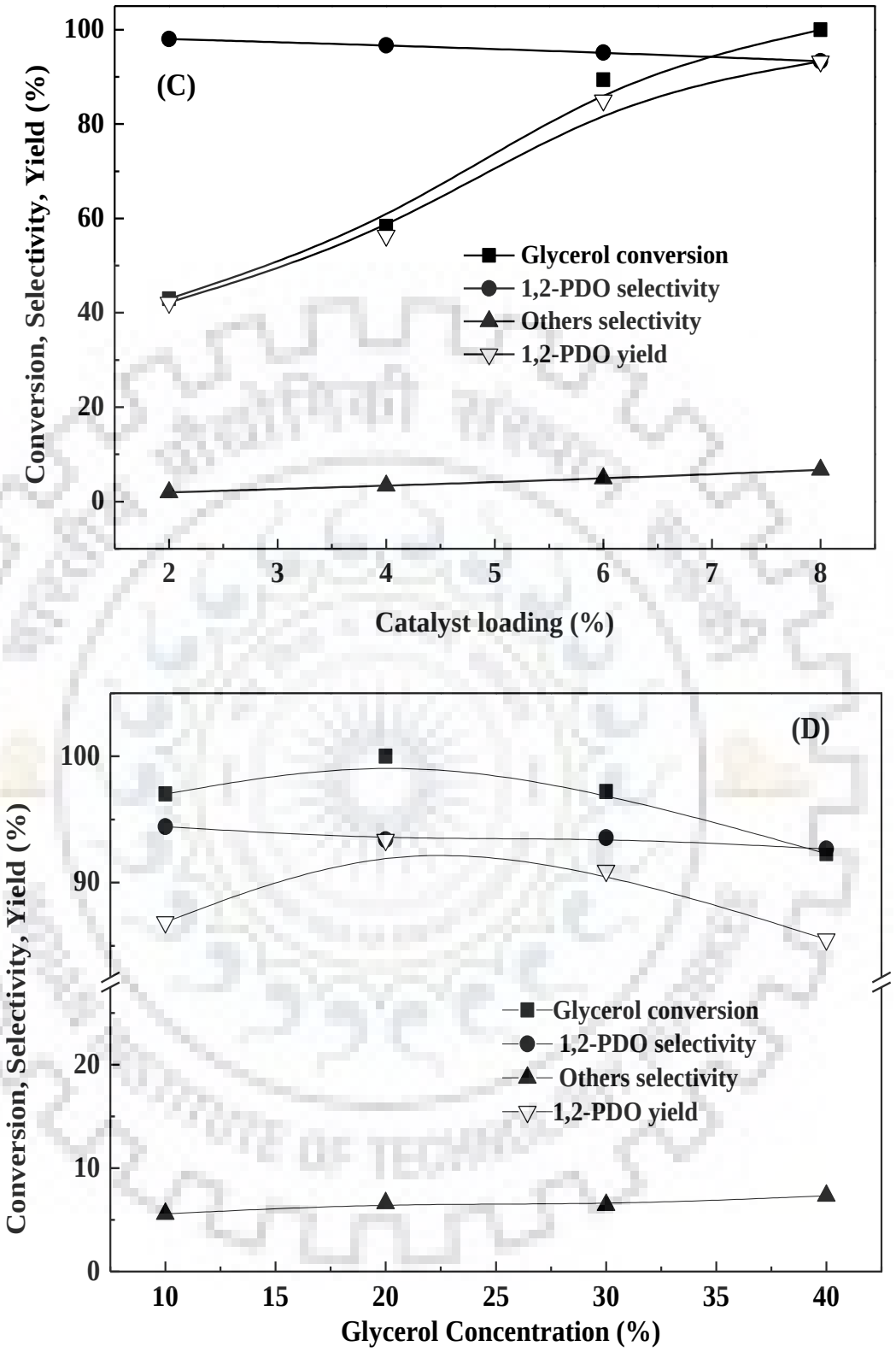

Figure 4.25. (C) Effect of catalyst loading, reaction condition: 210 °C temperature, 4.5 MPa H_2 pressure, 20 wt.% glycerol (20 g), reaction time 12 h (D) Effect of glycerol concentration, reaction condition: 210 °C temperature, 4.5 MPa H_2 pressure, (0.8-3.2) g catalyst, reaction time 12 h

4.4.3.4 Effect of glycerol concentration

Figure 4.25 (D) showing the dependence of glycerol concentration on glycerol conversion and the selectivity to the hydrogenolysis products. Glycerol concentration was varied from 10-40 wt.%. It was observed that, initially, conversion of glycerol increased from 96% to 100% as the feed concentration was varied from 10-20 wt.%. Further increasing the glycerol concentration up to 40 wt.%, glycerol conversion was decreased from 100% to 92.2%. Decreasing of glycerol conversion at higher concentration was because of higher viscosity and the availability of less number of hydrogen species [Sharma et al., (2014), Ameen et al., (2017)]. The selectivity towards 1,2-PDO decreased slightly from 94.6% to 92.6% with increasing the glycerol concentration from 10 wt.% to 40 wt.%. The overall yield of 1,2-PDO was passed through a maxima. Initially, it increased from 91.6% to 93.4% with increasing glycerol concentration from 10%-20%. Further, it decreased to 85.5% as the concentration of glycerol was increased up to 40 wt.%.

Reaction parameter study suggested that in presence of Cu:Zn(4:1)/MgO-La_2O_3 catalyst, 100% conversion with 93.3% selectivity towards 1,2-PDO was achieved at 210 ^oC temperature, 4.5 MPa pressure in presence of 8 wt.% catalyst and 20 wt.% aqueous glycerol solution as feed.

4.4.4 Reusability study

Stability and reusability of Cu:Zn(4:1)/MgO-La_2O_3 catalyst was investigated at the optimum reaction condition up to 4^{th} cycle. In a typical procedure, the catalyst was separated from the products and washed with distilled water several times followed by ethanol. Further, the solution was dried in an oven at 100 °C for 24 h followed by calcination at 400 °C for 4 h. Calcined catalyst was reduced at 350 °C for 2 h under the flow of H_2 before every reuse. The reusability results obtained are summarized in Table 4.19. It was found that after 4^{th} cycle, glycerol conversion was decreased by ~15 % with respect to fresh catalyst and the selectivity towards 1,2-PDO was decreased by ~30% with a simultaneous increase in the selectivity to 1-propanol (1-PO) from 10.7% to 29%. These results suggested that the selectivity to 1-PO was increased at the expense of the selectivity towards 1,2-PDO due to overhydrogenolysis process. With repetitive heat treatment and reduction of the catalyst after every cycle, the reducibility of the catalyst was increased significantly which was probably the primary reason to enhance the overhydrogenolysis activity of the catalyst.

To determine the deactivation reason, the structural and physico-chemical properties of the catalyst after the 4th cycle was characterized by XRD, BET, TEM and XPS, respectively. The characterization results of fresh reduced and used (after 4th cycle) catalyst were compared. XRD patterns of the used catalyst showed very sharp diffraction peaks for all the different phases present as marked in Figure 4.26. The intensity of the peaks corresponding to metallic copper were increased significantly which indicated the enhanced crystallinity of the copper metal on the catalyst surface after repetitive heat treatment and reduction before every use. By comparing both the XRD patterns, it was observed that, in addition to the original diffraction peaks, two more additional peaks at the 2θ value of 17.8°, 24.4° were detected. These additional peaks corresponded to a new crystal plane of $LaCO_3OH$ species [JCPDS: 49-0981] [Zheng et al., (2013)]. These new planes were formed might be due to the prolonged exposure of the catalyst with water in successive reuse. The formation of this new phase in the catalyst was might be another possible reason for the lower catalytic activity and 1,2-PDO selectivity after the 4th cycle.

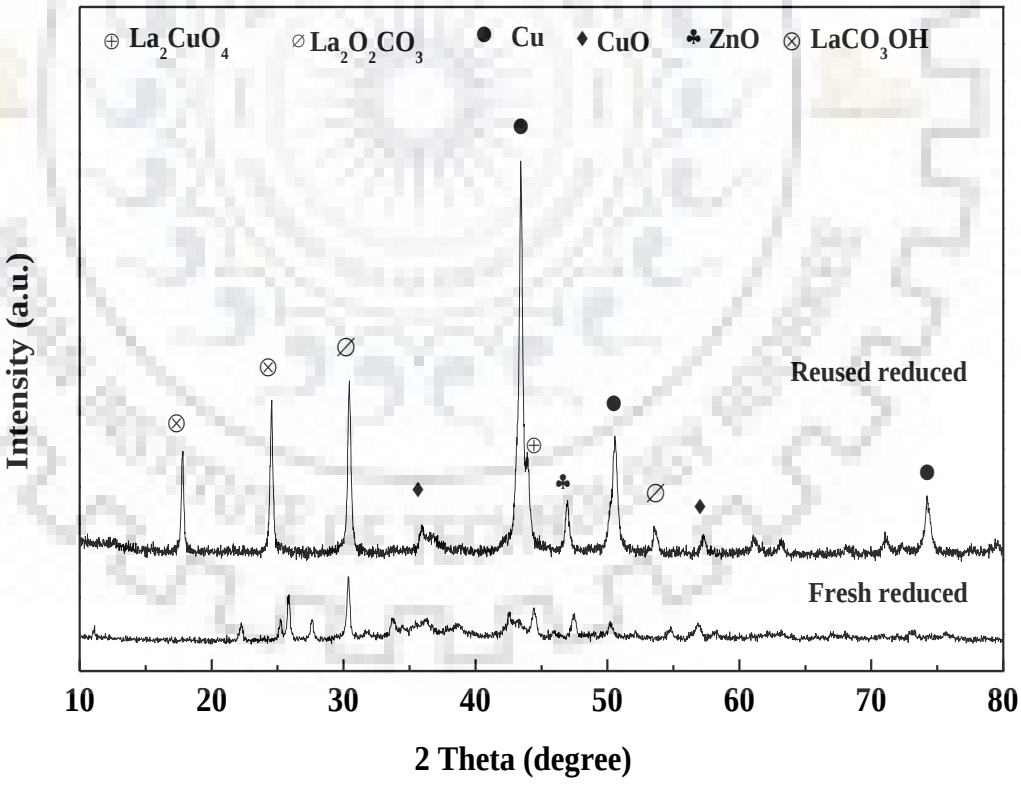

Figure 4.26. XRD pattern of fresh and used reduced Cu:Zn(4:1)/MgO-La_2O_3 catalyst

The average crystallite size of the used catalyst was calculated by using Scherrer's formula and the results are summarized in Table 4.20. It was estimated that the average crystallite size of used catalyst was increased from 27.8 nm to 41.8 nm and BET surface area was reduced slightly from 15.5 $m^2. g^{-1}$ to 12.1 $m^2. g^{-1}$ due to repetitive heat treatment of the catalyst. Further, AAS analysis was performed to verify the metal leaching in the reaction mixture during the reaction of fresh and used catalyst. AAS result reported in Table 4.20 suggested that the metal leaching in the solution was insignificant.

TEM images of fresh reduced and used catalysts were compared in Figure. 4.27 [(A) and (B)], respectively. The average particle size histogram obtained suggested that the average particle size was increased from 24 nm to 36 nm [Figure. 4.27 [(a) and (b)], due to agglomeration after successive reuse. All these characterization results suggested that the variation of physico-chemical properties, primarily, catalyst reducibility, and particle size were the key reasons for the reduction of catalyst activity and 1,2-PDO selectivity.

4.4.5 Summary

Effects of various basic supports (MgO, La_2O_3, CaO, BaO_2 and MgO-La_2O_3) on the performance of Cu:Zn bimetallic catalysts were evaluated for liquid phase glycerol hydrogenolysis reaction to enhance the catalytic activity, 1,2-PDO selectivity and durability of the catalyst. Cu:Zn(4:1)/MgO catalyst showed higher glycerol conversion (98.4%) with 93% selectivity towards 1,2-PDO at 210 °C temperature, 4.5 MPa of H_2 pressure compared to La_2O_3, CaO, BaO_2 supported catalysts. Higher activity of Cu:Zn(4:1)/MgO catalyst was because of the optimum amount of acidic (2.12 $mmol.gcat^{-1}$), basic sites (2.81 $mmol.gcat^{-1}$), higher reducibility (91.7%), higher Cu active sites [$(Cu^+ + Cu^o)/Cu$ ratio = 0.969]. The result suggested that, after incorporation of La_2O_3 to Cu:Zn(4:1)/MgO catalyst, complete glycerol conversion with 93% selectivity towards 1,2-PDO was achieved at 210 °C temperature, 4.5 MPa of H_2 pressure when 20 wt.% glycerol was used as a feed. Characterization study revealed that after addition of La_2O_3 to Cu:Zn(4:1)/MgO catalyst, basic sites increased from 2.81-2.86 $mmol.gcat^{-1}$, the degree of reduction increased significantly from 91.7-97% and average crystallite size decreased from 33.2 - 27.8 nm. These were the primary reason for enhancing the catalytic activity over Cu:Zn(4:1)/MgO- La_2O_3 catalyst. Further, influences of various reaction parameters such as temperature (170-210 °C), pressure (3-6 MPa), catalyst loading (2-8 wt.%) and feed concentration (10-40 wt.%) were investigated over Cu:Zn(4:1)/MgO-La_2O_3 catalyst. Effect of reaction temperature study suggested that the catalyst showed superior activity 80%

glycerol conversion with 94% selectivity towards 1,2-PDO even at 170 °C reaction temperature and 4.5 MPa of pressure whereas 66% conversion with 96% selectivity towards 1,2-PDO was achieved at 210 °C of temperature and 3.0 MPa of H_2 pressure. Stability and reusability of Cu:Zn(4:1)/MgO-La_2O_3 catalyst was investigated up to 4th cycle at the optimum reaction condition obtained by parameter study. Reusability study demonstrated that glycerol conversion decreased by 14.4% and selectivity towards 1,2-PDO decreased drastically from 93.4% to 63.2% with simultaneous increasing the selectivity to 1-propanol from 2.2% to 29% after 4th successive reuse. These results suggested that selectivity towards 1,2-PDO decreased because of overhydrogenolysis of 1,2-PDO to propanol. XRD pattern of reused catalyst suggested that Cu metal was highly reduced after repetitive heat treatment and reduction prior to each cycle, which might propagate overhydrogenolysis of 1,2-PDO to propanol. Therefore, although the addition of La_2O_3 in 50 wt.% Cu:Zn(4:1)/MgO catalyst enhanced the catalytic activity, however, it was not beneficial for the stability of the catalyst.

Table 4.19. Reusability test over Cu:Zn(4:1)/MgO-La_2O_3 catalyst

Cycles	Conversion (%)	Selectivity (%)				1,2-PDO yield (%)
		1,2-PDO	EG	1-PO	Others	
Fresh catalyst	100	93.4	2.1	2.2	2.3	93.4
2nd cycle	92.4	87.5	4.7	6.1	1.7	80.8
3rd cycle	87.7	83.8	3.7	10.7	1.8	73.5
4th cycle	85.6	63.2	3.9	29.0	3.9	54.1

Reaction condition: 20 wt.% glycerol (20 g), 4.5 MPa, 210 °C, catalyst/glycerol wt. ratio = 0.08, time = 12 h

Experimental errors for all the values (conversion, selectivity and yield) : x ± 1 %

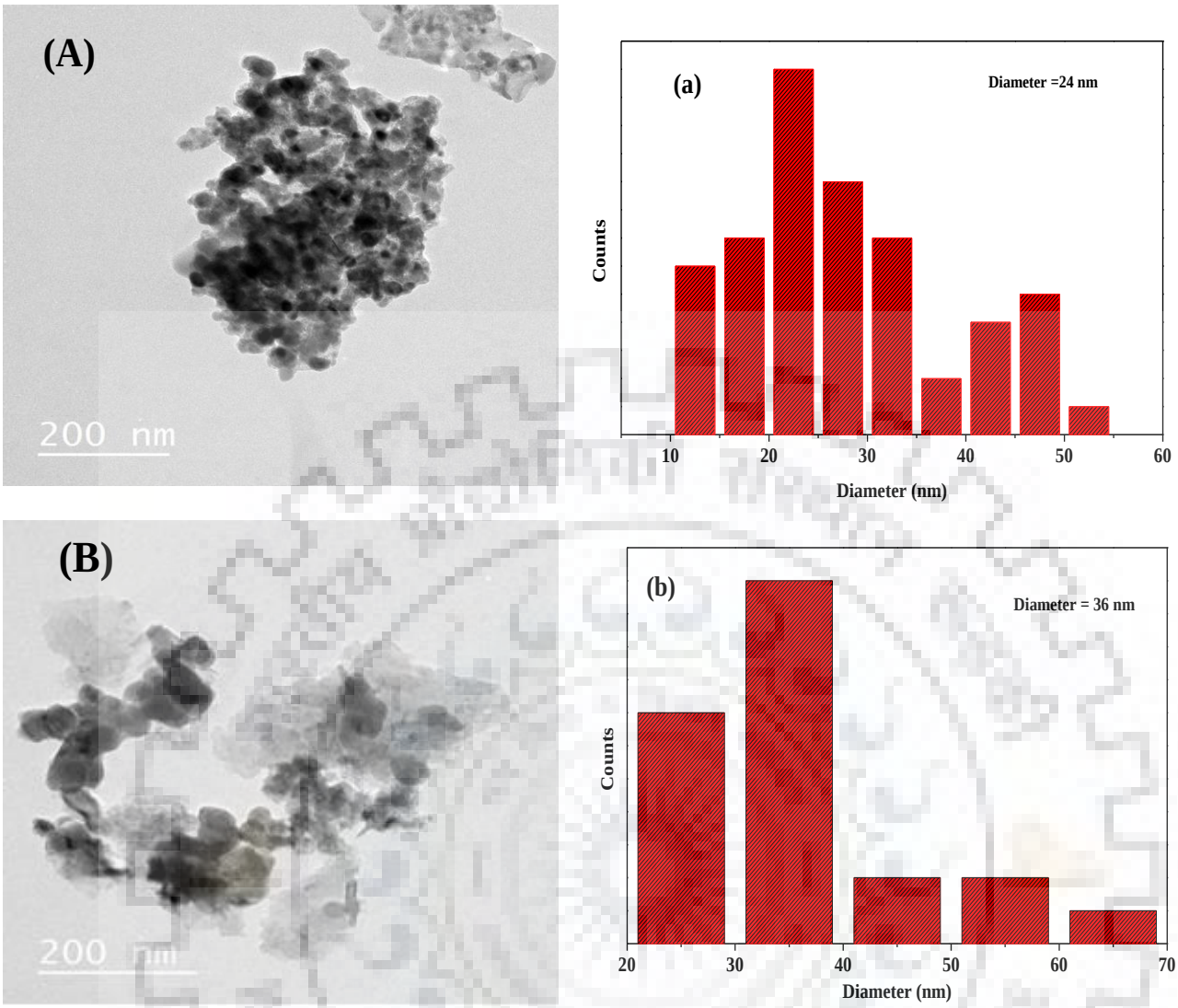

Figure 4.27. TEM micrograph and corresponding average particle size histogram: (A) and (a) fresh and reduced Cu:Zn(4:1)/MgO-La_2O_3 catalyst; (B) and (b) Cu:Zn(4:1)/MgO-La_2O_3 catalyst after cycle-4

Table 4.20. BET-surface area and XRD-results of used Cu:Zn(4:1)/MgO-La_2O_3 catalyst

Reusability	S_{BET} [a] ($m^2.g^{-1}$)	Cu [b] (wt.%)	Zn [b] (wt.%)	D_{Cu} XRD (nm) [c]						
				CuO	ZnO	$La_2O_2CO_3$	Cu	La_2CuO_4	$LaCO_3OH$	Average
Fresh reduced catalyst	15.5	40.2	10.5	18.3	25.3	37.12	32.2	26.3	-	27.8
4th cycle reduced	12.1	38.5	9.2	29.5	31.4	37.05	39.16	43.5	70.5	41.8

[a] Obtained from N_2 adsorption-desorption isotherm data

[b] Metal loading calculated from AAS analysis

[c] Average crystallite size calculated by using Scherrer's formula

Experimental errors for all the values (conversion, selectivity and yield) : x ± 1 %

CHAPTER V

KINETIC STUDY

This chapter discusses the kinetic study and the development of the kinetic models for liquid phase hydrogenolysis of glycerol in presence of Cu:Ni(1:1)/γ-Al_2O_3, Cu:Zn(4:1)/MgO, Cu:Zn(4:1)/MgO-La_2O_3 catalysts, respectively. Kinetic experiments were carried out in the temperature and H_2 pressure range of 170-220 ºC and 3-6 MPa, respectively, in presence of various catalysts. Approximately, twenty three different kinetic models were tried to fit the experimental data over various catalysts. However, the best-fitted models are discussed in this chapter and the rest of the models are shown in Appendix II. In presence of Cu:Ni(1:1)/γ-Al_2O_3 catalyst, 1,2-PDO and propanol were detected as the primary reaction products, and a series reaction scheme for the conversion of glycerol to 1,2-PDO followed by the conversion of 1,2-PDO to propanol was considered to develop the kinetic model. A new kinetic model in a combination of Langmuir–Hinshelwood-Hougen-Watson (LHHW) and Eley-Rideal (ER) approach was developed in presence of Cu:Ni(1:1)/γ-Al_2O_3 catalyst. Further, in presence of Cu:Zn(4:1)/MgO and Cu:Zn(4:1)/MgO-La_2O_3 catalysts, 1,2-PDO was detected as the main reaction product with very high selectivity to ~93%. For these catalysts, kinetic models were developed by using Langmuir–Hinshelwood-Hougen-Watson (LHHW) approach and the obtained results demonstrated very well fit between the experimental and models predicted data.

5.1 Development of kinetic model in presence of Cu:Ni(1:1)/γ-Al_2O_3 catalyst

Details of experimental study for liquid phase hydrogenolysis of glycerol in presence of Cu:Ni(1:1)/γ-Al_2O_3 catalyst at the different reaction temperatures (180-220 ºC) and pressures (3-6 MPa) are already discussed in Chapter IV. In this section, the development of various kinetic models and their validation are discussed. A series reaction scheme for the conversion of glycerol to 1,2-PDO followed by the hydrogenolysis of 1,2-PDO to propanol was considered to develop the kinetic model. Initially, power-law model was fitted, followed by a modified power-law model was tried by considering 1,2-PDO and propanols (1-propanol + 2-propanol) as the main reaction products. Further, to understand the intrinsic kinetic behavior, a more realistic heterogeneous kinetic model based on the combined Langmuir–Hinshelwood-Hougen-Watson (LHHW) and an Eley-Rideal (ER) approach was developed. Numerical solutions of the model equation were computed by using ode23 solver in MATLAB combined with genetic algorithm (GA).

5.1.1 Effect of external mass transfer resistance, intraparticle diffusion resistance, and heat transfer resistance

5.1.1.1 Effect of speed of agitation

To ensure the absence of external diffusion resistance, experiments were performed at different stirring speed (500-900 rpm) at the optimized reaction condition i.e. at 210 °C and at 4.5 MPa pressure in presence of 20 wt.% aqueous glycerol solution as a feed. 10 wt.% catalyst with respect to glycerol was used for the experiment. Each reaction data was collected after a run time of 12 h. The obtained glycerol conversion, the primary reaction products selectivity and the calculated average reaction rates are summed in Table 5.1. The calculated reaction rates were comparable with the previously reported values [Gandarias et al., (2011), Li and Yen (2018), Ma and He (2010)]. Results suggested that the variation of glycerol conversion, products selectivity, and the average reaction rate was not significant at the stirring speed of 700 rpm and higher. Lahr and Shanks (2003) showed that the variation of catalytic activity was unaffected at the stirring speed of 500 rpm and higher in presence Ru-based catalyst. Hichri et al., (1991) reported that the stirring speed of 800 rpm and higher was sufficient to eliminate the external mass transfer limitation for the hydrogenation of O-cresol in presence of Ni/SiO_2 catalyst. All the reaction kinetic data reported in this study were collected at the stirring speed of 700 rpm and it was supposed that the external mass transfer resistance was insignificant.

Table 5.1. Effect of stirring speed

	500 rpm	700 rpm	900 rpm
Glycerol Conversion (%)	69.6	71.6	71.4
Selectivity towards 1,2-PDO (%)	76.7	85.7	85.8
Selectivity to PO (%)	16.3	8.9	8.6
Average reaction rate (mol. $gcat^{-1}$. h^{-1})	6.41×10^{-3}	6.60×10^{-3}	6.58×10^{-3}

Experimental errors for all the values (conversion, selectivity and yield) : x ± 1 %
Reaction condition: 20 wt.% glycerol, 210 ^{o}C temperature, 4.5 MPa H_2, 2 g catalyst

5.1.1.2 Calculation of Weisz-Prater criterion and Prater number

It has been shown in various previous reports that the intra-particle diffusion resistance was insignificant for the powdered catalyst having the particle size of < 50 µm [Vasiliadou and Lemonidou (2013), Hao et al., (2010), Choudhary et al., (1998)]. To ensure the absence of intra-particle diffusion resistance in this study, Wiesz-Prater (WP) parameter was calculated [Appendix III] [Sharma et al., (2014), Smith et al., (1970), Pandhare et al., (2018)]. According to WP criteria, if the WP coefficient [$\varphi = \{r_{obs}\ \rho_p\ R_p^2 / D_e\ C_{AS}\}$] value is ≤ 1, the internal diffusion resistance can be neglected for a heterogeneous reaction. In this study, the estimated value of the WP parameter (φ) was obtained as 1.84×10^{-12} at the highest reaction temperature (220 ^oC) used for the reaction. This calculated value of WP coefficient ensured that the reaction was operated under a true kinetically controlled regime and the internal diffusion effect could be neglected. [Sharma et al., (2014), Pandhare et al., (2018)].

To investigate the thermal homogeneity of the reaction mixture, the Prater number was also calculated following the procedure mentioned in Appendix IV [Pandhare et al., (2018), Pankajakshan., (2018), Ameen et al., (2017)]. According to the Prater number, if $\beta = (T_{max} - T_s)$ is very low, then it can be assumed that the isothermal condition exists within the catalyst pellet. In this study, the estimated value of β was very low (~ 0.074 °C), which was less than 1 K [Rajkhowa et al., (2017)]. Therefore, it was supposed that the effect of heat transfer resistance was insignificant.

5.1.2 Development of kinetic model

A power-law, modified power-law and various heterogeneous kinetic models based on Langmuir-Hinshelwood-Hougen-Watson (LHHW) and Eley-Rideal (ER) approach were developed. These models were implemented to validate the experimental data obtained in presence of Cu:Ni(1:1)/γ-Al_2O_3 catalyst in the slurry batch reactor. Initially, the power-law model was used to estimate the global reaction rate and the preliminary reaction kinetic parameters were estimated by considering one-step rate expression model. Further, the modified power-law model was developed by considering all the major reaction products obtained in hydrogenolysis of glycerol in presence of Cu:Ni(1:1)/γ-Al_2O_3 catalyst [Torres et al., (2010)]. However, the primary drawback associated with the power-law model is that this model does not consider the different reaction steps, i.e. adsorption, surface reaction, and desorption, associated with a heterogeneously catalysed reaction. Therefore, the development of more realistic kinetic models based on LHHW and ER approaches is highly desirable. In this

study, various reaction kinetic models developed based on the LHHW, ER and combination of the LHHW-ER approaches were utilized to fit the experimental results. The best-fitted kinetic models developed based on certain assumptions are discussed in the following section.

The genetic algorithm (GA) optimization tool was used to optimize the fitness function and to determine the reaction kinetic variables of the models developed. The population size of 1000 and the optimum values of genetic parameters of 0.9 and 0.1 were used for crossover and mutation probability, respectively. In comparison to the traditional direct search method, GA is a well-accepted optimization approach to govern the parameters of complex fitting problems where seeking the global optima is complicated [McCall (2005), Maedar et al., (2004)]. GA approaches a multi-directional search within the surrounding and generates a population of candidate solutions randomly without depending on the initial estimated parameters. Further, it generates next generation population of solutions using the better-fitted value. The successive iteration process was repeated until it satisfied the minimum stopping criterion or until it acquired the best possible solution.

5.1.2.1 Power law model

According to the power-law model, the rate equation of the following one-step glycerol hydrogenolysis process was written as equation (5.1).

$$Glycerol\ (G) \xrightarrow{Catalyst} Product\ (P)$$

$$r = \frac{dC_G}{dt} = kC_G^n = k_0 \exp\left(-\frac{E}{RT}\right) C_G^n \quad (5.1)$$

where, C_G = concentration of glycerol, n = overall order of the equation, k = specific reaction rate constant, k_o = frequency factor, E = activation energy, R = gas constant, T = reaction temperature.

To determine the reaction kinetic parameter, rate equation (5.1) was solved by ode23 by using genetic algorithm in MATLAB. The kinetic variables were estimated by minimizing the residuals sum of squares of the experimental and simulated glycerol concentration. The objective function was defined as: $f = \sum_{i=1}^{N}[(C_{G,exp}^{i} - C_{G,sim}^{i})^2$ (5.2)

where, $C_{G,exp}^{i}$= experimental concentration of glycerol, $C_{G,sim}^{i}$= simulated concentration of glycerol.

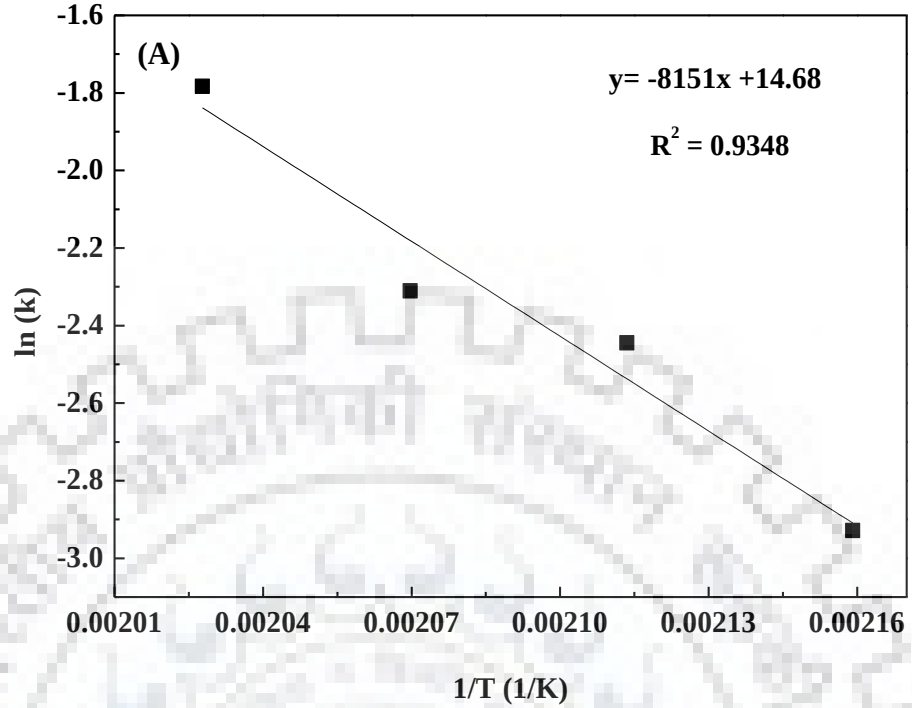

Figure 5.1 (A) Arrhenius plot to calculate the activation energy for glycerol hydrogenolysis to 1,2-PDO by power-law model.

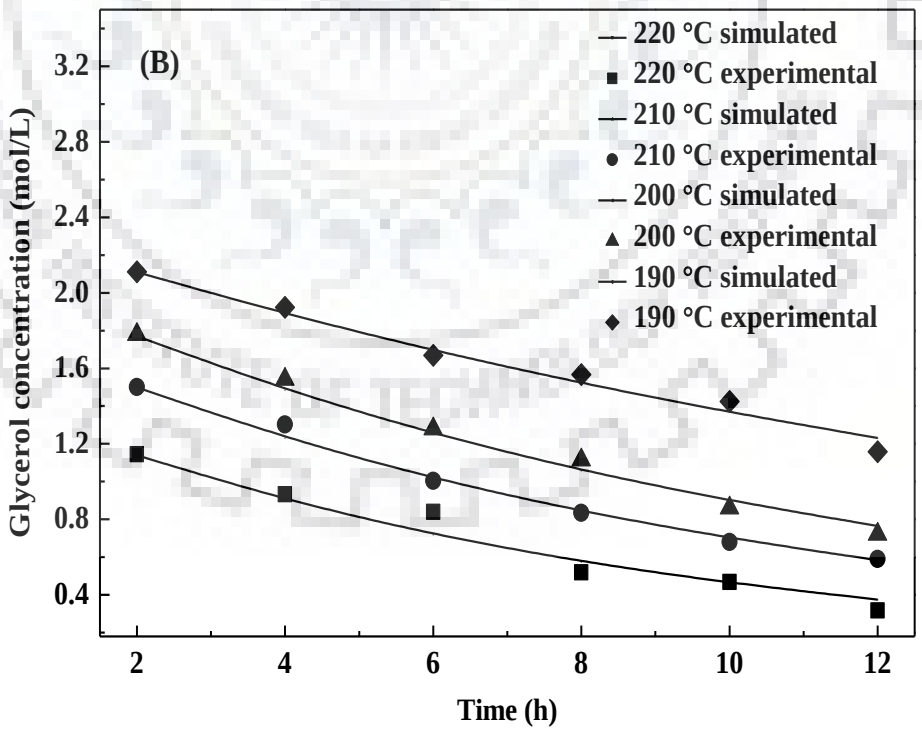

Figure 5.1 (B) Variation of simulated and experimental glycerol concentration at different temperature obtained by power-law model.

The apparent reaction order, 'n', for this reaction was obtained as 1.02 with respect to glycerol, which was approximately similar to the pseudo first order dependency. Activation energy and frequency factor calculated by Arrhenius equation were 67.7 kJ.mol^{-1} and 2.39 × 10^{6} mol.gcat^{-1}.h^{-1}, respectively. Earlier Xia et al., (2012b) reported an activation energy of 65.5 kJ.mol^{-1} and the frequency factor of 5.60×10^{6} mol.gcat^{-1}.h^{-1} for glycerol to 1,2-propanediol (1,2-PDO) formation in presence of $Cu_{0.4}/Zn_{0.6}Mg_{5.6}Al_2O_{8.6}$ catalyst. The plot of ln (k) vs 1/T is shown in Figure 5.1(A). The variation of experimental and simulated concentration of glycerol as a function of time at various reaction temperatures is presented in Figure 5.1 (B). The result showed that the power-law model simulated and the experimental values exhibited very good agreement with the R^2 value of ~1.

5.1.2.2 Modified power-law model

In simple power-law model, the global reaction rate equation was written based on the assumption that reactant glycerol was converted to only one product. However, the experimental results showed that in presence of Cu:Ni(1:1)/γ-Al_2O_3 catalyst, the primary reaction products were 1,2-PDO, propanol (PO) (1-propanol + 2-propanol), and trace amounts (~2-2.5%) of EG. To develop the modified power-law model, 1,2-PDO and propanol were only considered as primary reaction products. In this model, it was assumed that initially, glycerol reacted with H_2 to produce 1,2-PDO and EG simultaneously. Further, 1,2-PDO reacted with H_2 and produced PO [Equations (5.3) – (5.5)]. Mole balance and the rate equation for each and every step considered in the modified power-law model were described as follows [Torres et al., (2010)].

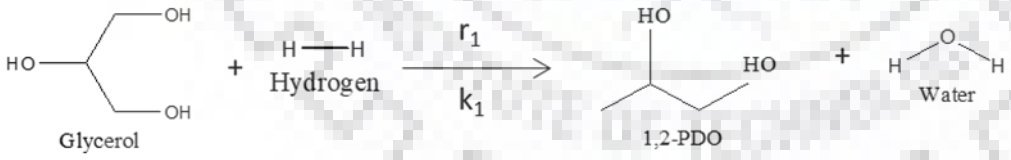

(5.3)

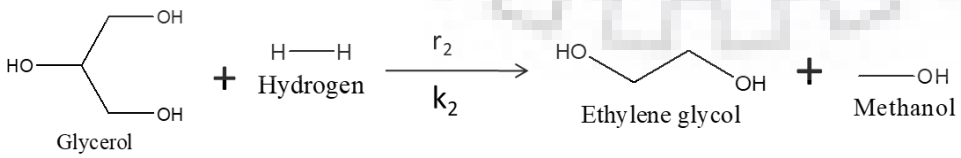

(5.4)

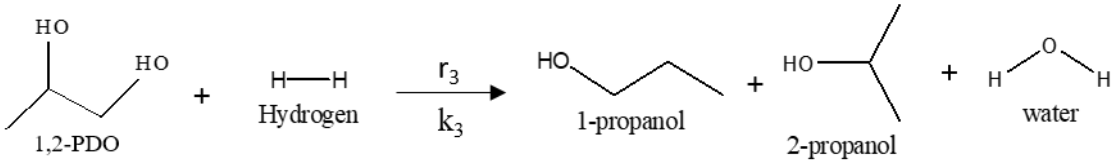

(5.5)

Mole balance equations

$$\frac{dC_G}{dt} = r_G = -r_1 - r_2 \quad (5.6)$$

$$\frac{dC_P}{dt} = r_P = r_1 - r_3 \quad (5.7)$$

$$\frac{dC_{PO}}{dt} = r_{PO} = r_3 \quad (5.8)$$

Rate terms for reaction steps

$$r_1 = k_1 C_G \frac{P_{H_2}}{H_{H_2}} \quad (5.9)$$

$$r_2 = k_2 C_G \frac{P_{H_2}}{H_{H_2}} \quad (5.10)$$

$$r_3 = k_3 C_P \frac{P_{H_2}}{H_{H_2}} \quad (5.11)$$

H_{H_2}= Henry's constant at 190 °C, 200 °C, 210 °C and 220 °C were 26.774, 24.75, 22.652, 20.488, respectively. The unit of Henry's constant was (m^3(liq)/m^3(gas)) [Torres et al., (2010)].

The objective function was defined as follows

$$f = \sum_{i=1}^{N}[(C_{G,exp}^i - C_{G,sim}^i)^2 + (C_{PG,exp}^i - C_{PG,sim}^i)^2 + (C_{PO,exp}^i - C_{PO,sim}^i)^2] \quad (5.12)$$

$C_{G,exp}^i$= experimental concentration of glycerol, $C_{G,sim}^i$= simulated concentration of glycerol,

$C_{PG,exp}^i$= experimental concentration of 1,2-PDO, $C_{PG,sim}^i$= simulated concentration of 1,2-PDO,

$C_{PO,exp}^i$= experimental concentration of propanol, $C_{PO,sim}^i$= simulated concentration of propanol.

Model equations [(5.6) - (5.8)] were solved by ode23 function using GA in MATLAB. The experimental and modified power-law model predicted concentrations of the reactant and products were plotted with the variation of time at various reaction temperature (190-220 ^oC) and at a constant pressure (4.5 MPa) (Figure 5.2 (A)-(D)). Model-predicted and experimentally obtained concentrations of reactant and products were also compared at different pressure (3-6

MPa) at constant temperature (210 ^{o}C) [Figure 5.2 (E) and (F)]. Results demonstrated that the experimental concentrations were very well fitted with the model predicted concentrations. Further, activation energy values for the formation of products (1,2-PDO and PO) were calculated from Arrhenius plot [ln (k) vs 1/T] [Figure 5.3 (A) and (B)]. Calculated values of activation energy for the formation of 1,2-PDO from glycerol, the formation of PO from 1,2-PDO were 45.7 kJ.mol^{-1} and 141.3 kJ.mol^{-1}, respectively. Frequency factors for the conversion of glycerol to 1,2-PDO and 1,2-PDO to PO were 8.3×10^{3} and 1.21×10^{15}, respectively. Torres et al., (2010) reported the activation energy for the formation of 1,2-PDO from glycerol and PO from 1,2-PDO were 54.2 kJ.mol^{-1} and 25.1 kJ.mol^{-1}, respectively. The frequency factors for these reactions were reported as 10.3×10^{2} and 4.86×10^{2}, respectively. The activation energy (141.3 kJ.mol^{-1}) obtained for the formation of propanol was comparable with the activation energy (124.1 kJ.mol^{-1}) obtained by C. T. Q. Mai (2016) in presence of 10Ni/30HSiW/Al_2O_3 catalyst. In contrast to that, the activation energy and the frequency factor for the formation of propanol reported by Torres et al., (2010) was little lower. The parity plots of the simulated and experimental concentration of glycerol, 1,2-PDO and PO at various temperature and pressure showed very good agreement with the R^2 value of 0.96-0.99 [Figure 5.4 (A)-(C)].

Although the modified power-law model was fitted very well with the experimental data, this model did not describe the realistic heterogeneous kinetic phenomena. This model did not involve all the steps related to a solid catalyzed reaction. Therefore, various heterogeneous kinetic models (~20) based on LHHW, ER and combined LHHW-ER approaches were developed and tried to validate with the help of the experimental data obtained over Cu:Ni(1:1)/γ-Al_2O_3 catalyst. The best-fitted model developed based on combined LHHW-ER approach is discussed in the following section.

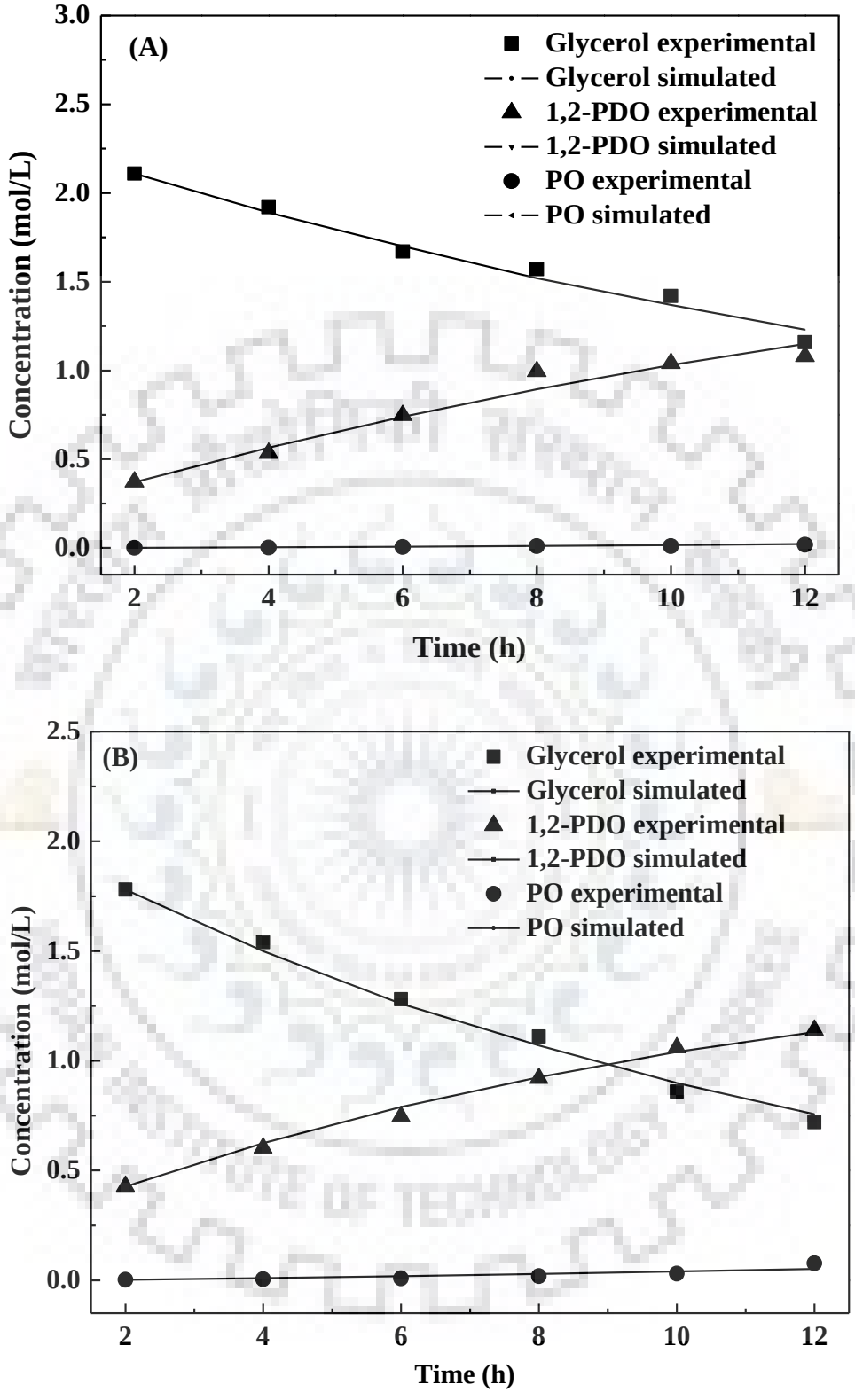

Figure 5.2 (A) Variation of experimental and simulated concentration of glycerol, 1,2-PDO and PO by modified power-law at 190 °C temperature (B) Variation of experimental and simulated concentration of glycerol, 1,2-PDO, and PO by modified power-law at 200 °C temperature

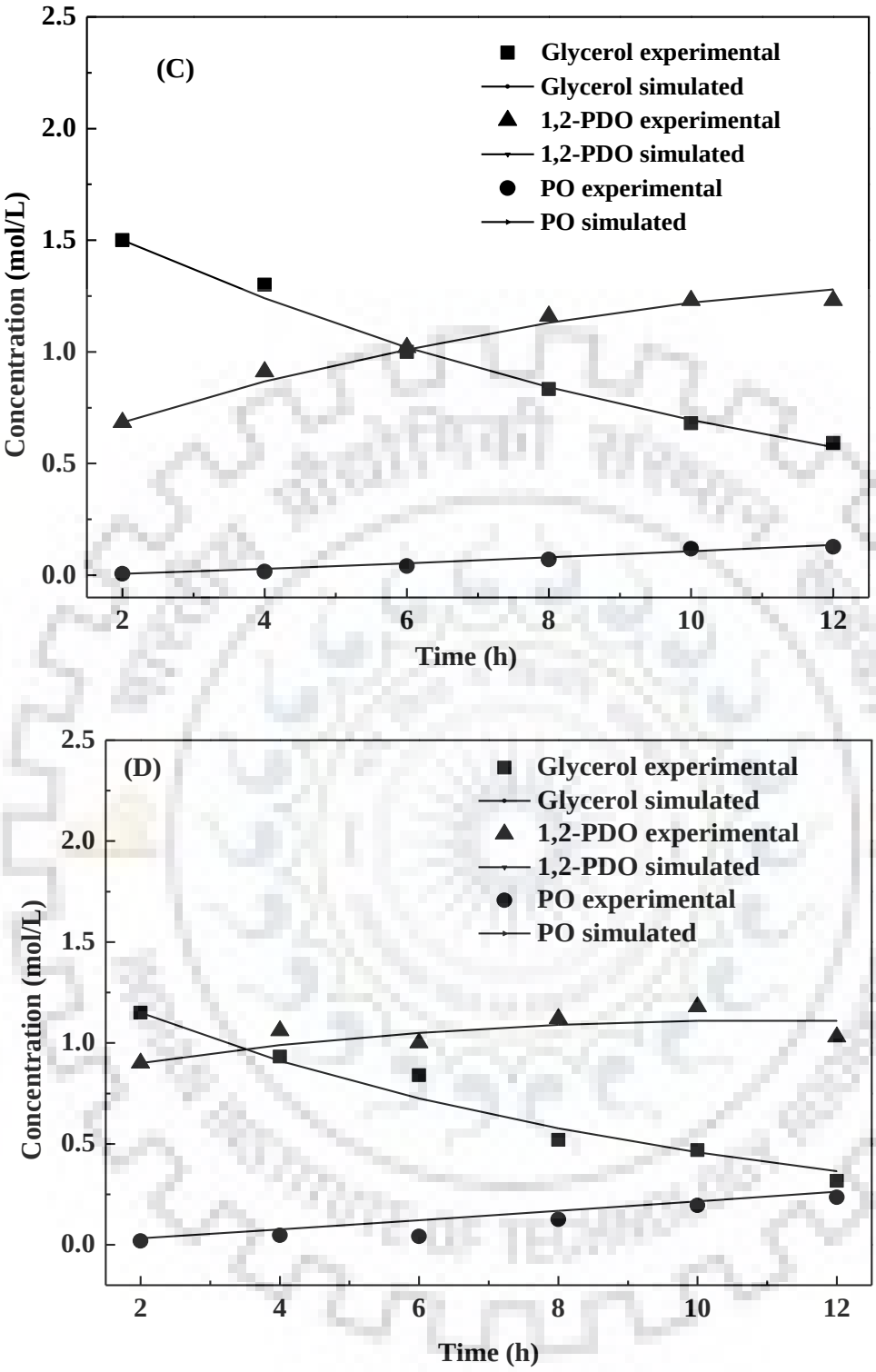

Figure 5.2 (C) Variation of experimental and simulated concentration of glycerol, 1,2-PDO, and PO by modified power-law at 210 °C temperature. (D) Variation of experimental and simulated concentration of glycerol, 1,2-PDO, and PO by modified power-law at different temperature 220 °C

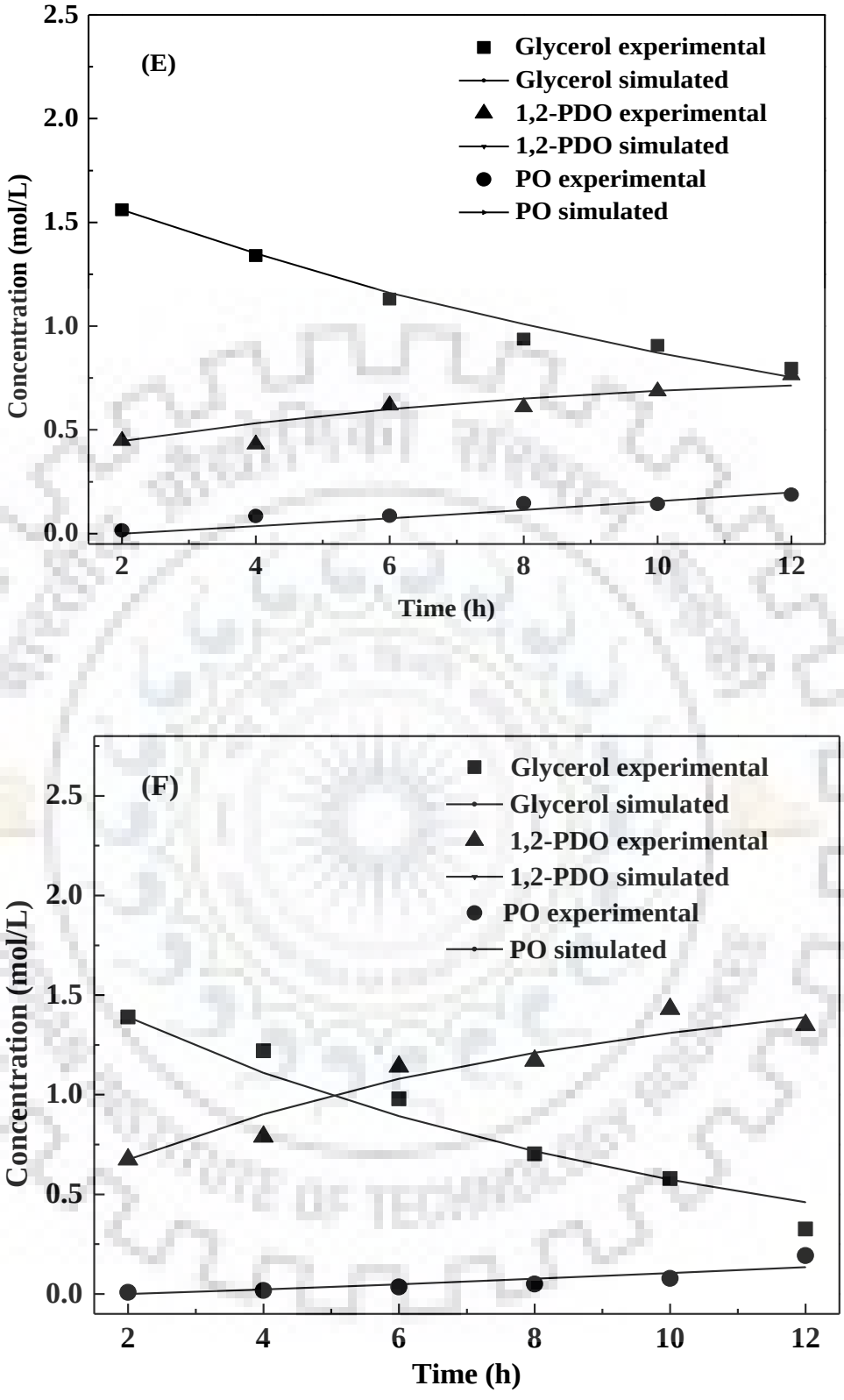

Figure 5.2 Variation of experimental and simulated concentration of glycerol, 1,2-PDO, and PO by modified power-law (E) at 3.0 MPa pressure, 210 °C temperature, 20 wt.% glycerol concentration of 20 g glycerol, 2 g catalyst. (F) at 6.0 MPa pressure, 210 °C temperature, 20 wt.% glycerol concentration of 20 g glycerol, 2 g catalyst

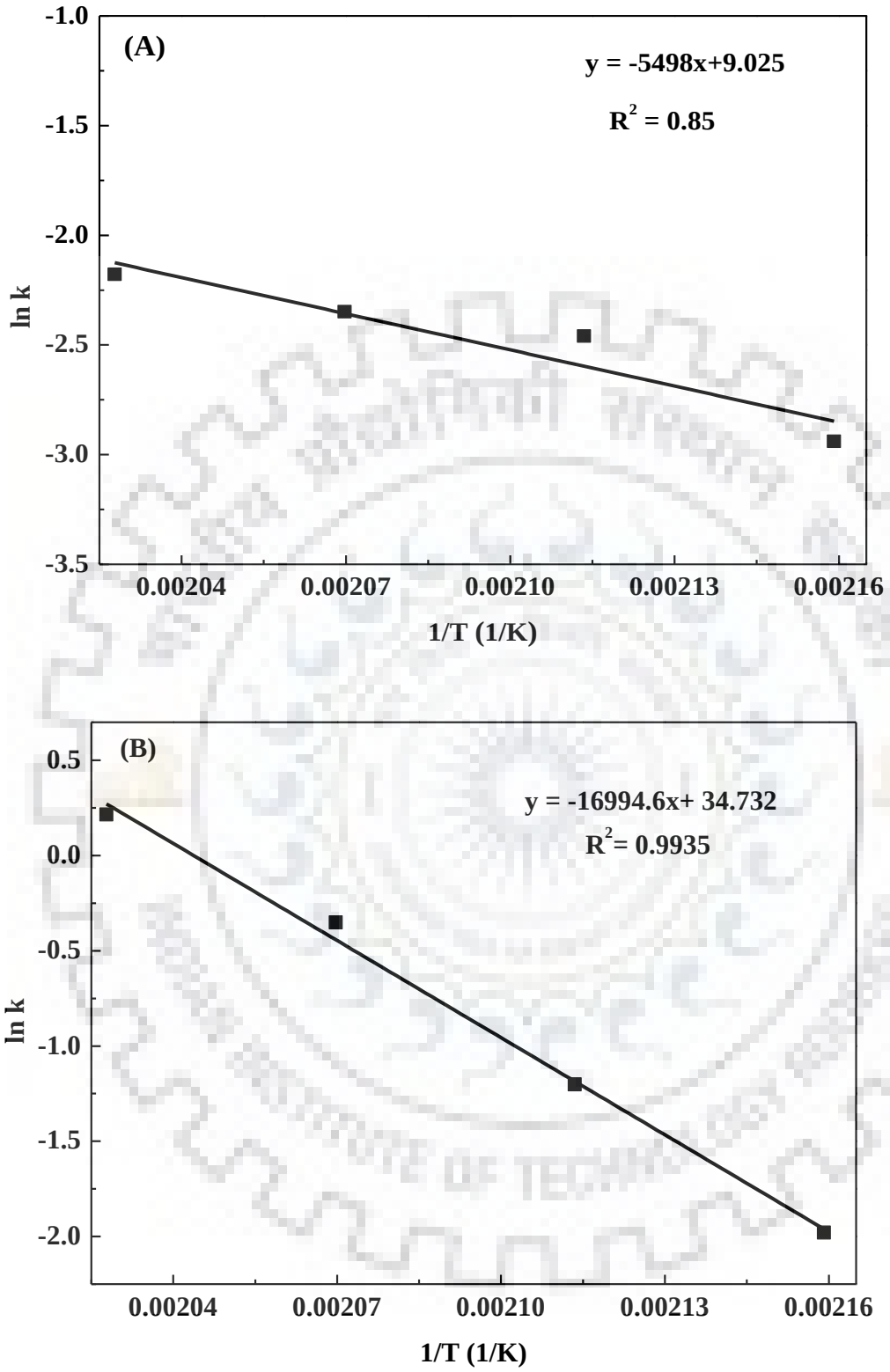

Figure 5.3. (A) Arrhenius plots used to calculate the activation energy using modified power-law model for the conversion of glycerol to 1,2-PDO (B) Arrhenius plots used to calculate the activation energy using modified power-law model for the conversion of 1,2-PDO to PO

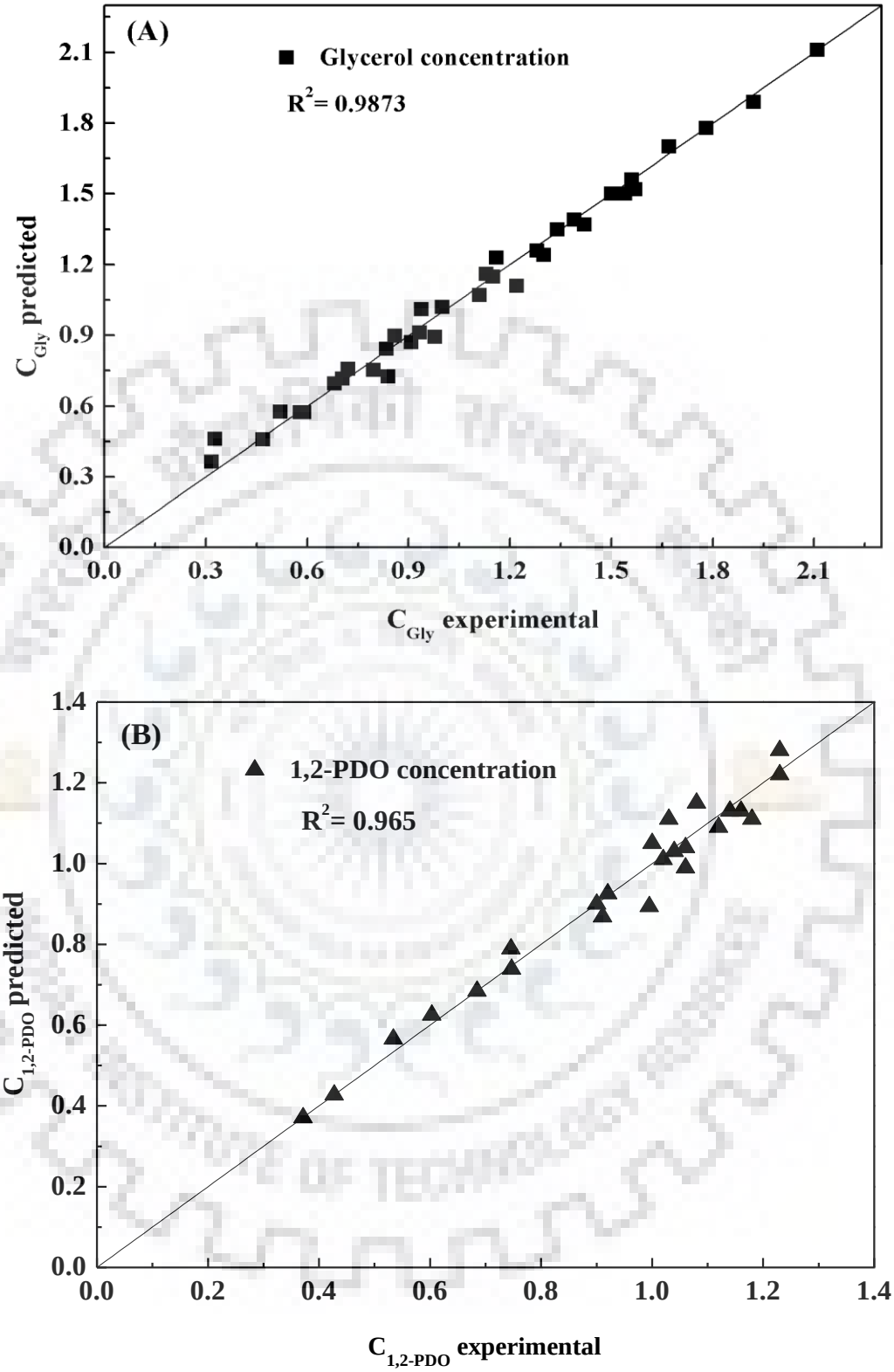

Figure 5.4 Parity plot of experimental and simulated concentration of (A) glycerol (B) 1-2-PDO by modified power-law model. Reaction condition: Temperature (190 °C, 200 °C, 210 °C, 220 °C) (other condition: 4.5 MPa pressure, 20 wt.% glycerol (20 g), 2 g catalyst) and pressure 3.0 MPa, 6.0 MPa (other condition: 210 °C, 20 wt.% glycerol (20 g), 2 g catalyst)

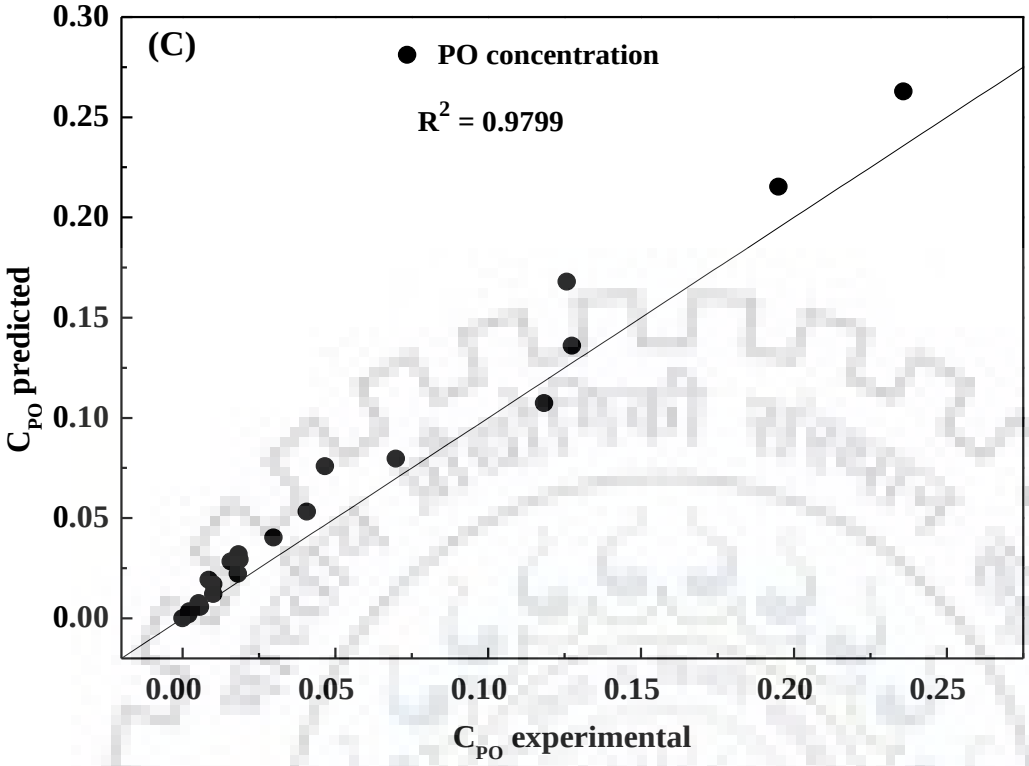

Figure 5.4 Parity plot of experimental and simulated concentration of (C) PO by modified power-law model. Reaction condition: Temperature (190 °C, 200 °C, 210 °C, 220 °C) (other condition: 4.5 MPa pressure, 20 wt.% glycerol (20 g), 2 g catalyst) and pressure 3.0 MPa, 6.0 MPa (other condition: 210 °C, 20 wt.% glycerol (20 g), 2 g catalyst)

5.1.2.3 Heterogeneous kinetic model

To develop the heterogeneous kinetic model, the reaction mechanism was proposed based on the combined assumptions of the LHHW and ER approaches. The schematic diagram of the heterogeneous kinetic model is shown in Scheme 5.1. In this model, it was assumed that glycerol molecules were adsorbed on the catalyst surface and molecular hydrogen was partially absorbed on the catalyst surface with the rest in the bulk phase since hydrogen was present in excess in the reactor. Initially, the adsorbed glycerol interacted with the molecular H_2 present in the bulk phase and produced adsorbed 1,2-PDO and adsorbed water [Xi et al., (2010), Anand et al., (2010)]. In the second step, the adsorbed 1,2-PDO interacted with the adjacent adsorbed hydrogen atoms and generated adsorbed PO. Finally, the adsorbed 1,2-PDO and PO were

desorbed from the surface of the catalyst and catalyst active sites were regenerated. The reaction steps considered to develop the rate equations were as follows:

Step 1: Adsorption of glycerol (G) and hydrogen (H_2) on the active site ($) of the catalyst occurred as follows:

$$G + \$ \underset{k_{-1}}{\overset{k_1}{\rightleftharpoons}} G.\$ \tag{5.13}$$

$$H_2 + 2\$ \underset{k_{-2}}{\overset{k_2}{\rightleftharpoons}} 2H.\$ \tag{5.14}$$

Step 2: Interaction of adsorbed glycerol with hydrogen molecule (H_2) present in the bulk phase and produced adsorbed 1,2-PDO followed by the surface reaction between adsorbed 1,2-PDO (P.$) and adsorbed atomic hydrogen (H.$) occurred as follows:

$$G.\$ + H_2 \underset{k_{-3}}{\overset{k_3}{\rightleftharpoons}} P.\$ + W \tag{5.15}$$

$$P.\$ + 2H.\$ \underset{k_{-4}}{\overset{k_4}{\rightleftharpoons}} PO.\$ + 2\$ \tag{5.16}$$

where, P, PO, and W represented 1,2-PDO, propanol, and water, respectively.

Step 3: Desorption of products (1,2-PDO and PO) from the catalyst surface and the active sites were regenerated as follows:

$$P.\$ \underset{k_{-5}}{\overset{k_5}{\rightleftharpoons}} P + \$ \tag{5.17}$$

$$PO.\$ \underset{k_{-6}}{\overset{k_6}{\rightleftharpoons}} PO + \$ \tag{5.18}$$

From equations (13) - (18), the rate equations for the individual step were written as follows:

$$(-r_1) = k_1\left(C_G C_\$ - \frac{C_{G.\$}}{K_1}\right); \quad K_1 = \frac{k_1}{k_{-1}} \tag{5.19}$$

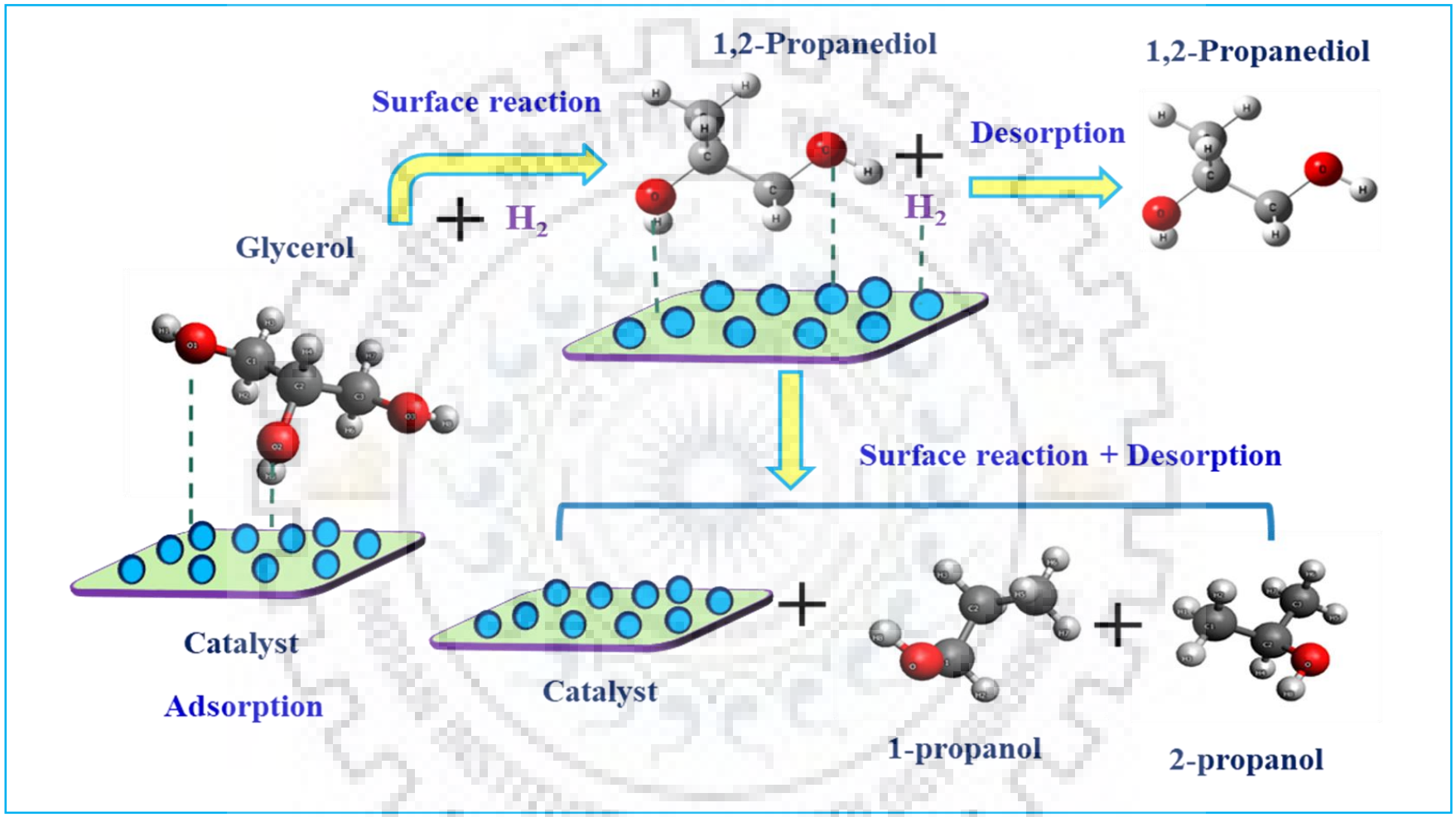

Scheme 5.1. LHHW-ER type reaction mechanism for glycerol hydrogenolysis reaction over Cu:Ni(1:1)/γ-Al_2O_3 catalyst

$$(-r_2) = k_2\left(P_{H_2}C_{\$}^2 - \frac{C_{H.\$}^2}{K_2}\right); \quad K_2 = \frac{k_2}{k_{-2}} \tag{5.20}$$

$$(-r_3) = k_3\left(C_{G.\$}P_{H_2} - \frac{C_{P.\$}C_W}{K_3}\right); \quad K_3 = \frac{k_3}{k_{-3}} \tag{5.21}$$

$$(-r_4) = k_4\left(C_{P.\$}C_{H.\$}^2 - \frac{C_{PO.\$}C_{\$}^2}{K_4}\right); \quad K_4 = \frac{k_4}{k_{-4}} \tag{5.22}$$

$$(-r_5) = k_5\left(C_{P.\$} - \frac{C_P C_{\$}}{K_5}\right); \quad K_5 = \frac{k_5}{k_{-5}} \tag{5.23}$$

$$(-r_6) = k_6\left(C_{PO.\$} - \frac{C_{PO}C_{\$}}{K_6}\right); \quad K_6 = \frac{k_6}{k_{-6}} \tag{5.24}$$

where K_1, K_2, K_3, K_4, K_5, and K_6 were the equilibrium constants for the above-mentioned steps.

To develop the final rate equation, three different rate equations were derived by considering the adsorption, surface reaction and desorption steps as the rate-limiting steps, separately. However, results suggested that the experimental data were fitted well for the rate expression developed based on the surface reaction step as rate controlling. Further, thermodynamic equilibrium constant for overall glycerol hydrogenolysis process was also calculated [Appendix V] [Ameen et al., (2017)]. Negative value of Gibbs free energy ($\Delta G_{298}^{o} = -93.479 \frac{kJ}{mol}$) and high value of equilibrium constant K_a at 210 °C = 6.99 ×10^{15} imply that the reaction is irreversible in nature and thermodynamically 100% conversion is feasible. Therefore, the final rate expression was formulated assuming the surface reaction as a rate controlling step and irreversible in nature [Lahr and Shanks (2003), Pandhare et al., (2018)] which is discussed as follows:

From Eq. (5.21),

$$(-r_3) = k_3 C_{G.\$} P_{H_2} \tag{5.25}$$

Now from Eq. (22),

$$(-r_4) = k_4 C_{P.\$} C_{H.\$}^2 \tag{5.26}$$

Adsorption and desorption steps were very fast when surface reaction step was rate limiting, then we had

From Eq. (5.19), $\frac{r_1}{k_1} = 0$ then

$$C_{G.\$} = K_1 C_G C_\$ \tag{5.27}$$

Similarly, from Eq. (5.20), $\frac{r_2}{k_2} = 0$ then

$$C_{H.\$} = C_\$ (K_2 P_{H_2})^{1/2} \tag{5.28}$$

Similarly, from Eq. (5.23), $\frac{r_5}{k_5} = 0$ then

$$C_{P.\$} = \frac{C_P C_\$}{K_5} \tag{5.29}$$

Similarly, from Eq. (5.24), $\frac{r_6}{k_6} = 0$ then

$$C_{PO.\$} = \frac{C_{PO} C_\$}{K_6} \tag{5.30}$$

On substituting these values in the surface reaction rate Eqs. (5.25) and (5.26) reduced to

$$(-r_3) = k_3 K_1 P_{H_2} C_G C_\$ \tag{5.31}$$

$$(-r_4) = \frac{k_4 K_2 P_{H_2} C_P C_\$^3}{K_5} \tag{5.32}$$

From the total site balance, we had

$$C_{T\$} = C_\$ + C_{G.\$} + C_{H.\$} + C_{P.\$} + C_{PO.\$} \tag{5.33}$$

Substituting concentrations of adsorbed species in Eq. (5.33) gave,

$$C_{T\$} = C_\$ + K_1 C_G C_\$ + (K_2 P_{H_2})^{1/2} C_\$ + \frac{C_P C_\$}{K_5} + \frac{C_{PO} C_\$}{K_6} \tag{5.34}$$

$$C_\$ = \frac{C_{T\$}}{\left[1 + K_1 C_G + (K_2 P_{H_2})^{1/2} + \frac{C_P}{K_5} + \frac{C_{PO}}{K_6}\right]} \tag{5.35}$$

Substituting Eq. (5.35) into Eq. (5.31) and (5.32) yielded,

$$(-r_3) = \frac{k_3 K_1 C_G P_{H_2} C_{T\$}}{\left[1 + K_1 C_G + (K_2 P_{H_2})^{1/2} + \frac{C_P}{K_5} + \frac{C_{PO}}{K_6}\right]} = \frac{k_3' K_1 P_{H_2} C_G}{\left[1 + K_1 C_G + (K_2 P_{H_2})^{1/2} + \frac{C_P}{K_5} + \frac{C_{PO}}{K_6}\right]} \tag{5.36}$$

where $k_3' = k_3 C_{T\$}$, apparent reaction rate constant for the conversion of glycerol to 1,2-PDO.

$$(-r_4) = \frac{k_4 K_2 C_P P_{H_2} C_{T\$}^3}{K_5\left[1 + K_1 C_G + (K_2 P_{H_2})^{1/2} + \frac{C_P}{K_5} + \frac{C_{PO}}{K_6}\right]^3} = \frac{k_4' K_2 C_P P_{H_2}}{K_5\left[1 + K_1 C_G + (K_2 P_{H_2})^{1/2} + \frac{C_P}{K_5} + \frac{C_{PO}}{K_6}\right]^3} \tag{5.37}$$

Where $k_4' = k_4 C_{T.\$}^3$ was the apparent reaction rate constant for the conversion of 1,2-PDO to PO.

Equations (5.36) and (5.37) represent the final rate expressions for the two series reactions, i.e.: hydrogenolysis of glycerol to 1,2-PDO followed by the hydrogenolysis of 1,2-PDO to PO.

To develop the model, the mole balance of individual species was written as follows:

$$\frac{\mathrm{d}\, C_G}{\mathrm{d}\, t} = -r_3 \tag{5.38}$$

$$\frac{\mathrm{d}\, C_P}{\mathrm{d}\, t} = r_3 - r_4 \tag{5.39}$$

$$\frac{\mathrm{d}\, C_{PO}}{\mathrm{d}\, t} = r_4 \tag{5.40}$$

where C_G, C_P, and C_{PO} were the steady-state concentration of glycerol, 1,2-PDO and PO, respectively, 't' was the reaction time.

In order to evaluate the unknown variables in the rate expressions, the sets of differential equations (Eqs. (5.38) - (5.40)) obtained were computed with the help of ode23s function for stiff systems in MATLAB together with genetic algorithm optimization tool. The residual sum of squares i.e. f (fitness function), between experimental and simulated concentrations of glycerol, 1,2-PDO, and PO were minimized with the help of GA. GA was used to minimize the objective function obtained from the model equations.

The objective function was elucidated as follows:

$$f = \sum_{i=1}^{N} \left[(C^{i}_{G,exp} - C^{i}_{G,sim})^2 + (C^{i}_{P,exp} - C^{i}_{P,sim})^2 + (C^{i}_{PO,exp} - C^{i}_{PO,sim})^2 \right] \quad (5.41)$$

where, N represented the number of experimental runs and $C^{i}_{G,exp}$, $C^{i}_{P,exp}$ and $C^{i}_{PO,exp}$ were the experimental and $C^{i}_{G,sim}$, $C^{i}_{P,sim}$ and $C^{i}_{PO,sim}$ were the simulated concentration of glycerol, 1,2-PDO, and PO obtained by solving the model equations, respectively.

The estimated values of the rate constant, adsorption constant, frequency factors and activation energies along with their respective confidence intervals for various reaction steps are summarized in Table 5.2. Confidence intervals (95%) for the parameters (K_1, K_2, k_3', k_4', K_5, K_6) were determined by t-statistic method [Rajkhowa et al., (2017)]. The activation energy for the conversion of glycerol to 1,2-PDO was lower as compared to the generation of PO from 1,2-PDO, and this result very well correlated with the experimental data. Activation energy values obtained for the adsorption of glycerol and desorption of 1,2-PDO was much lower in regard to the surface reaction steps, which also confirmed the assumption i.e. surface reaction steps were the rate limiting. Activation energy and frequency factor values obtained by solving the model developed comparable with the previously reported values [Zhou et al., (2010), Vasiliadou and Lemonidou (2013), Yfanti et al., (2018), Xia et al., (2012b), Nimlos et al., (2006)].

Table 5.2 Reaction kinetic parameters estimated by combining the LHHW and ER approaches

	Kinetic parameters		
	Rate constant at 210 °C ($mol.gcat^{-1}.h^{-1}$)	Activation energy ($kJ.mol^{-1}$)	Frequency factor ($mol.gcat^{-1}.h^{-1}$)
Conversion of glycerol to 1,2-PDO (k'_3)	12.6	70.5 ± 8.9	$17.62 \pm 0.03 \times 10^8$
Conversion of 1,2-PDO to PO (k'_4)	2.0	79.5 ± 2.1	$6.51 \pm 0.76 \times 10^8$
	Equilibrium constant at 210 °C ($L.\ mol^{-1}$)		($L.\ mol^{-1}$)
Adsorption of Glycerol (K_1)	1.17	12.1 ± 0.42	$2.12 \pm 0.21 \times 10^{-4}$
Adsorption of Hydrogen (K_2)	1.7	16.7 ± 3.6	$1.85 \pm 0.08 \times 10^{-7}$
Adsorption of 1,2-PDO ($1/K_5$)	2.41×10^{-2}	12.9 ± 2.8	$2.07 \pm 0.79 \times 10^{-6}$
Adsorption of propanol ($1/K_6$)	2.22×10^{-1}	14.8 ± 3.9	$7.14 \pm 1.07 \times 10^{-6}$

Experimental and simulated concentration of glycerol, 1,2-PDO and PO with time at various reaction temperature were plotted (Figure 5.5 (A)-(C)). The parity plots (Figure 5.6 (A)-(C)) depicted that the proposed heterogeneous model for the formation of 1,2-PDO and PO by hydrogenolysis of glycerol was fitted the experimental data satisfactorily. Since the proposed LHHW-ER model was validated very well with the experimental result, all the kinetic parameters estimated by solving this model were more appropriate.

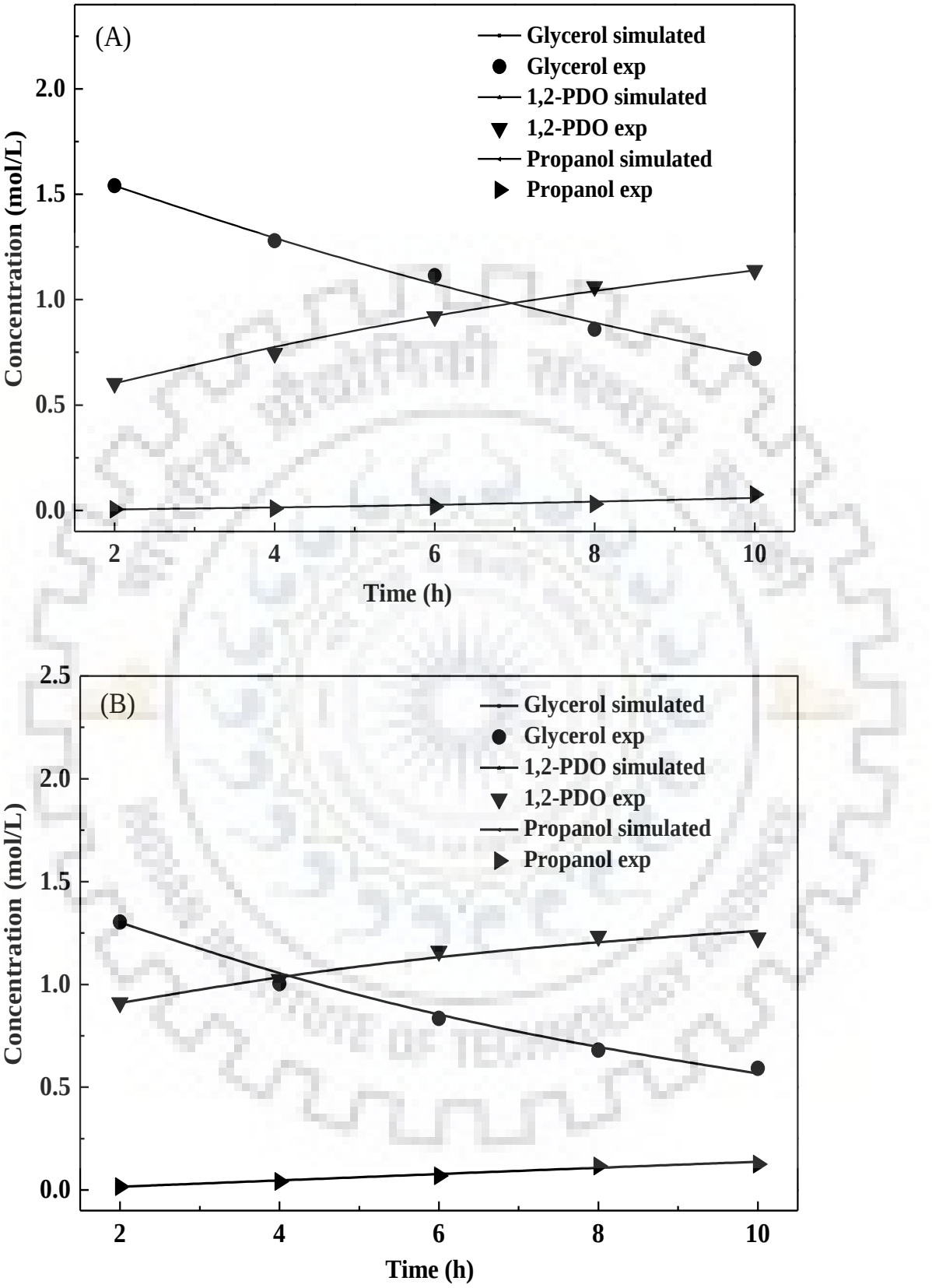

Figure 5.5. Comparison of experimental and model predicted concentration at (A) 200 °C, (B) 210 °C obtained by combined LHHW-ER approach

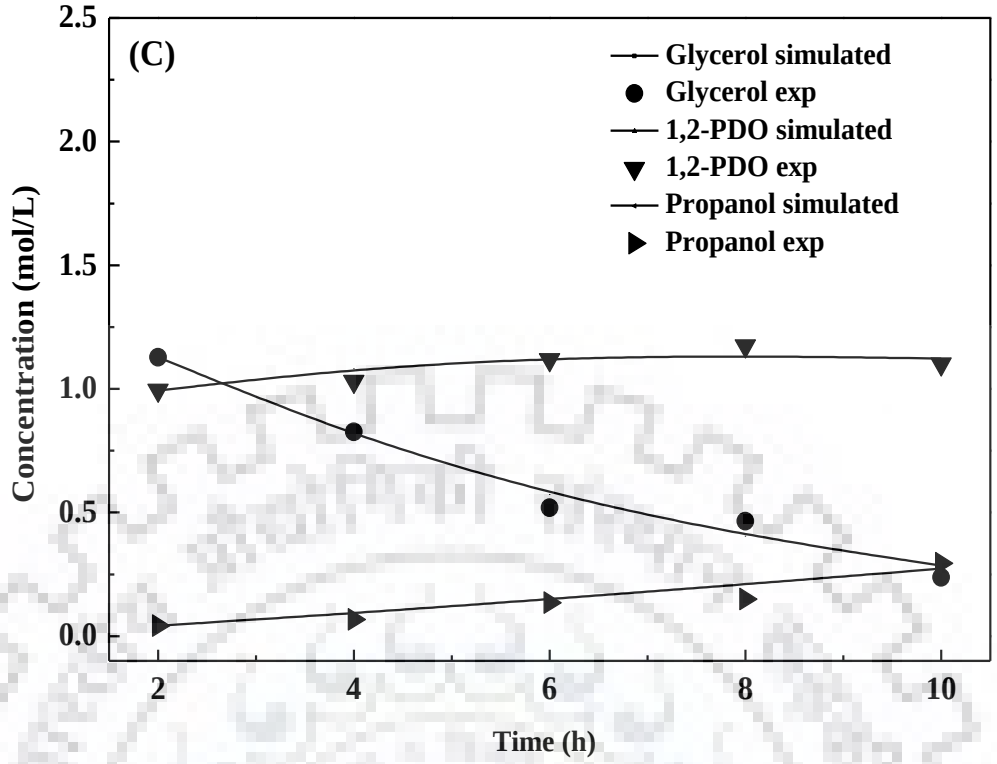

Figure 5.5. Comparison of experimental and model predicted concentration at (C) 220 °C, obtained by combined LHHW-ER approach

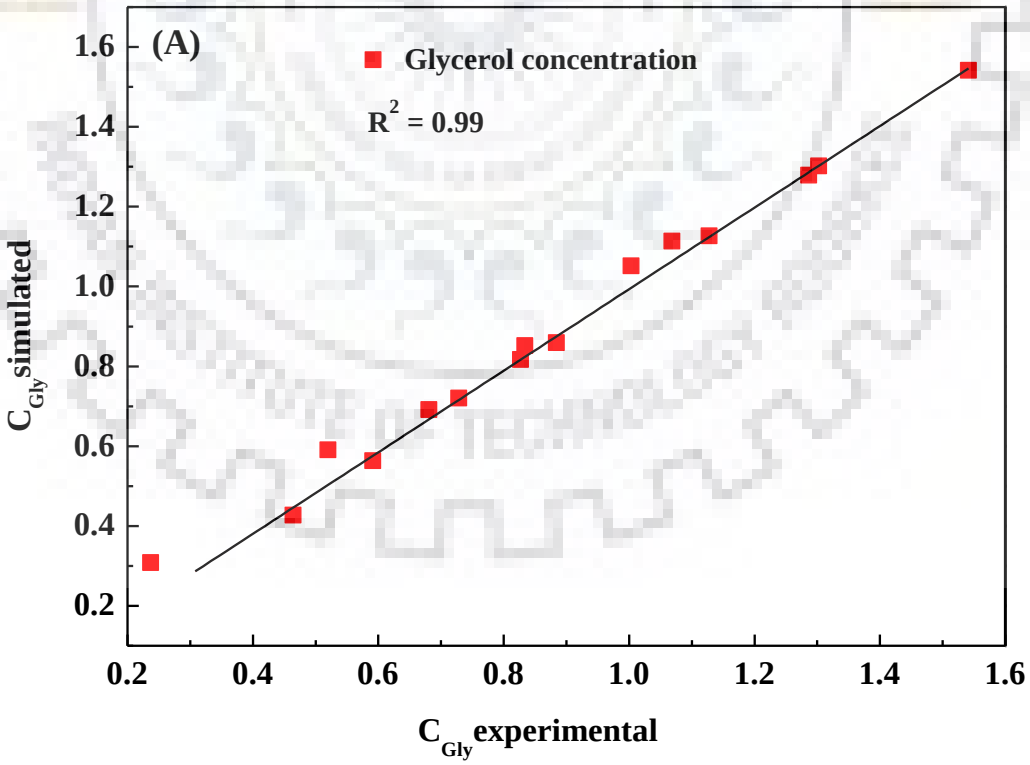

Figure 5.6. Parity plot of experimental and model predicted concentration of (A) glycerol obtained by combined LHHW-ER approach

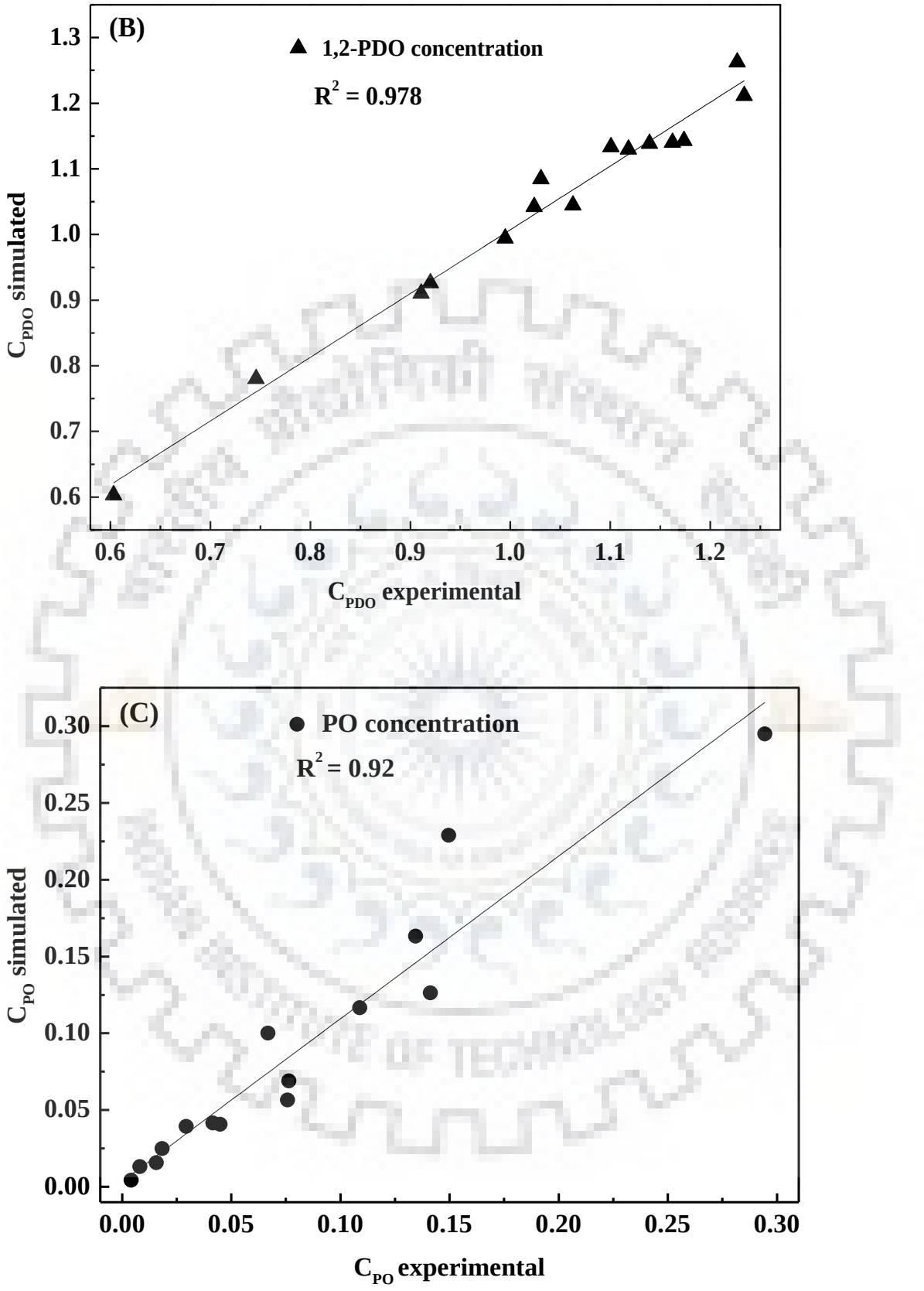

Figure 5.6. Parity plot of experimental and model predicted concentration of (B) 1-2-PDO (C) PO obtained by combined LHHW-ER approach

5.1.3 Summary

Kinetic study of hydrogenolysis of glycerol was carried out in a slurry batch reactor in presence of highly active bi-functional Cu:Ni(1:1)/γ-Al_2O_3 catalyst synthesized by wetness impregnation method. Experiments were performed at the various reaction temperature (180-220 °C) and pressure (4.5-6.0 MPa). 1,2-PDO and propanol (1-PO + 2-PO) were identified as the primary reaction products and trace amounts of other products, including EG, hydroxyacetone, ethanol, and methanol, were also identified.

Probable reaction pathway followed in the presence of bi-functional copper-nickel catalyst was tried to elucidate based on the product distribution obtained, and a reaction mechanism was proposed. The reaction mechanism study suggested two steps hydrogenolysis process i.e. dehydration of glycerol to hydroxyacetone on the acidic centres of the catalyst followed by hydrogenation of hydroxyacetone to 1,2-PDO on the metallic sides of the catalyst. Since 1,2-PDO and propanol were found as primary products, the series reaction of glycerol to 1,2-PDO and 1,2-PDO to propanol were taken into account for kinetic model development. WP criteria and Prater number were validated to make sure all the experimental data were collected in the true kinetic regime.

Various kinetic models including power-law, modified power-law and a heterogeneous kinetic model based on the assumptions of combined Langmuir-Hinshelwood-Hougen-Watson (LHHW) and Eley-Rideal (ER) approaches were developed. The kinetic models were validated with the help of experimental data generated in presence of Cu:Ni(1:1)/γ-Al_2O_3 catalyst in a slurry batch reactor. The model equations were solved by ode23s function for stiff systems in MATLAB together with GA optimization tool. Power law model suggested pseudo 1^{st} order kinetics with respect to glycerol concentration with an activation energy of 67.7 kJ.mol^{-1} for one step hydrogenolysis process. Further, modified power-law model was developed by considering 1,2-PDO and propanol (1-PO + 2-PO) as primary reaction products. Results demonstrated that the experimental concentrations of 1,2-PDO and propanol were very well aligned with the model predicted concentrations. Finally, a more realistic heterogeneous kinetic model based on the assumptions of combined LHHW and ER approaches was developed. The obtained activation energy (Table 5.2) were in synergy to the assumptions made to develop the model. The parity plot of the experimental and simulated concentration of reactant and products revealed that heterogeneous kinetic model was aptly fitted with the experimental data.

5.2 Development of kinetic model in presence of Cu:Zn(4:1)/MgO catalyst

This section describes the kinetic study of glycerol hydrogenolysis reaction in presence of Cu:Zn(4:1)/MgO catalyst. Experiments were carried out at different temperatures (170 °C-210 °C) and at 4.5 MPa H_2 pressure. For each experiment, 20 wt.% aqueous glycerol (20 g) as a feed with 1.6 g of catalyst was used. Langmuir-Hinshelwood type kinetic model was developed Rate equation developed based on this model was solved by MATLAB in combination with Genetic Algorithm. Results suggested that the predicted concentration data were satisfactorily fitted with the experimental data generated. Kinetic parameters i.e. activation energy and pre-exponential factors were estimated by solving the model equations.

5.2.1 Kinetic study

5.2.1.1 Effect of temperature

Effects of temperature and time on glycerol conversion and products selectivity are shown in Figure 5.7 [(A) and (B)]. Experimental errors for all the values (conversion, selectivity and yield) in Figure 5.7 are x ± 1 %. Conversion of glycerol was found to increases with reaction temperature and after 10 h of reaction, it was increased from 61% at 170 °C to 97.4% at 210 ºC. As shown in Fig. 5.7 (B), the selectivity towards 1,2-PDO was very high (> 92.6%) even at 210 ºC. Therefore, 1,2-PDO was considered as a primary reaction product. At higher temperature (210 °C), selectivity towards 1,2-PDO decreased slightly from 93.4% at 2 h to 92.6% at 10 h. Selectivity to EG increased from 3.9% to 4.5% with increasing of temperature from 170 °C to 210 °C after 10 h of reaction.

5.2.2 Development of kinetic model

5.2.2.1 Langmuir-Hinshelwood-Hougen-Watson Model

The schematic diagram of the Langmuir-Hinshelwood-Hougen-Watson Model model is shown in Scheme 5.2. In this model, it was assumed that glycerol and molecular hydrogen was adsorbed on the surface of the catalyst. The adsorbed glycerol interacted with the adsorbed H_2 and produced adsorbed 1,2-PDO and adsorbed water [Xi et al., (2010), Anand et al., (2010)]. Finally, adsorbed 1,2-PDO and water were desorbed from the surface of the catalyst and catalyst active sites were regenerated. The reaction steps considered to develop the rate equations were as follows:

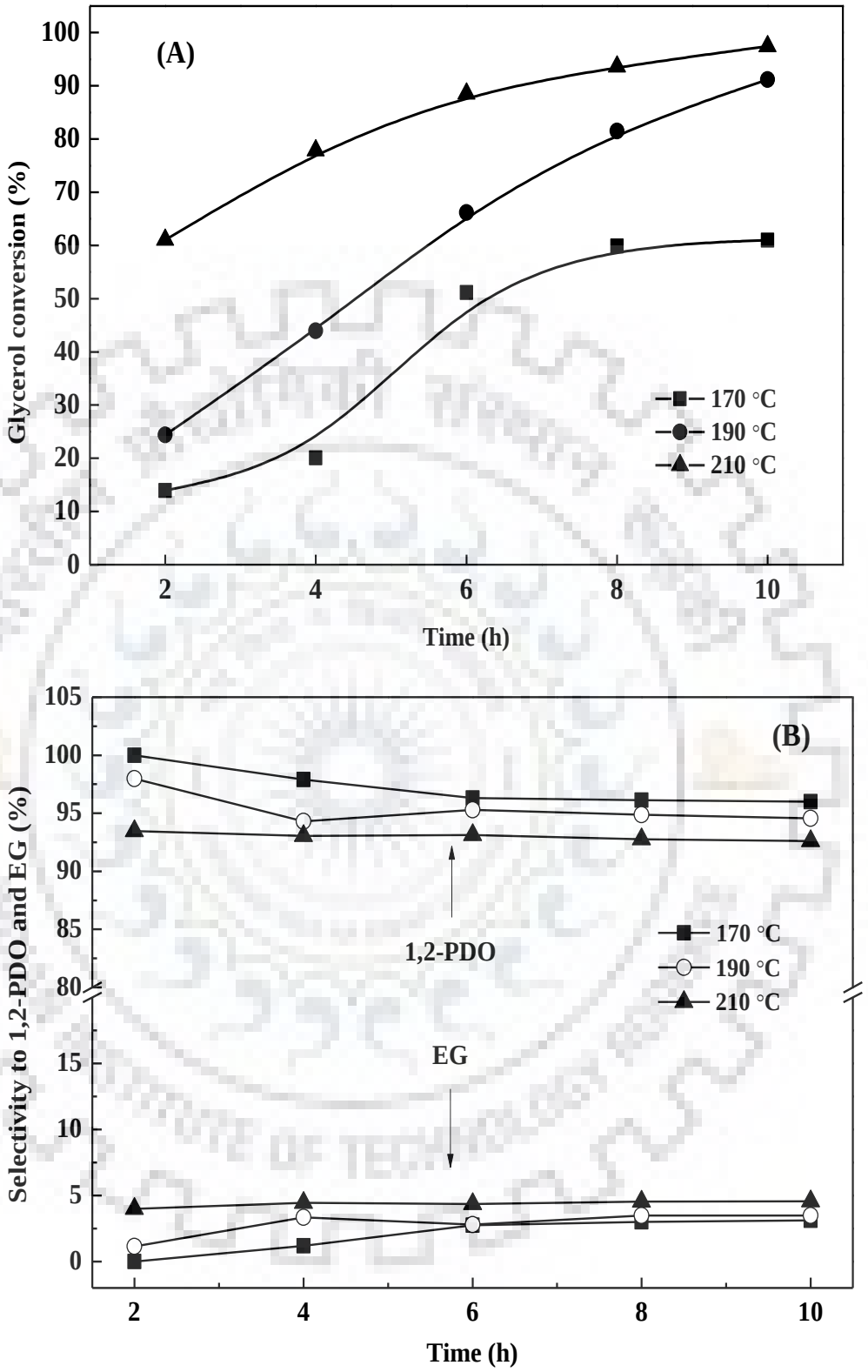

Figure 5.7. Variation of glycerol conversion and product selectivity with time at different temperature and pressure. Reaction condition for (A) and (B): Temperature = 170 °C-210 °C, Pressure = 4.5 MPa, Feed = 20 wt.% glycerol (20 g), catalyst = 1.6 g

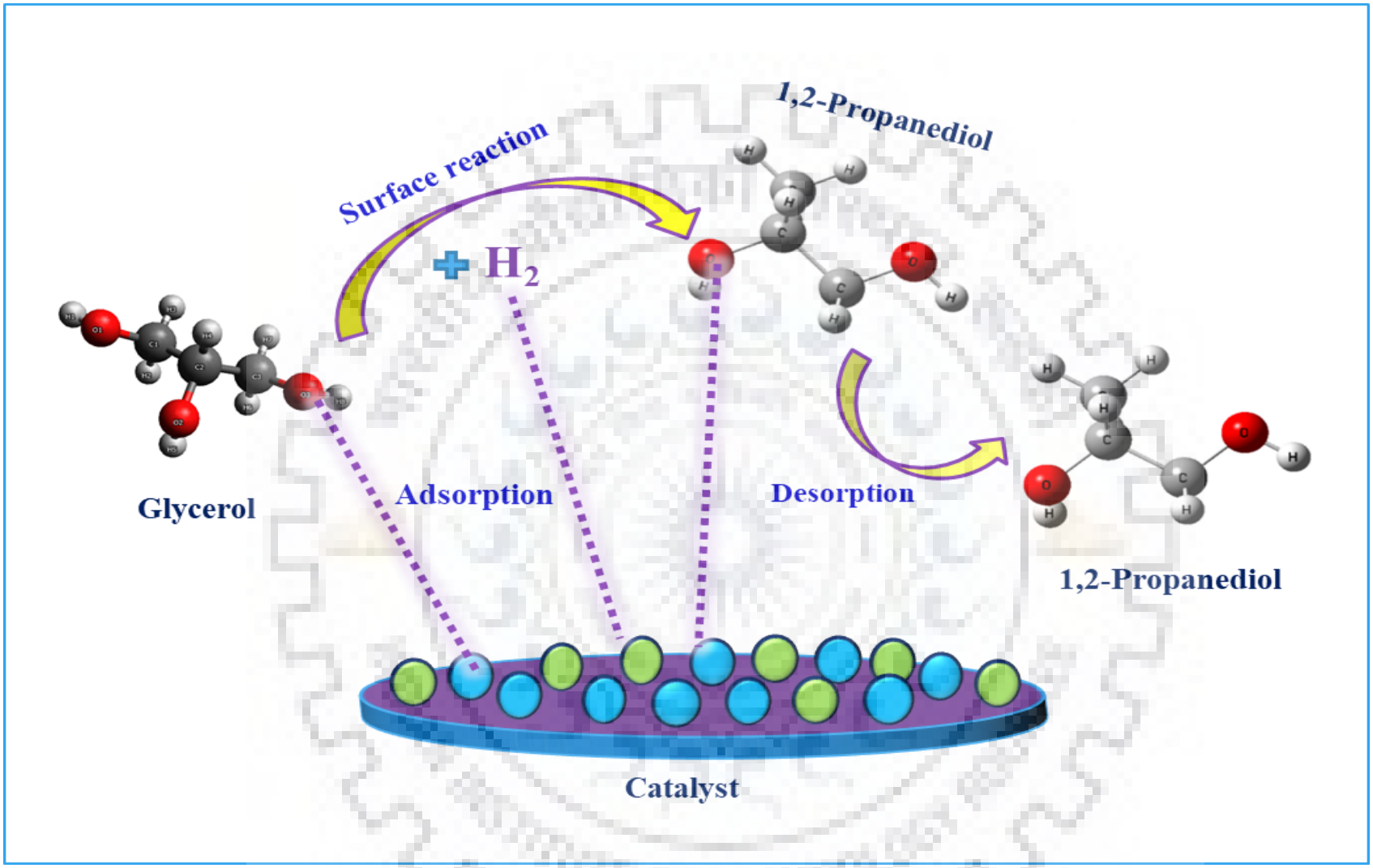

Scheme 5.2. LHHW type reaction mechanism for glycerol hydrogenolysis reaction over Cu:Zn(4:1)/MgO catalyst

Step 1: Adsorption of glycerol (G) and hydrogen (H_2) on the active site ($) of the catalyst

$$G + \$ \underset{k_{-1}}{\overset{k_1}{\rightleftharpoons}} G.\$ \tag{5.42}$$

$$H_2 + \$ \underset{k_{-2}}{\overset{k_2}{\rightleftharpoons}} H_2.\$ \tag{5.43}$$

Step 2: Interaction of adsorbed glycerol with adsorbed hydrogen molecule (H_2) produced adsorbed 1,2-PDO and adsorbed water.

$$G.\$ + H_2.\$ \underset{k_{-3}}{\overset{k_3}{\rightleftharpoons}} P.\$ + W.\$ \tag{5.44}$$

where, P and W represented 1,2-PDO and water, respectively.

Step 3: Desorption of products (1,2-PDO and water) from the catalyst surface and the active sites were regenerated as:

$$P.\$ \underset{k_{-4}}{\overset{k_4}{\rightleftharpoons}} P + \$ \tag{5.45}$$

$$W.\$ \underset{k_{-5}}{\overset{k_5}{\rightleftharpoons}} W + \$ \tag{5.46}$$

From the equations (5.42) - (5.46), the rate equations for the individual step were written as follows:

$$(-r_1) = k_1(C_G C_\$ - \frac{C_{G.\$}}{K_1}); \quad K_1 = \frac{k_1}{k_{-1}} \tag{5.47}$$

$$(-r_2) = k_2(P_{H_2} C_\$ - \frac{C_{H_2.\$}}{K_2}); \quad K_2 = \frac{k_2}{k_{-2}} \tag{5.48}$$

$$(-r_3) = k_3(C_{G.\$}.C_{H_2.\$} - \frac{C_{P.\$}C_{W.\$}}{K_3}); \quad K_3 = \frac{k_3}{k_{-3}} \tag{5.49}$$

$$(-r_4) = k_4(C_{P.\$} - \frac{C_P C_\$}{K_4}); \quad K_4 = \frac{k_4}{k_{-4}} \tag{5.50}$$

$$(-r_5) = k_5(C_{W.\$} - \frac{C_W C_\$}{K_5}); \quad K_5 = \frac{k_5}{k_{-5}} \tag{5.51}$$

where K_1, K_2, K_3, K_4, K_5 were the equilibrium constants for the above-mentioned steps.

Initially, three different rate equations were derived by considering adsorption, surface reaction and desorption steps as the rate-limiting steps separately. It was observed that the experimental data were fitted well with the rate equation developed based on the surface reaction step as the rate controlling step. Therefore, the final rate expression was formulated by assuming the surface reaction step as a rate controlling step and irreversible in nature as follows [Lahr and Shanks (2003), Pandhare et al., (2018), Ameen et al., (2017)].

From Eq. (5.49),

$$(-r_3) = k_3 C_{G.\$} C_{H_2.\$} \tag{5.52}$$

The adsorption and desorption steps were very fast when the surface reaction step was rate limiting, then we had

From Eq. (5.47), $-\frac{r_1}{k_1} = 0$ then

$$C_{G.\$} = K_1 C_G C_\$ \tag{5.53}$$

Similarly, from Eq. (5.48), $-\frac{r_2}{k_2} = 0$ then

$$C_{H_2.\$} = K_2 C_\$ P_{H_2} \tag{5.54}$$

Similarly, from Eq. (5.50), $-\frac{r_4}{k_4} = 0$ then

$$C_{P.\$} = \frac{C_P C_\$}{K_4} \tag{5.55}$$

Similarly, from Eq. (5.51), $-\frac{r_5}{k_5} = 0$ then

$$C_{W.\$} = \frac{C_W C_\$}{K_5} \tag{5.56}$$

On substituting these values in the surface reaction rate Eqs. (5.52) which reduced to

$$(-r_3) = k_3 K_1 C_G C_\$ K_2 C_\$ P_{H_2} \tag{5.57}$$

From the total site balance, we had

$$C_{T\$} = C_\$ + C_{G.\$} + C_{H2.\$} + C_{P.\$} + C_{W.\$} \tag{5.58}$$

Substituting concentrations of adsorbed species in the Eq. (5.58) gave,

$$C_{T\$} = C_\$ + K_1 C_G C_\$ + K_2 C_\$ P_{H_2} + \frac{C_P C_\$}{K_4} + \frac{C_W C_\$}{K_5} \tag{5.59}$$

$$C_\$ = \frac{C_{T\$}}{\left[1 + K_1 C_G + K_2 P_{H_2} + \frac{C_P}{K_4} + \frac{C_W}{K_5}\right]} \tag{5.60}$$

Substituting Eq. (5.60) into Eq. (5.57) yielded,

$$(-r_3) = \frac{k_3 C_{T\$}^2 K_1 K_2 C_G P_{H_2}}{\left[1 + K_1 C_G + K_2 P_{H_2} + \frac{C_P}{K_4} + \frac{C_W}{K_5}\right]^2} \tag{5.61}$$

At $t = 0$, $(-r_3) = (-r_3)_0$; C_P and $C_W = 0$,

Then, equation (5.61) will be $(-r_3) = \frac{k_3 C_{T\$}^2 K_1 K_2 C_G P_{H_2}}{\left[1 + K_1 C_G + K_2 P_{H_2}\right]^2}$ (5.62)

Assuming that adsorption of glycerol (G) and hydrogen (H_2) on the active sites of the catalysts did not inhibit the reaction, thereby neglecting the inhibition term $\left[1 + K_1 C_G + K_2 P_{H_2}\right]^2$

Now, Eq. (5.62) was modified as $(-r_3) = k_3' C_G P_{H_2}$ (5.63)

where $k_3' = k_3 C_{T\$}^2 K_1 K_2$ apparent reaction rate constant for the conversion of glycerol to 1,2-PDO.

Equations (5.63) represented the final rate expression for hydrogenolysis of glycerol to 1,2-PDO reaction.

To develop the model, the mole balance equation was written as follows:

$$\frac{dC_G}{dt} = -r_3 \tag{5.64}$$

where C_G was the steady-state concentration of glycerol, 't' was the reaction time.

In order to evaluate the unknown variables in the rate expressions, the differential equation (Eqs. (5.63)) obtained were computed with the help of ode23s function for stiff systems in MATLAB together with genetic algorithm tool. The residual sum of squares i.e. *f* (fitness function), between experimental and simulated concentrations of glycerol, 1,2-PDO, and PO were minimized with the help of GA.

GA was used to minimize the objective function.

The objective function was elucidated as follows:

$$f = \sum_{i=1}^{N} \left[(C^{i}_{G,exp} - C^{i}_{G,sim})^2 \right] \tag{5.65}$$

where, *N* represented the number of experimental runs and $C^{i}_{G,exp}$ were the experimental and $C^{i}_{G,sim}$ were the simulated concentrations of glycerol, 1,2-PDO and PO obtained by solving the model equations, respectively.

The kinetic parameters such as activation energy and frequency factor for glycerol conversion to 1,2-PDO were estimated by using the Arrhenius equation. The obtained activation energy and frequency factor were 42.62 kJ.mol^{-1} and 2.9×10^{4} mol.gcat^{-1}.h^{-1}, respectively. Experimental and simulated glycerol concentration at different reaction temperature with time is shown in Figure 5.8 (A). Parity plot of simulated glycerol concentration vs experimental concentration of glycerol shown in Figure 5.8 (B) suggested that experimental data were very well fitted with the model predicted concentrations.

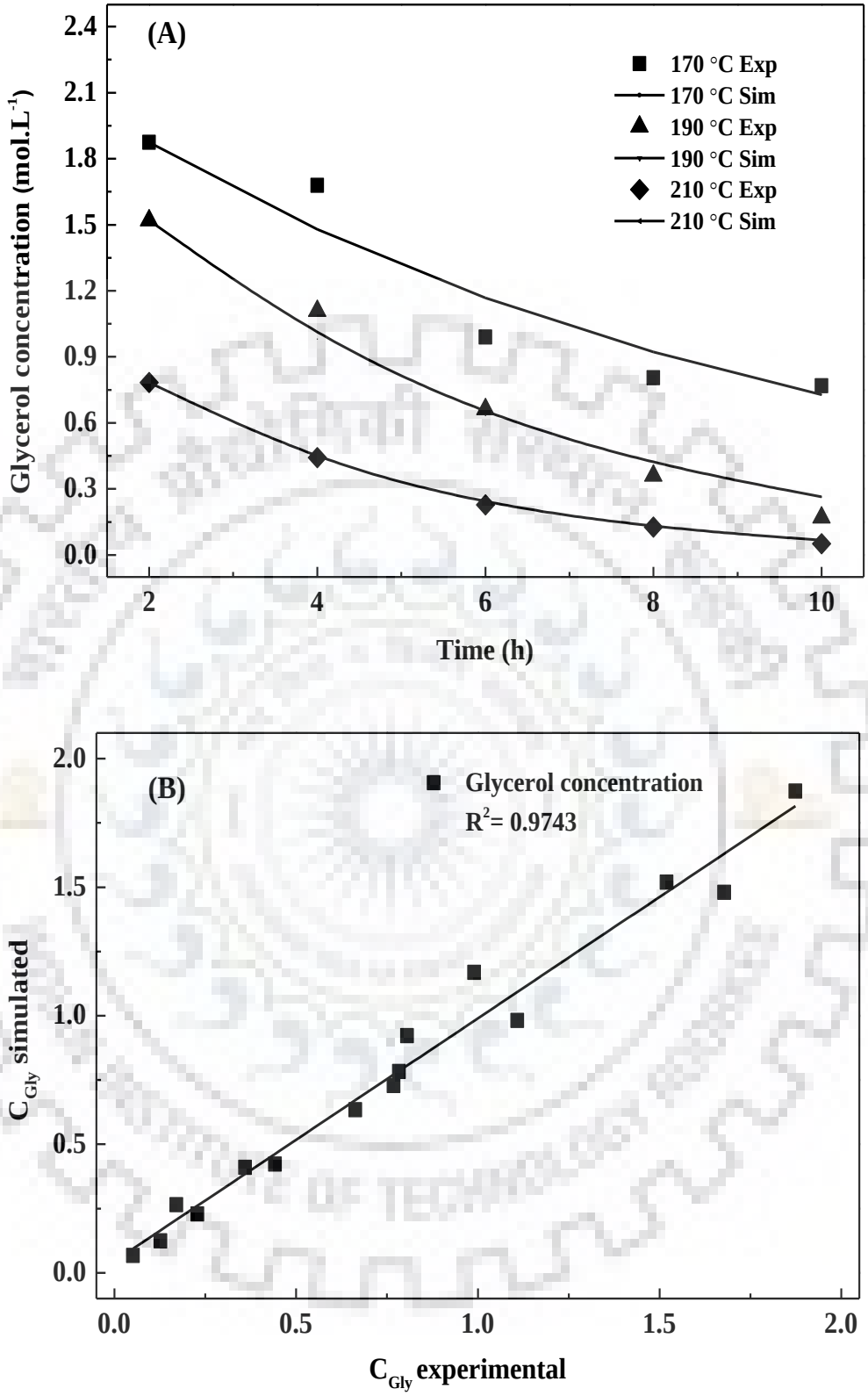

Figure 5.8. (A) Variation of experimental and simulated glycerol concentration at different temperature obtained by L-H model (B) Parity plots of the experimental and model-predicted concentrations of glycerol from the L-H model

5.2.3 Summary

The kinetic study of glycerol hydrogenolysis reaction using bi-functional, highly active Cu:Zn(4:1)/MgO catalyst was carried out in the temperature range of (170-210 °C) and at 4.5 MPa H_2 pressure. Results showed that Cu:Zn(4:1)/MgO catalyst very high selectivity (> 93%) to 1,2-PDO, and trace amounts of other products such as hydroxyacetone (1.2%), EG (2.7%), methanol (1.23%) and ethanol (0.35%) were also detected at different reaction condition used. A simple one-step glycerol conversion to 1,2-PDO reaction was considered to develop the kinetic model. LHHW approach was used to find out the final rate expression which was solved by ode23 with the help of GA. An activation energy of 42.6 $kJ.mol^{-1}$ was obtained for glycerol conversion to 1,2-PDO formation step. The kinetic model developed was satisfactorily correlated with the experimental data obtained.

5.3 Development of kinetic model in presence of Cu:Zn(4:1)/MgO-La_2O_3 catalyst

This section discusses the kinetic study of glycerol hydrogenolysis reaction over Cu:Zn(4:1)/MgO-La_2O_3 catalyst, as this catalyst showed highest catalytic activity among all other catalysts developed in this thesis. Kinetic experiments were performed by varying reaction temperature (170-210 °C) and pressure (3-6 MPa). In presence of this catalyst, 1,2-PDO was the primary product and the obtained 1,2-PDO selectivity (> 93%) was very high. As a results, a simple one step glycerol conversion of to 1,2-PDO was considered to develop LHHW type kinetic model. Kinetic parameters were obtained by solving the model equation by using MATLAB. GA was used to minimize the objective function.

5.3.1 Kinetic study

5.3.1.1 Effect of temperature

Effect of temperature on glycerol conversion and products selectivity with time was investigated in the range of 170 °C to 210 °C, and the results are shown in Figure 5.9 [(A) and (B)]. Experimental errors for all the values (conversion, selectivity and yield) : x ± 1 %. It was observed that conversion of glycerol was increased sharply with increasing temperature as well as time. At 170 °C, glycerol conversion was increased from 10% after 2 h to 81% after 12 h. At 210 ^oC, glycerol conversion was varied from 78% to 100% with the variation of time from 2 to 12 h of reaction time.

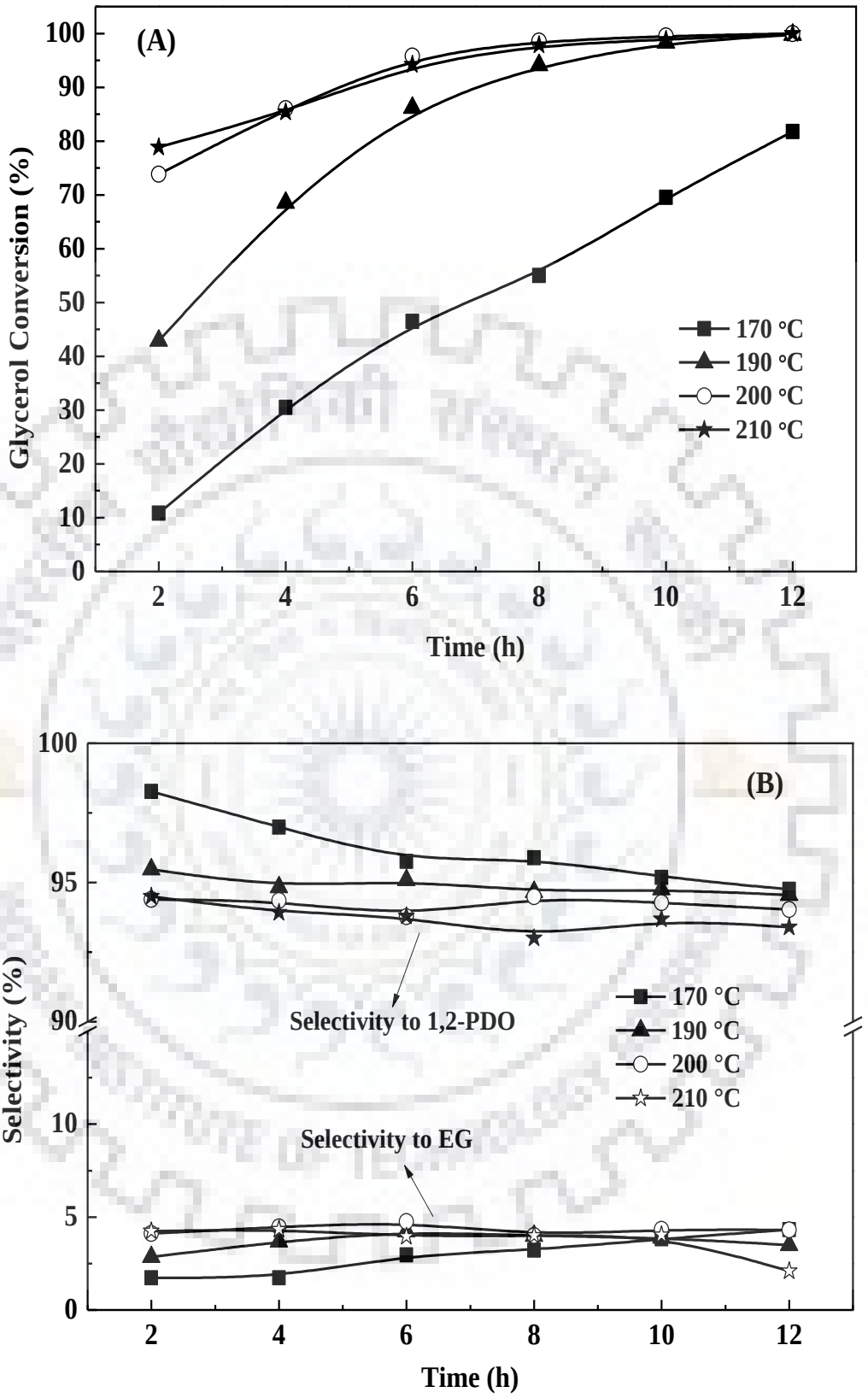

Figure 5.9. (A) Variation of glycerol conversion and (B) product selectivity with time at different temperature. Reaction condition: temperature = 170 °C-210 °C, pressure = 4.5 MPa, Feed = 20 wt.% glycerol (20 g), catalyst = 1.6 g

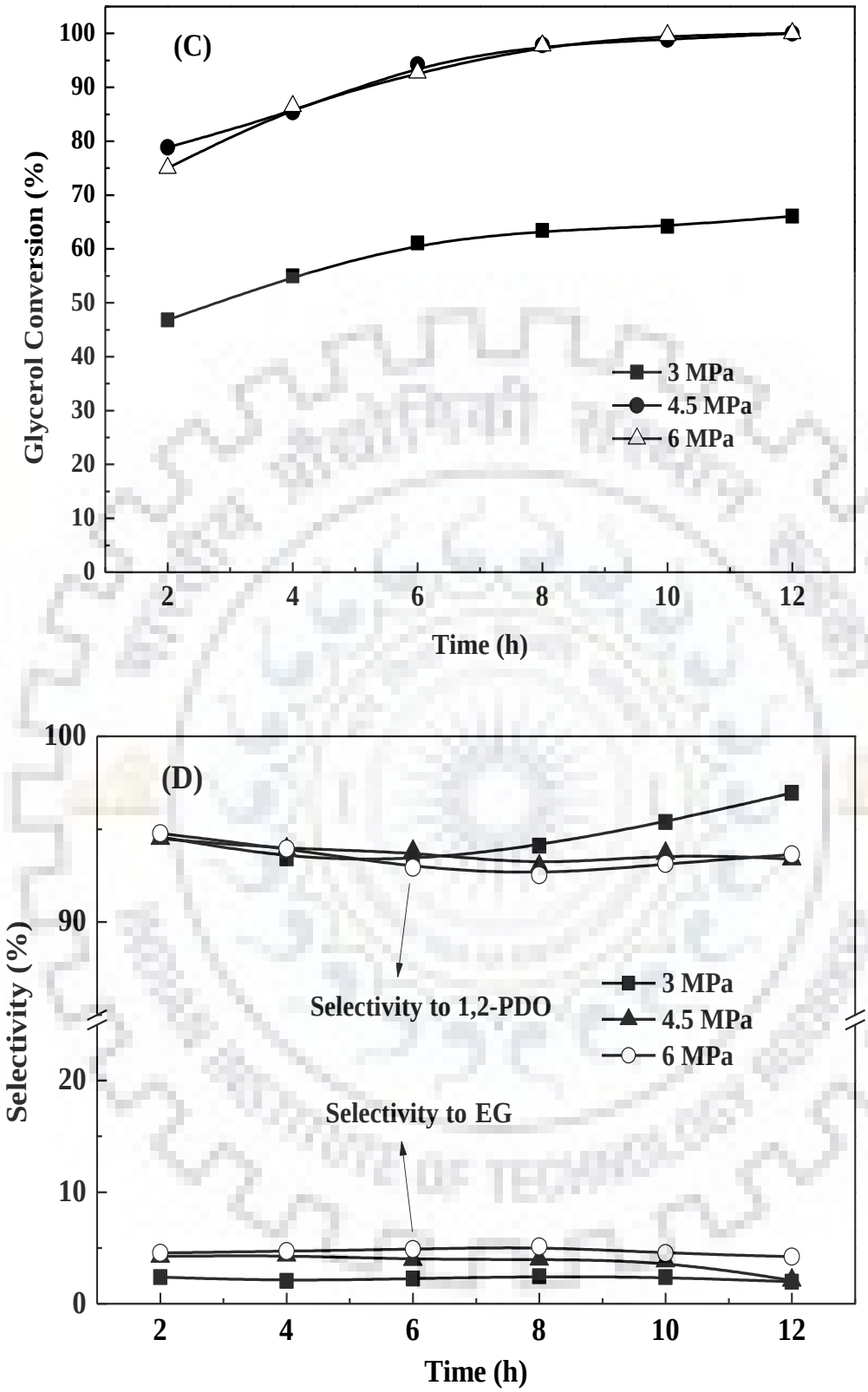

Figure 5.9. (C) Variation of glycerol conversion and (D) product selectivity with time at different pressure. Reaction condition: pressure = 3 MPa– 6 MPa, temperature = 210 °C, feed = 20 wt.% glycerol (20 g), catalyst = 1.6 g

In presence of Cu:Zn(4:1)/MgO-La_2O_3 catalyst, 1,2-PDO was obtained as a main reaction product (> 93%) and small amounts of degradation products such as EG, PO and methanol were also obtained. At 170 °C, the selectivity towards 1,2-PDO decreased slightly from 98% to 94.6% with the variation of reaction time from 2 to 12 h. However, at 210 °C, the selectivity towards 1,2-PDO remained almost constant (94.5- 93.5%) with the variation of time from 2-12 h. The slight decrease in selectivity towards 1,2-PDO with increasing temperature and time was obtained due to the formation of degradation products such as EG, PO, methanol etc. Figure 5.9 shows that the selectivity of ethylene glycol decreased with increasing temperature from ~4.2% at 170 ^oC to ~2.1% at 210 °C..

5.3.1.2 Effect of pressure

Influence of H_2 pressure on glycerol conversion and products selectivity with time is shown in Figure 5.9 [(C) and (D)]. Experimental errors for all the values (conversion, selectivity and yield) : x ± 1 %. It shows that, glycerol conversion increased from 46% at 2 h to 66% after 12 h at 3.0 MPa pressure and at 210 ^oC. However, at 4.5 MPa pressure, glycerol conversion increased sharply from ~80% to 100% within 8 h of reaction time. No significant variation in the glycerol conversion was found beyond the reaction pressure of 4.5 MPa. At 3 MPa, the selectivity to 1,2-PDO increased from 94.5% to 97% with increasing the reaction time from 2h to 12 h. Selectivity to EG was almost constant (~2.1%) within the reaction time period (2-12 h). Further increasing the pressure (> 3 MPa) the selectivity to 1,2-PDO and EG was also almost ~94% and ~4.2%, respectively.

5.3.2 Development of kinetic model

5.3.2.1 Langmuir-Hinshelwood-Hougen-Watson type Model

In this section, kinetic model was developed based on the same reaction mechanism which was already shown in Schematic 5.2.

Step 1: Adsorption of glycerol (G) and hydrogen (H_2) on the active site ($) of the catalyst as:

$$G + \$ \underset{k_{-1}}{\overset{k_1}{\rightleftharpoons}} G.\$ \tag{5.66}$$

$$H_2 + \$ \underset{k_{-2}}{\overset{k_2}{\rightleftharpoons}} H_2.\$ \tag{5.67}$$

Step 2: Interaction of adsorbed glycerol with hydrogen molecule (H_2) present in the bulk phase and produced adsorbed 1,2-PDO (P) and adsorbed water (W):

$$G.\$ + H_2.\$ \underset{k_{-3}}{\overset{k_3}{\rightleftharpoons}} P.\$ + W.\$ \tag{5.68}$$

Step 3: Desorption of products (1,2-PDO and water) from the catalyst surface and the active sites were regenerated as:

$$P.\$ \underset{k_{-4}}{\overset{k_4}{\rightleftharpoons}} P + \$ \tag{5.69}$$

$$W.\$ \underset{k_{-5}}{\overset{k_5}{\rightleftharpoons}} W + \$ \tag{5.70}$$

From the equations (5.66) - (5.70), the rate equations for individual step were written as follows:

$$(-r_1) = k_1\left(C_G C_\$ - \frac{C_{G.\$}}{K_1}\right); \quad K_1 = \frac{k_1}{k_{-1}} \tag{5.71}$$

$$(-r_2) = k_2\left(P_{H_2} C_\$ - \frac{C_{H_2.\$}}{K_2}\right); \quad K_2 = \frac{k_2}{k_{-2}} \tag{5.72}$$

$$(-r_3) = k_3\left(C_{G.\$}.C_{H_2.\$} - \frac{C_{P.\$}C_{W.\$}}{K_3}\right); \quad K_3 = \frac{k_3}{k_{-3}} \tag{5.73}$$

$$(-r_4) = k_4\left(C_{P.\$} - \frac{C_P C_\$}{K_4}\right); \quad K_4 = \frac{k_4}{k_{-4}} \tag{5.74}$$

$$(-r_5) = k_5\left(C_{W.\$} - \frac{C_W C_\$}{K_5}\right); \quad K_5 = \frac{k_5}{k_{-5}} \tag{5.75}$$

where K_1, K_2, K_3, K_4, K_5 were the equilibrium constants for the above mentioned steps.

To develop the final rate equation, three different rate equations were derived by considering adsorption, surface reaction and desorption steps as the rate limiting steps, separately. However, the final results suggested that, the experimental data were fitted well for the final rate expression developed based on the surface reaction step as the rate controlling step. As a result, the final rate expression was formulated by assuming the surface reaction step

as a rate controlling step and irreversible in nature [Lahr and Shanks (2003), Pandhare et al., (2018), Ameen et al., (2017)] as follows.

From Eq. (5.73),

$$(-r_3) = k_3 C_{G.\$} C_{H_2.\$} \tag{5.76}$$

The adsorption and desorption steps were very fast when surface reaction step was rate limiting, then we had

From Eq. (5.71), $-\frac{r_1}{k_1} = 0$ then

$$C_{G.\$} = K_1 C_G C_\$ \tag{5.77}$$

Similarly, from Eq. (5.72), $-\frac{r_2}{k_2} = 0$ then

$$C_{H_2.\$} = K_2 C_\$ P_{H_2} \tag{5.78}$$

Similarly, from Eq. (5.74), $-\frac{r_4}{k_4} = 0$ then

$$C_{P.\$} = \frac{C_P C_\$}{K_4} \tag{5.79}$$

Similarly, from Eq. (5.75), $-\frac{r_5}{k_5} = 0$ then

$$C_{W.\$} = \frac{C_W C_\$}{K_5} \tag{5.80}$$

On substituting these values in the surface reaction rate Eq. (5.76) which reduced to

$$(-r_3) = k_3 K_1 C_G C_\$ K_2 C_\$ P_{H_2} \tag{5.81}$$

From the total site balance, we had

$$C_{T\$} = C_\$ + C_{G.\$} + C_{H2.\$} + C_{P.\$} + C_{W.\$} \tag{5.82}$$

Substituting concentrations of adsorbed species in the Eq. (5.82) gave,

$$C_{T\$} = C_\$ + K_1 C_G C_\$ + K_2 C_\$ P_{H_2} + \frac{C_P C_\$}{K_4} + \frac{C_W C_\$}{K_5} \tag{5.83}$$

$$C_\$ = \frac{C_{T\$}}{\left[1 + K_1 C_G + K_2 P_{H_2} + \frac{C_P}{K_4} + \frac{C_W}{K_5}\right]} \tag{5.84}$$

Substituting Eq. (5.83) into Eq. (5.81) yielded,

$$(-r_3) = \frac{k_3 C_{T\$}^2 K_1 K_2 C_G P_{H_2}}{\left[1 + K_1 C_G + K_2 P_{H_2} + \frac{C_P}{K_4} + \frac{C_W}{K_5}\right]^2} \tag{5.85}$$

At $t = 0$, $(-r_3) = (-r_3)_0$; C_P and $C_W = 0$,

Then, equation (5.85) will be $(-r_3) = \frac{k_3 C_{T\$}^2 K_1 K_2 C_G P_{H_2}}{\left[1 + K_1 C_G + K_2 P_{H_2}\right]^2}$ (5.86)

Assuming that adsorption of Glycerol (G) and Hydrogen (H_2) on the catalysts active sites did not inhibit the reaction, thereby neglecting the inhibition term $\left[1 + K_1 C_G + K_2 P_{H_2}\right]^2$

Now, Eq. (5.86) was reduced to

$$(-r_3) = k_3' C_G P_{H_2} \tag{5.87}$$

where $k_3' = k_3 C_{T\$}^2 K_1 K_2$, apparent reaction rate constant for the conversion of glycerol to 1,2-PDO.

To develop the model, the mole balance equation was written as follows:

$$\frac{\mathrm{d}\, C_G}{\mathrm{d}\, t} = -r_3 \tag{5.88}$$

where C_G was the steady state concentration of glycerol, 't' was the reaction time.

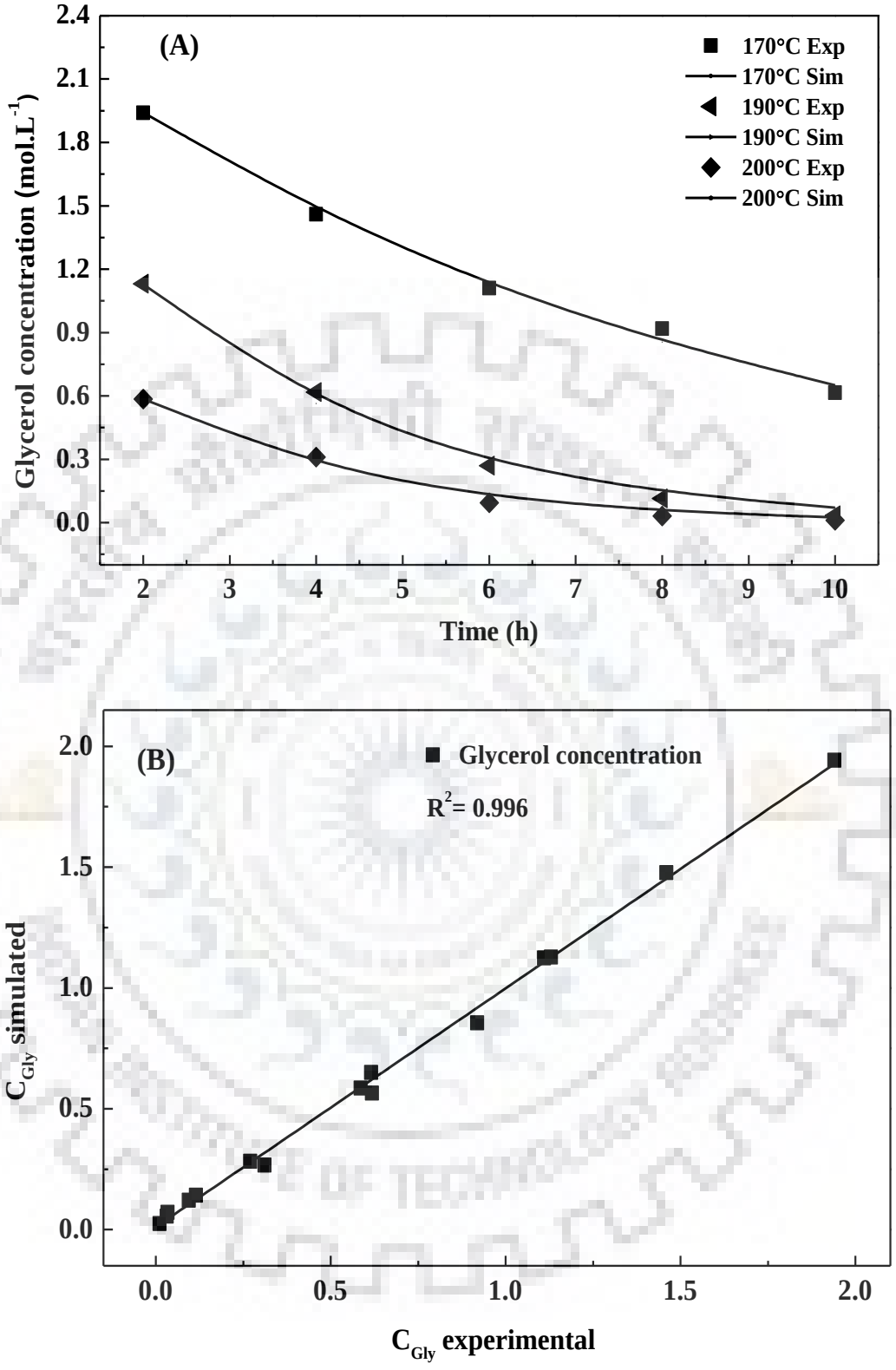

Figure 5.10. (A) Variation of experimental and simulated glycerol concentration at different temperature obtained by L-H model (B) Parity plots of the experimental and model-predicted concentrations of glycerol from the L-H model.

In order to evaluate the unknown variables in the rate expressions, the differential equation (Eqs. (5.88)) obtained was computed with the help of ode23s for stiff systems in MATLAB together with Genetic Algorithm. The residual sum of squares i.e. *f* (fitness function), between experimental and simulated concentrations of glycerol was minimized with the help of GA.

The objective function was elucidated as follows:

$$f = \sum_{i=1}^{N} \left[(C^{i}_{G,exp} - C^{i}_{G,sim})^2 \right] \quad (5.89)$$

where, *N* represented the number of experimental runs, $C^{i}_{G,exp}$ was the experimental and $C^{i}_{G,sim}$ was the simulated concentration of glycerol, obtained by solving the model equations.

The activation energy and frequency factor for the conversion of glycerol to 1,2-PDO were estimated by using Arrhenius equation. The obtained activation energy and frequency factor were 69.6 kJ.mol^{-1} and 4.2×10^{7} mol.gcat^{-1}.h^{-1}, respectively. The experimental and simulated glycerol concentration at various reaction temperature with time is shown in Figure 5.10 (A). Parity plot of simulated glycerol concentration vs experimental concentration shown in Figure 5.10 (B) dictated that experimental data were very well fitted with the model predicted concentrations

5.3.3 Summary

The kinetic study of liquid phase glycerol hydrogenolysis was performed in an autoclave reactor at various temperature (170-210 ^{o}C) and pressure (3-6 MPa) in presence of Cu:Zn(4:1)/MgO-La_2O_3 catalyst. LHHW type kinetic model was developed by considering a single step glycerol to 1,2-propanediol production and the model equation was solved by MATLAB coupled with genetic algorithm. Results showed that, the experimental concentrations of glycerol were very well fitted with the model predicted values. The activation energy and the frequency factor for the conversion of glycerol to 1,2-PDO was found to be 69.6 kJ.mol^{-1} and of 4.2×10^{7} mol.gcat^{-1}.h^{-1}, respectively.

CHAPTER VI

ECONOMIC ANALYSIS

Economic analysis for liquid phase hydrogenolysis of glycerol to 1,2-PDO production was carried out to determine the overall economic feasibility of the process by considering Cu:Zn(4:1)/MgO as a catalyst. Figure 6.1 illustrates the overall reaction process along with the manufacturing process of catalyst. Reactants (glycerol, H_2) and reduced catalyst, prepared by precipitation-deposition method were charged into the autoclave reactor and the reaction was continued for 12 h at the optimum temperature of 210 °C and H_2 pressure of 4.5 MPa. After the reaction, the reactor was allowed to cool to room temperature and the products were centrifuged to separate the catalyst. Per day 60 kg production of 1,2-PDO was assumed to be as the basis of the calculation. For this large scale production, the capacity of the reactor was considered as 500 L. For that purpose, 400 kg reaction mixture (80 kg glycerol + 320 kg distilled water) was considered to be processed per batch. The overall process considered is shown in Scheme 6.1.

6.1 Catalyst preparation cost

Catalyst amount required to process per batch of reaction was ~6.4 kg by considering 8 wt.% catalyst loading with respect to 80 kg of glycerol as feed. The manufacturing cost of catalyst was the summation of raw material cost and the total cost of energy consumed for catalyst preparation. The schematic diagram of the catalyst manufacturing process is shown in Figure 6.1. Details cost estimation for the synthesis of 6.4 kg of catalyst are summarized in Table 6.1.

- Raw material cost for the manufacturing of catalyst included the cost of metal precursors (copper nitrate, zinc nitrate), support (magnesium oxide), precipitating agent ($NaHCO_3$), deionized water and hydrogen which was used during the reduction of the catalyst.
- Energy cost included the amount of electricity consumption due to drying, calcination and reduction process.

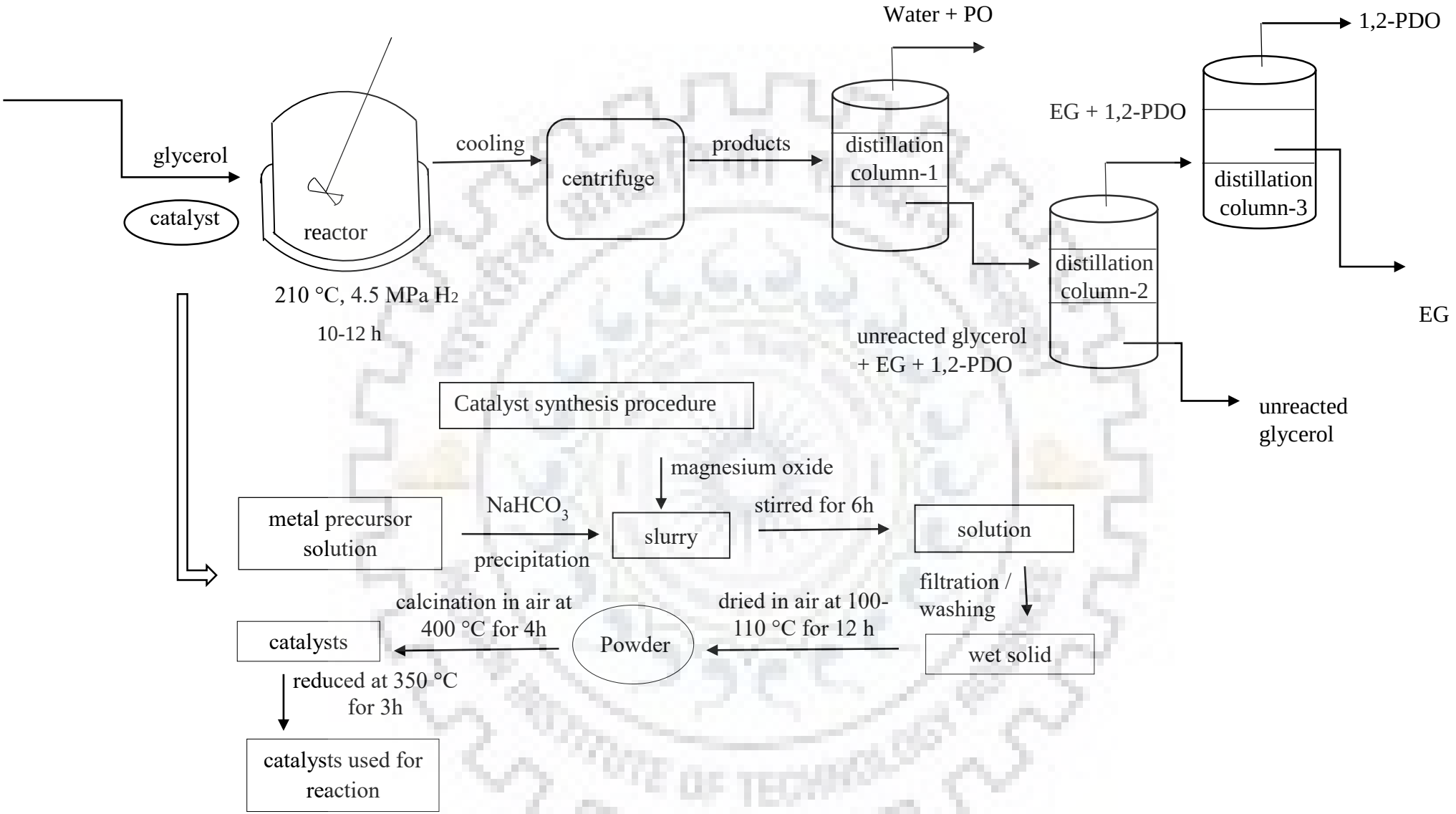

Figure 6.1. Overall reaction and catalyst synthesis process [products: 1-propanol (PO), 1,2-propanediol (1,2-PDO), ethylene glycol (EG)]

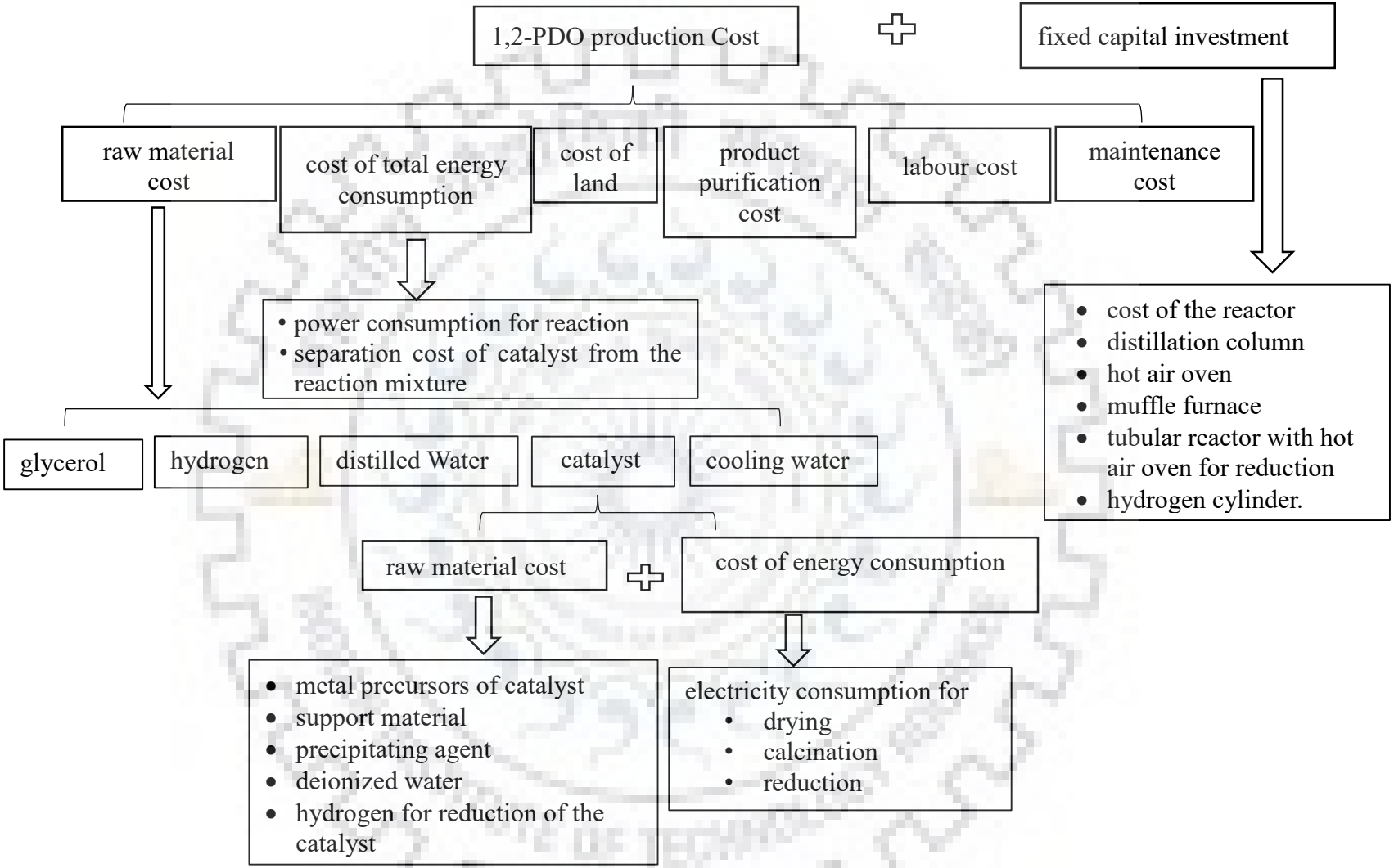

Scheme 6.1. Cost analysis of the overall process

Table 6.1. Catalyst manufacturing cost (6.4 kg catalyst)

Material Cost (Rs.)				Cost of energy (rate Rs. 3.85 per KWh) (as per local rate)			
Material	Amount required (kg)	Cost per kg	Cost for the synthesis of 6.4 kg catalyst (I)	Process	Rating (W)	Time duration (h)	Total cost of energy consumption (Rs.) (II)
Copper nitrate (>99%, Thomas Baker, India)	8516.41	2770.5/-	17731.2/-	Drying	3500	12	134.75/-
Zinc nitrate (>99%, Thomas Baker, India)	4367.86	726.15/-	4647.4/-	Calcination	6190	4	305.04/-
Magnesium oxide (Thomas Baker, India, 98%)	3200	1728/-	5529.6/-	Reduction	6190	4	71.49/-
Sodium bicarbonate (>99.8%, Thomas Baker, India)	37,632	410/-	15429.1/-	-	-	-	-
Hydrogen (99.99%, Sigma gas)		-	1152/-	-	-	-	-
Total		-	44489.3/-	-	-	-	511.2/-
Raw material cost for the synthesis of 6.4 kg catalyst (I) + Total cost of energy consumption (II)							Rs. 45000.6/-

Total cost for the synthesis of 6.4 kg catalyst (material cost and energy cost) was estimated to be Rs. 45000.6/-

Therefore, cost per kg of catalyst synthesis was calculated as Rs. 7031/-

6.2 Production cost of 1,2-propanediol

Now the total cost for the production of 1,2-PDO was considered as the sum of fixed capital investment and the manufacturing cost of 1,2-PDO.

Table 6.2. Fixed capital cost

Fixed capital	Unit	Cost per unit (Rs.)	Total cost (Rs.)
Cost of the reactor	1	50,00,000/-	50,00,000/-
Distillation column	3[a]	2,00,000/-	6,00,000/-
Hot air oven of 650 liter capacity	1	-	80,000/-
Muffle furnace	1	2,00,000/-	2,00,000/-
Tubular reactor with hot air oven for reduction	1	1,00,000/-	1,00,000/-
Hydrogen gas, 21000 liter	-	-	1,36,400/-
Land cost	285 m^2	Rs. 3500 /m^2 as per local cost	10,00,000/-
Distilled water plant	1	50,000/-	50,000/-
Total fixed cost			71,66,400/-

[a]Three units of distillation columns were required for the purification of 1,2-PDO in three stages as described by Gandarias et al., 2015. First to separate (glycerol+ ethylene glycol + 1,2-PDO) from water and lower alcohols. Second to separate (ethylene glycol + 1,2-PDO) from glycerol. Finally, 1,2-PDO from ethylene glycol.

6.2.1 Fixed capital investment

Table 6.2 summarizes fixed capital cost which included the cost of the reactor, cost of hot air oven for drying. Cost of 500 L autoclave reactor was provided by Amar Equipments Private Limited, Mumbai – 400070, Maharashtra, India. Cost of dry air oven was obtained from local supplier i.e. Bio Techno Lab. Mumbai – 400002, Maharashtra, India. Maximum 325 liters

(600 mm × 600 mm × 900 mm) capacity of hot air oven was available with the supplier. Therefore, it was assumed that 2 units of 325-liter capacity were equivalent to one large hot air oven. Cost of distilled water plant (capacity 50 $L.h^{-1}$) was collected from Total Industrial Solutions, Sonipat- 131001, Haryana, India. Cost of muffle furnace (metal loading capacity of 100 kg) was obtained from Sensoheat Engineering Equipments (I) Private Limited, Pune – 411019, Maharashtra, India. Cost of the tubular furnace (740 mm x 640 mm x 400 mm) was collected from Virtual Instrumentation & Software Applications Private Limited, Chennai – 600087, Tamil Nadu, India. Cost of H_2 cylinder was provided by Sigma gas service, India. Cost of distillation column was collected from Luthra Industrial Engineering Corporation, Sector 60, Mohali, India.

6.2.2 Production cost

It was considered that the production cost of 1,2-PDO was the summation of total raw material cost, total energy cost, product purification cost, cost of land, labor cost and maintenance cost.

- Raw material cost for the production of 1,2-PDO involved the cost of reactants [glycerol (99.9%, Thomas Baker, India), hydrogen (99.99%, Sigma gas), distilled water], the manufacturing cost of the required amount of catalyst per batch and cooling water. Total material cost per batch of reaction was calculated as Rs. 84,830.38/- (Table 6.3).
- Energy cost included the cost of power consumption for reaction and the separation cost of catalyst from the reaction mixture. Electricity cost was assumed to be as Rs. 3.85 per kWh (local rate) and the consumption of electricity for 12 h of reaction and for separation of catalyst and for distilled water were 96 kW, 5 kW, and 473 kW respectively. Details of raw material and energy cost were summarized in Table 6.3.
- Cost of purification of 1,2-PDO was calculated as Rs. 2438.4/- by considering 0.5 Euro per kg of 1,2-propanediol purification cost which includes utility cost, module cost and operating cost [Gandarias et al., 2015].
- Labour cost was calculated as Rs 500/- per day per person and three labours were considered for the operation of the process. In the cost estimation process, total 300 working days was considered in a year.
- Land requirement for this study was 285 m^2 and the cost of the land was considered as Rs. 3500 /m^2 as per local cost.

Table 6.3. Production cost of 1,2-PDO per batch (cost are in Indian rupee)

Cost of material required for the production of 60 kg 1,2-PDO				Cost of energy consumed per batch (II)			Cost of product separation (utility cost + operating cost + module cost) (Rs.) (III)	Cost of labor (Rs.) (IV)	Maintenance and other cost was assumed per batch of operation (Rs.) (V)
Material	Amount required	Rate of cost (Rs.)	Total cost (Rs.)	Cost of power consumption by reactor (Rs.)	Cost of power consumption by centrifuge for product separation (Rs.)	Cost of power consumption by distillation unit (Rs.)			
Glycerol (99.9%, Thomas Baker)	80 kg	464.12/- per kg	37,130.2/-	369.6/-	19.25/-	1821.2/-	2438.4/-	1500 /-	500/-
Hydrogen (99.99%, Sigma gas)	11998 litre	0.2/- per litre	2399.6/-						
Catalyst	6.4 kg	8081/- per kg	45,000.5/-						
Cooling water	30 litre	10/- per litre	300/-						
Total raw material cost (I)			84,830.38/-						
Total production cost (I) + (II) + (III) + (IV) + (V)			91,478.83/-						

Table 6.4. Economic benefits of the process

Year (j)	% of Full Capacity	Revenue (sj)	Operating Expenses (co,j)	Depreciation (dj)	Np,j (sj - co,j - dj)(1-φ)	Annual cash flow (sj - co,j - dj)(1-φ)+dj
1	1	3,60,00,000/-	2,70,54,000/-	7,16,640/-	57,37,802/-	64,77,192/-
2	1	3,60,00,000/-	2,70,54,000/-	6,44,976/-	57,90,241.8/-	64,55,692.8/-
3	1	3,60,00,000/-	2,70,54,000/-	5,80,478.4/-	58,37,437.62/-	64,36,343.52/-
4	1	3,60,00,000/-	2,70,54,000/-	5,22,430.56/-	58,79,913.85/-	64,18,929.17/-
5	1	3,60,00,000/-	2,70,54,000/-	4,70,187.50/-	59,18,142.47/-	64,03,256.25/-
6	1	3,60,00,000/-	2,70,54,000/-	4,23,168.75/-	59,52,548.22/-	63,89,150.62/-
7	1	3,60,00,000/-	2,70,54,000/-	3,80,851.87/-	59,83,513.40/-	63,76,455.56/-
8	1	3,60,00,000/-	2,70,54,000/-	3,42,766.69/-	60,11,382.06/-	63,65,030.00/-
9	1	3,60,00,000/-	2,70,54,000/-	3,08,490.02/-	60,36,463.85/-	63,54,747.00/-
10	1	3,60,00,000/-	2,70,54,000/-	2,77,641.02/-	60,59,037.47/-	63,45,492.30/-
Total (at the end of 10^{th} year)					5,92,06,482.77/-	6,40,22,289.25/-
Return on investment after taxes (%) = (total net profit/total year)/(fixed capital investment) [Peters et al., (2003)]				82.82%		
Payback period (years) = fixed capital investment/(total annual cash flow/ total year) [Peters et al., (2003)]				1.12		

6.3 Economic analysis

It can be seen from Table 6.3 that manufacturing cost of 60 kg 1,2-PDO was found to be Rs. 91,478.83/-. Therefore, production cost per kilograms of 1,2-PDO was estimated as Rs. 1502.4/-. Considering 300 working days in a year, 1,2-PDO production per year was considered to be 18,000 kg and its total manufacturing cost per year was calculated as Rs. 2,70,54,000/-. The market price of 1,2-PDO was found to be Rs. 4437.5/- per kg (Alfa aesar = 99.5% 1,2 PDO, Item no 030948) [Thermo Fisher Scientific]. In this study, selling cost per kilogram of 1,2-PDO was considered as Rs. 2,000/- and as a result revenue per year was estimated as Rs. 3,60,00,000/-. Fixed Capital Investment was calculated as Rs. 71,66,400/- (Table 6.2). Written down value depreciation method with 10% rate of depreciation for 10 years was considered for the economic analysis of the process [Depreciation rate chart under companies Act, 2013]. Annual income tax rate (φ) was considered as 30% of profit. [Income tax slabs in India for AY 2018-2019].

For the above process, return on investment after deduction of taxes was calculated as

Return on investment (ROI) = (total net profit/10)/ (fixed capital investment) [Peters et al., (2003)].

Payback period was calculated as = fixed capital investment/ (annual cash flow/10) [Peters et al., (2003)].

It can be seen from Table 6.4 that, ROI after taxes was calculated as 82.82% and the payback period was estimated as 1.12 years. The results showed that the 1,2-PDO production from glycerol hydrogenolysis reaction by using Cu:Zn(4:1)/MgO catalyst will be extremely cost-effective and profitable.

CHAPTER VII

CONCLUSIONS AND RECOMMENDATIONS

7.1 Conclusions

In this thesis work, liquid phase hydrogenolysis of glycerol was carried out over several highly active monometallic and bimetallic catalysts. Following conclusions can be made from this work:

1. Hydrogenolysis of glycerol was carried out in a slurry batch reactor in presence of Cu/γ-Al_2O_3, Ni/γ-Al_2O_3 and Cu:Ni(1:1)/γ-Al_2O_3 catalysts synthesized by wetness impregnation method. The bimetallic catalyst showed higher catalytic activity as compared to monometallic catalysts due to the formation of a new Cu-Ni mixed phase, the strong interaction between Cu and Ni metal.
2. Effects of reaction parameters study suggested that maximum 71.6% conversion with 85.6% selectivity towards 1,2-PDO and 8.9% selectivity to propanol were achieved at 210 °C temperature, and at 4.5 MPa pressure after 12 h of reaction. 20 wt.% aqueous glycerol solution as a feed and 10 wt.% catalyst loading with respect to glycerol was the optimum values for the maximum selectivity towards 1,2-PDO.
3. The reaction mechanism study suggested two steps hydrogenolysis process i.e. dehydration of glycerol to hydroxyacetone on the acidic centers of the catalyst followed by the hydrogenation of hydroxyacetone to 1,2-PDO on the metallic sides of the catalyst. It was also suggested that linear alcohols (1-propanol + 2-propanol) were obtained due to overhydrogenolysis of 1,2-PDO.
4. Layered double hydroxide (LDHs) derived Cu-Mg-Al-O based catalysts were synthesized by homogenous urea hydrolysis method and effects of urea concentrations on the catalytic performances were evaluated. Results demonstrated that the catalysts synthesized in presence of 2M urea showed the best catalytic activity due to the presence of optimum acidity, small copper crystallite size, and well developed curved lamellae structure.
5. Addition of Zn to Cu-Mg-Al-O catalyst increased the catalytic activity considerably. Whereas, ZnO helped to lower the reduction temperature of the catalyst by its hydrogen spillover effect.
6. The maximum glycerol conversion of 98.4% with 94.3% selectivity towards 1,2-PDO was achieved over Cu-Zn-Mg-Al-O-3 catalyst in the presence of 1g of NaOH at 210 ^oC,

at 4.5 MPa pressure and after 12 h of reaction when 20 wt.% glycerol was used as feed. Addition of base also reduced the formation of degradation products due to the cleavage of C-C bond of glycerol.

7. Catalyst reusability results revealed that conversion of glycerol was decreased by 30% due to structural changes of the catalyst after successive reuse and sintering of copper and ZnO species during the reaction. However, the selectivity towards 1,2-PDO increased from 94.3% to 96.3% at the expense of ethylene glycol (EG) after cycle -3.
8. A series of MgO supported Cu, Zn, Fe, Co-based mono-metallic and bi-metallic catalysts (Cu-Zn, Cu-Fe, Co-Zn, Co-Fe) were synthesized by precipitation-deposition method and the catalytic performances were evaluated in liquid phase. Bimetallic catalysts exhibited higher catalytic activity as compared to the monometallic catalysts. The effect was more pronounced for Cu based catalysts.
9. Among all the mono-metallic catalysts, Cu/MgO catalyst showed a 95.4% conversion with 94.2% selectivity towards 1,2-PDO at 210 ^{o}C and at 4.5 MPa pressure. After the addition of a small amount of zinc in the copper-magnesium system (Cu:Zn(4:1)/MgO), glycerol conversion (98.7%) and the selectivity (93.4%) to 1,2-PDO enhanced significantly. ZnO mainly enhanced the reducibility of CuO species due to the hydrogen spillover effect. NH_3 –TPD and CO_2 –TPD results revealed that copper introduced the acidic sites, whereas, Zn introduced the additional basicity in the catalyst.
10. Very high catalytic activity and 1,2-PDO selectivity over 50 wt.% Cu:Zn(4:1)/MgO catalyst was due to the presence of appropriate combinations of acidic (2.13 mmol NH_3. g^{-1}cat.) and/or basic (1.81 mmol CO_2.g^{-1}cat.) sites concentration on the catalyst, high hydrogen consumption (6.7 mmol.g^{-1}cat.), very high degree of reduction (91.7%), and presence of small average copper particle size (37.1 nm) in the reduced catalyst.
11. The product distribution obtained over 50 wt.% Cu:Zn(4:1)/MgO catalyst suggested two-step hydrogenolysis reaction process for the production of 1,2-PDO from glycerol i,e. dehydration of glycerol to hydroxyacetone followed by the hydrogenation of hydroxyacetone to 1,2-PDO. EG was produced due to the cleavage of C-C bond of glycerol.
12. Catalyst reusability study showed that glycerol conversion decreased by ~14% after cycle-3. However, the selectivity towards 1,2-PDO was almost constant (~94%). Deactivation of the catalyst was because of agglomeration of particles due to repetitive heat treatment of the catalyst before each cycle.

13. Effects of different supports (La_2O_3, CaO, BaO_2 and MgO-La_2O_3) on Cu-Zn bimetallic catalyst were evaluated. Cu:Zn(4:1)/MgO-La_2O_3 catalyst showed the highest activity. 100% conversion with 93.4% selectivity towards 1,2-PDO was achieved at 210 ^oC and at 4.5 MPa pressure.
14. Reusability study in presence of Cu:Zn(4:1)/MgO-La_2O_3 catalyst showed that glycerol conversion decreased by 14.4% after 4th cycle. The selectivity towards 1,2-PDO decreased from 93.4% to 63.2% with simultaneous increasing the selectivity to propanol from 2.2% to 29%. Deactivation of catalytic activity was because of decreasing the surface area and the agglomeration of Cu particle. XRD pattern of reused catalyst suggested that the degree of reduction of Cu was increased significantly after successive reuse. The presence of more reduced copper metal on the catalyst surface might propagate the over hydrogenolysis of 1,2-PDO to propanol. Therefore, although the addition of La_2O_3 in 50 wt.% Cu:Zn(4:1)/MgO catalyst enhanced the catalytic activity, however, it was not beneficial for the stability of the catalyst.
15. Kinetic study of hydrogenolysis of glycerol was carried out in presence of Cu:Ni(1:1)/γ-Al_2O_3 catalyst. Since 1,2-PDO and propanol were found to be as the primary reaction products, a series reaction for the conversion of glycerol to 1,2-PDO followed by the conversion of 1,2-PDO to propanol was taken into account to develop the kinetic model.
16. Various kinetic models including power-law, modified power-law and a heterogeneous kinetic model based on the assumptions of combined Langmuir-Hinshelwood-Hougen-Watson (LHHW) and Eley-Rideal (ER) approach were developed. Power law model suggested pseudo 1st order kinetics with respect to glycerol concentration with an activation energy of 67.7 kJ.mol^{-1} for one step hydrogenolysis process. Further, modified power-law model was developed by considering 1,2-PDO and propanol (1-PO + 2-PO) as primary reaction products. Results demonstrated that the experimental concentrations of 1,2-PDO and propanol were very well correlated with the model predicted concentrations. Finally, a more realistic heterogeneous kinetic model based on the assumptions of combined LHHW and ER approach was developed. The obtained activation energies explained very well the assumptions made to develop the heterogeneous model. The parity plot of the experimental and simulated concentration values of reactant and products revealed that heterogeneous kinetic model was aptly fitted with the experimental data.
17. Langmuir-Hinshelwood type kinetic model were developed for glycerol hydrogenolysis reaction over 50 wt.% Cu:Zn(4:1)/MgO and 50 wt.% Cu:Zn(4:1)/MgO-La_2O_3 catalysts.

The obtained activation energy and frequency factors over 50 wt.% Cu:Zn(4:1)/MgO catalyst were 42.62 kJ.mol^{-1} and 2.9×10^{4} mol.gcat^{-1}.h^{-1}, respectively. In presence of 50 wt.% Cu:Zn(4:1)/MgO-La_2O_3 catalyst, an activation energy of 69.6 kJ.mol^{-1} and a frequency factor of 4.2×10^{7} mol.gcat^{-1}.h^{-1} were obtained for the conversion of glycerol to 1,2-PDO.

18. The overall economic feasibility of liquid phase hydrogenolysis of glycerol to 1,2-PDO was carried out in presence of 50 wt.% Cu:Zn(4:1)/MgO catalyst, which showed best activity among all of the catalysts developed in this thesis. Results suggested that the production of 1,2-PDO from renewable glycerol is extremely profitable and it is highly promising for commercial application.

7.2 Recommendations

Based on the work presented in this thesis, the following recommendations are made for better understanding the insights of the catalyst structure, role of the catalyst, on catalytic activity 1,2-PDO selectivity and stability.

1. To determine better insites of the catalysts, Characterization of catalysts by using more advanced techniques such as X-ray absorption near edge structure (XANES), extended X-ray absorption fine structure (EXAFS), diffuse reflectance infrared fourier transform spectroscopy (DRIFTS), high resolution transmission electron microscopy (HRTEM), and nuclear magnetic resonance spectroscopy (NMR) may be useful. These techniques are quite helpful to identify the atomic structure, oxidation state, coordination of metal ions and microstructure of the catalyst. Pyridine-FTIR can be used to distinguish the lewis and bronsted acidic sites of the catalyst and their role on catalytic activity for the conversion of glycerol to 1,2-PDO.
2. To increase the stability of the catalyst, the inclusion of some noble metals (Pt, Pd), rare earth elements (Ce, Sc, Y) to Cu-Zn/MgO catalyst may be effective.
3. Use of various solvents such as formic acid, methanol, ethanol, propanol etc. as a hydrogen donor rather using gaseous hydrogen may be beneficial.
4. A more rigorous and robust kinetic model for glycerol hydrogenolysis process can be developed by LHHW and/or ER model by considering all the individual products detected.

5. Density functional theory (DFT) calculation may be employed to elucidate the reaction mechanism theoretically for glycerol hydrogenolysis process involving C-C, C-H and C-O bond cleavage of glycerol in presence of various catalysts.
6. DFT calculation may help to design a new and promising catalyst.

REFERENCES

- Akiyama, M.; Sato, S.; Takahashi, R.; Inui, K.; Yokota, M. Dehydration–hydrogenation of glycerol into 1,2-propanediol at ambient hydrogen pressure. *Appl. Catal. A.* **2009**, *371*(1-2), 60-66.
- Amada, Y.; Shinmi, Y.; Koso, S.; Kubota, T.; Nakagawa, Y.; Tomishige, K. Reaction mechanism of the glycerol hydrogenolysis to 1,3-propanediol over Ir–ReOx/SiO_2 catalyst. *Appl. Catal. B.* **2011**, *105*, 117–127.
- Ameen, A. A.; Mondal, S.; Pudi, S. M.; Pandhare, N. N.; Biswas, P. Liquid phase hydrogenolysis of glycerol over highly active 50%Cu–Zn(8:2)/MgO catalyst: Reaction Parameter Optimization by Using Response Surface Methodology. *Energy Fuels.* **2017**, *31*, 8521-8533.
- Anand, K. A.; Anisia, K. S.; Agarwal, A. K.; Kumar, A. Hydrogenolysis of glycerol with FeCo macrocyclic complex bonded to raney nickel support under mild reaction conditions. *Can. J. Chem. Eng*. **2010**, *88*, 208–216.
- Ansari, S. G.; Wahab, R.; Ansari, Z. A.; Kim, Y. S.; Khang, G.; Al-Hajry, A.; Shin, H. S. Effect of nanostructure on the urea sensing properties of sol-gel synthesized ZnO, *Sensor. Actuat. B: Chem.* **2009**, *137*, 566–573. doi: 10.1016/j.snb.2009.01.018.
- Balan, V. Current challenges in commercially producing biofuels from lignocellulosic biomass, *ISRN Biotechnol*. **2014**, *2014*, 463074
- Balaraju, M.; Rekha, V.; Prasad, P. S. S.; Prasad, R. B. N.; Lingaiah, N. Selective hydrogenolysis of glycerol to 1,2 Propanediol over Cu-ZnO catalysts. *Catal. Lett.* **2008**, *126*, 119-124. doi:10.1007/s10562-008-9590-6.
- Balaraju, M.; Rekha, V.; Prasad, P. S. S.; Devi, B. L. A. P.; Prasad, R. B. N.; Lingaiah, N. Influence of solid acids as co-catalysts on glycerol hydrogenolysis to propylene glycol over Ru/C catalysts. *Appl. Catal. A.* **2009**, *354*, 82–87.
- Balaraju, M.; Jagadeeswaraiah, K.; Prasad, P. S. S.; Lingaiah, N. Catalytic hydrogenolysis of biodiesel derived glycerol to 1,2-propanediol over Cu–MgO catalysts. *Catal. Sci. Technol.* **2012**, *2*, 1967-1976. doi:10.1039/c2cy20059g.
- Basahel, S. N.; Al-Thabaiti, S. A.; Narasimharao, K.; Ahmed, N. S.; Mokhtar, M. Nanostructured Mg–Al hydrotalcite as catalyst for fine chemical synthesis, *J. Nanosci. Nanotechnol.* **2014**, *14*, 1931–1946. doi:10.1166/jnn.2014.9193.

- Bej, B.; Bepari, S.; Pradhan, N. C.; Neogi, S. Production of hydrogen by dry reforming of ethanol over alumina supported nano-NiO/SiO_2 catalyst. *Catal. Today*. **2017,** *291*, 58-66. DOI: 10.1016/j.cattod.2016.12.010.
- Bepari, S.; Pradhan, N. C.; Dalai, A. K. Selective production of hydrogen by steam reforming of glycerol over Ni/Fly ash catalyst. *Catal. Today*. **2017**a, *291*, 36-46.
- Bepari, S.; Basu, S.; Pradhan, N. C.; Dalai, A. K. Steam reforming of ethanol over cerium-promoted Ni-Mg-Al hydrotalcite catalysts. *Catal. Today*. **2017**b, 291, 47-57. DOI: 10.1016/j.cattod.2017.01.027.
- Biswas, P.; Kunzru, D. Steam reforming of ethanol for production of hydrogen over Ni/CeO_2–ZrO_2 catalyst: effect of support and metal loading. *Int. J. Hydrogen Energ*. **2007**, *32*(8), 969-80.
- Chaminand, J.; Djakovitch, L.; Gallezot, P.; Marion, P.; Pinel, C.; Rosier, C. Glycerol hydrogenolysis on heterogeneous catalysts. *Green. Chem*. **2004**, *6*(8), 359-361.
- Checa, M.; Auneau, F.; Hidalgo-Carrillo, J.; Marinas, A.; Marinas, J. M.; Pinel, C.; Urbano, F. J. Catalytic transformation of glycerol on several metal systems supported on ZnO. *Catal. Today*. **2012**, *196*(1), 91-100.
- Choudhary, V. R.; Sane, M. K.; Tambe, S. S. Kinetics of hydrogenation of o-nitrophenol to o-aminophenol on Pd/Carbon catalysts in a stirred three-phase slurry reactor. *Ind. Eng. Chem. Res.* **1998**, *37*, 3879–3887.
- Costantino, U.; Costantino, F.; Elisei, F.; Latterini, L.; Nocchetti, M. Coupling physical chemical techniques with hydrotalcite-like compounds to exploit their structural features and new multifunctional hybrids with luminescent properties, *Phys. Chem. Chem. Phys*. **2013**, *15*, 13254-13269. doi:10.1039/c3cp51581h.
- Da Silva, G. P.; Mack M.; Contiero, J. Glycerol: A promising and abundant carbon source for industrial microbiology. *J. Biotechnol. Adv*. **2009**, *27*, 30–39.
- Daniel, O. M.; DeLaRiva, A.; Kunkes, E. L.; Datye, A. K.; Dumesic, J. A.; Davis, R. J. X-ray absorption spectroscopy of bimetallic Pt–Re catalysts for hydrogenolysis of glycerol to propanediols. *ChemCatChem*. **2010**, *2*(9), 1107-1114.
- Dasari, M. A.; Kiatsimkul, P. P.; Sutterlin, W. R.; Suppes, G. J. Low pressure hydrogenolysis of glycerol to propylene glycol. *Appl. Catal. A.* **2005**, *281*, 225-231. doi:10.1016/j.apcata.2004.11.033.
- Dedecek, J.; Sobalik, Z.; Tvaruzkova, Z.; Kaucky, D.; Wichterlova, B.; Coordination of Cu ions in high-silica zeolite matrices - Cu^+ photoluminescence, Ir of NO adsorbed on

Cu^{2+}, and Cu^{2+} ESR Study, *J. Phy. Chem.* **1995**, *99*, 16327–16337. doi:10.1021/j100044a020.

- Delgado, S. N.; Yap, D.; Vivier, L.; Especel, C. Influence of the nature of the support on the catalytic properties of Pt-based catalysts for hydrogenolysis of glycerol. *J. Mol. Catal. A.* **2013**, *367*, 89-98.
- Deng, C.; Duan, X.; Zhou, J.; Chen, D.; Zhou, X.; Yuan, W. Size effects of Pt-Re bimetallic catalysts for glycerol hydrogenolysis. *Catal. Today*. **2014**, *234*, 208-214.
- Deng, C.; Leng, L.; Duan, X.; Zhou, J.; Zhou, X.; Yuan, W. Support effect on the bimetallic structure of Ir–Re catalysts and their performances in glycerol hydrogenolysis. *J. Mol. Catal. A.* **2015**, *410*, 81-88.
- Depreciation rate chart under companies Act, 2013, https://taxguru.in/company-law/rates-depriciation-companies-act-2013.html.
- Dhanala, V.; Maity, S. K.; Shee, D. Oxidative steam reforming of isobutanol over Ni/γ-Al_2O_3 catalysts: A comparison with thermodynamic equilibrium analysis. *J. Ind. Eng. Chem.* **2015**, *27*, 153-63.
- Dieuzeide, M. L.; De Urtiaga, R.; Jobbagy, M.; Amadeo, N. Vapor phase hydrogenolysis of glycerol to 1,2-propanediol at atmospheric pressure over copper catalysts supported on mesoporous alumina. *Catal. Today*. **2017**, *296*, 19-25.
- Du, Y.; Wang, C.; Jiang, H.; Chen, C.; Chen, R. Insights into deactivation mechanism of Cu–ZnO catalyst in hydrogenolysis of glycerol to 1,2-propanediol, *J. Ind. Eng. Chem.* **2016**, *35*, 262–267.
- Durán-Martín, D.; Ojeda, M.; Granados, M. L.; Fierro, J. L. G.; Mariscal, R. Stability and regeneration of Cu–ZrO_2 catalysts used in glycerol hydrogenolysis to 1,2-propanediol. *Catal. Today*. **2013**, *210*, 98-105.
- Duran-Martin, D.; Granados, M. L.; Fierro, J. L. G.; Pinel, C.; Mariscal, R. Deactivation of CuZn catalysts used in glycerol hydrogenolysis to obtain 1,2-propanediol. *Top. Catal*. **2017**, *60*(15-16), 1062-1071.
- Feng, Y.; Yin, H.; Shen, L.; Wang, A.; Shen, Y.; Jiang, T. Gas-phase hydrogenolysis of glycerol catalyzed by Cu/MOx catalysts, *Chem. Eng. Technol.* **2013**, *36*(1), 73-82.
- Feng, J.; Fu, H.; Wang, J.; Li, R.; Chen, H.; Li, X. Hydrogenolysis of glycerol to glycols over ruthenium catalysts: Effect of support and catalyst reduction temperature. *Catal. Commun.* **2008**, *9*, 1458-1464. doi:10.1016/j.catcom.2007.12.011.

- Feng, Y. S.; Liu, C.; Kang, Y. M.; Zhou, X. M.; Liu, L. L.; Deng, J.; Xu, H. J.; Fu, Y. Selective hydrogenolysis of glycerol to 1,2-propanediol catalyzed by supported bimetallic PdCu-KF/γ-Al_2O_3. *Chem. Eng. J.* **2015**, *281*, 96-101.
- Fernandez, Y.; Menendez, J. A.; Arenillas, A.; Fuente, E.; Peng, J. H.; Zhang, Z. B.; Li, W.; Zhang, Z. Y.; Microwave-assisted synthesis of CuO/ZnO and CuO/ZnO/Al_2O_3 precursors using urea hydrolysis, *Solid State Ionics.* **2009**, *180*, 1372–1378. doi:10.1016/j.ssi. 2009.08.014.
- Gandarias, I.; Arias, P. L.; Requies, J.; Güemez, M. B.; Fierro, J. L. G. Hydrogenolysis of glycerol to propanediols over a Pt/ASA catalyst: The role of acid and metal sites on product selectivity and the reaction mechanism. *Appl. Catal. B.* **2010**, *97*, 248–256.
- Gandarias, I.; Fernandez, S. G.; El Doukkali, M.; Requies, J.; Arias, P. L. Physico-chemical study of glycerol hydrogenolysis over a Ni–Cu/Al_2O_3 catalyst using formic acid as the hydrogen source. *Top. Catal*. **2013,** *56*(11), 995-1007.
- Garcia-Fernandez, S.; Gandarias, I.; Requies, J.; Soulimani, F.; Arias, P. L.; Weckhuysen, B. M. The role of tungsten oxide in the selective hydrogenolysis of glycerol to 1,3-propanediol over Pt/WOx/Al_2O_3. *Appl. Catal. B.* **2017**, *204*, 260-272.
- Guo, L.; Zhou, J.; Mao, J.; Guo, X.; Shuguang, Z. Supported Cu catalysts for the selective hydrogenolysis of glycerol to propanediols. *Appl. Catal. A.* **2009**, *367*, 93-98. doi:10.1016/j.apcata.2009.07.040.
- Guo, X.; Li, Y.; Song, W. Glycerol hydrogenolysis over Co catalysts derived from a layered double hydroxide precursor, *Catal. Lett*. **2011**, *141*, 1458–1463.
- Gupta, M.; Schwartz, V.; Overbury, S. H.; More, K.; Meyer III, H. M.; Spivey, J. J. Novel Pulse Electrodeposited Co–Cu–ZnO Nanowire/tube Catalysts for C1–C4 Alcohols and C2–C6 (Except C5) Hydrocarbons from CO and H_2. *J. Phys. Chem. C.* **2012**, *116*, 10924−10933. http://dx.doi.org/10.1021/jp301965s.
- Gupta, M.; He, J.; Nguyen, T.; Petzold, F.; Fonseca, D.; Jasinski, J. B.; Sunkara. M. K.; Nanowire catalysts for ultra-deep hydro-desulfurization and aromatic hydrogenation. *Appl. Catal. B.* **2016**, *180*, 246–254.
- Gupta, M.; Spivey, J. J. Electrodeposited Cu-ZnO and Mn-Cu-ZnO nanowire/tube catalysts for higher alcohols from syngas. *Catal. Today*. **2009**, *147*(2), 126-132.
- Hamzah, N.; Nordin, N. M.; Nadzri, A. H. A.; Nik, Y. A.; Kassim, M. B.; Yarmo, M. A. Enhanced activity of Ru/TiO_2 catalyst using bisupport, bentonite-TiO_2 for hydrogenolysis of glycerol in aqueous media, *Appl. Catal. A.* **2012**, *419-420*, 133-141.

- Hao, M.; Yang, B.; Wang, H.; Liu, G.; Qi, S.; Yang, J.; Li, C.; Lv, J. Hydrogenolysis of glycerol to 1,2-propanediol catalyzed by Cu-$H_4SiW_{12}O_{40}/Al_2O_3$ in liquid phase. *J. Phys. Chem. A.* **2010**, *114*, 3811–3817.
- Huang, L.; Zhu, Y.; Zheng, H.; Li, Y.; Zeng, Z. Continuous production of 1,2-propanediol by the selective hydrogenolysis of solvent-free glycerol under mild conditions, *J. Chem. Technol. Biotechnol.* **2008**, *83*(12),1670–1675.
- Huang, Z.; Cui, F.; Xue, J.; Zuo, J.; Chen, J.; Xia, C. Cu/SiO_2 catalysts prepared by hom- and heterogeneous deposition–precipitation methods: Texture, structure, and catalytic performance in the hydrogenolysis of glycerol to 1,2-propanediol. *Catal. Today*. **2012**, *183*, 42–51. doi:10.1016/j.cattod.2011.08.038.
- Iglesia, E.; Barton, D. G.; Biscardi, J. A.; Gines, M. J.; Soled, S. L. Bifunctional pathways in catalysis by solid acids and bases. *Catal. Today*. **1997**, *38*, 339-360.
- Income Tax Slabs in India for AY 2018-2019. https://business.mapsofindia.com.
- James, O.O.; Chowdhury, B.; Maity, S. TPR and TPD studies of effects of Cu and Ca promotion on Fe–Zn-based Fischer–Tropsch catalysts. *J. Chem. Sci.* **2013**, *125*(3), 679-686.
- Jimenez-Morales, I.; Vila, F.; Mariscal, R.; Jimenez-Lopez, A. Hydrogenolysis of glycerol to obtain 1,2-propanediol on Ce-promoted Ni/SBA-15 catalysts. *Appl. Catal. B.* **2012**, *117-118*, 253-259.
- Jiang, Z.; Hao, Z.; Yu, J.; Hou, H.; Hu, C.; Su, J. Catalytic combustion of methane on novel catalysts derived from Cu-Mg/Al-hydrotalcites. *Catal. Lett.* **2005**, *99*,157-163.
- Jingfa, D.; Qi, S.; Yulong, Z.; Songying, C.; Dong, W. A novel process for preparation of a $Cu/ZnO/Al_2O_3$ ultrafine catalyst for methanol synthesis from CO_2 + H_2: comparison of various preparation methods. *Appl. Catal. A.* **1996**, *139*, 75–85. doi:http://dx.doi.org/10.1016/0926-860X(95)00324-X.
- Kant, A.; He, Y.; Jawad, A.; Li, X.; Rezaei, F.; Smith, J. D.; Rownaghi, A. A. Hydrogenolysis of glycerol over Ni, Cu, Zn, and Zr supported on H-beta. *Chem. Eng. J.* **2017**, *317*, 1-8.
- Karinen, R. S.; Krause, A. O. I. New biocomponents from glycerol. *Appl. Catal. A.* **2006,** *306*, 128-133.
- Kim, J. Y.; Rodriguez, J. A.; Hanson, J. C.; Frenkel, A. I.; Lee, P. L. Reduction of CuO and Cu_2O with H_2: H embedding and kinetic effects in the formation of suboxides. *J. Am. Chem. Soc.* **2003**, *125*, 10684-10692.

- Khandan, N.; Kazemeini, M.; Aghaziarati, M. Determining an optimum catalyst for liquid-phase dehydration of methanol to dimethyl ether. *Appl. Catal. A.* **2008**, *349*, 6-12.
- Kolena, J.; Skuhrovcova, L.; Kocik, J.; Safar, J.; Kupcik, J. Catalyst for selective hydrogenolysis of glycerol, prepared from hydrotalcite-like structures. *Top. Catal.* **2018,** *61*(15-17).
- Kumar, V. A.; Pant, K. K.; Kunzru, D. Potassium-containing calcium aluminate catalysts for pyrolysis of n-heptane. *Appl. Catal. A.* **199**7, *162*(1), 193-200.
- Kusunoki, Y.; Miyazawa, T.; Kunimori, K.; Tomishige, K. Highly active metal – acid bifunctional catalyst system for hydrogenolysis of glycerol under mild reaction conditions, *Catal. Commun.* **2005**, *6*, 645–649.
- Kwak, B. K.; Park, D. S.; Yun, Y. S.; Yi, J. Preparation and characterization of nanocrystalline $CuAl_2O_4$ spinel catalysts by sol–gel method for the hydrogenolysis of glycerol. *Catal. Commun*. **2012**, *24*, 90-95.
- Lahr, D. G.; Shanks, B. H. Kinetic analysis of the hydrogenolysis of lower polyhydric alcohols: Glycerol to glycols. *Ind. Eng. Chem. Res.* **2003**, *42*, 5467–5472.
- Lee, S.; Schneider, K.; Schumann, J.; Mogalicherla, A. K.; Pfeifer, P.; Dittmeyer, R. Effect of metal precursor on $Cu/ZnO/Al_2O_3$ synthesized by flame spray pyrolysis for direct DME production. *Chem. Eng. Sci*. **2015**, *138*, 194-202. http://dx.doi.org/10.1016/j.ces.2015.08.021.
- Li, X.; Zhang, C.; Cheng, H.; He, L.; Lin, W.; Yu, Y.; Zhao, F. Effect of Zn doping on the hydrogenolysis of glycerol over ZnNiAl catalyst. *J. Mol. Catal. A. Chem.* **2014**, *395*, 1-6.
- Li, X.; Xiang, M.; Wu, D. Hydrogenolysis of glycerol over bimetallic CuNi catalysts supported on hierarchically porous SAPO-11 zeolite. *Catal. Commun.* **2019**, *119*, 170-175.
- Lin, J. H.; Biswas, P.; Guliants, V. V.; Misture, S. Hydrogen production by water–gas shift reaction over bimetallic Cu–Ni catalysts supported on La-doped mesoporous ceria. *Appl. Catal. A.* **2010**, *387*(1-2), 87-94.
- Lin, J. H.; Guliants, V. V. Alumina-supported Cu@Ni and Ni@Cu core–shell nanoparticles: Synthesis, characterization, and catalytic activity in water–gas-shift reaction. *Appl. Catal. A.* **2012**, *445*, 187-194.

- Liu, Y.; Pasupulety, N.; Gunda, K.; Rempel, G. L.; Ng, F. T .T. Glycerol hydrogenolysis to 1,2-propanediol by Cu/ZnO/Al catalysts. *Top. Catal*. **2014**, *57*, 1454–1462. doi:10.1007/s11244-014-0318-0.
- Liu, C.; Zhang, C.; Hao, S.; Sun, S.; Liu, K.; Xu, J.; Zhu, Y.; Li, Y. WO_x modified Cu/Al_2O_3 as a high-performance catalyst for the hydrogenolysis of glucose to 1,2-propanediol. *Catal. Today*. **2016**, *261*, 116-127.
- Maedar, M.; Neuhold, Y. M.; Puxty, G. Application of a genetic algorithm: near optimal estimation of the rate and equilibrium constants of complex reaction mechanisms. *Chemom. Intell. Lab. Syst*. **2004**, *70*(2), 193-203.
- Mallesham, B.; Sudarsanam, P.; Reddy, B. V. S.; Reddy, B. M. Development of cerium promoted copper–magnesium catalysts for biomass valorization: selective hydrogenolysis of bioglycerol. *Appl. Catal. B*. **2016**, *181*, 47-57.
- Ma, L.; He, D. Hydrogenolysis of glycerol to propanediols over highly active Ru–Re bimetallic catalysts. *Top. Catal*. **2009**, *52*, 834–844. DOI 10.1007/s11244-009-9231-3
- Mai, C. T. Q. Catalytic Hydrogenolysis of glycerol to 1-propanol using bifunctional catalysts in an aqueous media, University of Waterloo, **2016**. *http://hdl.handle.net/10012/11032*.
- Maity S. K. Opportunities, recent trends and challenges of integrated biorefinery: Part I. *Renew. Sust. Energ. Rev.* **2015**a, *43*, 1427–1445.
- Maity S. K. Opportunities, recent trends and challenges of integrated biorefinery: Part II. *Renew. Sust. Energ. Rev.* **2015**b, *43*, 1446–1466.
- Mane, R. B.; Hengne, A. M.; Ghalwadkar, A. A.; Vijayanand, S.; Mohite, P. H.; Potdar, H. S.; Rode, C. V. Cu: Al nano catalyst for selective hydrogenolysis of glycerol to 1,2-propanediol. *Catal. Lett*. **2010**, *135*(1-2), 141-147. https://doi.org/10.1007/s10562-010-0276-5.
- Mane R. B.; Rode, C. V. Simultaneous glycerol dehydration and in situ hydrogenolysis over Cu–Al oxide under an inert atmosphere. *Green. Chem*. **2012**a, *14*(10), 2780-2789.
- Mane R. B.; Rode, C. V. Continuous dehydration and hydrogenolysis of glycerol over nonchromium copper catalyst: laboratory-scale process studies. *Org. Process Res. Dev*. **2012**b, *16*(5), 1043-1052.
- Maris, E.; Davis, R. J. Hydrogenolysis of glycerol over carbon-supported Ru and Pt catalysts. *J. Catal.* **2007**a, *249*, 328–337.

- Maris, E.; Ketchie, W. C.; Murayama, M.; Davis, R. J. Glycerol hydrogenolysis on carbon-supported PtRu and AuRu bimetallic catalysts. *J. Catal.* **2007**b, *251*, 281-294.
- McCall. J. Genetic algorithms for modelling and optimization. *J. Comput. Appl. Math.* **2005**, *184*(1), 205-222.
- Meher, L. C.; Gopinath, R.; Naik, S.N.; Dalai, A.K. Catalytic hydrogenolysis of glycerol to propylene glycol over mixed oxides derived from a hydrotalcite-type precursor. *Ind. Eng. Chem. Res.* **2009**, *48*, 1840-1846. doi:10.1021/ie8011424.
- Menchavez, R. N.; Morra, M. J.; He, B. B. Glycerol hydrogenolysis using a Ni/Ce-Mg catalyst for improved ethanol and 1,2-propanediol selectivities. *Can. J. Chem. Eng.* **2017**, *95*, 1332-1339.
- Mirzaei, F.; Rezaei, M.; Meshkani, F.; Fattah, Z. Carbon dioxide reforming of methane for syngas production over Co–MgO mixed oxide nanocatalysts, *J. Ind. Eng. Chem.* **2015**, *21*, 662–667.
- Mitta, H.; Vanama P. V.; Samudrala S. P.; Komandur V. R. C. Vapour phase hydrogenolysis of glycerol to propanediols over Cu/SBA-15 catalysts. *J. Chem. Technol. Biotechnol*. **2015**, *90*(10), 1906-1917.
- Mitta, H.; Seelam, P. K.; Ojala, S.; Keiski, R. L.; Balla, P. Tuning Y-zeolite based catalyst with copper for enhanced activity and selectivity in vapor phase hydrogenolysis of glycerol to 1, 2-propanediol. *Appl. Catal. A.* **2018**, *550*, 308-319.
- Miyazawa, T.; Kusunoki, Y.; Kunimori, K.; Tomishige, K. Glycerol conversion in the aqueous solution under hydrogen over Ru/C plus an ion-exchange resin and its reaction mechanism. *J. Catal.* **2006**, *240*, 213–221. doi:10.1016/j.jcat.2006.03.023.
- Miyazawa, T.; Koso, S.; Kunimori, K.; Tomishige, K. Glycerol hydrogenolysis to 1,2-propanediol catalyzed by a heat-resistant ion-exchange resin combined with Ru/C, *Appl. Catal. A.* **2007**, *329*, 30–35. doi:10.1016/j.apcata.2007.06.019.
- Montassier, C.; Dumas, J.M.; Granger, P.; Barbier, J. Deactivation of supported copper based catalysts during polyol conversion in aqueous phase. *Appl. Catal. A.* **1995**, *121*, 231-244.
- Mogalicherla, A. K.; Kunzru, D. Effect of method of preparation on activity of Pd/Al_2O_3 monolith catalysts. *Can. J. Chem. Eng.* **2010**, *88*(3), 367-375.
- Mogalicherla, A. K.; Kunzru, D. The Effect of prewetting on the loading of γ-alumina washcoated cordierite monolith. *Int. J. Appl. Ceram. Tec.* **2011**, *8*(2), 430-436.

- Mohanty, S.; Kunzru, D.; Saraf, D. N. Hydrocracking: a review. *Fuel*. **1990**, *69*(12), 1467-73.
- Moura, J. S.; Fonseca, J. D. S. L.; Bion, N.; Epron, F.; de Freitas Silva, T., Maciel, C. G., Assaf, J. M. and do Carmo Rangel, M. Effect of lanthanum on the properties of copper, cerium and zirconium catalysts for preferential oxidation of carbon monoxide. *Catal. Today*. **2014**, *228*, 40-50.
- Nagaraja, B. M.; Padmasri, A. H.; David Raju, B.; Rama Rao, K. S. Vapor phase selective hydrogenation of furfural to furfuryl alcohol over Cu–MgO coprecipitated catalysts. *J. Mol. Catal. A. Chem.* **2007**, *265*, 90–97. doi:10.1016/j.molcata.2006.09.037.
- Naik, S. N.; Goud, V. V.; Rout, P. K.; Dalai, A. K. Production of first and second generation biofuels: a comprehensive review. *Renew. Sust. Energ. Rev*. **2010**, *14*(2), 578-597.
- Nakagawa, Y.; Tomishige, K. Heterogeneous catalysis of the glycerol hydrogenolysis. *Catal. Sci. Technol.* **2011**, *1*, 179-190. doi:10.1039/c0cy00054j.
- Nakagawa Y.; Tamura, M; Tomishige, K. Catalytic materials for the hydrogenolysis of glycerol to 1,3-propanediol. *J. Mater. Chem. A*. **2014**, *2*, 6688-6702.
- National policy on biofuels **2018**, Ministry of Petroleum and Natural gas, Government of India, http://petroleum.nic.in/sites/default/files/biofuelpolicy2018_1.pdf.
- Nimlos, M. R.; Blanksby, S. J.; Qian, X.; Himmel, M. E.; Johnson, D. K. Mechanism of glycerol dehydration. *J. Phys. Chem. A.* **2006**, *110*, 6145-6156.
- Niu, L.; Wei, R.; Yang, H.; Li, X.; Jiang, F.; Xiao, G. Hydrogenolysis of glycerol to propanediols over Cu-MgO/USY catalyst, *Chin. J. Catal*. **2013**, *34*, 2230-2235.
- Ogawa, M.; Kaiho, H. Homogeneous precipitation of uniform hydrotalcite particles, *Langmuir*. **2002**, *18*, 4240–4242. doi:10.1021/la0117045.
- Pagliaro, M.; Ciriminna, R.; Kimura, H.; Rossi, M.; Della Pina, C. From glycerol to value-added products. *Angew. Chem. Int. Ed*. **2007**, *46*(24), 4434-4440.
- Pal, D.; Mitra S. K. Asymmetric oil product pricing in India: Evidence from a multiple threshold nonlinear ARDL model. *Economic Modelling*. **2016**, 59, 314-328.
- Pandhare, N. N.; Pudi, S. M.; Biswas, P.; Sinha S. Selective hydrogenolysis of glycerol to 1,2-propanediol over highly active and stable Cu/MgO catalyst in the vapor phase, *Org. Process. Res. Dev.* **2016**, *20*, 1059-1067.

- Pandhare, N. N.; Pudi, S. M.; Mondal, S.; Pareta, K.; Kumar M.; Biswas, P. Development of kinetic model for hydrogenolysis of glycerol over Cu/MgO catalyst in a slurry reactor. *Ind. Eng. Chem. Res.* **2018**, *57*(1), 101-110. DOI: 10.1021/acs.iecr.7b03684.
- Pankajakshan, A.; Pudi, S. M.; Biswas, P. Acetylation of glycerol over highly stable and active sulfated alumina catalyst: reaction mechanism, kinetic modeling and estimation of kinetic parameters. *Inc. Int. J. Chem. Kinet.* **2018**, *50*, 98–111.
- Pathak, K.; Reddy, K. M.; Bakhshi, N. N.; Dalai, A. K. Catalytic conversion of glycerol to value added liquid products. *Appl. Catal. A.* **2010**, *372*(2), 224-238. https://doi.org/10.1016/j.apcata.2009.10.036.
- Peters M. S.; Timmerhaus K. D.; West R. E. *Plant design and economics for chemical engineers*. Fifth edition. McGraw-Hill, New York. **2003**.
- Phoohinkong, W.; Foophow, T.; Pecharapa, W. Synthesis and characterization of copper zinc oxide nanoparticles obtained via metathesis process, *Adv. Nat. Sci: Nanosci Nanotechnol.* **2017**, *8*(3), 035003-035011.
- Pudi, S. M.; Biswas, P.; Kumar, S. Selective hydrogenolysis of glycerol to 1,2-propanediol over highly active copper-magnesia catalysts: Reaction parameter, catalyst stability and mechanism study, *J. Chem. Technol. Biotechnol*. **2015**a, *91*, 2063-2075. doi:10.1002/jctb.4802.
- Pudi, S. M.; Biswas, P.; Kumar, S.; Sarkar, B. Selective hydrogenolysis of glycerol to 1,2-propanediol over bimetallic Cu-Ni catalysts supported on γ-Al_2O_3, *J. Braz. Chem. Soc.* **2015**b, *26*, 1551-1564.
- Pudi, S. M.; Mondal, T.; Biswas, P.; Biswas, S.; Sinha, S. Conversion of glycerol into value-added products over Cu-Ni catalyst supported on γ-Al_2O_3 and activated carbon, *Int. J. Chem. React. Eng.* **2014**, *12*(1), 151–162. doi:10.1515/ijcre-2013-0102.
- Rajkhowa, T.; Marin, G. B.; Thybaut, J. W. A comprehensive kinetic model for Cu catalyzed liquid phase glycerol hydrogenolysis. *Appl. Catal. B.* **2017**, *205*, 469–480.
- Rao, T. V. M.; Deo, G. Kinetic parameter analysis for propane ODH: V_2O_5/Al_2O_3 and MoO_3/Al_2O_3 catalysts. *AIChE J*. **2007**, *53*(6), 1538-1549.
- Rao, T. V. M.; Vico-Ruiz, E.; Banares, M. A.; Deo, G. Obtaining the best composition of supported V_2O_5–MoO_3/TiO_2 catalyst for propane ODH reaction. *J. Catal*. **2008**, *258*(2), 324-333.

- Rao, T. M.; Yang, Y.; Sayari, A. Ethane dehydrogenation over pore-expanded mesoporous silica supported chromium oxide: 1. Catalysts preparation and characterization. *J. Mol. Catal. A.* **2009**, *301*(1-2), 152-158.
- Rekha, V.; Sumana, C.; Douglas, S. P.; Lingaiah, N. Understanding the role of Co in Co–ZnO mixed oxide catalysts for the selective hydrogenolysis of glycerol, *Appl. Catal. A.* **2015**, *491*, 155–162.
- Rekha, V.; Raju, N.; Sumana, C.; Douglas, S. P.; Lingaiah, N. Selective Hydrogenolysis of Glycerol Over Cu–ZrO_2–MgO Catalysts. *Catal. Lett.* **2016**, *146*(8), 1487-1496.
- REN21-Renewable Energy Policy Network for the 21st century, http://www.ren21.net/REN21Activities/GlobalStatusReport.aspx.
- Rode, C. V.; Ghalwadkar, A. A.; Mane, R. B.; Hengne, A. M.; Jadkar, S. T.; Biradar, N. S. Selective hydrogenolysis of glycerol to 1,2-propanediol: Comparison of batch and continuous process operations. *Org. Process Res. Dev.* **2010**, *17*, 1385-1392.
- Rodrigues, R.; Isoda, N.; Gonçalves, M.; Figueiredo, F. C. A.; Mandelli, D.; Carvalho, W. A. Effect of niobia and alumina as support for Pt catalysts in the hydrogenolysis of glycerol. *Chem. Eng. J.* **2012,** *198*, 457-467.
- Rogatis, L. D.; Montini, T.; Lorenzut, B.; Fornasiero, P. Ni_xCu_y/Al_2O_3 based catalysts for hydrogen production. *Energ. Environ. Sci*. **2008**, *1*, 501-509.
- Sato, S.; Akiyama, M.; Takahashi, R.; Hara, T.; Inui, K.; Yokota, M. Vapor-phase reaction of polyols over copper catalysts. *Appl. Catal. A. Gen.* **2008**, *347*, 186-191.
- Sato, S.; Akiyama, M.; Inui, K.; Yokota, M. Selective conversion of glycerol into 1, 2-propanediol at ambient hydrogen pressure. *Chem. Lett.* **2009**, *38*(6), 560-561.
- Schlaf, M. Selective deoxygenation of sugar polyols to a, ω-diols and other oxygen content reduced materials-a new challenge to homogeneous ionic hydrogenation and hydrogenolysis catalysis. *Dalton Transactions*. **2006**, *0*, 4646-4653.
- Sepulveda, J.; Manuale, D.; Santiago, L.; Carrara, N.; Torres, G.; Vera, C.; Goncalves, M.; Carvalho, W.; and Mandelli, D. Selective hydrogenolysis of glycerol to propylene glycol in a continuous flow trickle bed reactor using copper chromite and Cu/Al_2O_3 catalysts. *Quim. Nova.*, **2017**, *40*(4), 371-377. http://dx.doi.org/10.21577/0100-4042.20170018.
- Sharma, R. V.; Kumar, P.; Dalai, A. K. Selective hydrogenolysis of glycerol to propylene glycol by using Cu:Zn:Cr:Zr mixed metal oxides catalyst. *Appl. Catal. A.* **2014**, *477*, 147–156. doi:10.1016/j.apcata.2014.03.007.

- Shiju, N. R.; Guliants, V. V. Recent developments in catalysis using nanostructured materials. Appl. Catal. A. **2009**, *356*, 1-17.
- Smith, J. M. Chemical engineering kinetics. McGraw-Hill, New York, **1970**.
- Special chem. industrial news, retrieved from http://adhesives.specialchem.com/ news/ industry news/global-market-for-glycerin/ on June 19, **2014**.
- Sun, J.; Zhu, K.; Gao, F.; Wang, C.; Liu, J.; Peden, C. H. F.; Wang, Y. Direct conversion of bio-ethanol to isobutene on nanosized $Zn_xZr_yO_z$ mixed oxides with balanced acid–base sites, *J. Am. Chem. Soc.* **2011**, *33*, 11096–11099.
- Surendar, M.; Padmakar, D.; Lingaiah, N.; Rao, K. R.; Prasad, P. S. Influence of La_2O_3 composition in MgO–La_2O_3 mixed oxide-supported Co catalysts on the hydrogen yield in glycerol steam reforming. *Sustain. Energ. Fuels*. **2017**, *1*(2), 354-361.
- ThermoFisher Scientific, https://portal.thermofisher.co.in/WOP/IndiaStockCheck.aspx.
- Torres, A.; Roy, D.; Subramaniam, B.; Chaudhari, R. V. Kinetic modeling of aqueous-phase glycerol hydrogenolysis in a batch slurry reactor. *Ind. Eng. Chem. Res.* **2010**, *49*, 10826–10835.
- Tsoncheva, T.; Dal Santo, V.; Gallo, A.; Scotti, N.; Dimitrov, M.; Kovacheva, D. Structure and catalytic activity of hosted in mesoporous silicas copper species: effect of preparation procedure and support pore topology. *Appl. Catal. A*. **2011**, *406*(1-2), 13-21.
- Turco, M.; Bagnasco, G.; Costantino, U.; Marmottini, F.; Montanari, T.; Ramis, G.; Busca, G. Production of hydrogen from oxidative steam reforming of methanol. I. Preparation and characterization of Cu/ZnO/Al_2O_3 catalysts from a hydrotalcite-like LDH precursor. *J. Catal.* **2004**, *228*, 43–55. doi:10.1016/j.jcat.2004.08.026.
- Vanama, P. K.; Kumar, A; Ginjupalli, S. R; Komandur, V. R. C. Vapor-phase hydrogenolysis of glycerol over nanostructured Ru/MCM-41 catalysts. *Catal. Today*. **2015**, *250*, 226-238.
- Vantblik, H. F. J and Prins, R. Characterization of supported cobalt and cobalt-rhodium catalysts. *J. Catal.* **1986**, *97*, 188-199.
- Vasiliadou, E. S.; Heracleous E.; Vasalos, I. A.; Lemonidou, A. A. Ru-based catalysts for glycerol hydrogenolysis-effect of support and metal precursor. *Appl. Catal. B.* **2009**, *92*, 90–99.
- Vasiliadou, E. S.; Lemonidou, A. A. Investigating the performance and deactivation behavior of silica-supported copper catalysts in glycerol hydrogenolysis. *Appl. Catal. A. Gen.* **2011**, *396*, 177-185. doi:10.1016/j.apcata.2011.02.014.

- Vasiliadou, E. S.; Lemonidou, A. A. Kinetic study of liquid-phase glycerol hydrogenolysis over Cu/SiO_2 catalyst. *Chem. Eng. J.* **2013**, *231*, 103–112.
- Vasiliadou, E. S.; Eggenhuisen, T. M.; Munnik, P.; De Jongh, P. E.; De Jong, K. P.; Lemonidou, A. A. Synthesis and performance of highly dispersed Cu/SiO_2 catalysts for the hydrogenolysis of glycerol. *Appl. Catal. B.* **2014**, *145*, 108-119.
- Vila, F.; Granados, M. L.; Ojeda, M.; Fierro, J. L. G.; Mariscal, R. Glycerol hydrogenolysis to 1,2-propanediol with $Cu/\gamma\text{-}Al_2O_3$: Effect of the activation process. *Catal. Today*. **2012**, *187*(1), 122-128.
- Wang, S.; Zhang, Y.; Liu, H. Selective hydrogenolysis of glycerol to propylene glycol on Cu-ZnO composite catalysts: structural requirements and reaction mechanism. *Chem. Asian J.* **2010**, *5*, 1100-1111.
- Wang, Y.; Zhou, J.; Guo, X. Catalytic hydrogenolysis of glycerol to propanediols: a review. *RSC. Adv.* **2015**a, *5*, 74611-74628.
- Wang, C.; Jiang, H.; Chen, C.; Chen, R.; Xing, W. Solvent effect on hydrogenolysis of glycerol to 1,2-propanediol over Cu–ZnO catalyst, *Chem. Eng. J.* **2015**b, *264*, 344–350.
- Wang, J.; Lei, N.; Yang, C.; Su, Y.; Zhao, X.; Wang, A. Effect of promoters on the selective hydrogenolysis of glycerol over Pt/W-containing catalysts. *Chin. J. Catal.* **2016**, *37*(9), 1513-1519.
- Wu, Z., Mao, Y., Song, M., Yin, X., Zhang, M. Cu/boehmite: A highly active catalyst for hydrogenolysis of glycerol to 1,2-propanediol. *Catal. Commun.* **2013**, *32*, 52-57.
- Xi, Y.; Holladay, J. E.; Frye, J. G.; Oberg, A. A.; Jackson, J. E.; Miller, D. J. A kinetic and mass transfer model for glycerol hydrogenolysis in a trickle-bed reactor. *Org. Process Res. Dev*. **2010**, 14, 1304–1312.
- Xia, S.; Yuan, Z.; Wang, L.; Chen, P.; Hou, Z. Hydrogenolysis of glycerol on bimetallic Pd-Cu/solid-base catalysts prepared via layered double hydroxides precursors. *Appl. Catal. A.* **2011**, *403*(1-2), 173-182.
- Xia, S.; Yuan, Z.; Wang, L.; Chen, P.; Hou, Z. Catalytic production of 1,2-propanediol from glycerol in bio-ethanol solvent, *Bioresour. Technol.* **2012**a, *104*, 814–817. doi:10.1016/j.biortech.2011.11.031.
- Xia, S.; Nie, R.; Lu, X.; Wang, L.; Chen, P.; Hou, Z. Hydrogenolysis of glycerol over $Cu_{0.4}/Zn_{5.6-x}MgxAl_2O_{8.6}$ catalysts: The role of basicity and hydrogen spillover, *J. Catal.* **2012**b**,** *296*, 1–11. doi:10.1016/j.jcat.2012.08.007.

- Xia, S.; Zheng, L.; Wang, L.; Chen, P.; Hou, Z. Hydrogen-free synthesis of 1,2-propanediol from glycerol over Cu–Mg–Al catalysts, *RSC. Adv*. **2013**, *3*, 16569. doi:10.1039/c3ra42543f.
- Xiao, Z.; Wang, X.; Xiu, J.; Wang, Y.; Williams, C. T.; Liang, C. Synergetic effect between Cu^0 and Cu^+ in the Cu-Cr catalysts for hydrogenolysis of glycerol. *Catal. Today*. **2014,** *234*, 200-207.
- Yadav, G. D.; Chandan, P. A.; Tekale, D. P. Hydrogenolysis of Glycerol to 1 , 2-Propanediol over Nano-Fibrous Ag-OMS-2 Catalysts, *Ind. Eng. Chem. Res.* **2012**, *51*, 1549–1562.
- Yang, Z.; Choi, K. M.; Jiang, N.; Park, S. E. Microwave synthesis of hydrotalcite by urea hydrolysis. *B. Korean Chem. Soc.* **2007**, *28*(11), 2029-2033.
- Yang, W.; Feng, Y.; Chu, W.; Promotion effect of CaO modification on mesoporous Al_2O_3-supported Ni catalysts for CO_2 methanation. *Int. J. of Chem. Eng.* **2016**.
- Yfanti, V. L.; Ipsakis, D.; Lemonidou, A. A. Kinetic study of liquid phase glycerol hydrodeoxygenation under inert conditions over a Cu-based catalyst. **2018**, *3*, 559-571 *React. Chem. Eng.* DOI: 10.1039/c8re00061a.
- Yuan, Z.; Wu, P.; Gao, J.; Lu, X.; Hou, Z.; Zheng, X. Pt/Solid-Base: a predominant catalyst for glycerol hydrogenolysis in a base-free aqueous solution. *Catal. Lett.* **2009**, *130*, 261–265, DOI 10.1007/s10562-009-9879-0
- Yuan, Z.; Wang, L.; Wang, J.; Xia, S.; Chen, P.; Hou, Z.; Zheng, X. Hydrogenolysis of glycerol over homogenously dispersed copper on solid base catalysts. *Appl. Catal. B.* **2011**, *101*, 431-440. doi:10.1016/j.apcatb.2010.10.013.
- Yuan, Z.; Wang, J.; Wang, L.; Xie, W.; Chen, P.; Hou, Z.; Zheng, X. Biodiesel derived glycerol hydrogenolysis to 1,2-propanediol on Cu/MgO catalysts. *Bioresour. Technol.* **2010**, *101*, 7088–7092.
- Yue, C. J.; Gu, L. P.; Su, Y.; Zhu, S. P. Selective hydrogenolysis of glycerol to 1,2-propanediol over MgO-nested Raney Cu. *React. Kinet. Mech. Catal.* **2014**, *111*, 633–645.
- Yu, C.; Xu, H.; Ge, Q.; Li, W. Properties of the metallic phase of zinc-doped platinum catalysts for propane dehydrogenation, *J. Mol. Catal. A. Chem.* **2007**, *266*, 80-87.
- Yu, W.; Zhao, J.; Ma, H.; Miao, H.; Song, Q.; Xu, J. Aqueous hydrogenolysis of glycerol over Ni–Ce/AC catalyst: Promoting effect of Ce on catalytic performance. *Appl. Catal. A.* **2010**, *383*, 73-78.

- Yun, Y. S.; Park, D. S.; Yi, J. Effect of nickel on catalytic behaviour of bimetallic Cu–Ni catalyst supported on mesoporous alumina for the hydrogenolysis of glycerol to 1,2-propanediol, *Catal. Sci. Technol.* **2014**, *4*, 3191–3202. doi:10.1039/c4cy00320a.
- Zelazny, A.; Samson, K.; Grabowski, R.; Sliwa, M.; Ruggiero-Mikolajczyk, M.; Kornas, A. Hydrogenolysis of glycerol to propylene glycol over Cu/oxide catalysts: influence of the support and reaction conditions, *React. Kinet. Mech. Cat.* **2017**, *121*(1), 329-343. doi:10.1007/s11144-017-1154-6.
- Zheng, X.; Lin, H.; Zheng, J.; Duan, X.; Yuan, Y. Lanthanum oxide-modified Cu/SiO_2 as a high-performance catalyst for chemoselective hydrogenation of dimethyl oxalate to ethylene glycol. *ACS Catal.* **2013**, *3*(12), 2738-2749.
- Zhong, H.; Zhou, Yi.; Ye, M.; He, Y.; Ye, J. He, C.; Yang, C.; Li Y. Controlled synthesis and optical properties of colloidal ternary chalcogenide $CuInS_2$ nanocrystals. *Chem. Mater.* **2008**, *20*(20), 6434-6443.
- Zhou, Z.; Li, X.; Zeng, T.; Hong, W.; Cheng, Z.; Yuan, W. Kinetics of hydrogenolysis of glycerol to propylene glycol over Cu-ZnO-Al_2O_3 catalysts. *Chin. J. Chem. Eng.* **2010**, *18*, 384–390.
- Zhou, J.; Zhang, J.; Guo, X.; Zhang, S. Ag/Al_2O_3 for glycerol hydrogenolysis to 1,2-propanediol: activity, selectivity and deactivation, *Green Chem.* **2012**, *14*(1), 156–163.
- Zhou, C. H.; Deng, K.; Serio, M. D.; Xiao, S.; Tong, D. S.; Li, L.; Lin, C. X.; Beltramini, J.; Zhang, H.; Yu, W. H. Cleaner hydrothermal hydrogenolysis of glycerol to 1,2-propanediol over Cu/oxide catalysts without addition of external hydrogen. *Mol. Catal.* **2017**, *432*, 274-284.
- Zhu, Y. Y.; Wang, S. R.; Zhu, L. J.; Ge, X. L.; Li, X. B.; Luo, Z. Y. The Influence of Copper Particle Dispersion in Cu/SiO_2 Catalysts on the Hydrogenation Synthesis of Ethylene Glycol. *Catal. Lett.* **2010**, *135*, 275-281. https://doi.org/10.1007/s10562-010-0298-z.
- Zou, H.; Shen, J. Microcalorimetric and infrared spectroscopic studies of γ-Al_2O_3 modified by zinc oxide. *Thermochima. Acta.* **2000**, *351*, 165-170.

APPENDIX I

Table A1.1. Physico-chemical properties of Cu:Ni(1:1)/γ-Al_2O_3 catalyst with the variation of calcination temperature

Calcination temperature	BET surface area (m^2g^{-1})	Pore volume ($cm^3.g^{-1}$)	Average Cu-Ni crystallite size (nm)	Acidity (mmol NH_3. $gcat^{-1}$)	Degree of reduction (%)
350	92.0	0.15	17.2	2.8	68.3
400	90.0	0.15	16.2	2.9	74.3
450	86.0	0.14	20.2	1.5	54.8
500	83.0	0.13	19.1	0.2	68.2

CALCULATION OF CALIBRATION FACOTRS

Calibration factors were used to calculate the mole ratios of different components in the product mixture and it was defined as follow.

Calibration factor of X with respect to Y,

$$K_{XY} = \frac{\frac{\text{weight of X in the standard mixture}}{\text{weight of Y in the standard mixture}}}{\frac{\text{area of X}}{\text{area of Y}}}$$

1. Calibration factor for glycerol, 1,2-PDO, hydroxyacetone, EG, 1-propanol, 2-propanol, ethanol, and methanol

For the calculation of calibration factors of all reactants and products, n-butanol was used as an internal standard.

Calibration factor of glycerol with respect to n-butanol = 3.02

Calibration factor of 1,2-PDO with respect to n-butanol = 1.56

Calibration factor of hydroxyacetone with respect to n-butanol = 2.33

Calibration factor of EG with respect to n-butanol = 2.33

Calibration factor of 1-propanol with respect to n-butanol = 1.01

Calibration factor of 2-propanol with respect to n-butanol = 1.11

Calibration factor of ethanol with respect to n-butanol = 1.37

Calibration factor of methanol with respect to n-butanol = 2.30

Carrier gas: Nitrogen (flow rate: 50 cc min^{-1})

Detector: Flame inonization detector (FID)

Column: Chromosorb-101 packed column (1.52 m x 3.1 mm o.d. x 2 mm i.d.)

2. Chromatogram of identified obtained by GC

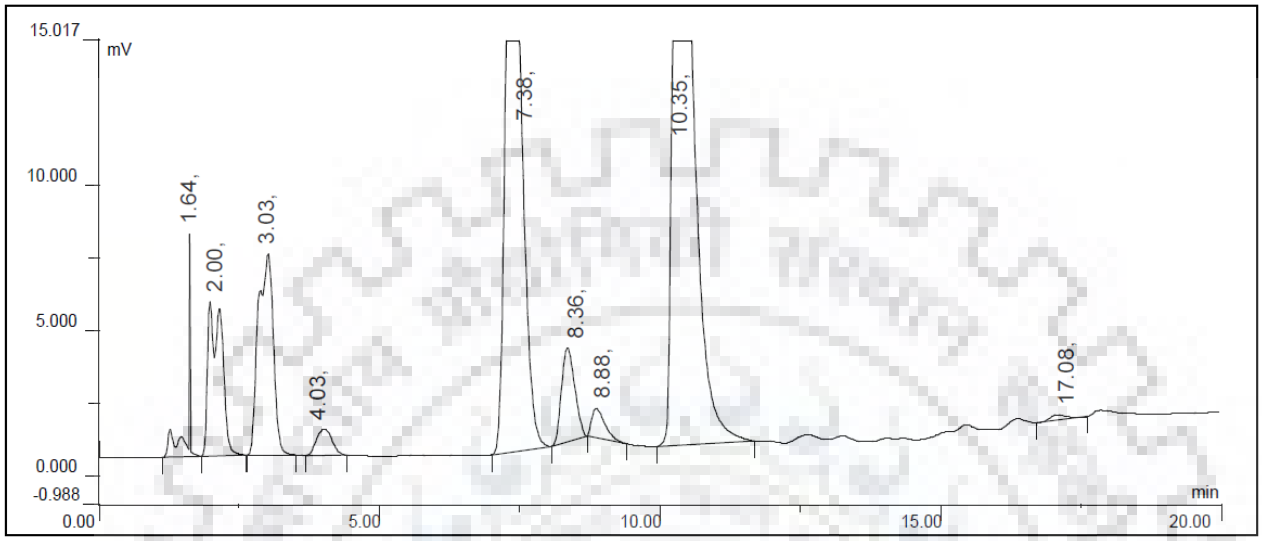

Figure A1.1. Chromatogram of identified products obtained by GC

Table A1.2. Components detected by GC and their retention times

Compound name	Retention time
Methanol	1.64
Ethanol	2.00
2-propanol (2-PO)	3.03
1-propanol (1-PO)	4.03
n-butanol	7.38
Hydroxyacetone	8.36
Ethylene glycol (EG)	8.88
1,2-propanediol (1,2-PDO)	10.35
Glycerol	17.08

APPENDIX II

KINETIC MODELS

Model 1. $G \rightarrow P$

Step 1: Adsorption of glycerol (G) and hydrogen (H_2) on the active site ($) of the catalyst as:

$$G + 2\$ \underset{k_{-1}}{\overset{k_1}{\rightleftharpoons}} G.\$_2$$

$$H_2 + 2\$ \underset{k_{-2}}{\overset{k_2}{\rightleftharpoons}} 2H.\$$$

Step 2: Interaction of adsorbed glycerol with adsorbed hydrogen produced adsorbed 1,2-PDO as:

$$G.\$_2 + 2H.\$ \underset{k_{-3}}{\overset{k_3}{\rightleftharpoons}} P.\$ + W + 3\$$$

where, P and W represented 1,2-PDO and water, respectively.

Step 3: Desorption of 1,2-PDO from the catalyst surface and the active sites were regenerated as:

$$P.\$ \underset{k_{-4}}{\overset{k_4}{\rightleftharpoons}} P + \$$$

Model 2. $G \rightarrow P$

Step 1: Adsorption of glycerol (G) on the active site ($) of the catalyst as:

$$G + \$ \underset{k_{-1}}{\overset{k_1}{\rightleftharpoons}} G.\$$$

Step 2: Interaction of adsorbed glycerol with hydrogen molecule (H_2) produced adsorbed 1,2-PDO as:

$$G.\$ + H_2 \underset{k_{-2}}{\overset{k_2}{\rightleftharpoons}} P.\$ + W$$

where, P and W represented 1,2-PDO and water, respectively.

Step 3: Desorption of 1,2-PDO from the catalyst surface and the active sites were regenerated as:

$$P.\$ \underset{k_{-3}}{\overset{k_3}{\rightleftharpoons}} P + \$$$

Model 3. $G \rightarrow P$

Step 1: Adsorption of glycerol (G) and hydrogen (H_2) on the active site ($) of the catalyst as:

$$G + \$ \underset{k_{-1}}{\overset{k_1}{\rightleftharpoons}} G.\$$$

$$H_2 + \$ \underset{k_{-2}}{\overset{k_2}{\rightleftharpoons}} H_2.\$$$

Step 2: Interaction of adsorbed glycerol with adsorbed hydrogen produced adsorbed 1,2-PDO as:

$$G.\$ + H_2.\$ \underset{k_{-3}}{\overset{k_3}{\rightleftharpoons}} P.\$ + W.\$$$

where, P and W represented 1,2-PDO and water, respectively.

Step 3: Desorption of 1,2-PDO and water from the catalyst surface and the active sites were regenerated as:

$$P.\$ \underset{k_{-4}}{\overset{k_4}{\rightleftharpoons}} P + \$$$

$$W.\$ \underset{k_{-5}}{\overset{k_5}{\rightleftharpoons}} W + \$$$

Model 4. $G \rightarrow P \rightarrow PO$

Step 1: Adsorption of glycerol (G) and hydrogen (H_2) on the active site ($) of the catalyst as:

$$G + \$ \underset{k_{-1}}{\overset{k_1}{\rightleftharpoons}} G.\$$$

$$H_2 + 2\$ \underset{k_{-2}}{\overset{k_2}{\rightleftharpoons}} 2H.\$$$

Step 2: Interaction of adsorbed glycerol with adsorbed atomic hydrogen produced adsorbed 1,2-PDO followed by the surface reaction between adsorbed 1,2-PDO (P.$) and adsorbed atomic hydrogen (H.$) occurred as:

$$G.\$ + 2H.\$ \underset{k_{-3}}{\overset{k_3}{\rightleftharpoons}} P.\$ + 2\$$$

$$P.\$ + 2H.\$ \underset{k_{-4}}{\overset{k_4}{\rightleftharpoons}} PO.\$ + 2\$$$

where, P, PO represented 1,2-PDO, propanol, respectively.

Step 3: Desorption of products (1,2-PDO and PO) from the catalyst surface and the active sites were regenerated as:

$$P.\$ \underset{k_{-5}}{\overset{k_5}{\rightleftharpoons}} P + \$$$

$$PO.\$ \underset{k_{-6}}{\overset{k_6}{\rightleftharpoons}} PO + \$$$

Model 5. $G \rightarrow P \rightarrow PO$

Step 1: Adsorption of glycerol (G) on the active site ($) of the catalyst as:

$$G + \$ \underset{k_{-1}}{\overset{k_1}{\rightleftharpoons}} G.\$$$

Step 2: Interaction of adsorbed glycerol with hydrogen molecule (H_2) and produced adsorbed 1,2-PDO followed by the surface reaction between adsorbed 1,2-PDO (P.$) and hydrogen molecule (H_2) occurred as:

$$G.\$ + H_2 \underset{k_{-3}}{\overset{k_3}{\rightleftharpoons}} P.\$ + W$$

$$P.\$ + H_2 \underset{k_{-4}}{\overset{k_4}{\rightleftharpoons}} PO.\$ + W$$

where, P, PO, and W represented 1,2-PDO, propanol, and water, respectively.

Step 3: Desorption of products (1,2-PDO and PO) from the catalyst surface and the active sites were regenerated as:

$$P.\$ \underset{k_{-5}}{\overset{k_5}{\rightleftharpoons}} P + \$$$

$$PO.\$ \underset{k_{-6}}{\overset{k_6}{\rightleftharpoons}} PO + \$$$

Model 6. $G \rightarrow P \rightarrow PO$

Step 1: Adsorption of glycerol (G) and hydrogen (H_2) on the active site ($) of the catalyst as:

$$G + \$ \underset{k_{-1}}{\overset{k_1}{\rightleftharpoons}} G.\$$$

$$H_2 + \$ \underset{k_{-2}}{\overset{k_2}{\rightleftharpoons}} H_2.\$$$

Step 2: Interaction of adsorbed glycerol with adsorbed hydrogen molecule and produced adsorbed 1,2-PDO followed by the surface reaction between adsorbed 1,2-PDO (P.$) and adsorbed molecular hydrogen (H_2.$) occurred as:

$$G.\$ + H_2.\$ \underset{k_{-3}}{\overset{k_3}{\rightleftharpoons}} P.\$ + \$$$

$$P.\$ + H_2.\$ \underset{k_{-4}}{\overset{k_4}{\rightleftharpoons}} PO.\$ + \$$$

where, P, PO, and W represented 1,2-PDO, propanol, and water, respectively.

Step 3: Desorption of products (1,2-PDO and PO) from the catalyst surface and the active sites were regenerated as:

$$P.\$ \underset{k_{-5}}{\overset{k_5}{\rightleftharpoons}} P + \$$$

$$PO.\$ \underset{k_{-6}}{\overset{k_6}{\rightleftharpoons}} PO + \$$$

Model 7. $G \rightarrow P \rightarrow PO$

Step 1: Adsorption of glycerol (G) and hydrogen (H_2) on the active site ($) of the catalyst as:

$$G + \$ \underset{k_{-1}}{\overset{k_1}{\rightleftharpoons}} G.\$$$

$$H_2 + \$ \underset{k_{-2}}{\overset{k_2}{\rightleftharpoons}} H_2.\$$$

Step 2: Interaction of adsorbed glycerol with adsorbed hydrogen molecule and produced adsorbed 1,2-PDO followed by the surface reaction between adsorbed 1,2-PDO (P.$) and adsorbed molecular hydrogen (H_2.$) occurred as:

$$G.\$ + H_2.\$ \underset{k_{-3}}{\overset{k_3}{\rightleftharpoons}} P.\$ + \$$$

$$P.\$ + H_2.\$ \underset{k_{-4}}{\overset{k_4}{\rightleftharpoons}} PO.\$ + \$$$

where, P, PO represented 1,2-PDO, propanol, respectively.

Step 3: Desorption of products (1,2-PDO and PO) from the catalyst surface and the active sites were regenerated as:

$$P.\$ \underset{k_{-5}}{\overset{k_5}{\rightleftharpoons}} P + \$$$

$$PO.\$ \underset{k_{-6}}{\overset{k_6}{\rightleftharpoons}} PO + \$$$

Model 8. $G \rightarrow P \rightarrow PO$

Step 1: Adsorption of glycerol (G) and hydrogen (H_2) on the active site ($) of the catalyst as:

$$G + \$ \underset{k_{-1}}{\overset{k_1}{\rightleftharpoons}} G.\$$$

$$H_2 + \$ \underset{k_{-2}}{\overset{k_2}{\rightleftharpoons}} H_2.\$$$

Step 2: Interaction of adsorbed glycerol produced adsorbed 1,2-PDO followed by the surface reaction between adsorbed 1,2-PDO (P.$) and adsorbed molecular hydrogen (H.$) occurred as:

$$G.\$ \underset{k_{-3}}{\overset{k_3}{\rightleftharpoons}} P.\$ + W$$

$$P.\$ + H_2.\$ \underset{k_{-4}}{\overset{k_4}{\rightleftharpoons}} PO.\$ + \$$$

where, P, PO, and W represented 1,2-PDO, propanol, and water, respectively.

Step 3: Desorption of products (1,2-PDO and PO) from the catalyst surface and the active sites were regenerated as:

$$P.\$ \underset{k_{-5}}{\overset{k_5}{\rightleftharpoons}} P + \$$$

$$PO.\$ \underset{k_{-6}}{\overset{k_6}{\rightleftharpoons}} PO + \$$$

Model 9.

Step 1: Adsorption of glycerol (G) and hydrogen (H_2) on the active site ($) of the catalyst as:

$$G + \$ \underset{k_{-1}}{\overset{k_1}{\rightleftharpoons}} G.\$$$

$$H_2 + \$ \underset{k_{-2}}{\overset{k_2}{\rightleftharpoons}} H_2.\$$$

Step 2: Interaction of adsorbed glycerol with adsorbed hydrogen molecule and produced adsorbed 1,2-PDO followed by the surface reaction between adsorbed 1,2-PDO (P.$) and adsorbed molecular hydrogen (H_2.$) occurred as:

$$G.\$ + H_2.\$ \underset{k_{-3}}{\overset{k_3}{\rightleftharpoons}} P.\$ + W + \$$$

$$G.\$ + H_2.\$ \underset{k_{-4}}{\overset{k_4}{\rightleftharpoons}} PO.\$ + \$$$

where, P, PO, and W represented 1,2-PDO, propanol, and water, respectively.

Step 3: Desorption of products (1,2-PDO and PO) from the catalyst surface and the active sites were regenerated as:

$$P.\$ \underset{k_{-5}}{\overset{k_5}{\rightleftharpoons}} P + \$$$

$$PO.\$ \underset{k_{-6}}{\overset{k_6}{\rightleftharpoons}} PO + \$$$

Model 10.

Step 1: Adsorption of glycerol (G) on the active site ($) of the catalyst as:

$$G + 2\$ \underset{k_{-1}}{\overset{k_1}{\rightleftharpoons}} G.\$_2$$

Step 2: Interaction of adsorbed glycerol with hydrogen molecule (H_2) present in the bulk phase and produced adsorbed 1,2-PDO and propanol :

$$G.\$_2 + H_2 \underset{k_{-2}}{\overset{k_2}{\rightleftharpoons}} P.\$ + PO.\$ + W$$

where, P, PO, and W represented 1,2-PDO, propanol, and water, respectively.

Step 3: Desorption of products (1,2-PDO and PO) from the catalyst surface and the active sites were regenerated as:

$$P.\$ \underset{k_{-3}}{\overset{k_3}{\rightleftharpoons}} P + \$$$

$$PO.\$ \underset{k_{-4}}{\overset{k_4}{\rightleftharpoons}} PO + \$$$

Model 11.

Step 1: Adsorption of glycerol (G) and hydrogen (H_2) on the active site ($) of the catalyst as:

$$G + \$ \underset{k_{-1}}{\overset{k_1}{\rightleftharpoons}} G.\$$$

$$H_2 + \$ \underset{k_{-2}}{\overset{k_2}{\rightleftharpoons}} H_2.\$$$

Step 2: Interaction of adsorbed glycerol with adsorbed hydrogen molecule produced adsorbed 1,2-PDO followed by the surface reaction between adsorbed 1,2-PDO (P.$) and propanol (PO.$) occurred as:

$$G.\$ + H_2.\$ \underset{k_{-3}}{\overset{k_3}{\rightleftharpoons}} P.\$ + PO.\$$$

where, P, PO represented 1,2-PDO, propanol, respectively.

Step 3: Desorption of products (1,2-PDO and PO) from the catalyst surface and the active sites were regenerated as:

$$P.\$ \underset{k_{-4}}{\overset{k_4}{\rightleftharpoons}} P + \$$$

$$PO.\$ \underset{k_{-5}}{\overset{k_5}{\rightleftharpoons}} PO + \$$$

Model 12.

Step 1: Adsorption of glycerol (G) on the active site ($) of the catalyst as:

$$G + \$ \underset{k_{-1}}{\overset{k_1}{\rightleftharpoons}} G.\$$$

Step 2: Interaction of adsorbed glycerol with hydrogen molecule (H_2) produced adsorbed 1,2-PDO. Further, interaction of adsorbed glycerol with hydrogen molecule (H_2) produced propanol as:

$$G.\$ + H_2 \underset{k_{-2}}{\overset{k_2}{\rightleftharpoons}} P.\$ + W$$

$$G.\$ + H_2 \underset{k_{-3}}{\overset{k_3}{\rightleftharpoons}} PO.\$ + W$$

where, P, PO, and W represented 1,2-PDO, propanol, and water, respectively.

Step 3: Desorption of products (1,2-PDO and PO) from the catalyst surface and the active sites were regenerated as:

$$P.\$ \underset{k_{-4}}{\overset{k_4}{\rightleftharpoons}} P + \$$$

$$PO.\$ \underset{k_{-5}}{\overset{k_5}{\rightleftharpoons}} PO + \$$$

Model 13.

Step 1: Adsorption of glycerol (G) and hydrogen (H_2) on the active site ($) of the catalyst as:

$$G + \$ \underset{k_{-1}}{\overset{k_1}{\rightleftharpoons}} G.\$$$

$$H_2 + \$ \underset{k_{-2}}{\overset{k_2}{\rightleftharpoons}} H_2.\$$$

Step 2: Interaction of adsorbed glycerol with adsorbed hydrogen molecule produced adsorbed 1,2-PDO followed by the surface reaction between adsorbed 1,2-PDO (P.$) and adsorbed hydrogen produced adsorbed propanol (PO.$). Further, interaction of adsorbed glycerol with adsorbed hydrogen molecule produced Ethelyene glycol (E.$).

$$G.\$ + H_2.\$ \underset{k_{-3}}{\overset{k_3}{\rightleftharpoons}} P.\$ + \$$$

$$P.\$ + H_2.\$ \underset{k_{-4}}{\overset{k_4}{\rightleftharpoons}} PO.\$ + \$$$

$$G.\$ + H_2.\$ \underset{k_{-5}}{\overset{k_5}{\rightleftharpoons}} E.\$ + \$$$

where, P, PO, and E represented 1,2-PDO, propanol, and ethylene glycol, respectively.

Step 3: Desorption of products (1,2-PDO, PO and ethylene glycol) from the catalyst surface and the active sites were regenerated as:

$$P.\$ \underset{k_{-6}}{\overset{k_6}{\rightleftharpoons}} P + \$$$

$$PO.\$ \underset{k_{-7}}{\overset{k_7}{\rightleftharpoons}} PO + \$$$

$$E.\$ \underset{k_{-8}}{\overset{k_8}{\rightleftharpoons}} E + \$$$

Model 14. $G \rightarrow A \rightarrow P$

Step 1: Adsorption of glycerol (G) and adsorption of hydrogen on the active site ($) of the catalyst in which hydrogen is adsorbed as hydrogen atoms as:

$$G + \$ \underset{k_{-1}}{\overset{k_1}{\rightleftharpoons}} G.\$$$

$$H_2 + 2\$ \underset{k_{-2}}{\overset{k_2}{\rightleftharpoons}} 2H.\$$$

Step 2: Interaction of adsorbed glycerol produced adsorbed hydroxyacetone (A.$) followed by the surface reaction between adsorbed hydroxyacetone (A.$) and adsorbed atomic hydrogen (H.$) occurred as:

$$G.\$ \underset{k_{-3}}{\overset{k_3}{\rightleftharpoons}} A.\$ + W$$

$$A.\$ + 2H.\$ \underset{k_{-4}}{\overset{k_4}{\rightleftharpoons}} P.\$ + 2\$$$

where, A, P, and W represented hydroxyacetone, 1,2-PDO, and water, respectively.

Step 3: Desorption of products (hydroxyacetone and 1,2-PDO) from the catalyst surface and the active sites were regenerated as:

$$A.\$ \underset{k_{-5}}{\overset{k_5}{\rightleftharpoons}} A + \$$$

$$P.\$ \underset{k_{-6}}{\overset{k_6}{\rightleftharpoons}} P + \$$$

Model 15. $G \rightarrow A \rightarrow P$

Step 1: Adsorption of glycerol (G) and hydrogen (H_2) on the active site ($) of the catalyst as:

$$G + \$ \underset{k_{-1}}{\overset{k_1}{\rightleftharpoons}} G.\$$$

$$H_2 + \$ \underset{k_{-2}}{\overset{k_2}{\rightleftharpoons}} H_2.\$$$

Step 2: Interaction of adsorbed glycerol produced adsorbed hydroxyacetone (A.$) followed by the surface reaction between adsorbed hydroxyacetone (A.$) and adsorbed molecular hydrogen (H_2.$) occurred as:

$$G.\$ \underset{k_{-3}}{\overset{k_3}{\rightleftharpoons}} A.\$ + W$$

$$A.\$ + H_2.\$ \underset{k_{-4}}{\overset{k_4}{\rightleftharpoons}} P.\$ + \$$$

where, A, P, and W represented hydroxyacetone, 1,2-PDO, and water, respectively.

Step 3: Desorption of products (hydroxyacetone and 1,2-PDO) from the catalyst surface and the active sites were regenerated as:

$$A.\$ \underset{k_{-5}}{\overset{k_5}{\rightleftharpoons}} A + \$$$

$$P.\$ \underset{k_{-6}}{\overset{k_6}{\rightleftharpoons}} P + \$$$

Model 16. $G \rightarrow A \rightarrow P$

Step 1: Adsorption of glycerol on the active site ($) of the catalyst as:

$$G + \$ \underset{k_{-1}}{\overset{k_1}{\rightleftharpoons}} G.\$$$

Step 2: Interaction of adsorbed glycerol produced adsorbed hydroxyacetone (A.$) followed by the surface reaction between adsorbed hydroxyacetone (A.$) and hydrogen molecule (H_2) occurred as:

$$G.\$ \underset{k_{-2}}{\overset{k_2}{\rightleftharpoons}} A.\$ + W$$

$$A.\$ + H_2 \underset{k_{-3}}{\overset{k_3}{\rightleftharpoons}} P.\$$$

where, A, P, and W represented hydroxyacetone, 1,2-PDO, and water, respectively.

Step 3: Desorption of products (hydroxyacetone and 1,2-PDO) from the catalyst surface and the active sites were regenerated as:

$$A.\$ \underset{k_{-4}}{\overset{k_4}{\rightleftharpoons}} A + \$$$

$$P.\$ \underset{k_{-5}}{\overset{k_5}{\rightleftharpoons}} P + \$$$

Model 17. $G \rightarrow A \rightarrow P$

Step 1: Adsorption of glycerol (G) and hydrogen (H_2) on two different active sites of the catalyst $ and S, respectively:

$$G + \$ \underset{k_{-1}}{\overset{k_1}{\rightleftharpoons}} G.\$$$

$$H_2 + S \underset{k_{-2}}{\overset{k_2}{\rightleftharpoons}} H_2.S$$

Step 2: Interaction of adsorbed glycerol produced adsorbed hydroxyacetone (A.$) followed by the surface reaction between adsorbed hydroxyacetone (A.$) and adsorbed molecular hydrogen (H_2.S) occurred as:

$$G.\$ \underset{k_{-3}}{\overset{k_3}{\rightleftharpoons}} A.\$ + W$$

$$A.\$ + H_2.S \underset{k_{-4}}{\overset{k_4}{\rightleftharpoons}} P.\$ + S$$

where, A, P, and W represented hydroxyacetone, 1,2-PDO, and water, respectively.

Step 3: Desorption of products (hydroxyacetone and 1,2-PDO) from the catalyst surface and the active sites were regenerated as:

$$A.\$ \underset{k_{-5}}{\overset{k_5}{\rightleftharpoons}} A + \$$$

$$P.\$ \underset{k_{-6}}{\overset{k_6}{\rightleftharpoons}} P + \$$$

Model 18. $G \rightarrow A \rightarrow P$

Step 1: Adsorption of glycerol (G) and hydrogen (H_2) on two different active sites of the catalyst \$ and S, respectively, in which hydrogen (H_2) is adsorbed as hydrogen atoms:

$$G + \$ \underset{k_{-1}}{\overset{k_1}{\rightleftharpoons}} G.\$$$

$$H_2 + 2S \underset{k_{-2}}{\overset{k_2}{\rightleftharpoons}} 2H.S$$

Step 2: Interaction of adsorbed glycerol produced adsorbed hydroxyacetone (A.\$) followed by the surface reaction between adsorbed hydroxyacetone (A.\$) and adsorbed atomic hydrogen (H.S) occurred as:

$$G.\$ \underset{k_{-3}}{\overset{k_3}{\rightleftharpoons}} A.\$ + W$$

$$A.\$ + 2H.S \underset{k_{-4}}{\overset{k_4}{\rightleftharpoons}} P.\$ + 2S$$

where, A, P, and W represented hydroxyacetone, 1,2-PDO, and water, respectively.

Step 3: Desorption of products (hydroxyacetone and 1,2-PDO) from the catalyst surface and the active sites were regenerated as:

$$A.\$ \underset{k_{-5}}{\overset{k_5}{\rightleftharpoons}} A + \$$$

$$P.\$ \underset{k_{-6}}{\overset{k_6}{\rightleftharpoons}} P + \$$$

Model 19. $G \rightarrow A \rightarrow P$

Step 1: Adsorption of glycerol (G) on the active site ($) of the catalyst as:

$$G + 2.\$ \underset{k_{-1}}{\overset{k_1}{\rightleftharpoons}} G.\$_2$$

Step 2: Interaction of adsorbed glycerol produced adsorbed hydroxyacetone (A.$) followed by the surface reaction between adsorbed hydroxyacetone (A.$) and hydrogen molecule (H_2) occurred as:

$$G.\$_2 \underset{k_{-2}}{\overset{k_2}{\rightleftharpoons}} A.\$ + W.\$$$

$$A.\$ + H_2 \underset{k_{-3}}{\overset{k_3}{\rightleftharpoons}} P.\$$$

where, A, P, and W represented hydroxyacetone, 1,2-PDO, and water, respectively.

Step 3: Desorption of products (hydroxyacetone, 1,2-PDO, and water) from the catalyst surface and the active sites were regenerated as:

$$A.\$ \underset{k_{-4}}{\overset{k_4}{\rightleftharpoons}} A + \$$$

$$W.\$ \underset{k_{-5}}{\overset{k_5}{\rightleftharpoons}} W + \$$$

$$P.\$ \underset{k_{-6}}{\overset{k_6}{\rightleftharpoons}} P + \$$$

APPENDIX III

WEISZ-PRATER CRITERION

Table A2.1. Calculation of Weisz-Prater criterion

According to Wiesz- Prater criterion: intra particle diffusion can be neglected if Wiesz- Prater criterion: $\varphi = \frac{r_{obs}\rho_p R_p^2}{D_e C_{AS}} \leq 1$ where $'\varphi'$ is known as Wiesz- Prater parameter		
Symbol	Term	Value
r_{obs}	Observed reaction rate at bulk concentration	7.5×10^{-6} mol glycerol.gcat^{-1}.s^{-1}
R_p	Radius of the catalyst particle	0.62×10^{-6} cm
C_{AS}	Reactant concentration at external particle surface	2.2×10^{-3} mol.cm^{-3}
ρ_p	True density of the catalyst	2.2 g.cc^{-1}
ξ	Catalyst porosity	0.5
T	Reaction temperature	493 K
$M_{glycerol}$	Molecular weight of glycerol (reactant)	92.5 g.mol^{-1}
α	Pore radius	2.8×10^{-7} cm
D_k	Knudsen diffusivity of glycerol = $9.7\times 10^{3} \times \alpha \left[\frac{T}{M_{glycerol}}\right]^{1/2}$	6.27×10^{-3} cm^2.s^{-1}
D_e	Effective diffusivity = $D_k \xi^2$	1.567×10^{-3} cm^2.s^{-1}
Φ	Weisz-Prater parameter	1.84×10^{-12}

In the present work, the calculated value of Weisz-Prater parameter was very low <<1 at the maximum reaction temperature (220 °C), so intra particle diffusion resistance was negligible.

APPENDIX IV

PRATER NUMBER

Table A3.1. Calculation of Prater Number

According to Prater no, if $\beta = T_{max} - T_S = \frac{-\Delta H_{Rx} D_e C_{AS}}{\lambda_{eff}}$ is very low, then the isothermal condition exists within the catalyst pellet.		
Symbol	Term	Value
$-\Delta H_{Rx}$	Heat of reaction	103×10^3 J.mol^{-1}
D_e	Effective diffusivity	1.567×10^{-3} cm^2.s^{-1}
C_{AS}	Concentration of reactant at the external surface of the catalyst particle	2.2×10^{-3} mol.cm^{-3}
T_S	Surface temperature	493 K
$\lambda_{eff} = \lambda_S \left(\frac{\lambda_f}{\lambda_S} \right)^{\xi}$	Effective thermal conductivity of catalyst pellet	4.792 W.m^{-1}.K^{-1}
λ_S	Thermal conductivity of catalyst pellet	38.8 W.m^{-1}.K^{-1}
λ_f	Thermal conductivity of fluid (glycerol + water + solubility of hydrogen)	0.5908 W.m^{-1}.K^{-1}
ξ	Porosity of catalyst pellet	0.5
β	Prater no	0.074 K

In this study, the estimated value of β was very low 0.074 K, which was less than 1 K. This result suggested that heat transfer resistance was insignificant.

APPENDIX V

THERMODYNAMIC EQUILIBRIUM CALCULATION FOR HYDROGENOLYSIS OF GLYCEROL

Standard Gibbs free energy of the following reaction was calculated by using standard method

At the standard reaction condition

$C_3H_8O_3$ (l) + H_2 (g) $\rightleftharpoons$ $C_3H_8O_2$ (l) + H_2O (g)

The Gibbs free energy at 298 °C

ΔG^o_{298} = (-333687.96 - 237129)-(-477337.068) = -93.479 kJ/mol

$-\ln(K_{298}) = (\Delta G^o)/RT$ = -93479.892 /8.314×298.15 = -37.7111

ΔH^o_{298} for this reaction $= -500.3 - 285.958 - 0 + 669.6 = -116.658$ kJ/mol

$C_P^o = a + bT + cT^2 + dT^3 + eT^{-2}$

C_P of glycerol = $137.654 + 0.3184T - 0.0001125T^2$

C_P of H_2 = $27.012 + 3.509\times10^3\ T + cT^2 + 0.690\times10^{-5}\ eT^{-2}$

C_P of H_2O = $28.850 + 12.055\times10^3\ T + 1.006\times10^{-5}\ eT^{-2}$

C_P of C_3H_8O at 210°C = 276.64 J/mol/K

$\Delta H^o_{298} = \Delta H_O + \Delta aT + \frac{\Delta b}{2}T^2 + \frac{\Delta c}{3}T^3 + \frac{\Delta d}{4}T^4 - \frac{\Delta e}{T}$

From van't Hoff equation,

$\left(\frac{\partial \ln K_a}{\partial T} = \frac{\Delta H^O}{RT^2}\right)$

$\ln K_T = 1/R\ [\ (\Delta H_O/T) + \Delta a \ln T + \frac{\Delta b}{2}T + \frac{\Delta c}{6}T^2 + \frac{\Delta d}{12}T^3 - \frac{\Delta e}{2T^2}\ ] + I$

The equilibrium constant can be calculated by solving these above equations

The calculated value of equilibrium constant K_a at 210 °C = 6.99×10^{15}

Negative value of Gibbs free energy ($\Delta G^o_{298} = -93.479 \frac{kJ}{mol}$) and high value of equilibrium constant K_a at 210 °C = 6.99×10^{15} imply that the reaction is irreversible in nature and thermodynamically 100% conversion is feasible.

APPENDIX VI

SPRINGER NATURE LICENSE TERMS AND CONDITIONS

May 07, 2019

This Agreement between g-14, sarojini bhawan iit roorkee ("You") and Springer Nature ("Springer Nature") consists of your license details and the terms and conditions provided by Springer Nature and Copyright Clearance Center.

License Number	4583580579043
License date	May 07, 2019
Licensed Content Publisher	Springer Nature
Licensed Content Publication	Catalysis Letters
Licensed Content Title	Production of 1,2-Propanediol from Renewable Glycerol Over Highly Stable and Efficient Cu–Zn(4:1)/MgO Catalyst
Licensed Content Author	Smita Mondal, Al Ameen Arifa, Prakash Biswas
Licensed Content Date	Jan 1, 2017
Licensed Content Volume	147
Licensed Content Issue	11
Type of Use	Thesis/Dissertation
Requestor type	academic/university or research institute
Format	print
Portion	full article/chapter
Will you be translating?	no
Circulation/distribution	<501
Author of this Springer Nature content	yes
Title	Conversion of glycerol to propanediol using heterogenous catalysts
Institution name	Indian Institute of Technology Roorkee
Expected presentation date	May 2019
Requestor Location	g-14, sarojini bhawan iit roorkee g-14, sarojini bhawan iit roorkee roorkee, haridwar 247667 India Attn: g-14, sarojini bhawan iit roorkee
Total	0.00 USD
Terms and Conditions	

Springer Nature Terms and Conditions for RightsLink Permissions

Springer Nature Customer Service Centre GmbH (the Licensor) hereby grants you a non-exclusive, world-wide licence to reproduce the material and for the purpose and requirements specified in the attached copy of your order form, and for no other use, subject to the conditions below:

1. The Licensor warrants that it has, to the best of its knowledge, the rights to license reuse of this material. However, you should ensure that the material you are requesting is original to the Licensor and does not carry the copyright of another entity (as credited in the published version).

   If the credit line on any part of the material you have requested indicates that it was reprinted or adapted with permission from another source, then you should also seek

permission from that source to reuse the material.

2. Where **print only** permission has been granted for a fee, separate permission must be obtained for any additional electronic re-use.

3. Permission granted **free of charge** for material in print is also usually granted for any electronic version of that work, provided that the material is incidental to your work as a whole and that the electronic version is essentially equivalent to, or substitutes for, the print version.

4. A licence for 'post on a website' is valid for 12 months from the licence date. This licence does not cover use of full text articles on websites.

5. Where **'reuse in a dissertation/thesis'** has been selected the following terms apply: Print rights of the final author's accepted manuscript (for clarity, NOT the published version) for up to 100 copies, electronic rights for use only on a personal website or institutional repository as defined by the Sherpa guideline (www.sherpa.ac.uk/romeo/).

6. Permission granted for books and journals is granted for the lifetime of the first edition and does not apply to second and subsequent editions (except where the first edition permission was granted free of charge or for signatories to the STM Permissions Guidelines http://www.stm-assoc.org/copyright-legal-affairs/permissions/permissions-guidelines/), and does not apply for editions in other languages unless additional translation rights have been granted separately in the licence.

7. Rights for additional components such as custom editions and derivatives require additional permission and may be subject to an additional fee. Please apply to Journalpermissions@springernature.com/bookpermissions@springernature.com for these rights.

8. The Licensor's permission must be acknowledged next to the licensed material in print. In electronic form, this acknowledgement must be visible at the same time as the figures/tables/illustrations or abstract, and must be hyperlinked to the journal/book's homepage. Our required acknowledgement format is in the Appendix below.

9. Use of the material for incidental promotional use, minor editing privileges (this does not include cropping, adapting, omitting material or any other changes that affect the meaning, intention or moral rights of the author) and copies for the disabled are permitted under this licence.

10. Minor adaptations of single figures (changes of format, colour and style) do not require the Licensor's approval. However, the adaptation should be credited as shown in Appendix below.

Appendix — Acknowledgements:

For Journal Content:
Reprinted by permission from [**the Licensor**]: [**Journal Publisher** (e.g. Nature/Springer/Palgrave)] [**JOURNAL NAME**] [**REFERENCE CITATION** (Article name, Author(s) Name), [**COPYRIGHT**] (year of publication)

For **Advance Online Publication papers:**
Reprinted by permission from [**the Licensor**]: [**Journal Publisher** (e.g. Nature/Springer/Palgrave)] [**JOURNAL NAME**] [**REFERENCE CITATION** (Article name, Author(s) Name), [**COPYRIGHT**] (year of publication), advance online publication, day month year (doi: 10.1038/sj.[JOURNAL ACRONYM].)

For Adaptations/Translations:
Adapted/Translated by permission from [**the Licensor**]: [**Journal Publisher** (e.g. Nature/Springer/Palgrave)] [**JOURNAL NAME**] [**REFERENCE CITATION** (Article name, Author(s) Name), [**COPYRIGHT**] (year of publication)

Note: For any republication from the British Journal of Cancer, the following credit line style applies:

Reprinted/adapted/translated by permission from [**the Licensor**]: on behalf of Cancer Research UK: : [**Journal Publisher** (e.g. Nature/Springer/Palgrave)] [**JOURNAL NAME**] [**REFERENCE CITATION** (Article name, Author(s) Name), [**COPYRIGHT]** (year of publication)

For **Advance Online Publication** papers:
Reprinted by permission from The [**the Licensor**]: on behalf of Cancer Research UK: [**Journal Publisher** (e.g. Nature/Springer/Palgrave)] [**JOURNAL NAME**] [**REFERENCE CITATION** (Article name, Author(s) Name), [**COPYRIGHT**] (year of publication), advance online publication, day month year (doi: 10.1038/sj. [JOURNAL ACRONYM])

For Book content:
Reprinted/adapted by permission from [**the Licensor**]: [**Book Publisher** (e.g. Palgrave Macmillan, Springer etc) [**Book Title**] by [**Book author**(s)] [**COPYRIGHT**] (year of publication)

Other Conditions:

Version 1.1

Title:	Highly active Cu-Zn-Mg-Al-O catalyst derived from layered double hydroxides (LDHs) precursor for selective hydrogenolysis of glycerol to 1,2-propanediol
Author:	Smita Mondal,Rathikanti Janardhan,Mohan Lal Meena,Prakash Biswas
Publication:	Journal of Environmental Chemical Engineering
Publisher:	Elsevier
Date:	December 2017

Gmail **smita mondal <s08mondal@gmail.com>**

Fwd:RE: Request for a no objection letter

prakashbiswas <prakashbiswas@gmail.com> Fri, May 10, 2019 at 7:03 AM
To: s08mondal <s08mondal@gmail.com>

Sent from OPPO Mail
---------- Forwarded Message ----------
From: "CONTRACTS-COPYRIGHT (shared)" <Contracts-Copyright@rsc.org>
Date: 9 May 2019 7:28 pm
Subject: RE: Request for a no objection letter
To: "'prakashbiswas@gmail.com'" <prakashbiswas@gmail.com>
Cc:

> Dear Prakash Biswas,
>
> Could you please forward the below to Mrs Mondal?
>
> Best wishes,
> Chloe Szebrat
>
> **********
> Dear Mrs Mondal,
>
> The Royal Society of Chemistry (RSC) hereby grants permission for the use of your paper(s) specified below in the printed and microfilm version of your thesis. You may also make available the PDF version of your paper(s) that the RSC sent to the corresponding author(s) of your paper(s) upon publication of the paper(s) in the following ways: in your thesis via any website that your university may have for the deposition of theses, via your university's Intranet or via your own personal website. We are however unable to grant you permission to include the PDF version of the paper(s) on its own in your institutional repository. The Royal Society of Chemistry is a signatory to the STM Guidelines on Permissions (available on request).
>
> Please note that if the material specified below or any part of it appears with credit or acknowledgement to a third party then you must also secure permission from that third party before reproducing that material.
>
> Please ensure that the thesis states the following:
>
> Reproduced by permission of The Royal Society of Chemistry
>
> and include a link to the paper on the Royal Society of Chemistry's website.
>
> Please ensure that your co-authors are aware that you are including the paper in your thesis.
>
> Best wishes,
> Chloe Szebrat
> Contracts and Copyright Executive
> Royal Society of Chemistry
> Thomas Graham House
> Science Park, Milton Road
> Cambridge, CB4 0WF, UK
> Tel: +44 (0) 1223 438329
> www.rsc.org
>
> -----Original Message-----
> From: prakashbiswas@gmail.com <prakashbiswas@gmail.com>

Sent: 03 May 2019 15:04
To: CONTRACTS-COPYRIGHT (shared) <Contracts-Copyright@rsc.org>
Subject: Request for a no objection letter

Name: Prakash Biswas
Message: Dear Sir/Madam,
This is requested to you for a no objection letter from RSC to publish the research content of a manuscript published in Reaction Chemistry & Engineering, in the PhD thesis of first author Mrs. Smita Mondal.
This is required based on a comment received from a PhD thesis examiner.
The paper detail is as follows:
Smita Mondal , Himanshu Malviya and Prakash Biswas, "Kinetic modelling for the hydrogenolysis of bio-glycerol in the presence of a highly selective Cu–Ni–Al2O3 catalyst in a slurry reactor",
DOI: 10.1039/C8RE00138C (Paper) React. Chem. Eng., 2019, 4, 595-609

Your kind help in this regard will be highly appreciated.

Thanking you
With best regards
Prakash Biswas
Corresponding Author